THE UNIVERSITY OF NOTTINGHAM

RESEARCH ON THE UNCONTROLLED ZERO-SEQUENCE CURRENT OF AN OPEN-END WINDING PMSM WITH COMMON DC LINK

PhD Thesis

by

NICK HUNTER

Submitted to the University of Nottingham for the degree of Doctor of Philosophy

March 2020

In memory of

Vladimir Alekseevich Krukhmalev

(my lovely grandad who passed away during the first year of my PhD)

and

Everton Alfanso Blake

(my good friend and a colleague who gave me the whole new insight into the world of practical engineering and had been always motivating me to achieve more from the very first day of my journey to becoming an engineer)

ABSTRACT

This thesis describes the research based on a particular type of the motor drives called an open-end winding permanent magnet synchronous motor drive with common DC link. These types of drives are an arrangement of two three phase inverters connected to both ends of a permanent magnet synchronous motor and are fed from a single direct current source. Therefore, it has a return path between the two inverters. This allows the most prominent third harmonic back EMF to introduce the zero-sequence current. Hence, these kinds of motor drives suffer from the circulating zero-sequence current. Although this current usually is undesired and, therefore, suppressed using various control techniques, there are some cases when the suppression of this current is unfeasible. Hence, the zero-sequence current could be left flowing in the system. High-speed drives could be considered to be an example of such a system.

The research introduced in this thesis is centred on the analysis of the mentioned zero-sequence current that is flowing in the system due to the specific properties of the machine. It features a full mathematical derivation of the nature of the zero-sequence current flowing in the system because of the machine side of the drive and a comprehensive analysis of the power loss in conductor due to this zero-sequence component.

The analysis performed in this thesis resulted in a proposal of a couple of novel solutions for the mitigation of the zero-sequence component's impact on the drive such as the torque ripple and the power loss in conductor. In addition, one of the research outcomes was the development of a novel technique that turns the disadvantage of having the zero-sequence component flowing freely in the drive to its advantage.

In addition, the research produced in this thesis led to the development of a software solution that is meant to aid design and control engineers to mitigate the power losses in an open-end winding permanent magnet synchronous motor drive with common DC link.

ACKNOWLEDGEMENTS

I would like to pay my special regards to my supervisors, Dr Thomas Cox, Prof. Pericle Zanchetta, Dr Shafiq Odhano and Dr Giovanni Lo Calzo for their support.

I am indebted to Dr Luca Rovere, Dr Fausto Stella and Dr Jonathan Blissett along with Dr Dmitry Golovanov for their invaluable assistance. Thanks to Dr Alessandro Galassini, Dr Luca Tarisciotti, Dr Alessandro Costabebe, Mr Stuart Marchant, Dr Bilal Arif and all of the people who were supporting me by giving me the valuable advices.

A special thank you to my lovely wife Elena Hunter and my mother Elena Mellard for their intensive physical and mental support throughout the years of my PhD. I would like to thank my father, Oleg together with his wife Marina and her parents Tamara and Nikolay, my brother Konstantin and my cousin Alexander for their emotional support. Also, thanks to both of my grandmothers: Maria and Natalia together with the rest of the family for having faith in me through these years, including my wife's side of the family: my father-in-law, Alexander, my mother-in-law, Galina and my sisters-in-law, Svetlana and Tanya.

Thanks to my friend, Albert Gallini who has emotionally supported me throughout these years and kept me on track with his motivational speeches when I was going off course. Thanks to Sanya for sending me over9000 memes making sure my mood remains positive throughout the day. Also, I am indebted to Fatima Ihab for the invaluable mental health support that appeared to be the turning point in my PhD.

I would also like to pay special regards to my colleagues, Shirley, Moe, Iain and Tom for being such understanding and supportive line managers. Also, thanks to all of the Foundation Engineering and Science team that supported me physically and mentally throughout my time at work: John, Jez, Cathy, Francesco, Rob, Ruth, Sobia, Rachel, Peter and the maths team: David, Alan, Christina and James.

I also wish to express my deepest gratitude to Prof. Sergey Bozhko who has inspired me to pursue my degree in Electrical and Electronic Engineering and has kept motivating me throughout the years in academia.

SYMBOLS & ABBREVIATIONS

PMSM	Permanent Magnet Synchronous Motor
OEW	Open-End Winding
ZSC	Zero-Sequence Current
ZSV	Zero-Sequence Voltage
VSC	Voltage Source Converter
EMF	Electromotive Force
BEMF	Back Electromotive Force
IMD	Integrated Motor Drive
FEA	Finite element analysis
PE	Power Electronics
MRAS	Model Reference Adaptive System
FFT	Fast Fourier Transform
SiC	Silicon Carbide
IGBT	Insulated Gate Bipolar Transistor
MTPA	Maximum Torque Per Ampere
ZSMBSC	Zero-Sequence Model-Based Sensorless Control
ZSMBPO	Zero-Sequence Model-Based Position Observer
IPMSM	Interior Permanent Magnet Synchronous Motor
SMPMSM	Surface Mount Permanent Magnet Synchronous Motor
DSP	Digital Signal Processor
PID	Proportional Integral Derivative Controller
SOGI	Second Order General Integrator
ADC	Analog to Digital Converter
MSE	Mean Squared Error
MSEI	Mean Squared Error Improvement

TABLE OF CONTENTS

1 Introduction 17

1.1 High-Speed Drives 18

1.2 Motivation and Research Objective 20

1.3 Thesis Organisation 22

2 Literature Review on Control Techniques for High-Speed Open-End Winding PMSM Drives 24

2.1 Permanent Magnet Synchronous Machines Configurations 25

2.2 OEW PMSM Drives with common DC link 30

2.2.1 Torque ripple suppression 30

2.2.2 Temperature Estimation 32

2.2.3 Sensorless Control in OEW PMSM with common DC Link 34

2.2.4 Power Losses in an OEW PMSM with common DC Link 34

2.3 Integrated drives 36

3 Open-End Winding PMSM with Common DC Link Theory 37

3.1 OEW PMSM voltage equations in Machine Variables 38

3.2 OEW PMSM Voltage Equations in Rotor Reference Frame 42

3.3 Torque produced by an OEW PMSM 46

3.4 Effect of ZSC on the OEW PMSM performance 48

3.4.1 Controlled Zero-Sequence Current 48

3.4.2 Uncontrolled Zero-Sequence Current 55

3.5 Discussion 64

4 Simulation Model Design and Experimental Test System 65

4.1 Open-End Winding PMSM with Common DC link Simulation Model 66

4.1.1 Design of the Open-End Winding PMSM Model in Simulink. 67

4.1.2 Adding Non-linearity to the Open-End Winding PMSM model 69

4.1.3 Inverter Simulation Design 73

4.2 Experimental Test System 77

4.2.1 Experimental SiC Inverter 77

4.2.2 High-Speed High Power Density Open-End Winding Test Machine 78

4.2.3 Control Board 79

4.2.4 High-Speed Machines Testing Rig 80

4.2.5 The Experimental Setup Parameters Estimation 81

4.3 Discussion 85

5 Proposed Torque Quality Improvement Technique for an Open-End Winding PMSM 87

5.1 Modeling of the OEW PMSM Output Torque 88

5.2 Design of the Torque Ripple Compensator 89

5.3 Simulation Results 93

5.3.1 Ideal Simulation Case 93

5.3.2 Non-Ideal Simulation Case 96

5.4 Experimental Results 111

5.5 Discussion 131

6 Proposed Non-Intrusive Online Stator Temperature Estimation Technique for an Open-End Winding PMSM 133

6.1 Zero-Sequence Current Analysis 134

6.2 Resistance and Temperature Estimation 138

6.2.1 Resistance Estimation 138

6.2.2 Temperature Estimation 138

6.2.3 Implementation of Resistance and Temperature Estimation ...140

6.2.4 Parameter Sensitivity Analysis 142

6.3 Simulation Results 146

6.4 Discussion 148

7 Further Improvements of the OEW PMSM control..150

7.1 Power Loss Reduction for OEW PMSM 151

7.1.1 Power Loss due to the ZSC Analysis 151

7.1.2 Proposed Power Loss in Conductor Reduction Technique 175

7.1.3 Discussion 198

7.2 Current Limit of OEW PMSM with common DC Link 201

7.2.1 RMS Current Limiter for OEW PMSM 201

7.2.2 Peak Current Limiter..205

7.3 Development of a Design Aid Algorithm for OEW PMSM with Common DC Link 209

7.3.1 Power Loss Reduction Aid 209

7.3.2 Discussion 223

8 Conclusions, Contributions and Recommendations for Future Research 224

8.1 Conclusions and Contributions 225

8.2 Recommendation for Future Work 228

8.2.1 Torque Quality Improvement Technique 228

8.2.2 Non-Intrusive Online Stator Temperature Estimation Technique 228

8.2.3 Reduction of Power Loss in Conductor Technique..................229

8.2.4 Current Limiting Technique...230

8.2.5 Other Further Work 230

Appendix A – Special FFT Algorithm i

Appendix B – OEW PMSM Model for Simulink simulation vi

Appendix C - Sample Calculations... xii

Appendix D - Power Loss Reduction Algorithm xiii

Appendix E - Power Loss Reduction App..................................xxvi

Appendix F - Published Papers lvii

TABLE OF FIGURES

Fig. 1.1 – OEW PMSM with common DC link 20
Fig. 2.1 – Synthesising voltage vectors of different configurations 26
Fig. 2.2 – Star Connected PMSM schematic...26
Fig. 2.3 – Delta Connected PMSM schematic 27
Fig. 2.4 – OEW PMSM with common DC link schematic...........................27
Fig. 2.5 – Characteristic curves of each of the winding configuration [15] .28
Fig. 2.6 – OEW PMSM with dual DC supply..28
Fig. 2.7 – OEW PMSM with floating bridge 29
Fig. 2.8 – Modularised converter unit attached to the motor casing..........36
Fig. 3.1 – OEW PMSM with common DC bus..38
Fig. 3.2 – Zero-Sequence Voltage phasor diagram 49
Fig. 3.3 – Zero-Sequence Voltage phasor diagram when V_0=0V 49
Fig. 3.4 – Zero-Sequence Current phasor diagram 51
Fig. 3.5 – Phasor diagram of the Zero-Sequence Voltage and Current 51
Fig. 3.6 – Electromagnetic torque's DC component due to ZSC................60
Fig. 3.7 – Electromagnetic torque's AC component due to ZSC. 63
Fig. 4.1 – Diagram of a basic OEW PMSM drive simulation structure 66
Fig. 4.2 – Linear behaviour of quadrature (Lq) and direct (Ld) inductances 69
Fig. 4.3 – Non-linear behaviour of quadrature (Lq) and direct (Ld) inductances 70
Fig. 4.4 – Difference between non-linear Ld and quadrature Lq inductances 70
Fig. 4.5 – Non-linear inductance behaviour block diagram 71
Fig. 4.6 – Frequency content of OEW PMSM phase back EMF derived from FEA..72
Fig. 4.7 – OEW PMSM Matlab/Simulink model for common DC link...........73
Fig. 4.8 – Modulation scheme for Open-End Winding PMSM control [97]...74
Fig. 4.9 – SVM diagram for the dual fed inverter in $qd0$ plane..................75
Fig. 4.10 – SVM diagram for the dual fed inverter in qd plane 76
Fig. 4.11 – High power SiC Inveter for the OEW drive configuration 77

Fig. 4.12 – High-speed high torque machine 78
Fig. 4.13 – Control Platform based on ZynQ 7020 SoC 79
Fig. 4.14 – 4-Quadrant starter/generator test rig with schematic [102] 81
Fig. 4.15 – Comparison of quadrature current with its approximation 82
Fig. 4.16 – Comparison of the motor speed with its approximation 83
Fig. 5.1 – Equivalent circuit of zero-sequence component of OEW PMSM ..88
Fig. 5.2 – Basic Quadrature Current PI+RC simulation setup 91
Fig. 5.3 – Bode diagram of the resonant controller according to the range of the input frequencies 92
Fig. 5.4 – Electromagnetic torque (top) and phase current (bottom) at 200Hz electrical speed 94
Fig. 5.5 – Quadrature, direct and zero currents (top, middle and bottom, respectively) at 200 Hz electrical speed...95
Fig. 5.6 – The full detailed simulation block diagram featuring voltage modulation 97
Fig. 5.7 – SOGI based single phase PLL amplitude estimator...................98
Fig. 5.8 – Electromagnetic torque comparison with MSE values 99
Fig. 5.9 – Electromagnetic torque FFT comparison (No load) 99
Fig. 5.10 – Electromagnetic torque FFT comparison (Load torque 10 Nm) 100
Fig. 5.11 – Electromagnetic torque FFT comparison (Load torque 20 Nm) 100
Fig. 5.12 – Electromagnetic torque FFT comparison (Load torque 30 Nm) 101
Fig. 5.13 – Electromagnetic torque FFT comparison (Load torque 40 Nm) 101
Fig. 5.14 – Zero-sequence current ($i0$) comparison 102
Fig. 5.15 – AC part of the quadrature axis voltage ($VqAC$).....................102
Fig. 5.16 – DC part of the quadrature axis voltage ($VqDC$) 103
Fig. 5.17 – Quadrature axis voltage (Vq) 103
Fig. 5.18 – Quadrature axis current (iq) comparison 104
Fig. 5.19 – Quadrature axis current with reference (proposed control method) 104

Fig. 5.20 – Direct axis current (id) comparison 105
Fig. 5.21 – Phase A current (ia) comparison 105
Fig. 5.22 – Phase A voltage (Va) comparison 106
Fig. 5.23 – Electrical rotor speed during load transient 106
Fig. 5.24 – Electromagnetic torque during speed transient 107
Fig. 5.25 – Torque comparison across the range of load currents at 500 rpm 112
Fig. 5.26 – Torque comparison across the range of load currents at 1000 rpm 113
Fig. 5.27 – Torque comparison across the range of load currents at 1500 rpm 114
Fig. 5.28 – Torque comparison across the range of load currents at 2000 rpm 115
Fig. 5.29 – Torque comparison across the range of load currents at 2500 rpm 116
Fig. 5.30 – Torque comparison across the range of load currents at 3000 rpm 117
Fig. 5.31 – Torque comparison across the range of load currents at 3500 rpm 118
Fig. 5.32 – Torque comparison across the range of load currents at 4000 rpm 119
Fig. 5.33 – Torque comparison across the range of load currents at 4500 rpm 120
Fig. 5.34 – Torque comparison across the range of load currents at 5000 rpm 121
Fig. 5.35 – Torque comparison across the range of load currents at 5500 rpm 122
Fig. 5.36 – Torque quality improvement across the range of speeds and load currents 125
Fig. 5.37 – Mean Squared Error improvement (MSEI) of the torque across the range of speeds and load currents 128
Fig. 5.38 – The quadrature current iq at No Load condition 129
Fig. 5.39 – The quadrature current iq at 10 A load condition 129

Fig. 5.40 – The quadrature current iq at 30 A load condition 130
Fig. 5.41 – The quadrature current iq at 50 A load condition 130
Fig. 6.1 – Equivalent circuit of zero-sequence component of OEW PMSM.134
Fig. 6.2 – Relationship between the ZSC amplitude and the rotor electrical speed...136
Fig. 6.3 – Relationship between the frequency constant multiplier and the ZSC amplitude. 137
Fig. 6.4 – OEW PMSM temperature estimation block diagram. 140
Fig. 6.5 – SOGI based single phase PLL amplitude estimator. 141
Fig. 6.6 – Temperature estimation simulation block diagram. 142
Fig. 6.7 – Resistance estimation parameter sensitivity with increasing electrical speed from 10 to 800 Hz at T = 45°C. 143
Fig. 6.8 – Temperature estimation parameter sensitivity with increasing electrical speed from 10 to 800 Hz at T = 45°C. 144
Fig. 6.9 – Resistance estimation parameter sensitivity with increasing electrical speed from 10 to 800 Hz at T = 100°C. 144
Fig. 6.10 – Temperature estimation parameter sensitivity with increasing electrical speed from 10 to 800 Hz at T = 100°C. 145
Fig. 6.11 – Simulation results: (a – stator winding temperature, b – phase resistance, c – electromagnetic torque) – 800Hz constant electrical speed, (d – stator winding temperature, e – phase resistance, f – electromagnetic torque) – 100Hz constant electrical speed 146
Fig. 7.1 – ZSC amplitude along a range of electrical angular speeds 152
Fig. 7.2 – ZSC amplitude at constant base frequency (nominal rs) 154
Fig. 7.3 – ZSC amplitude at constant base frequency (increased rs) 154
Fig. 7.4 – Amplitude of zero-sequence current 155
Fig. 7.5 – Zero-sequence back EMF $rs = 0.164\ \Omega$ 158
Fig. 7.6 – Zero-sequence current $rs = 0.164\ \Omega$ 158
Fig. 7.7 – Total power loss due to zero-sequence component $rs = 0.164\ \Omega$ 158
Fig. 7.8 – Power loss in conductor due to ZSC $rs = 0.164\ \Omega$ 158
Fig. 7.9 – Zero-sequence back EMF $rs = 0.597\ \Omega$ 159
Fig. 7.10 – Zero-sequence current $rs = 0.597\ \Omega$ 159

Fig. 7.11 – Total power loss due to zero-sequence component $rs = 0.597\ \Omega$ 159
Fig. 7.12 – Power loss in conductor due to ZSC $rs = 0.597\ \Omega$......159
Fig. 7.13 – Zero-sequence back EMF $rs = 1.031\ \Omega$ 160
Fig. 7.14 – Zero-sequence current $rs = 1.031\ \Omega$ 160
Fig. 7.15 – Total power loss due to zero-sequence component $rs = 1.031\ \Omega$ 160
Fig. 7.16 – Power loss in conductor due to ZSC $rs = 1.031\ \Omega$......160
Fig. 7.17 – Zero-sequence back EMF $rs = 1.464\ \Omega$ 161
Fig. 7.18 – Zero-sequence current $rs = 1.464\ \Omega$ 161
Fig. 7.19 – Total power loss due to zero-sequence component $rs = 1.464\ \Omega$ 161
Fig. 7.20 – Power loss in conductor due to ZSC $rs = 1.464\ \Omega$......161
Fig. 7.21 – Zero-sequence back EMF $rs = 2\ \Omega$ 162
Fig. 7.22 – Zero-sequence current $rs = 2\ \Omega$......162
Fig. 7.23 – Total power loss due to zero-sequence component $rs = 2\ \Omega$ ...162
Fig. 7.24 – Power loss in conductor due to ZSC $rs = 2\ \Omega$......162
Fig. 7.25 – Steady state zero-sequence back EMF......164
Fig. 7.26 – Steady state zero-sequence current......164
Fig. 7.27 – Steady state total power loss due to zero-sequence component 165
Fig. 7.28 – Steady state power loss in conductor due to ZSC 165
Fig. 7.29 – Components of power loss due to ZSC 166
Fig. 7.30 – Power loss in conductor due to ZSC with crossing active and reactive planes points. 167
Fig. 7.31 – Power loss in conductor due to the torque producing current iq 169
Fig. 7.32 – Power loss in conductor due to zero-sequence current 171
Fig. 7.33 – Power loss in conductor due to ZSC (resistance domain) 173
Fig. 7.34 – Power loss in conductor due to iq 174
Fig. 7.35 – Components of the power loss in conductor 174
Fig. 7.36 – Total power loss in conductor......175
Fig. 7.37 – Total power loss in conductor (resistance domain)......176

Fig. 7.38 – Total power loss in conductor with max/min points 183
Fig. 7.39 – Max/min power loss in conductor points (resistance domain) 183
Fig. 7.40 – Total maximum and minimum power loss in conductor.........184
Fig. 7.41 – Absolute maximum reduction of power loss in conductor 185
Fig. 7.42 – Relative maximum reduction of power loss in conductor 186
Fig. 7.43 – Maximum relative reduction of power loss in conductor 187
Fig. 7.44 – Potential reduction of power loss in conductor at $iq\ max2$ 188
Fig. 7.45 – Potential reduction of power loss in conductor (fe domain) ...189
Fig. 7.46 – Operational points for the minimum power loss in conductor. 196
Fig. 7.47 – Potential reduction of power loss in conductor at $fe\ o/p$ 197
Fig. 7.48 – Surface of potential reduction of power loss in conductor......198
Fig. 7.49 – Phase current peak control block 206
Fig. 7.50 – Minimum of the peak fundamentals at various γ 3D 207
Fig. 7.51 – Minimum of the peak fundamentals at various γ 2D 207
Fig. 7.52 – Fundamental, 3rd Harmonic and Phase Current 208
Fig. 7.53 – Phase current peak according to change in Ia1 and Ia3 208
Fig. 7.54 – Text output of the developed Matlab algorithm 210
Fig. 7.55 – Total power loss in conductor with max/min points and the user's operating point...211
Fig. 7.56 – Potential reduction of power loss in conductor with the user's operating point...211
Fig. 7.57 – Power loss due to the zero-sequence component with the user's operating point...212
Fig. 7.58 – Potential reduction of power loss in conductor at $iq\ o/p$ with the user's operating point 213
Fig. 7.59 – Potential reduction of power loss in conductor at $fe\ o/p$ with the user's operating point 213
Fig. 7.60 – Operational points for the minimum power loss in conductor at the current resistance value...214
Fig. 7.61 – Operational points for the minimum power loss in conductor at the suggested resistance value 214
Fig. 7.62 – Power Loss in Conductor Reduction Calculator app (3D view) 215
Fig. 7.63 – Text output of the application 216

Fig. 7.64 – Power Loss in Conductor Reduction Calculator App (2D view) 217
Fig. 7.65 – Graphical 1D outputs of the application 218
Fig. 7.66 – Power loss in conductor is already at minimum GUI (3D view) 219
Fig. 7.67 – Power loss in conductor is already at minimum text message 219
Fig. 7.68 – Error handling: operating speed exceeds rated speed 221
Fig. 7.69 – Error handling: (a) – high operating point current, (b) - high leakage inductance 221
Fig. 7.70 – Error handling: (a) – phase resistance, (b) - leakage inductance, (c) – 3rd harmonic flux coefficient 222
Fig. 7.71 – Error handling: (a) – flux linkage, (b) – pole number condition, (c) – rated speed value 222

LIST OF TABLES

TABLE I 3-phase OEW PMSM Specification according to FEA 67
TABLE II - Flux coefficients estimation 83
TABLE III 3-phase OEW PMSM Drive's Estimated Parameters 84
TABLE IV Torque quality improvement – Peak-to-Peak (Simulation)...108
TABLE V Torque quality improvement – MSE (Simulation)..................109
TABLE VI Torque quality improvement – Experimental (No load) 123
TABLE VII Torque quality improvement – Experimental (10 A load) 123
TABLE VIII Torque quality improvement – Experimental (30 A load)..124
TABLE IX Torque quality improvement – Experimental (50 A load) 124
TABLE X MSE improvement (MSEI) – Experimental (No load) 126
TABLE XI MSE improvement (MSEI) – Experimental (10A load).........126
TABLE XII MSE improvement (MSEI) – Experimental (30A load).........127
TABLE XIII MSE improvement (MSEI) – Experimental (50A load) 127
TABLE XIV Estimation error with $L0 = \pm 5\%$ and $\lambda pm3 = \pm 10\%$ 145
TABLE XV Electrical angle domain plots..157

Chapter 1

1 Introduction

This chapter introduces the concept of the high-speed drives and describes the motivation for the research and its objectives. In addition, the described thesis organisation section is meant to guide through the subsequent chapters.

1.1High-Speed Drives

An electrical drive is a system that converts energy from an electrical power source to a mechanical load. It consists of the three main elements: the controller, converter and machine - the primary electro-mechanical energy converter of the drive.

High-Speed Drives are used in applications where the operational speed is over 10 000 r/min. [1] The significant advantage of High-Speed Drives is the reduction of system weight for a given power conversion. The reduction of weight and size, in turn, also results in a better efficiency of a system the drive is used in, for example, an automotive industry, particularly in mobile applications such as vehicles where the reduction of weight is beneficial due to the minimisation of the fuel consumption. [2] [3] [4]

A rapid growth of the industrial and academic interests in the area of high-speed machines and drives pushing the research towards the improvements in this area. [5] [6] These interests are stimulated by the numerous potential applications of High-Speed Drives such as aeroengine spools, helicopter and racing engines, electric spindles for milling cutters and grinding, fuel pumps and turbochargers. In addition, due to the reduced weight/volume of the motor drive such a trend in research is beneficial for the "more electric" systems intended to replace hydraulic and pneumatic power sources in transportation and automotive industries. [7] Currently, research in the area of High-Speed Drives is mainly concentrated around the increase of power density of electrical machines, power converters, embedded control and communication links. [8]

The power output of an electrical machine is the product of the shaft torque and its rotational speed. In order to increase the torque without increasing the current density the rotor volume or/and the maximum flux density must be increased. [9] However, there has not been a considerable improvement in the maximum flux density over the past century. [10] [11] In addition, the increase of the volume of the machine is contradicting the goal of increasing the power density when the drive has to be a part of an aerospace or an automotive application. Hence, the increase of power of the machine was achieved by raising the operating speed. [12] [13] This is the major reason why the high-speed machines and, subsequently, the high-speed drives technology emerged. [14]

The increase of the operating speed has, however, introduced a lot of problems in the converter and the controller side of the drive. The converter side is now forced to use a higher frequency higher power switching technology along with the more efficient drives topology.

1.2Motivation and Research Objective

First and foremost, as it is stated in the introduction of this chapter on page 17, with the development of the aerospace and the automotive industries the research focus naturally gravitated towards the high-speed high power density drives due to the volume and weight limitations that applications in these fields are typically subjected to.

An open-end winding (OEW) with common DC link configuration for a PMSM drive shown in Fig. 1.1 was chosen as the subject of the research due to its increased potential power output compared to other configurations. [15] [16]

An Open-End Winding PMSM is a type of an electrical motor that has some key advantages with other configurations which include a good fault tolerance [17] [18], reduced complexity of the drive when compared to multi-level inverter drives [19] and which is usually particularly designed for the high-speed operation as it can take advantage from the full bus voltage. [20]

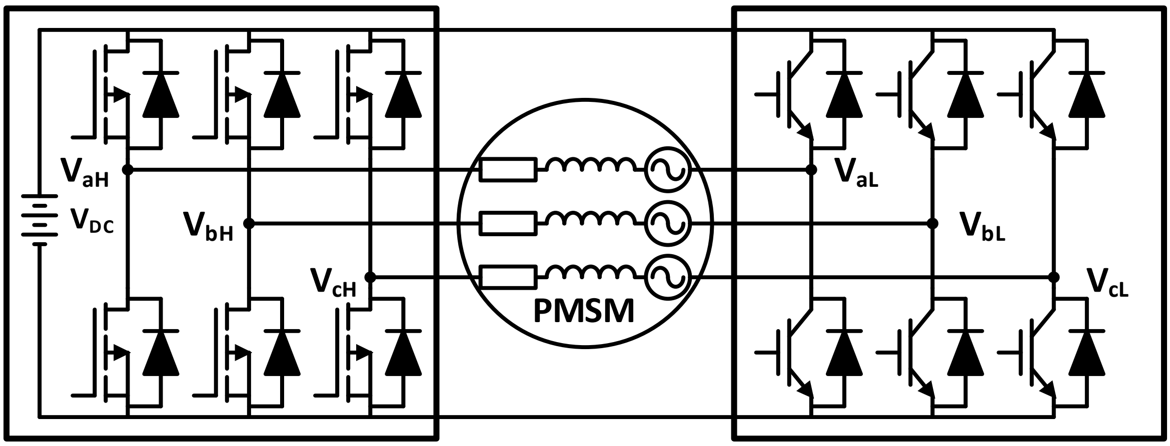

Fig. 1.1 – OEW PMSM with common DC link

Unfortunately, the open-end winding configuration of a permanent magnet synchronous motor comes with its drawbacks such as an additional power loss along with an additional torque ripple due to the circulating zero-sequence current in the stator windings. Not only does this circulating zero-sequence current not contribute to the rotation of the rotor, but also the analysis presented in this thesis showed that it results in the degradation of the performance.

In order to eliminate the negative influence of the zero-sequence current in the system, most of the research papers suggest the use of suppression techniques involving a zero-sequence voltage that has to be introduced by the inverter side of the drive. [21] [22] [23] [24] [25] [26] [27] [28] [29] However, when a machine is designed to be both high-speed and high torque, the number of the stator turns tends to be greatly reduced. Hence, the inductance of such a machine is generally low. Low phase inductance leads to low leakage inductance, especially when a drive is closely integrated giving only short electrical connections between the inverter and the machine itself. Low leakage inductance can also lead to spikes of zero-sequence current when a high voltage source is used for the bus that feeds the inverter. Depending on the value of this low leakage inductance, large spikes of zero-sequence current could be observed in the system if zero-sequence voltage is introduced even for as little as one microsecond when the drive is controlled using the voltage switching techniques. The suppression of the zero-sequence current for those kinds of open-end winding permanent magnet synchronous motor drive configurations does not seem feasible due to the mentioned large spikes of zero-sequence current.

The motivation that drove this research was as follows. It is not always feasible to eliminate the downsides of the OEW PMSM with common DC link configuration when it has low leakage inductance. In order to keep the advantages of OEW, research can be focused around ways to mitigate the influence of the zero-sequence current or to even use its presence in order to do something useful, in other words, to turn the disadvantage of the open-end winding PMSM configuration into its advantage.

1.3Thesis Organisation

Chapter 1 provides with the background along with the motivation and the objective of the research, briefly explaining the challenges associated with the high-speed drives, especially with the particular configuration of a drive that is considered in this thesis – open-end winding permanent magnet synchronous drive with common DC link.

Chapter 2 gives an overview of the work that has already been done in the field of the open-end winding permanent magnet synchronous motor drives with common DC link.

Chapter 3 shows the mathematical concept and the theory behind the open-end winding permanent magnet motor with common DC bus and demonstrates its challenges.

Chapter 4 describes the simulation model design derivations for the open-end winding system with common DC Link and its implementation along with the high-speed high power experimental test system.

Chapter 5 introduces a proposed method to mitigate the influence of the zero-sequence current on the quality of the torque production of the open-end winding permanent magnet synchronous motor drive with common DC Link without introducing zero-sequence voltage in the system.

Chapter 6 explains how a disadvantage of an open-end winding permanent magnet synchronous motor with common DC Link in a form of the unwanted zero-sequence current could be turned into its advantage by proposing a novel method for the non-intrusive online stator temperature estimation.

Chapter 7 develops a thorough understanding of the influence of an uncontrolled zero-sequence current on the power loss in conductor of an open-end winding permanent magnet synchronous motor drive with common DC link and proposes a novel method of reducing this power loss. Also, not only does this chapter propose a new current limiting technique for an open-end winding permanent magnet synchronous motor drive with common DC link, but also it reveals an erroneous idea of a current limiting technique introduced in some of the research papers.

Chapter 8 draws the conclusions and contributions of the research, stating the limitations of the proposed ideas and discussing the further research work that could be done in the field.

Chapter 2

2 Literature Review on Control Techniques for High-Speed Open-End Winding PMSM Drives

This chapter describes the difference between the most common three phase motor configurations, outlining their advantages and disadvantages. Moreover, a review of the existing control techniques and ideas of utilising the zero-sequence current in an open-end winding permanent magnet synchronous motor drives configuration with common DC link are also discussed.

2.1 Permanent Magnet Synchronous Machines Configurations

The constant development of the automotive and aerospace industries require higher power drives for the same volume/mass of the motor. This leads the research into the usage of the 3 phase permanent magnet synchronous motors (PMSM) due to their efficiency, high power density and a rather reduced complexity of its control. [30]

There are different types of the winding configurations for a 3 phase PMSM motor. The most common ones are depicted in Fig. 2.2-Fig. 2.4: the star connection, the delta connection, and the open-end winding (OEW) configuration, respectively. In case of an OEW configuration a star's neutral point is opened and each of the ends of the stator phases are connected to one leg of the inverter of that drive system, Fig. 2.4. [31] All of the three different types presented have their own advantages and disadvantages.

Let us consider, for example, a switching state of (110) in a star mode depicted in Fig. 2.2 and the delta mode illustrated in Fig. 2.3. The synthesising voltage vectors for these modes are shown in Fig. 2.1(a) and Fig. 2.1(b), respectively. The synthesising voltage vectors for the OEW configuration are shown in Fig. 2.1(c). Those vectors arise from one side of the inverter having a switching state (110) and the other side (001).

The amplitudes of the basic voltage vectors can be constructed from Fig. 2.1 (a), (b) and (c) as $\sqrt{2/3} \cdot V_{dc}$, $\sqrt{2/3} \cdot \sqrt{3}V_{dc}$, and $\sqrt{2/3} \cdot 2V_{dc}$, respectively, where $\sqrt{2/3}$ is the equal-power conversion coefficient. [15]

Hence, when a motor is connected in a delta configuration as per Fig. 2.3, the amplitude of the basic voltage vector is $\sqrt{3}$ times of that of the star configuration, however, the open-end winding configuration depicted in Fig. 2.4 has the amplitude of the basics voltage vector which is $\frac{2}{\sqrt{3}}$ times of the amplitude of the basic voltage vector in delta configuration.

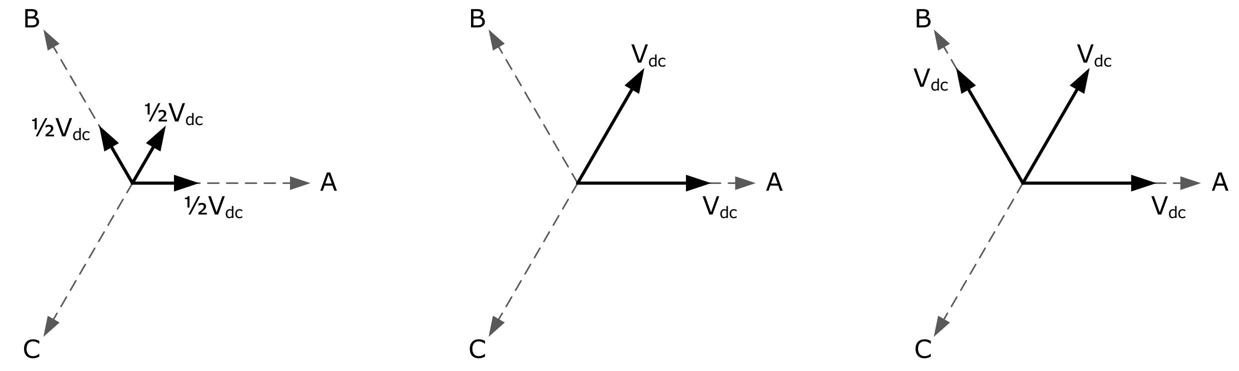

(a) Star mode (b) Delta mode (c) OEW mode

Fig. 2.1 – Synthesising voltage vectors of different configurations

The amplitude of the phase current in the star or the OEW configurations is the same as the amplitude of the line current, however, the amplitude of the phase current in delta mode is $1/\sqrt{3}$ of the line current. This means that the maximum amplitude of a synthesised stator current vector in delta mode is $1/\sqrt{3}$ of that in star or the OWE configuration.

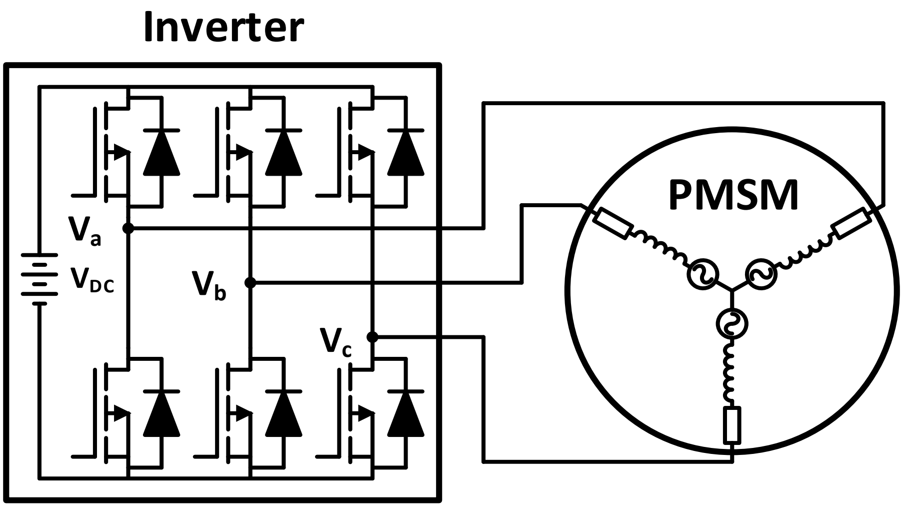

Fig. 2.2 – Star Connected PMSM schematic

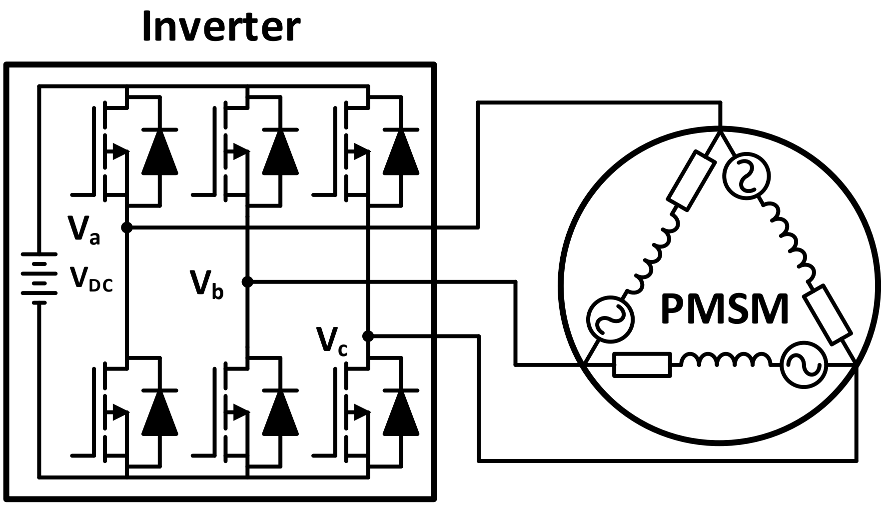

Fig. 2.3 – Delta Connected PMSM schematic

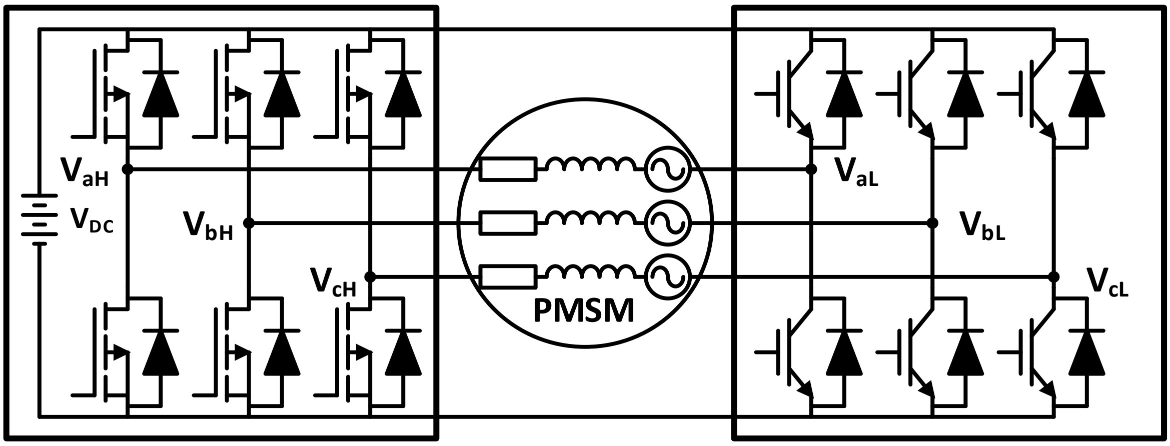

Fig. 2.4 – OEW PMSM with common DC link schematic

An example of the electromagnetic torque comparison between the different configurations is presented in Fig. 2.5.

Fig. 2.5 represents the typical characteristic curves of each of the motor configurations. The star configuration is represented with the blue line. The delta configuration or the triangular mode is represented in red. The open-end winding (OEW) configuration is shown in black and is called an independent mode. Fig. 2.5 shows that the torque in the delta configuration is $\frac{1}{\sqrt{3}}$ times of that of the star configuration. However, its speed range is around $\sqrt{3}$ times wider.

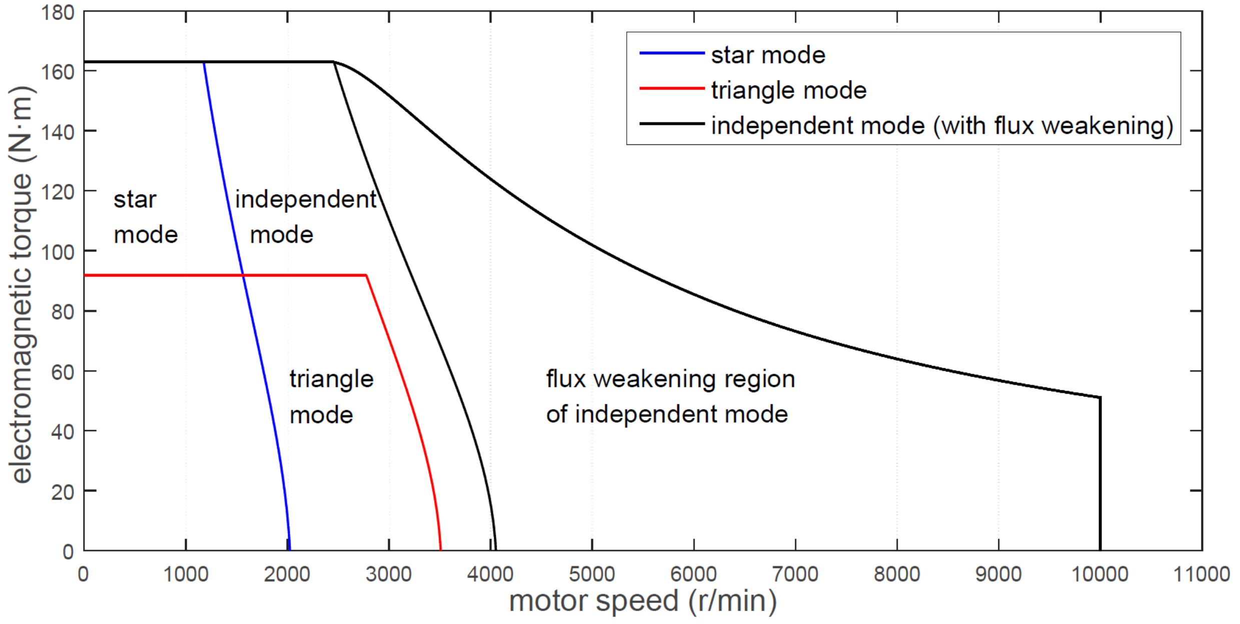

Fig. 2.5 – Characteristic curves of each of the winding configuration [15]

According to [15], a drive connected in the open-end winding configuration appears to be the best of both worlds: the torque is the same as with the star connection, however, the speed range is around twice of it. The OEW configuration is superior when it comes to the DC bus voltage utilisation, efficiency and power rating of the entire system comparing to the most commonly used star connection. [27] [32].

There are, of course, other types of the open-end winding configurations [20] [33], such as an OEW PMSM configuration with two isolated DC power supplies [34] [35] [36] [37] shown in Fig. 2.6 and another one with a floating bridge [38] [39] [40] [41] [42] depicted in Fig. 2.7.

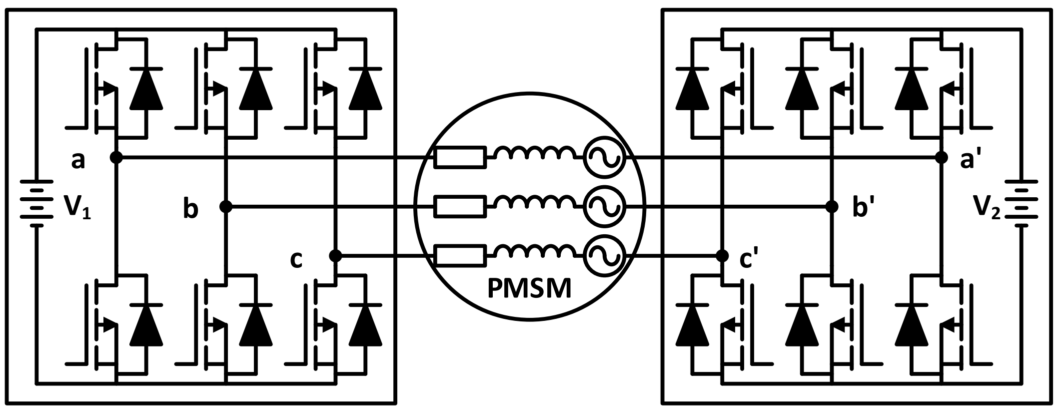

Fig. 2.6 – OEW PMSM with dual DC supply

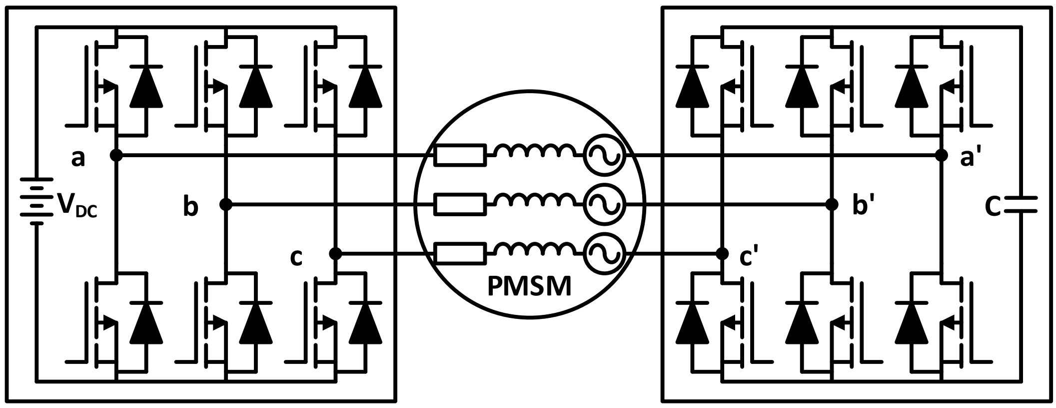

Fig. 2.7 – OEW PMSM with floating bridge

The OEW configuration with the common DC supply, Fig. 2.4, has a relatively easy implementation and a simpler structure comparing to the dual power supply, Fig. 2.6, version [43]. The OEW PMSM connection with floating bridge topology has a limited fault tolerant capability and a relatively complex control algorithm. [16] [44] [45]

However only the open-end winding PMSM drive configuration with the common DC link shown in Fig. 2.4 is considered in this thesis. According to [16] such a configuration is capable of a relatively high grade fault tolerance. [46] [47] [48] [49] [50] Fault tolerance is crucial in automotive including aerospace applications. [51] [52] [53]. In addition, the configuration of an OEW PMSM with common DC link has a relatively reduced complexity and low cost comparing with the configurations presented in Fig. 2.6 and Fig. 2.7 [54].

2.2OEW PMSM Drives with common DC link

Unlike in the star connection, the OEW configuration introduces a zero-sequence current (ZSC) that is circulating in the system. [55]

2.2.1Torque ripple suppression

Open-End Winding PMSM drive with a common DC bus features a dual inverter topology and a single DC power source. According to the comparison of the inverter arrangements considered in [56] its major advantages are fault tolerance, compact design, and high torque per volume ratio. In addition, such an arrangement is well suited for the implementation of different power device technologies such as IGBT and Silicon Carbide (SiC). Moreover, such an arrangement allows an increase of output power for a given inverter due to utilisation of the full bus voltage. Due to the aforementioned advantages, not only is the OEW PMSM topology a good candidate for aerospace applications, but also it is appropriate for wind power generation and motor drives operating above certain speeds [28].

However, such a topology does have some drawbacks. One issue is that the output electromagnetic torque becomes a function of both the third harmonic back EMF and the ZSC. Moreover, there are two parts of the OEW PMSM drive that happen to be the sources of ZSC: the inverter side and the actual OEW PMSM side. The ZSC caused by the inverter side can be minimised by introducing a special modulation [57] that eliminates the zero-sequence voltage (ZSV). In addition, the ZSV caused by dead-time [58] can also be compensated [59] [60]. Hence, in this chapter only the torque ripple due to the third harmonic back EMF is considered as the source of the oscillation. [61]

Different torque ripple minimisation techniques were considered previously such as the usage of proportional integral control (PI) [62] with back EMF Feed Forward Compensation [63] or the use of proportional resonant control (PR) to minimise the ZSC [43]. However, all of the mentioned methods of minimisation of the torque ripple are based on the suppression or minimisation of the zero-sequence current by introducing zero-sequence voltage in the system. It appears that there is no research work that has been focused on the minimisation of the torque ripple using alternative methods, rather than the suppression of ZSC. Moreover, in cases when a machine has a considerably low leakage inductance none of those methods will work because the low leakage inductance dramatically restricts the amount of ZSV that can be applied to the system. Some high-speed machines would not tolerate any ZSV in the drive due to their tendency of having a very low leakage inductance. The argument is that the high-speed machines have less stator coil turns. Thereby, the inductance happens to be considerably low. Less wire turns also usually result in a lower leakage inductance. Such an inductance could induce a high ZSC spikes in the stator if ZSV is introduces even for a short period of time. However, when the ZSV is not applied, the ZSC becomes induced from another source, such as the third harmonic back EMF. According to the analysis performed in chapter 3, his current causes a torque disturbance. A new, alternative control method that improves the torque quality of such an open-end winding drive configuration has been proposed. The developed method uses a proportional integral plus adaptive resonant controller (PI+RC) [64] on the quadrature current branch in order to compensate the torque ripple caused by the ZSC due to the 3rd harmonic of the back EMF.

The most recent work done on the suppression of the torque ripple in an open-end winding PMSM with common DC link configuration is described in [65], where the researchers introduced a Model Predictive Current Control. Model Predictive Control is a technique that is able to both regulate the system’s states and drive the outputs to the desired values in an optimal way while satisfying the physical and operational constraints. [66]

There are different factors influencing the torque ripple. One of the studies revealed how torque ripple increases with increasing rotor position error [67]

2.2.2Temperature Estimation

OEW PMSM drives with common DC bus voltage are gaining increasing popularity in the pursuit of a low volume high power density solutions [56] for the aerospace [68], electric/hybrid vehicles [69] and wind power applications [61]. Moreover, such an arrangement is well suited for the implementation of different power device technology such as IGBT and Silicon Carbide (SiC) [57]. However, this topology has its drawbacks. The OEW PMSM drives with common DC link suffer from the circulating ZSC [70] due to the third harmonic back EMF [71]. In the case when a machine is designed to be a high-speed, high power and low volume it tends to have a considerably low leakage inductance. The argument is that the high-speed machines have less stator coil turns. Thereby, the inductance happens to be considerably low. Less wire turns also result in a lower leakage inductance. Such a low leakage inductance prevents the drive from applying any zero-sequence voltage (ZSV) [58], hence, the suppression of the aforementioned ZSC becomes impossible. The unsuppressed ZSC due to the third harmonic back EMF produces additional power loss that is converted to heat. Hence, the additional monitor of the phase winding temperature should increase the robustness of the overall system. In addition, due to a low volume and a high power density such machines tend to have either an integrated or attached liquid cooling [72]. Hence, it is crucial to track the stator temperature variations in order to ensure an optimal performance and the overall robustness of the system. This commonly requires a temperature sensor to be either integrated in or attached to the machine. In this chapter a new non-invasive method of identification of the online stator temperature without the usage of a temperature sensor is proposed. The temperature is estimated using an estimation of the stator phase resistance. There are resistance estimation methods, such as the one that has been proposed in [73] involving high frequency injection, however, it tends to have an estimation error directly proportional to the rotor electrical speed, thereby, this method is not suitable for the high electrical speed machines. Another method proposed recently in [74] depends on a very accurate zero crossing detection and is rather hard to implement. The method, proposed in [75] requires cooling system model. Another method requires a use of Kalman filter [76]. A rather recent paper on real-time resistance estimation requires a construction of a special function according to multiple simulations along with the access to the direct axis voltage information [77].

A thorough analysis revealed that the information about the phase resistance is hidden inside the amplitude of ZSC caused by the third harmonic back EMF. The analysis showed that this information can be derived using a maximum zero-sequence current concept introduced in this thesis, the actual value of ZSC amplitude and the rotor electrical speed. Hence, a new method was proposed which utilises the ZSC due to the third harmonic back EMF freely flowing in the system in order to extract the information on the phase resistance and, thereby, estimate the online stator temperature of the system. In addition, the freely flowing ZSC due to the third harmonic back EMF in an OEW PMSM with common DC link is a convenient opportunity for utilisation of the benefits of either a sensorless control or the proposed winding temperature estimation or even both, because the temperature estimation method proposed in this thesis could also potentially be combined with, for example, a novel zero-sequence model-based sensorless control. [28] It could be used to improve the accuracy of the rotor position estimation in any other sensorless techniques which heavily depend on the winding resistance value. Furthermore, the proposed new temperature estimation method gives an intimate temperature prediction comparing to the reading from an added temperature sensor, because the temperature sensor can only be attached to the winding insulation rather than to the winding itself. Moreover, the method could be especially beneficial for the high power low volume high-speed OEW PMSM drives with common DC bus due to their problems with suppression of the ZSC, described above.

2.2.3Sensorless Control in OEW PMSM with common DC Link

Sensorless control is a type of control which uses the estimated motor parameters such as the position of the rotor and the load torque. These parameters are obtained from the current and the voltage signals of the machine itself [78]. The major reason for the popularity of sensorless control in high-speed drives is the reliability. Encoders and resolvers may have a negative impact on aerodynamics in such high-speed applications as compressors and blowers due to the extrusion of sensors. In addition, high-speed rotational force is likely to cause the mechanical stresses that a position sensor will not be able to withstand. [79]

Although there are multiple methods of the Sensorless Control implementation particularly for the high-speed drives [80] [81] [82] [83], Model Reference Adaptive System (MRAS) method [84] [85] appears to be a good option for the high-speed drives as it works best at high-speed . [86]

It was found that one of the researchers succeeded in turning the disadvantage of the zero-sequence current into its advantage and used it in order to estimate the position of the rotor. This novel zero-sequence model-based sensorless method in [28] enabled elimination of both the voltage transducer and the three phase resistance network that conventional sensorless control methods of this type require.

2.2.4Power Losses in an OEW PMSM with common DC Link

Nearly every scientific paper [87] [25] [43] [54] [85] [88] as to the OEW PMSM with common DC link states that the power of the motor is lost due to the circulation of the zero-sequence current, however, it has been noted that there are no papers describing how much power is lost exactly. Some of the papers refer to the other papers when the power loss due to the zero-sequence current is mentioned. However, the referred papers do not explain how this current influences the power of the motor in a particular open-end winding permanent magnet synchronous motor drive configuration with common DC. Hence, it was decided to investigate this very phenomenon.

2.3Integrated drives

The permanent magnet synchronous motors are widely used across the industries due to their compact structure, high torque to inertia ratio, high airgap flux density and high efficiency. [89] The potential increase of power density of a drive system can be obtained by introducing the modularised converter units to a PMSM making an Integrated Motor Drive (IMD). [90] An example of such a drive is illustrated in Fig. 2.8 [91] below.

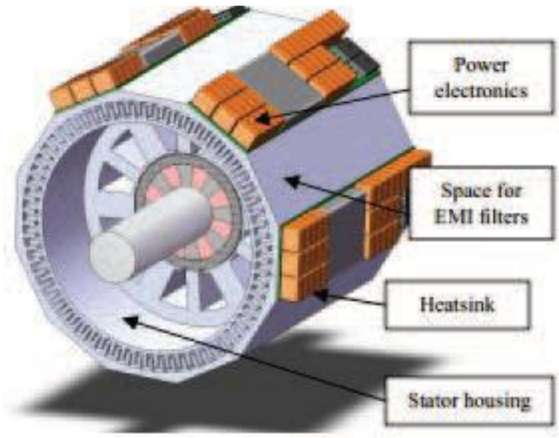

Fig. 2.8 – Modularised converter unit attached to the motor casing

Usually the power electronics (PE) modules of these kinds of drives are meant to be easily replaceable in case of malfunctioning or degradation in performance. [92] The integrated motor drives seem to be the way forward in the transportation applications due to the potential reduction in mass and volume even though there are still some problems yet to be overcome, such as electromechanical integration and the temperature management. [93]

In addition, the integrated motor drives will not suffer from all of the issues that the drives with the long feeder cables do. [94] There will be less overall internal resistance and the leakage inductance due to the absence of long wires connecting the PMSM and the inverter.

Chapter 3

3 Open-End Winding PMSM with Common DC Link Theory

This chapter introduces a mathematical analysis of the origin of a zero-sequence current in the machine side of an open-end winding permanent magnet synchronous motor drive with common DC link. In addition, the equations that describe the influence of this zero-sequence current onto the machine's performance is also derived. The presented mathematical analysis is used as a reference for all of the proposed ideas described in the subsequent chapters.

3.1 OEW PMSM voltage equations in Machine Variables

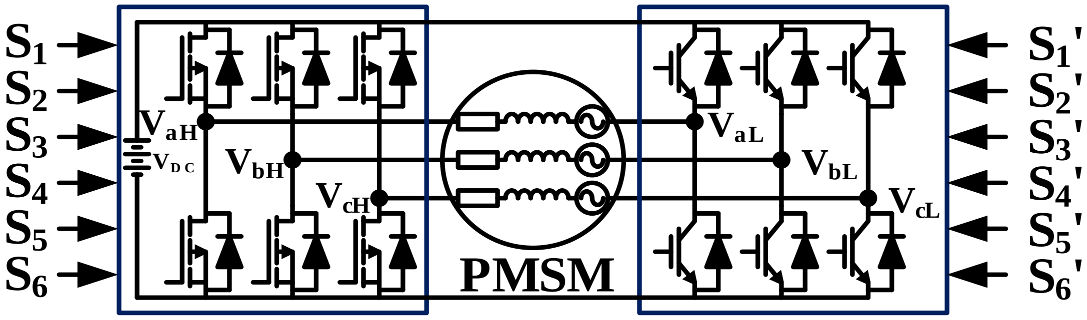

Fig. 3.1 – OEW PMSM with common DC bus

The diagram of an OEW PMSM drive with common DC link is presented in Fig. 3.1. The stator voltage equation, represented in machine variables:

$$V_{abc} = r_s i_{abc} + p\lambda_{abc} \tag{3.1}$$

where, r_s – stator winding resistance diagonal matrix, i_{abc} – stator phase currents matrix, λ_{abc} – stator phase flux linkage matrix and p is a derivative with respect to time $\left(\frac{d}{dt}\right)$ operator:

$$r_s = \begin{bmatrix} r_s & 0 & 0 \\ 0 & r_s & 0 \\ 0 & 0 & r_s \end{bmatrix};\ V_{abc} = \begin{bmatrix} V_a \\ V_b \\ V_c \end{bmatrix};\ i_{abc} = \begin{bmatrix} i_a \\ i_b \\ i_c \end{bmatrix};\ \lambda_{abc} = \begin{bmatrix} \lambda_a \\ \lambda_b \\ \lambda_c \end{bmatrix} \tag{3.2}$$

The stator phase flux linkage λ_{abc}, in turn, is related to the stator currents i_{abc} and the rotor permanent magnet flux through the following equation:

$$\lambda_{abc} = \lambda_{abc(s)} + \lambda_{abc(r)} \tag{3.3}$$

where, the flux linkage due to the stator currents $\lambda_{abc(s)}$ is a product of the inductance matrix L_s and the matrix of the stator phase currents i_{abc}:

$$\lambda_{abc(s)} = L_s i_{abc} \tag{3.4}$$

The inductance matrix L_s, in turn, is a 3×3 matrix [95]:

$$L_s = \begin{bmatrix} L_{ls} + L_A + L_B\cos(2\theta_e) & -\frac{1}{2}L_A + L_B\cos\left(2\left(\theta_e - \frac{\pi}{3}\right)\right) & -\frac{1}{2}L_A + L_B\cos\left(2\left(\theta_e + \frac{\pi}{3}\right)\right) \\ -\frac{1}{2}L_A + L_B\cos\left(2\left(\theta_e - \frac{\pi}{3}\right)\right) & L_{ls} + L_A + L_B\cos\left(2\left(\theta_e - \frac{2}{3}\pi\right)\right) & -\frac{1}{2}L_A + L_B\cos(2(\theta_e + \pi)) \\ -\frac{1}{2}L_A + L_B\cos\left(2\left(\theta_e + \frac{\pi}{3}\right)\right) & -\frac{1}{2}L_A + L_B\cos(2(\theta_e + \pi)) & L_{ls} + L_A + L_B\cos\left(2\left(\theta_e + \frac{2}{3}\pi\right)\right) \end{bmatrix} \quad (3.5)$$

The flux linkage due to the rotor permanent magnet $\lambda_{abc(r)}$, in turn, can be expressed as the sum of the fundamental $\lambda_{abc(r1)}$ and the 3rd harmonic $\lambda_{abc(r3)}$ components:

$$\lambda_{abc(r)} = \lambda_{abc(r1)} + \lambda_{abc(r3)} \quad (3.6)$$

The reason behind representing the flux linkage as the sum of the fundamental and the third harmonic components is that the third harmonic results in the zero-sequence current in the open-end winding PMSM drives with common DC link. [71]

The mentioned fundamental $\left(\lambda_{abc(r1)}\right)$ and the 3rd $\left(\lambda_{abc(r3)}\right)$ harmonic components of the flux linkage due to the rotor permanent magnet are expressed, respectively, as follows:

$$\lambda_{abc(r1)} = \lambda_{pm}\begin{bmatrix} \sin(\theta_e) \\ \sin\left(\theta_e - \frac{2}{3}\pi\right) \\ \sin\left(\theta_e + \frac{2}{3}\pi\right) \end{bmatrix} \quad (3.7)$$

$$\lambda_{abc(r3)} = \lambda_{pm}K_{pm3}\begin{bmatrix} \sin(3\theta_e) \\ \sin\left(3\left(\theta_e - \frac{2}{3}\pi\right)\right) \\ \sin\left(3\left(\theta_e + \frac{2}{3}\pi\right)\right) \end{bmatrix} \quad (3.8)$$

where, λ_{pm} is the amplitude of flux linkage established by the permanent magnet and K_{pm3} is one third of the ratio of the amplitude of the open circuit 3rd harmonic voltage $\hat{E}_{abc3}$ and fundamental voltage $\hat{E}_{abc1}$, respectively, induced in either of the stator windings:

$$K_{pm3} = \frac{1}{3}\frac{\hat{E}_{abc3}}{\hat{E}_{abc1}} \tag{3.9}$$

Analytically, the open circuit fundamental (E_{abc1}) and the 3rd harmonic (E_{abc3}) voltage components or the back EMF components are identified as the rate of change of flux linkage of the corresponding harmonics $\lambda_{abc(r1)}$ and $\lambda_{abc(r3)}$:

$$E_{abc1} = p\lambda_{abc(r1)} \tag{3.10}$$

$$E_{abc3} = p\lambda_{abc(r3)} \tag{3.11}$$

where, p is a derivative with respect to time operator.

Substituting equations (3.7) and (3.8) into (3.10) and (3.11), respectively, and assuming that a PMSM motor rotates at a constant speed the back EMF fundamental and third harmonic components become:

$$E_{abc1} = \omega_e\lambda_{pm}\begin{bmatrix}\cos(\theta_e)\\ \cos\left(\theta_e - \frac{2}{3}\pi\right)\\ \cos\left(\theta_e + \frac{2}{3}\pi\right)\end{bmatrix} \tag{3.12}$$

$$E_{abc3} = 3\omega_e\lambda_{pm}K_{pm3}\begin{bmatrix}\cos(3\theta_e)\\ \cos\left(3\left(\theta_e - \frac{2}{3}\pi\right)\right)\\ \cos\left(3\left(\theta_e + \frac{2}{3}\pi\right)\right)\end{bmatrix} \tag{3.13}$$

Hence, the amplitudes of the corresponding back EMF components are as follows:

$$\hat{E}_{abc1} = \omega_e \lambda_{pm} \tag{3.14}$$

$$\hat{E}_{abc3} = 3\omega_e \lambda_{pm} K_{pm3} \tag{3.15}$$

Substituting equation (3.14) into (3.15) the coefficient K_{pm3} can be found using the following formula:

$$K_{pm3} = \frac{\hat{E}_{abc3}}{3\hat{E}_{abc1}} \tag{3.16}$$

Hence, K_{pm3} is indeed one third of the ratio of the amplitude of the open circuit 3rd harmonic voltage $\hat{E}_{abc3}$ and fundamental voltage $\hat{E}_{abc1}$ induced in either of the stator windings.

In order to obtain the new stator phase flux linkage λ_{abc} the equations (3.4) and (3.6) are substituted into (3.3):

$$\lambda_{abc} = L_s i_{abc} + \lambda_{abc(r1)} + \lambda_{abc(r3)} \tag{3.17}$$

Therefore, substituting (3.17) into (3.1) the stator voltage equation becomes:

$$V_{abc} = r_s i_{abc} + p[L_s i_{abc}] + p\lambda_{abc(r1)} + p\lambda_{abc(r3)} \tag{3.18}$$

Since $p[L_s i_{abc}] = pL_s i_{abc} + L_s p i_{abc}$, the voltage equation becomes:

$$V_{abc} = r_s i_{abc} + pL_s i_{abc} + L_s p i_{abc} + p\lambda_{abc(r1)} + p\lambda_{abc(r3)} \tag{3.19}$$

3.2OEW PMSM Voltage Equations in Rotor Reference Frame

Converting the voltage equation from the machine variables, V_{abc} , into the rotor reference frame V_{qd0} in order to see the effect of the 3rd back EMF harmonic on the torque production of the machine:

$$V_{qd0} = KV_{abc} = Kr_s i_{abc} + KpL_s i_{abc} + Kp\lambda_{abc(r1)} + Kp\lambda_{abc(r3)} \tag{3.20}$$

$$\begin{aligned} V_{qd0} = K(Kr_s)\left[K^{-1} i_{qd0}\right] + Kp\left[(KL_s)\left(K^{-1} i_{qd0}\right)\right] + Kp\left[K^{-1}\lambda_{qd0(r1)}\right] \\ + Kp\left[K^{-1}\lambda_{qd0(r3)}\right] \end{aligned} \tag{3.21}$$

where, K and K^{-1} are the change of variable coefficient and the inverse of the change of variable coefficient, respectively:

$$K = \frac{2}{3}\begin{bmatrix} \cos(\theta_e) & \cos\left(\theta_e - \frac{2}{3}\pi\right) & \cos\left(\theta_e + \frac{2}{3}\pi\right) \\ \sin(\theta_e) & \sin\left(\theta_e - \frac{2}{3}\pi\right) & \sin\left(\theta_e + \frac{2}{3}\pi\right) \\ \frac{1}{2} & \frac{1}{2} & \frac{1}{2} \end{bmatrix} \tag{3.22}$$

$$K^{-1} = \begin{bmatrix} \cos(\theta_e) & \sin(\theta_e) & 1 \\ \cos\left(\theta_e - \frac{2}{3}\pi\right) & \sin\left(\theta_e - \frac{2}{3}\pi\right) & 1 \\ \cos\left(\theta_e + \frac{2}{3}\pi\right) & \sin\left(\theta_e + \frac{2}{3}\pi\right) & 1 \end{bmatrix} \tag{3.23}$$

Since resistance r_s and inductance L_s, the matrices in qd0 can be represented as:

$$r_s = K\begin{bmatrix} r_s & 0 & 0 \\ 0 & r_s & 0 \\ 0 & 0 & r_s \end{bmatrix} = \begin{bmatrix} r_s & 0 & 0 \\ 0 & r_s & 0 \\ 0 & 0 & r_s \end{bmatrix} \tag{3.24}$$

$$L_s = K\begin{bmatrix} L_{aa} & L_{ab} & L_{ac} \\ L_{ba} & L_{bb} & L_{bc} \\ L_{ca} & L_{cb} & L_{cc} \end{bmatrix} = \begin{bmatrix} L_{ls}+L_{mq} & 0 & 0 \\ 0 & L_{ls}+L_{md} & 0 \\ 0 & 0 & L_{ls} \end{bmatrix} = \begin{bmatrix} L_q & 0 & 0 \\ 0 & L_d & 0 \\ 0 & 0 & L_0 \end{bmatrix} \quad (3.25)$$

where, L_{aa}, L_{bb} and L_{cc} are the self-inductances of the phases A, B and C, respectively, and the off-diagonal terms are the mutual inductances between the phases. According to (3.5) these inductances could be written as follow.

$$\left[\begin{array}{c} L_{aa} = L_{ls} + L_A + L_B\cos(2\theta_e) \\ L_{bb} = L_{ls} + L_A + L_B\cos\left(2\left(\theta_e - \frac{2}{3}\pi\right)\right) \\ L_{cc} = L_{ls} + L_A + L_B\cos\left(2\left(\theta_e + \frac{2}{3}\pi\right)\right) \\ L_{ab} = L_{ba} = -\frac{1}{2}L_A + L_B\cos\left(2\left(\theta_e - \frac{\pi}{3}\right)\right) \\ L_{ac} = L_{ca} = -\frac{1}{2}L_A + L_B\cos\left(2\left(\theta_e + \frac{\pi}{3}\right)\right) \\ L_{bc} = L_{cb} = -\frac{1}{2}L_A + L_B\cos\big(2(\theta_e + \pi)\big) \end{array}\right. \quad (3.26)$$

also,

$$L_{mq} = \frac{3}{2}(L_A - L_B) \quad (3.27)$$

$$L_{md} = \frac{3}{2}(L_A + L_B) \quad (3.28)$$

The voltage equation in the rotor reference frame becomes:

$$V_{qd0} = r_s i_{qd0} + Kp\left[L_s\left(K^{-1}i_{qd0}\right)\right] + Kp\left[K^{-1}\lambda_{qd0(r1)}\right] + Kp\left[K^{-1}\lambda_{qd0(r3)}\right] \quad (3.29)$$

Since $k[AB] = kAB + AkB$, where k is a scalar, A and B are the matrices, the voltage equation becomes:

$$\begin{aligned} V_{qd0} = r_s i_{qd0} &+ \left[KpK^{-1}L_s i_{qd0} + KK^{-1}pL_s i_{qd0}\right] \\ &+ \left[KpK^{-1}\lambda_{qd0(r1)} + KK^{-1}p\lambda_{qd0(r1)}\right] \\ &+ \left[KpK^{-1}\lambda_{qd0(r3)} + KK^{-1}p\lambda_{qd0(r3)}\right] \end{aligned} \quad (3.30)$$

Since,

$$KK^{-1} = \frac{2}{3}\begin{bmatrix} \cos(\theta_e) & \cos\left(\theta_e - \frac{2}{3}\pi\right) & \cos\left(\theta_e + \frac{2}{3}\pi\right) \\ \sin(\theta_e) & \sin\left(\theta_e - \frac{2}{3}\pi\right) & \sin\left(\theta_e + \frac{2}{3}\pi\right) \\ \frac{1}{2} & \frac{1}{2} & \frac{1}{2} \end{bmatrix}\begin{bmatrix} \cos(\theta_e) & \sin(\theta_e) & 1 \\ \cos\left(\theta_e - \frac{2}{3}\pi\right) & \sin\left(\theta_e - \frac{2}{3}\pi\right) & 1 \\ \cos\left(\theta_e + \frac{2}{3}\pi\right) & \sin\left(\theta_e + \frac{2}{3}\pi\right) & 1 \end{bmatrix} = \boldsymbol{I} \quad (3.31)$$

and

$$KpK^{-1} = \frac{2}{3}\begin{bmatrix} \cos(\theta_e) & \cos\left(\theta_e - \frac{2}{3}\pi\right) & \cos\left(\theta_e + \frac{2}{3}\pi\right) \\ \sin(\theta_e) & \sin\left(\theta_e - \frac{2}{3}\pi\right) & \sin\left(\theta_e + \frac{2}{3}\pi\right) \\ \frac{1}{2} & \frac{1}{2} & \frac{1}{2} \end{bmatrix}\frac{d}{dt}\begin{bmatrix} \cos(\theta_e) & \sin(\theta_e) & 1 \\ \cos\left(\theta_e - \frac{2}{3}\pi\right) & \sin\left(\theta_e - \frac{2}{3}\pi\right) & 1 \\ \cos\left(\theta_e + \frac{2}{3}\pi\right) & \sin\left(\theta_e + \frac{2}{3}\pi\right) & 1 \end{bmatrix} = \boldsymbol{\omega_e} \quad (3.32)$$

where,

$$\boldsymbol{\omega_e} = \begin{bmatrix} 0 & \omega_e & 0 \\ -\omega_e & 0 & 0 \\ 0 & 0 & 0 \end{bmatrix} \quad (3.33)$$

the voltage equation becomes:

$$\begin{aligned} V_{qd0} = r_s i_{qd0} + \left[\boldsymbol{\omega_e} L_s i_{qd0} + pL_s i_{qd0}\right] + \left[\boldsymbol{\omega_e}\lambda_{qd0(r1)} + p\lambda_{qd0(r1)}\right] \\ + \left[\boldsymbol{\omega_e}\lambda_{qd0(r3)} + p\lambda_{qd0(r3)}\right] \end{aligned} \quad (3.34)$$

Since,

$$\lambda_{qd0(r1)} = K\lambda_{abc(r1)} = K\lambda_{pm}\begin{bmatrix} \sin(\theta_e) \\ \sin\left(\theta_e - \frac{2}{3}\pi\right) \\ \sin\left(\theta_e + \frac{2}{3}\pi\right) \end{bmatrix} = \begin{bmatrix} 0 \\ \lambda_{pm} \\ 0 \end{bmatrix} \quad (3.35)$$

and

$$\lambda_{qd0(r3)} = K\lambda_{abc(r3)} = K\lambda_{pm}K_{pm3}\begin{bmatrix} \sin(3\theta_e) \\ \sin\left(3\left(\theta_e - \frac{2}{3}\pi\right)\right) \\ \sin\left(3\left(\theta_e + \frac{2}{3}\pi\right)\right) \end{bmatrix} = \begin{bmatrix} 0 \\ 0 \\ \lambda_{pm}K_{pm3}\sin(3\theta_e) \end{bmatrix} \quad (3.36)$$

the voltage equation becomes:

$$V_{qd0} = r_s i_{qd0} + \boldsymbol{\omega_e} L_s i_{qd0} + pL_s i_{qd0} + \boldsymbol{\omega_e}\lambda_{qd0(r1)} + p\lambda_{qd0(r3)} \quad (3.37)$$

Assuming L_A, L_B and L_{ls} in the inductance matrix L_s are constant:

$$\begin{aligned} \begin{bmatrix} V_q \\ V_d \\ V_0 \end{bmatrix} = \begin{bmatrix} r_s & 0 & 0 \\ 0 & r_s & 0 \\ 0 & 0 & r_s \end{bmatrix}\begin{bmatrix} i_q \\ i_d \\ i_0 \end{bmatrix} + \begin{bmatrix} 0 & \omega_e & 0 \\ -\omega_e & 0 & 0 \\ 0 & 0 & 0 \end{bmatrix}\begin{bmatrix} L_q & 0 & 0 \\ 0 & L_d & 0 \\ 0 & 0 & L_0 \end{bmatrix}\begin{bmatrix} i_q \\ i_d \\ i_0 \end{bmatrix} \\ + \begin{bmatrix} L_q & 0 & 0 \\ 0 & L_d & 0 \\ 0 & 0 & L_0 \end{bmatrix}\frac{d}{dt}\begin{bmatrix} i_q \\ i_d \\ i_0 \end{bmatrix} + \omega_e\begin{bmatrix} 0 \\ \lambda_{pm} \\ 0 \end{bmatrix} \\ + \frac{d}{dt}\begin{bmatrix} 0 \\ 0 \\ \lambda_{pm}K_{pm3}\sin(3\theta_e) \end{bmatrix} \end{aligned} \quad (3.38)$$

Therefore, a set of the rotor reference frame PMSM voltage equations can be written as:

$$\begin{cases} V_q = r_s i_q + L_q\dfrac{di_q}{dt} + \omega_e L_d i_d + \omega_e\lambda_{pm} \\ V_d = r_s i_d + L_d\dfrac{di_d}{dt} - \omega_e L_q i_q \\ V_0 = r_s i_0 + L_0\dfrac{di_0}{dt} + 3\omega_e\lambda_{pm}K_{pm3}\cos(3\theta_e) \end{cases} \quad (3.39)$$

3.3Torque produced by an OEW PMSM

Instantaneous power P_e flowing in the machine can be written in both the machine variables and the rotor reference frame, respectively, as:

$$P_e = V_a i_a + V_b i_b + V_c i_c = \frac{3}{2}\left(V_q i_q + V_d i_d + 2V_0 i_0\right) \tag{3.40}$$

Substituting (3.39) into the second part of (3.40), the instantaneous power equation becomes:

$$P_e = P_c + P_f + P_{em} \tag{3.41}$$

where, P_c is the power loss in the conductors, P_f is the rate of change of stored energy in the magnetic fields and P_{em} is the electromechanical power:

$$P_c = \frac{3}{2}\left(r_s {i_q}^2 + r_s {i_d}^2 + 2r_s {i_0}^2\right) \tag{3.42}$$

$$P_f = \frac{3}{2}\left(pL_q {i_q}^2 + pL_d {i_d}^2 + 2pL_0 {i_0}^2\right) \tag{3.43}$$

$$P_{em} = \left(\frac{3}{2}\right)\omega_e\left[i_q\lambda_{pm} + i_q i_d\left(L_d - L_q\right) + 6i_0\lambda_{pm}K_{pm3}\cos(3\theta_e)\right] \tag{3.44}$$

The power P_{em} is utilised for the conversion of energy from electrical to mechanical and is equal to the power output from the motor shaft. Hence, the electromechanical power P_{em} can be written as the product of the machine produced torque T_e and the mechanical angular rotor speed $\left(\frac{2}{P}\omega_e\right)$, where, P is the number of poles and ω_e is an electrical angular speed:

$$P_{em} = T_e\left(\frac{2}{P}\right)\omega_e \tag{3.45}$$

Substituting (3.45) into (3.44) the equation becomes:

$$T_e\left(\frac{2}{P}\right)\omega_e = \left(\frac{3}{2}\right)\omega_e\left[i_q\lambda_{pm} + i_q i_d\left(L_d - L_q\right) + 6i_0\lambda_{pm}K_{pm3}\cos(3\theta_e)\right] \quad (3.46)$$

Therefore, the torque produced by the machine is:

$$T_e = \left(\frac{3}{2}\right)\left(\frac{P}{2}\right)\left[i_q\lambda_{pm} + i_q i_d\left(L_d - L_q\right) + 6i_0\lambda_{pm}K_{pm3}\cos(3\theta_e)\right] \quad (3.47)$$

3.4 Effect of ZSC on the OEW PMSM performance

The effect of the Zero-Sequence Current due the 3rd harmonic back EMF on the Open-End Winding PMSM was studied considering the system in the steady state.

3.4.1 Controlled Zero-Sequence Current

The OEW PMSM steady state analysis is required in order to identify the influence of the 3rd harmonic back EMF on the system. The analysis is performed using the rotor reference frame voltage and torque equations. All of the corresponding phasor diagrams are drawn for the visual representation.

3.4.1.1 Steady State Zero-Sequence Voltage and Current

A zero-sequence voltage V_0 equation is one of the OEW PMSM rotor reference frame equations in (3.39). It is written as follows:

$$V_0 = r_s i_0 + L_0 \frac{di_0}{dt} + 3\omega_e \lambda_{pm} K_{pm3} \cos(3\theta_e) \tag{3.48}$$

The steady state phasor form of the equation (3.48) is

$$\tilde{V}_0 = r_s \tilde{I}_0 + jX_0 \tilde{I}_0 + \tilde{E}_0 \tag{3.49}$$

where, $\tilde{V}_0$ and $\tilde{I}_0$ are the zero-sequence voltage and current phasors, respectively, r_s is the phase resistance, $\tilde{E}_0$ is the zero-sequence back EMF phasor with a zero phase shift:

$$\tilde{E}_0 = \left|\tilde{E}_0\right| \cos(3\theta_e) \tag{3.50}$$

where, the amplitude $\left|\tilde{E}_0\right|$ is denoted in equation (3.51).

$$\left|\tilde{E}_0\right| = 3\omega_e \lambda_{pm} K_{pm3} \tag{3.51}$$

X_0 is the zero-sequence inductive reactance:

$$X_0 = 3\omega_e L_0 \tag{3.52}$$

Rearranging the equation (3.49) in order to construct a phasor diagram:

$$\tilde{V}_0 - \tilde{E}_0 = r_s \tilde{I}_0 + jX_0 \tilde{I}_0 \tag{3.53}$$

According to the equation (3.53) above the voltage phasor diagram, shown in Fig. 3.2, is drawn. Fig. 3.3, in turn, illustrates the case when the control zero voltage V_0 is equal to zero. The zero-sequence current in this case depends entirely on the value of the zero-sequence back EMF E_0, hence, according to (3.51) it is proportional to the electrical angular speed ω_e.

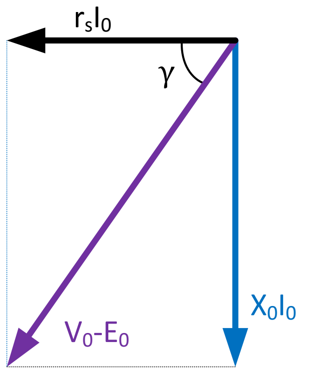

Fig. 3.2 – Zero-Sequence Voltage phasor diagram

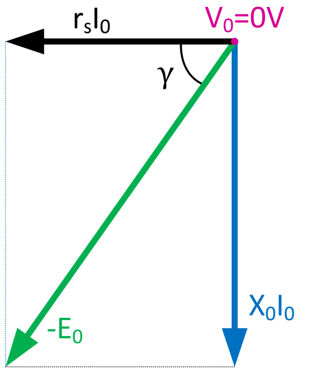

Fig. 3.3 – Zero-Sequence Voltage phasor diagram when V_0=0V

Rearranging the equation (3.53) in order to obtain the phasor current $\tilde{I}_0$:

$$\tilde{I}_0 = \frac{\tilde{V}_0 - \tilde{E}_0}{r_s + jX_0} \tag{3.54}$$

It is clear from Fig. 3.2 and the equation (3.54) that the zero-sequence current $\tilde{I}_0$ depends on the difference between the input zero-sequence voltage vector $\tilde{V}_0$ and the back EMF vector due to the 3rd harmonic $\tilde{E}_0$.

Further simplification of (3.54) results in the following equation of the zero-sequence phasor current:

$$\tilde{I}_0 = I_{0\_Re} - jI_{0\_Im} \tag{3.55}$$

where, I_{0_Re} is the real part of the phase current vector $\tilde{I}_0$:

$$I_{0\_Re} = \left(\tilde{V}_0 - \tilde{E}_0\right)\frac{r_s}{{r_s}^2 + {X_0}^2} \tag{3.56}$$

and I_{0_Im} is the imaginary part of the phase current vector $\tilde{I}_0$:

$$I_{0\_Im} = \left(\tilde{V}_0 - \tilde{E}_0\right)\frac{X_0}{{r_s}^2 + {X_0}^2} \tag{3.57}$$

The graphical representation of the zero-sequence phase current equation (3.55) is shown in Fig. 3.4.

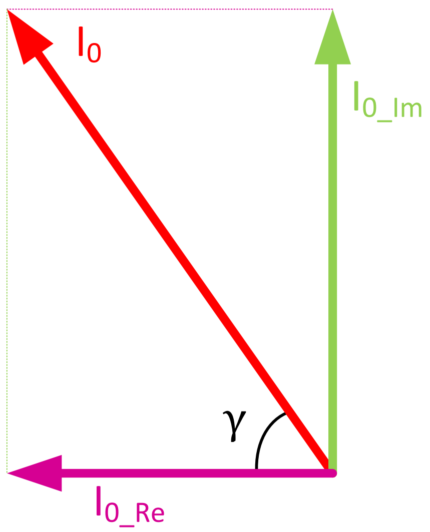

Fig. 3.4 – Zero-Sequence Current phasor diagram

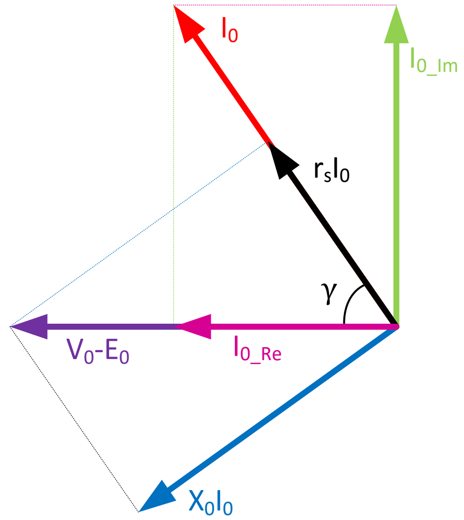

Fig. 3.5 – Phasor diagram of the Zero-Sequence Voltage and Current

Fig. 3.5 shows the combination of the Zero-Sequence Voltage (Fig. 3.2) and Current (Fig. 3.4) phasor diagrams. This diagram shows that the angle γ between the zero-sequence voltage and current phase vectors can be found using either the zero phase voltage components or the zero phase current components:

$$\gamma = \tan^{-1}\left(\frac{X_0 \tilde{I}_0}{r_s \tilde{I}_0}\right) = \tan^{-1}\left(\frac{I_{0\_Im}}{I_{0\_Re}}\right) = \tan^{-1}\left(\frac{X_0}{r_s}\right) \tag{3.58}$$

Therefore, using the equation of zero-sequence inductive reactance (3.52), the phase γ between the zero-sequence voltage and current phasors, becomes:

$$\gamma = \tan^{-1}\left(3\omega_e \frac{L_0}{r_s}\right) \tag{3.59}$$

The magnitude of the zero phase current vector:

$$\left|\tilde{I}_0\right| = \frac{\left|\tilde{V}_0 - \tilde{E}_0\right|}{\sqrt{{r_s}^2 + {X_0}^2}} \tag{3.60}$$

3.4.1.2Steady State Electrical Power

According to the equations of the zero-sequence phase angle (3.59) and its amplitude (3.60) the electrical angle domain equation of the zero-sequence current can be written as:

$$i_0 = \left|\tilde{I}_0\right| \cos(3\theta_e + \gamma) \tag{3.61}$$

where, $\left|\tilde{I}_0\right|$ is the amplitude of the zero-sequence current i_0, θ_e is the electrical phase angle and γ is the phase between the zero-sequence voltage and the zero-sequence current phasors.

Considering the derived equation of the motor power in the rotor reference frame (3.40) and the electrical angle domain equation of the zero-sequence current (3.61), the total electrical power equation can be rewritten as follows:

$$P_e = \frac{3}{2}\left(V_q i_q + V_d i_d + 2V_0\left|\tilde{I}_0\right| \cos(3\theta_e + \gamma)\right) \tag{3.62}$$

Incorporating ZSC equation (3.61) into the power loss in the conductor P_c equation (3.42)

$$P_c = \frac{3}{2}\left(r_s {i_q}^2 + r_s {i_d}^2 + 2r_s\left|\tilde{I}_0\right|^2 \cos^2(3\theta_e + \gamma)\right) \tag{3.63}$$

Using trigonometric identity of (3.64)

$$\cos^2(3\theta_e + \gamma) = \frac{1}{2}(\cos(6\theta + 2\gamma) + 1) \tag{3.64}$$

The formula for the power loss in conductor can be written as follows.

$$P_c = \frac{3}{2}\left(r_s {i_q}^2 + r_s {i_d}^2 + r_s\left|\tilde{I}_0\right|^2 + r_s\left|\tilde{I}_0\right|^2 \cos(6\theta + 2\gamma)\right) \tag{3.65}$$

The term causing power loss in conductor oscillation is $\frac{3}{2}\left(r_s\left|\tilde{I}_0\right|^2 \cos(6\theta + 2\gamma)\right)$.

Combining equation (3.43) and the ZSC in (3.61), the rate of change of stored energy in magnetic field P_f appears to be as follows:

$$P_f = \frac{3}{2}\left(pL_q {i_q}^2 + pL_d {i_d}^2 + 2pL_0\left|\tilde{I}_0\right|^2 \cos^2(3\theta_e + \gamma)\right) \tag{3.66}$$

Applying the same trigonometric identity (3.64), the equation becomes:

$$P_f = \frac{3}{2}\left(pL_q {i_q}^2 + pL_d {i_d}^2 + pL_0\left|\tilde{I}_0\right|^2 + pL_0\left|\tilde{I}_0\right|^2 \cos(6\theta + 2\gamma)\right) \tag{3.67}$$

where, $\left(pL_0\left|\tilde{I}_0\right|^2 \cos(6\theta + 2\gamma)\right)$ term is the oscillatory term.

Considering the electromechanical power P_{em} of equation (3.44) that is used to convert electrical to mechanical energy and combining it with (3.61), the equation (3.68) is obtained.

$$\begin{aligned} P_{em} = \left(\frac{3}{2}\right)\omega_e\big[&i_q\lambda_{pm} + i_q i_d\left(L_d - L_q\right) \\ &+ 6\left|\tilde{I}_0\right|\cos(3\theta_e + \gamma)\,\lambda_{pm}K_{pm3}\cos(3\theta_e)\big] \end{aligned} \tag{3.68}$$

Using a trigonometric identity:

$$A\cos(\theta+\gamma)\cos(\theta)=\frac{A}{2}\cos(2\theta+\gamma)+\frac{A}{2}\cos(\gamma) \tag{3.69}$$

The new equation of the electromechanical power becomes:

$$\begin{aligned}P_{em}=\left(\frac{3}{2}\right)\omega_e\big[i_q\lambda_{pm}+i_q i_d\big(L_d-L_q\big)+3\big|\tilde{I}_0\big|\lambda_{pm}K_{pm3}\cos(\gamma)\\+3\big|\tilde{I}_0\big|\lambda_{pm}K_{pm3}\cos(6\theta_e+\gamma)\big]\end{aligned} \tag{3.70}$$

The term causing the power oscillation is $\big(3\big|\tilde{I}_0\big|\lambda_{pm}K_{pm3}\cos(6\theta_e+\gamma)\big)$. The power is oscillating six times faster than the fundamental harmonic with the amplitude of the oscillation proportional to the zero-sequence current amplitude $\big(3\big|\tilde{I}_0\big|\lambda_{pm}K_{pm3}\big)$. There is also a DC offset of $\big(3\big|\tilde{I}_0\big|\lambda_{pm}K_{pm3}\cos(\gamma)\big)$ due to the ZSC.

3.4.1.3Steady State Electromagnetic Torque

Considering the derived equation of the electromagnetic torque in rotor reference frame (3.47) and the electrical angle domain equation of the zero-sequence current (3.61), the electromagnetic torque equation can be rewritten as follows:

$$\begin{aligned}T_e=\left(\frac{3}{2}\right)\left(\frac{P}{2}\right)\big[i_q\lambda_{pm}+i_q i_d\big(L_d-L_q\big)\\+6\big|\tilde{I}_0\big|\lambda_{pm}K_{pm3}\cos(3\theta_e+\gamma)\cos(3\theta_e)\big]\end{aligned} \tag{3.71}$$

Using the trigonometric identity introduced in (3.69) the new equation of the electromagnetic torque becomes:

$$\begin{aligned}T_e=\left(\frac{3}{2}\right)\left(\frac{P}{2}\right)\big[i_q\lambda_{pm}+i_q i_d\big(L_d-L_q\big)+3\big|\tilde{I}_0\big|\lambda_{pm}K_{pm3}\cos(\gamma)\\+3\big|\tilde{I}_0\big|\lambda_{pm}K_{pm3}\cos(6\theta_e+\gamma)\big]\end{aligned} \tag{3.72}$$

The term causing the torque oscillation is $\left(3\left|\tilde{I}_0\right|\lambda_{pm}K_{pm3}\cos(6\theta_e+\gamma)\right)$. The torque is oscillating six times faster than the fundamental harmonic with the amplitude of the oscillation proportional to the zero-sequence current amplitude $\left(3\left|\tilde{I}_0\right|\lambda_{pm}K_{pm3}\right)$.

3.4.2Uncontrolled Zero-Sequence Current

3.4.2.1Steady State uncontrolled Zero-Sequence Current

When there is no zero-sequence voltage (ZSV) generated by the inverter side of the drive, the zero-sequence current in this case is considered to be uncontrolled. The behaviour of this current depends entirely on the machine's parameters.

In case if the zero-sequence current is not controlled, in other words $\tilde{V}_0 = 0V$ as shown in Fig. 3.3, its magnitude becomes:

$$\left|\tilde{I}_0\right|_{(V_0=0)} = \frac{-\left|\tilde{E}_0\right|}{\sqrt{{r_s}^2 + {X_0}^2}} \tag{3.73}$$

Using the equations (3.51) and (3.52), this current can be rewritten as:

$$\left|\tilde{I}_0\right|_{(V_0=0)} = \frac{-3\omega_e\lambda_{pm}K_{pm3}}{\sqrt{{r_s}^2 + 9{\omega_e}^2{L_0}^2}} \tag{3.74}$$

It is clear from the equation (3.74) that when the zero-sequence current is not controlled its amplitude depends on the internal machine parameters and the angular speed of the motor itself.

In order to determine the minimum ($\left|\tilde{I}_0\right|_{min}$) and the maximum ($\left|\tilde{I}_0\right|_{\pm max}$) values of the uncontrolled zero-sequence current amplitude the limit of equation (3.74) is taken when the angular speed ω_e tends to zero, positive and negative infinity, respectively:

$$\left|\tilde{I}_0\right|_{min} = \lim_{\omega_e \to 0}\left(\left|\tilde{I}_0\right|_{(V_0=0)}\right) = \lim_{\omega_e \to 0}\left(\frac{-3\omega_e \lambda_{pm} K_{pm3}}{\sqrt{{r_s}^2 + 9{\omega_e}^2{L_0}^2}}\right) = 0 \tag{3.75}$$

$$\begin{aligned}\left|\tilde{I}_0\right|_{+max} &= \lim_{\omega_e \to +\infty}\left(\left|\tilde{I}_0\right|_{(V_0=0)}\right) = \lim_{\omega_e \to +\infty}\left(\frac{-3\omega_e \lambda_{pm} K_{pm3}}{\sqrt{{r_s}^2 + 9{\omega_e}^2{L_0}^2}}\right) = -\frac{\lambda_{pm} K_{pm3}}{L_0} \\ &= -\frac{\lambda_{pm3}}{L_0}\end{aligned} \tag{3.76}$$

$$\begin{aligned}\left|\tilde{I}_0\right|_{-max} &= \lim_{\omega_e \to -\infty}\left(\left|\tilde{I}_0\right|_{(V_0=0)}\right) = \lim_{\omega_e \to -\infty}\left(\frac{-3\omega_e \lambda_{pm} K_{pm3}}{\sqrt{{r_s}^2 + 9{\omega_e}^2{L_0}^2}}\right) = \frac{\lambda_{pm} K_{pm3}}{L_0} \\ &= \frac{\lambda_{pm3}}{L_0}\end{aligned} \tag{3.77}$$

According to the equations (3.75) and (3.76), the minimum and the maximum amplitudes of the uncontrolled zero-sequence phase current are zero and $\frac{\lambda_{pm3}}{L_0}$, respectively. Where, L_0 is the leakage inductance and λ_{pm3} is the amplitude of the 3rd harmonic flux linkage established by the permanent magnet rotor:

$$\lambda_{pm3} = \lambda_{pm} K_{pm3} \tag{3.78}$$

3.4.2.2Steady State Power due to the uncontrolled ZSC

The total electric power can be represented by the sum of power loss in conductor P_c, power loss that represents the rate of change of stored energy P_f and the electromechanical power P_{em} that is utilised to convert electrical energy to mechanical. This is shown in equation (3.41). In order to determine the influence of the uncontrolled zero-sequence current on each of the constituents of the total electrical power shown in equations (3.41)-(3.44), the zero-sequence current (3.74) and its phase shift (3.59) were substituted in equation of P_c (3.65), equation P_f (3.67) and equation P_{em} (3.70), subsequently.

Substituting (3.74) and (3.59) into (3.65) on page 53, the loss in the conductor P_c becomes a function of the electrical angular speed ω_e:

$$\begin{aligned} P_c = \frac{3}{2}\Bigg(& r_s {i_q}^2 + r_s {i_d}^2 + r_s \frac{9{\omega_e}^2{\lambda_{pm}}^2{K_{pm3}}^2}{{r_s}^2 + 9{\omega_e}^2{L_0}^2} \\ & + r_s \frac{9{\omega_e}^2{\lambda_{pm}}^2{K_{pm3}}^2}{{r_s}^2 + 9{\omega_e}^2{L_0}^2} \cos\left(6\theta + 2\tan^{-1}\left(3\omega_e \frac{L_0}{r_s}\right)\right)\Bigg) \end{aligned} \tag{3.79}$$

Substituting (3.74) and (3.59) into (3.67) on page 53, the power that is responsible for the rate of change of stored energy in magnetic field P_f appears to be as follows:

$$\begin{aligned} P_f = \frac{3}{2}\Bigg(& pL_q {i_q}^2 + pL_d {i_d}^2 + pL_0 \frac{9{\omega_e}^2{\lambda_{pm}}^2{K_{pm3}}^2}{{r_s}^2 + 9{\omega_e}^2{L_0}^2} \\ & + pL_0 \frac{9{\omega_e}^2{\lambda_{pm}}^2{K_{pm3}}^2}{{r_s}^2 + 9{\omega_e}^2{L_0}^2} \cos\left(6\theta + 2\tan^{-1}\left(3\omega_e \frac{L_0}{r_s}\right)\right)\Bigg) \end{aligned} \tag{3.80}$$

According to equation (3.80), P_f now is also a function of the electrical angular frequency ω_e.

Considering the power P_{em} from equation (3.70) on page 54 that is used to convert electrical to mechanical energy and combining it with equations (3.74) and (3.59), the equation (3.81) is obtained.

$$P_{em} = \left(\frac{3}{2}\right)\omega_e\left[i_q\lambda_{pm} + i_q i_d(L_d - L_q) - \frac{9\omega_e{\lambda_{pm}}^2{K_{pm3}}^2}{\sqrt{{r_s}^2 + 9{\omega_e}^2{L_0}^2}}\cos\left(\tan^{-1}\left(3\omega_e\frac{L_0}{r_s}\right)\right) - \frac{9\omega_e{\lambda_{pm}}^2{K_{pm3}}^2}{\sqrt{{r_s}^2 + 9{\omega_e}^2{L_0}^2}}\cos\left(6\theta_e + \tan^{-1}\left(3\omega_e\frac{L_0}{r_s}\right)\right)\right] \tag{3.81}$$

Although the electromechanical power P_{em} has already been a dependent of the electrical angular frequency ω_e, it is clear from (3.81) that the dependency now revealed to be non-linear.

3.4.2.3 Steady State Electromagnetic Torque due to the uncontrolled ZSC

When the zero-sequence current is not controlled its amplitude depends on the angular speed ω_e. Hence substituting equations (3.59) and (3.74) into (3.72) the electromagnetic torque equation becomes:

$$T_e = \left(\frac{3}{2}\right)\left(\frac{P}{2}\right)\left[i_q\lambda_{pm} + i_q i_d(L_d - L_q) - \frac{9\omega_e{\lambda_{pm}}^2{K_{pm3}}^2}{\sqrt{{r_s}^2 + 9{\omega_e}^2{L_0}^2}}\cos\left(\tan^{-1}\left(3\omega_e\frac{L_0}{r_s}\right)\right) - \frac{9\omega_e{\lambda_{pm}}^2{K_{pm3}}^2}{\sqrt{{r_s}^2 + 9{\omega_e}^2{L_0}^2}}\cos\left(6\theta_e + \tan^{-1}\left(3\omega_e\frac{L_0}{r_s}\right)\right)\right] \tag{3.82}$$

The above equation can be rewritten in the following form:

$$T_e = T_{qd} + T_{0DC} + T_{0AC} \tag{3.83}$$

where, T_{qd} is the torque produced by the projection of the current vector i_s onto the qd currents plane, T_{0DC} and T_{0AC} are the DC and AC components of the torque due to the zero current, respectively.

The equation of the torque produced by the qd currents has a form of the equation of the electromagnetic torque of a conventional star connected machine:

$$T_{qd} = \left(\frac{3}{2}\right)\left(\frac{P}{2}\right)\left[i_q\lambda_{pm} + i_q i_d\left(L_d - L_q\right)\right] \tag{3.84}$$

According to the expanded equation of the electromagnetic torque (3.82) and the equation (3.83) when i_0 is not controlled, the average torque is reduced with the increase of the machines angular speed ω_e. The term responsible for the decrease in the average torque production is:

$$\begin{aligned} T_{0DC} &= -\left(\frac{3}{2}\right)\left(\frac{P}{2}\right)\frac{9\omega_e{\lambda_{pm}}^2{K_{pm3}}^2}{\sqrt{{r_s}^2 + 9{\omega_e}^2{L_0}^2}}\cos\left(\tan^{-1}\left(3\omega_e\frac{L_0}{r_s}\right)\right) \\ &= -\left(\frac{3}{2}\right)\left(\frac{P}{2}\right)\frac{9\omega_e{\lambda_{pm}}^2{K_{pm3}}^2}{\sqrt{{r_s}^2 + 9{\omega_e}^2{L_0}^2}}\frac{r_s}{\sqrt{{r_s}^2 + 9{\omega_e}^2{L_0}^2}} \\ &= -\left(\frac{3}{2}\right)\left(\frac{P}{2}\right)\frac{9\omega_e r_s{\lambda_{pm}}^2{K_{pm3}}^2}{{r_s}^2 + 9{\omega_e}^2{L_0}^2} \end{aligned} \tag{3.85}$$

The DC component of the electromagnetic torque due to the zero-sequence current shown in (3.85) has its minimum value when the relationship stated in (3.86) is true.

$$\omega_e = \frac{r_s}{3L_0} \tag{3.86}$$

Substituting equation (3.86) into (3.85), the minimum value of the constant component of the electromagnetic torque due to the zero-sequence current could be found using the formula below.

$$T_{0DCmin} = -\left(\frac{9}{4}\right)\left(\frac{P}{2}\right)\frac{{\lambda_{pm}}^2 {K_{pm3}}^2}{L_0} \tag{3.87}$$

A rather interesting observation was made from (3.87): the increase of the rotor speed does not always result in the further reduction of the constant electromagnetic torque. There will always be a point at (3.86) when the further increase of speed would result in the increase of the average torque production. The maximum magnitude of the average torque reduction due to the zero-sequence current is the modulus of (3.87). In order to visualise the behaviour of the DC component of the electromagnetic torque T_{0DC}, Fig. 3.6 was drawn.

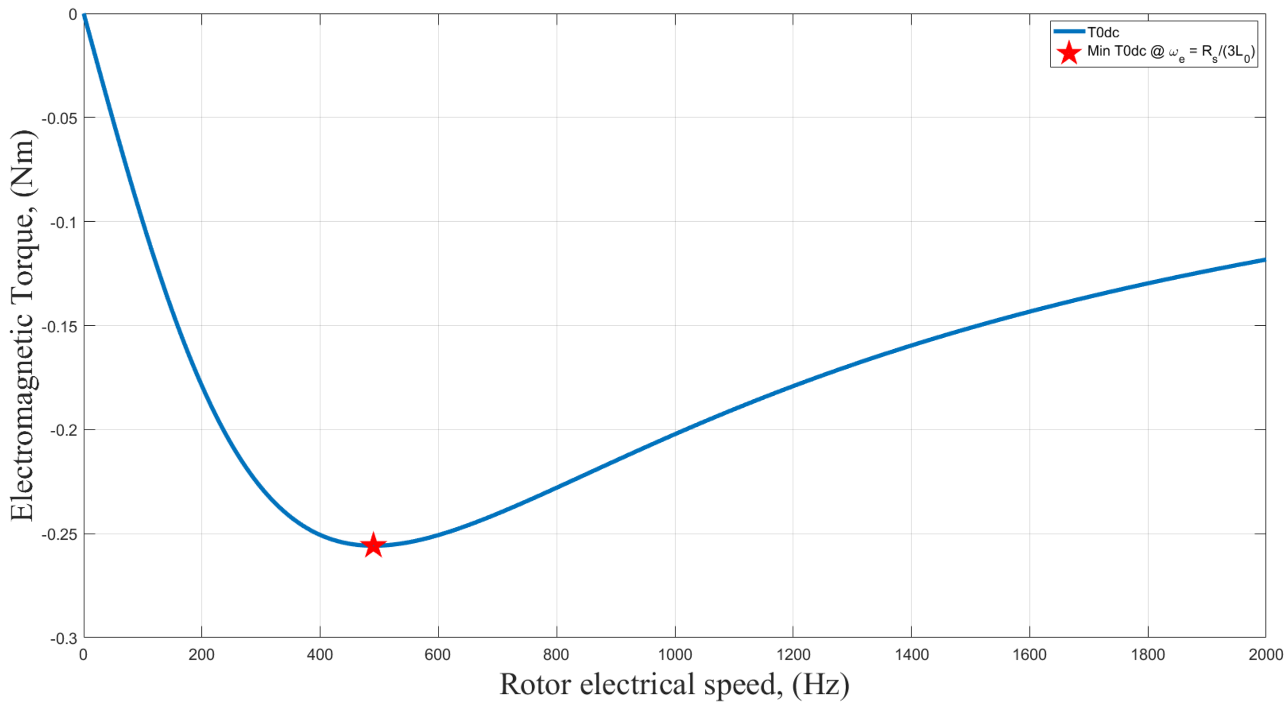

Fig. 3.6 – Electromagnetic torque's DC component due to ZSC.

The simulation of (3.85) shown in Fig. 3.6 confirms that the value of the average electromagnetic torque of the machine will not be reduced more than the modulus of (3.87) which will occur at the condition stated in (3.86). Passing the speed condition (3.86) depicted as a red pentagram in Fig. 3.6 will result in the recovery of the lost average torque as the limit of (3.85) when the speed tends to infinity is zero as per (3.88) below.

$$T_{0DCmax} = \lim_{\omega_e \to \infty} \left(-\left(\frac{3}{2}\right)\left(\frac{P}{2}\right) \frac{9\omega_e r_s {\lambda_{pm}}^2 {K_{pm3}}^2}{{r_s}^2 + 9{\omega_e}^2 {L_0}^2} \right) = 0 \tag{3.88}$$

The term responsible for the torque oscillation:

$$T_{0AC} = -\left(\frac{3}{2}\right)\left(\frac{P}{2}\right) \frac{9\omega_e {\lambda_{pm}}^2 {K_{pm3}}^2}{\sqrt{{r_s}^2 + 9{\omega_e}^2 {L_0}^2}} \cos\left(6\theta_e + \tan^{-1}\left(3\omega_e \frac{L_0}{r_s}\right)\right) \tag{3.89}$$

The amplitude of the torque oscillation is:

$$|T_{0AC}| = \left(\frac{3}{2}\right)\left(\frac{P}{2}\right) \frac{9\omega_e {\lambda_{pm}}^2 {K_{pm3}}^2}{\sqrt{{r_s}^2 + 9{\omega_e}^2 {L_0}^2}} \tag{3.90}$$

The phase of the torque oscillation is the same as the phase of the zero-sequence current described in the equation (3.59).

In order to determine the minimum and the maximum values of the amplitude of the electromagnetic torque oscillation $|T_0|$ the limit of the equation (3.90) must be taken when the electrical angular speed ω_e tends to zero, positive and negative infinity, respectively:

$$|T_{0AC}|_{min} = \lim_{\omega_e \to 0} \left(\left(\frac{3}{2}\right)\left(\frac{P}{2}\right) \frac{9\omega_e {\lambda_{pm}}^2 {K_{pm3}}^2}{\sqrt{{r_s}^2 + 9{\omega_e}^2 {L_0}^2}} \right) = 0 \tag{3.91}$$

$$|T_{0AC}|_{+max} = \lim_{\omega_e \to \infty} \left(\left(\frac{3}{2}\right)\left(\frac{P}{2}\right) \frac{9\omega_e {\lambda_{pm}}^2 {K_{pm3}}^2}{\sqrt{{r_s}^2 + 9{\omega_e}^2 {L_0}^2}} \right) = \left(\frac{9}{2}\right)\left(\frac{P}{2}\right) \frac{{\lambda_{pm}}^2 {K_{pm3}}^2}{L_0}$$
$$= \left(\frac{9}{2}\right)\left(\frac{P}{2}\right) \frac{{\lambda_{pm3}}^2}{L_0} \tag{3.92}$$

$$|T_{0AC}|_{-max} = \lim_{\omega_e \to -\infty} \left(\left(\frac{3}{2}\right)\left(\frac{P}{2}\right) \frac{9\omega_e {\lambda_{pm}}^2 {K_{pm3}}^2}{\sqrt{{r_s}^2 + 9{\omega_e}^2 {L_0}^2}} \right) = -\left(\frac{9}{2}\right)\left(\frac{P}{2}\right) \frac{{\lambda_{pm}}^2 {K_{pm3}}^2}{L_0}$$
$$= -\left(\frac{9}{2}\right)\left(\frac{P}{2}\right) \frac{{\lambda_{pm3}}^2}{L_0} \tag{3.93}$$

According to the equations (3.91) and (3.92), the minimum and the maximum amplitudes of the torque oscillation are zero and $\left(\frac{9}{2}\right)\left(\frac{P}{2}\right)\frac{{\lambda_{pm3}}^2}{L_0}$, respectively. λ_{pm3} is the amplitude of the 3rd harmonic of the flux leakage due to the permanent magnet rotor, L_0 is the leakage inductance.

The component of the electromagnetic torque due to the zero-sequence current that results in the torque oscillation presented in equation (3.89) was plotted in Fig. 3.7 below. Its instantaneous value depends on the speed of the motor as well as on the position of the rotor. Fig. 3.7 represents the same surface graph from different sides in order to visualise the dependencies. Fig. 3.7 (a) along with the colour bar show the whole picture of the torque/speed/angle dependency. Fig. 3.7 (b) shows how the instantaneous value of the electromagnetic torque's oscillating component due to the zero-sequence current depends on the angle of the rotor. Fig. 3.7 (c) depicts the dependency of the amplitude of T_{0AC} deduced in equation (3.90) on the electrical speed of the machine. Fig. 3.7 (d) is the perspective view.

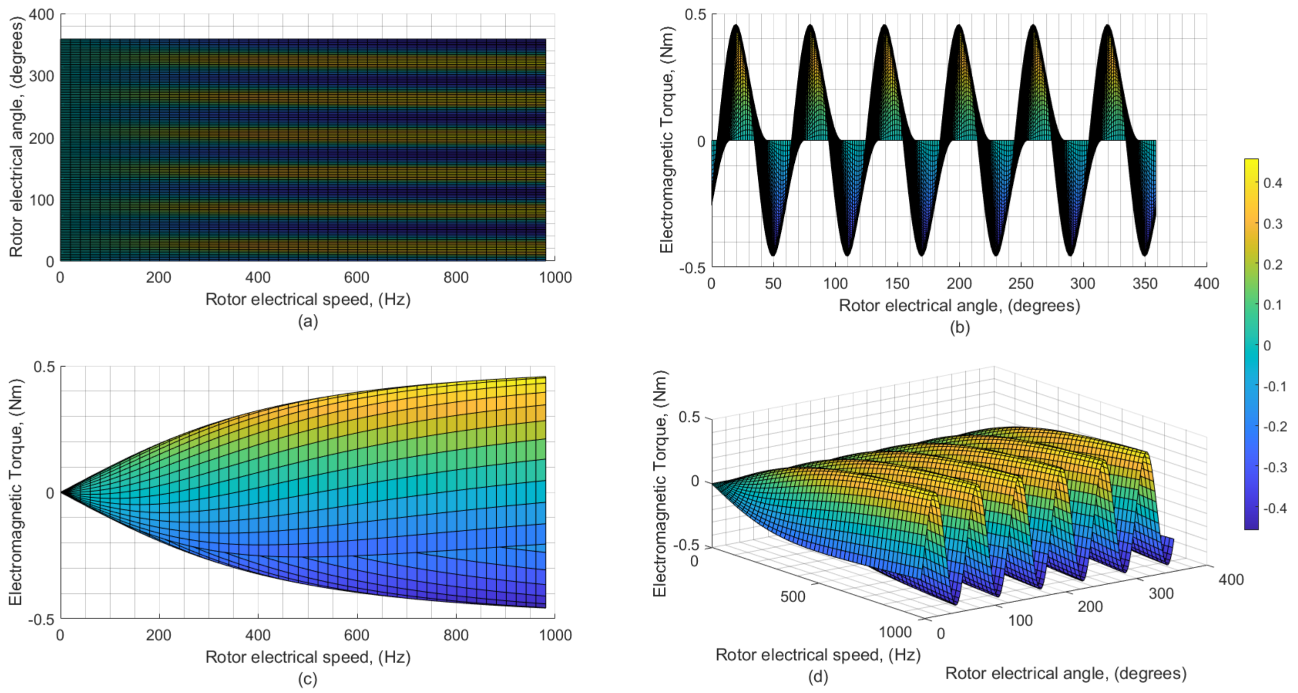

Fig. 3.7 – Electromagnetic torque's AC component due to ZSC.

3.5Discussion

A thorough mathematical analysis presented in this chapter revealed the origin of the zero-sequence current due to the machine side of the open-end winding permanent magnet synchronous motor with common DC bus. Some of the important concepts have also been established such as the equation of the maximum zero-sequence current amplitude value which showed that regardless of the speed of the rotor, the amplitude of the zero-sequence current cannot go over a certain limit. This helped to identify some regularities that led to the development of a novel online temperature identification technique introduced in chapter 6.

In addition, the presented analysis established the dependency of the motor's characteristics, such as power and torque, on the circulating zero-sequence current. In case the zero-sequence current is not controlled from the inverter side, in other words, the zero-sequence voltage generated by the inverter is zero, then the aforementioned motor's characteristics become dependent on the electrical angular frequency which in turn directly proportional to the rotor speed. This analysis enabled the research to both move towards understanding of the influence of the uncontrolled zero-sequence current on the power losses in conductor and think about the possible solution to reduce those losses. The influence of the uncontrolled zero-sequence current due to the machine side of the OEW PMSM drive was based on the analysis produced in this chapter and is investigated further in chapter 7.

Moreover, the analysis of the electromagnetic torque production presented in this chapter laid the basis for the proposal of a technique to mitigate the influence of the zero-sequence current due to the machine side of the drive on the torque production of an open-end winding permanent magnet synchronous motor drive with common DC link. This proposed technique is explained in chapter 5.

Besides, the analysis produced in this chapter also enabled the design of the Matlab/Simulink OEW PMSM with common DC link simulation model described in chapter 4.

Chapter 4

4 Simulation Model Design and Experimental Test System

This chapter focuses on the simulation model design of an open-end winding permanent magnet synchronous motor drive with common DC link in Matlab/Simulink and presents the simulation motor parameters that are going to be used in all of the subsequent chapters for the reference. In addition, the experimental rig that is used in order to validate some of the proposed techniques is also described in this chapter and will be used for the reference in future chapters.

4.1 Open-End Winding PMSM with Common DC link Simulation Model

In order to simulate the behaviour of the drive Matlab/Simulink software was chosen. The basic simulation model structure is presented in Fig. 4.1 below. It consists of a Matlab OEW PMSM model incorporated with the non-linear behaviour due to the non-linearity of the inductance together with a model of a dual fed inverter. In addition, the basic control structure features a Proportional Integral (PI) based current loop control and PI based speed loop control. The SVM block is the Space Vector Modulation that converts the control voltages V_{abc} to the inverter input signals for the switching of the MOSFETs. The control structure depicted in Fig. 4.1 also contains the $abc \rightarrow qd0$ transformation blocks based on the change of variable coefficients K and K^{-1} discussed in chapter 3 (equations (3.22) and (3.23), respectively).

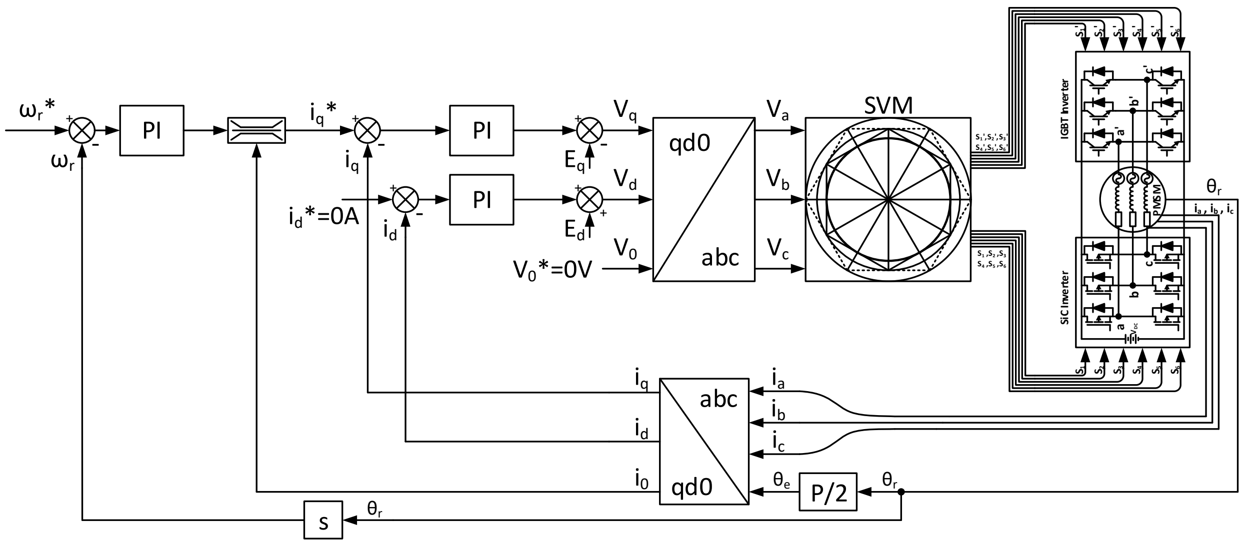

Fig. 4.1 – Diagram of a basic OEW PMSM drive simulation structure

The simulation model was based on the parameters of the drive system derived from the FEA analysis of the high-speed high torque motor that was developed as a part of an EPSRC project by Dr Gaurang Vakil from the University of Nottingham, stated in TABLE I.

TABLE I 3-phase OEW PMSM Specification according to FEA

Parameter	Value
Rated Speed, $\omega_{r\,rated}$	20kRPM
Phase Resistance, R_s	164mΩ
q- and d-axis Inductance, $L_q = L_d$	355μH
Leakage Inductance, L_0	17.75μH
PM Flux Linkage, λ_{pm}	71.5mVs
3rd Harmonic Flux Linkage coefficient, K_{pm3}	0.0115
Poles, P	6
Rated Current, I_{max}	150A
Rated Voltage, V_{DC}	540V
Bearings friction coefficient, B	0.0117 Ns/rad
Total inertia, J	0.1795 kgm2

4.1.1Design of the Open-End Winding PMSM Model in Simulink.

According to the derived equations for the OEW PMSM motor presented in chapter 3 a model was constructed using a single Matlab block for the Simulink simulation.

In order to obtain a discrete model for the phase currents of the motor, it was necessary to perform the following mathematical manipulations.

Rearranging the equation (3.19) for the change in current pi_{abc}:

$$pi_{abc} = {L_s}^{-1}\left[V_{abc} - (r_s + pL_s)i_{abc} - p\left(\lambda_{abc(r1)} + \lambda_{abc(r3)}\right)\right] \quad (4.1)$$

Using the Euler approximation [96] in order to obtain the instantaneous phase current values:

$$i_{abc}[k] = i_{abc}[k-1] + \delta(pi_{abc}[k]) \quad (4.2)$$

where, δ is the simulation sampling time.

The equations (4.1) and (4.2) were used in the PMSM simulation model for the calculation of all of the phase currents.

In order to model the angular speed of the motor, the mechanical PMSM model of the electromagnetic torque T_e has to be defined as follows.

$$T_e = J\left(\frac{2}{P}\right)\frac{d\omega_e}{dt} + B\left(\frac{2}{P}\right)\omega_e + T_L \tag{4.3}$$

where, the mechanical angular rotor speed is represented as $\left(\frac{2}{P}\omega_e\right)$, P is the number of poles, ω_e is the electrical angular speed, J is the total inertia, B is the friction coefficient and T_L is the load torque.

Rearranging the equation (4.3) to obtain the change in the electrical speed:

$$\frac{d\omega_e}{dt} = \frac{1}{J}\left[\left(\frac{P}{2}\right)(T_e - T_L) - B\omega_e\right] \tag{4.4}$$

Applying the Euler approximation to get an instantaneous value of the motor angular electrical speed $\omega_e[k]$:

$$\omega_e[k] = \omega_e[k-1] + \delta\dot{\omega}_e[k] \tag{4.5}$$

where, δ is the simulation sampling time.

In order to simulate the instantaneous current electrical angle $\theta_e[k]$, the instantaneous electrical angular frequency $\omega_e[k]$ is integrated as per (4.6) below.

$$\theta_e[k] = \theta_e[k-1] + \delta\omega_e[k] \tag{4.6}$$

where, δ is the simulation sampling time.

The mechanical rotor angle θ_m is found using the equation (4.7)

$$\theta_m[k] = \left(\frac{P}{2}\right)\theta_e[k] \tag{4.7}$$

4.1.2 Adding Non-linearity to the Open-End Winding PMSM model

The Linear and Non-Linear quadrature and direct inductance behaviours of the OEW PMSM were obtained using a finite element analysis (FEA) produced by Dr Gaurang Vakil from the University of Nottingham during the design of the machine for the EPSRC project. The result is represented in Fig. 4.2-Fig. 4.4. The graph in Fig. 4.2 represents the linear behaviour of the direct and quadrature inductances, whereas the graph in Fig. 4.3 represents the non-linear behaviour according to the corresponding quadrature and the direct currents. Fig. 4.4 represents the difference between the direct and the quadrature inductances $(L_d - L_q)$ according to the different combinations of the direct and quadrature currents. Inductance change along the corresponding currents occurs due to the saturation of the stator core. Such a behaviour could result in the power losses when a conventional SMPMSM control is applied to the machine.

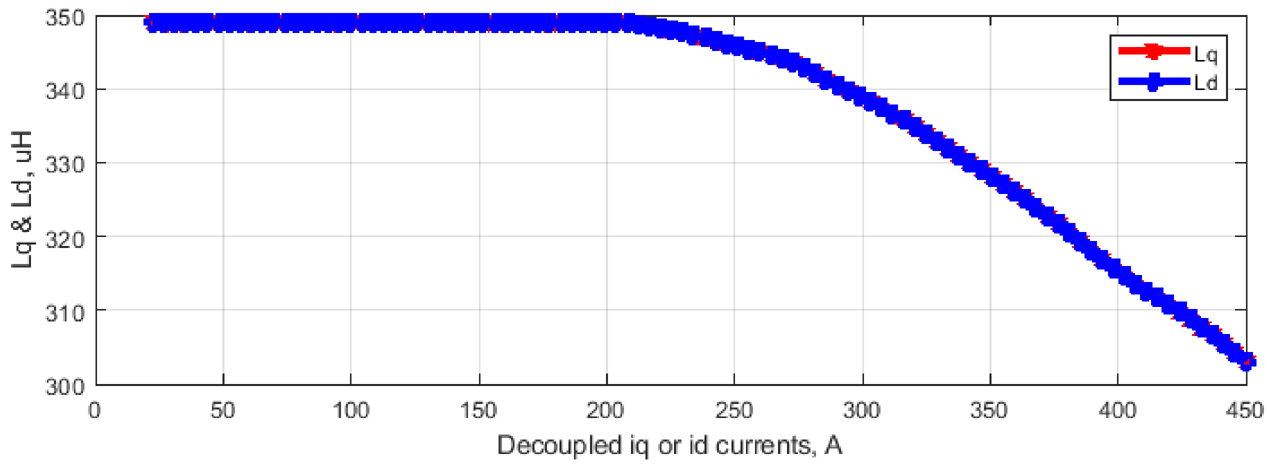

Fig. 4.2 – Linear behaviour of quadrature (L_q) and direct (L_d) inductances

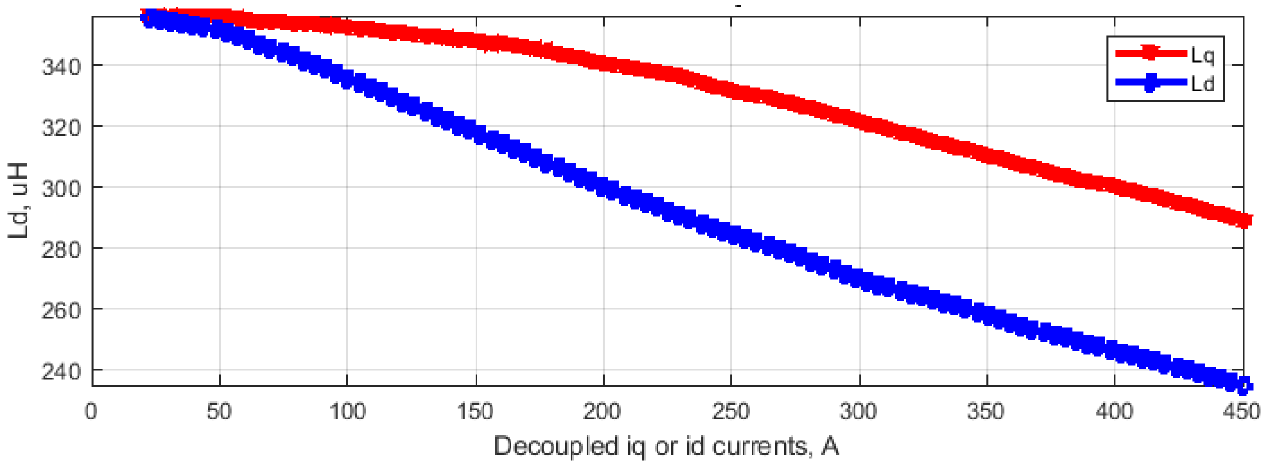

Fig. 4.3 – Non-linear behaviour of quadrature (L_q) and direct (L_d) inductances

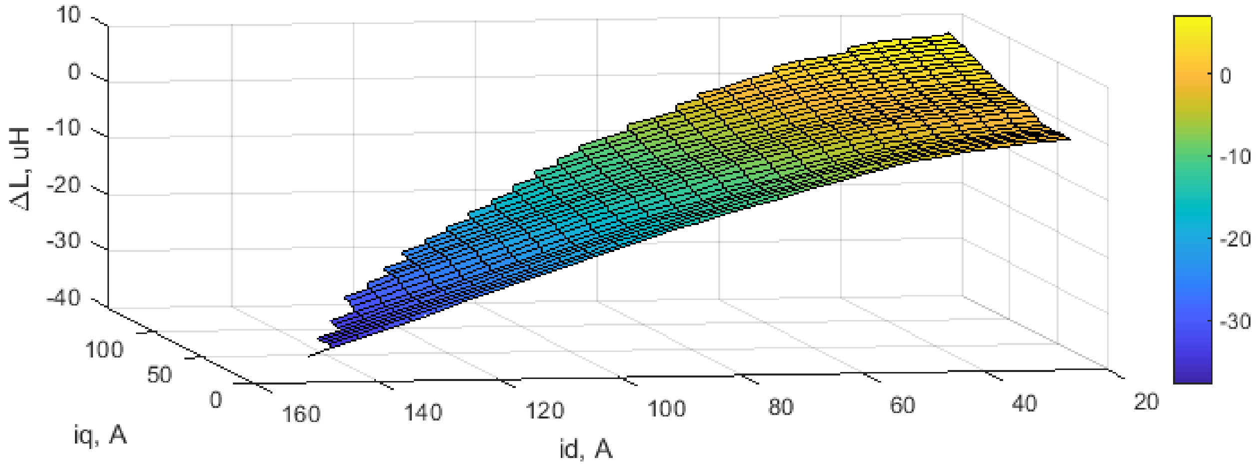

Fig. 4.4 – Difference between non-linear L_d and quadrature L_q inductances

Such a non-linear behaviour of the quadrature and direct inductances was considered in the simulation model in order to investigate its influence on the machine control.

L_A and L_B inductances of the L_s inductance matrix (3.5) from chapter 3 on page 39 can be found from the following formulae:

$$L_A = \frac{(L_q + L_d - 2L_{ls})}{3} \tag{4.8}$$

$$L_B = \frac{(L_q - L_d)}{3} \tag{4.9}$$

The value of leakage inductance L_{ls} is set to be no more than 5% of the quadrature inductance L_q according to FEA performed by the researcher who designed the particular high power OEW PMSM starter/generator considered in this thesis.

The non-linear values of the inductances are derived from the curves represented in Fig. 4.3 using a Look-Up Table (LUT) and an algorithm illustrated in Fig. 4.5.

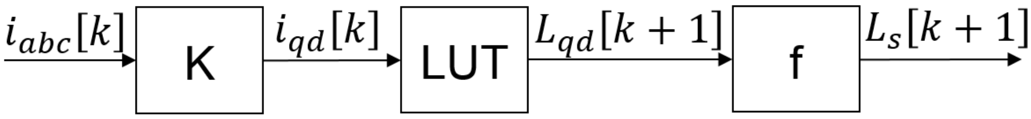

Fig. 4.5 – Non-linear inductance behaviour block diagram

However, the considered machine's maximum operating current is 150A. Fig. 4.2 - Fig. 4.4 concluded that the variation in the quadrature and direct inductances in a range from 0A to 150A (the designed operating range of the motor) are rather small to have caused an effect on the control. This effect was neglected; however, the slight non-linearity was added to the motor simulation in hopes of some unexpected behaviour that could be researched further. The equation (4.1) was considered to be sufficient to describe the motor behaviour without introducing unnecessary complications. Throughout the research presented in this thesis, the introduction of Fig. 4.5 had not resulted in any complications or concerns regarding the results.

In addition, the back EMF waveform produced by the FEA was analysed in order to find the third harmonic coefficient of the back EMF component. In order to accurately analyse such a waveform a Fast Fourier Transform was implemented using Matlab, (*FFTsim.m* algorithm in Appendix A). The outcome of the analysis is shown in Fig. 4.6.

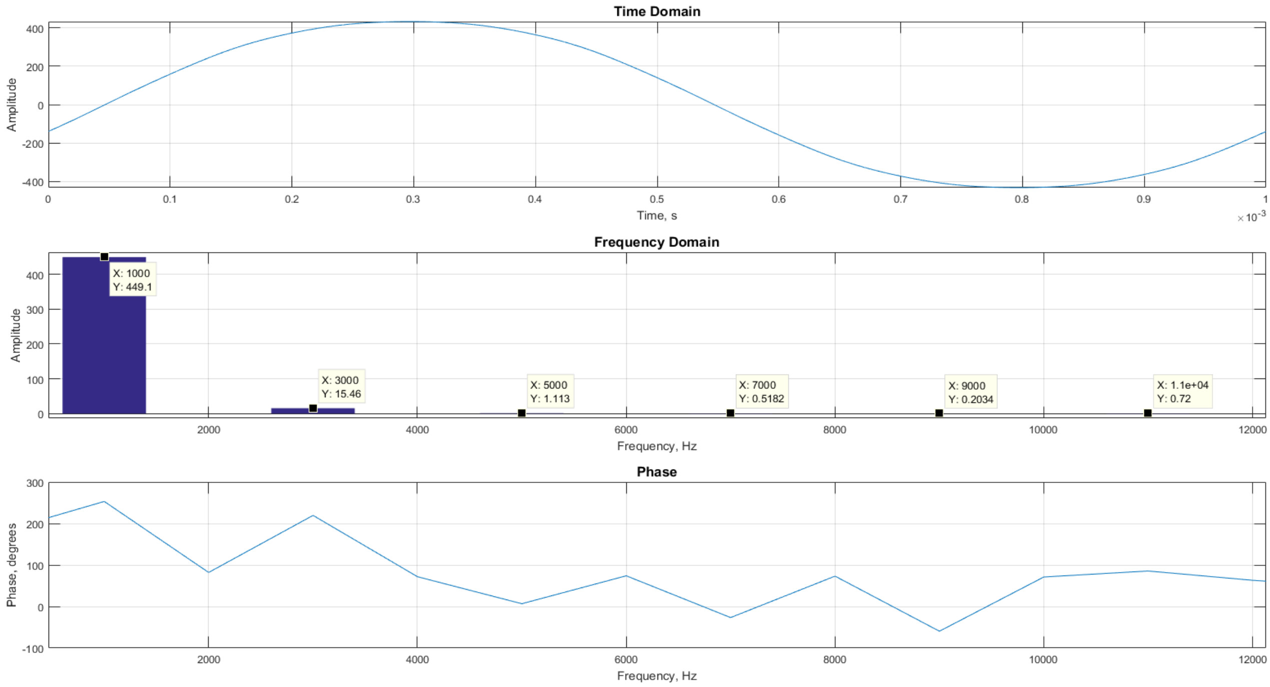

Fig. 4.6 – Frequency content of OEW PMSM phase back EMF derived from FEA

According to the produced results of the developed *FFTsim.m* algorithm presented in Fig. 4.6, the fundamental $\hat{E}_{abc1}$ and the third $\hat{E}_{abc3}$ harmonics are the two most pronounced harmonics, having values of 449.1 V and 15.46 V, respectively. The frequency of the fundamental back EMF was established to be 1 kHz. The value of λ_{pm} - the amplitude of the flux linkage established by the permanent magnet was found by rearranging the equation (3.14) from chapter 3 on page 41. The coefficient of the third harmonic flux linkage K_{pm3} was found using the equation (3.16) on page 41 of the same chapter. Both of these values were recorded to TABLE I, presented on page 67.

The equations (4.1) and (4.2) along with (4.5) were incorporated together to design a Matlab model that could be found in Appendix B in order to simulate the proposed ideas in Simulink, Fig. 4.7.

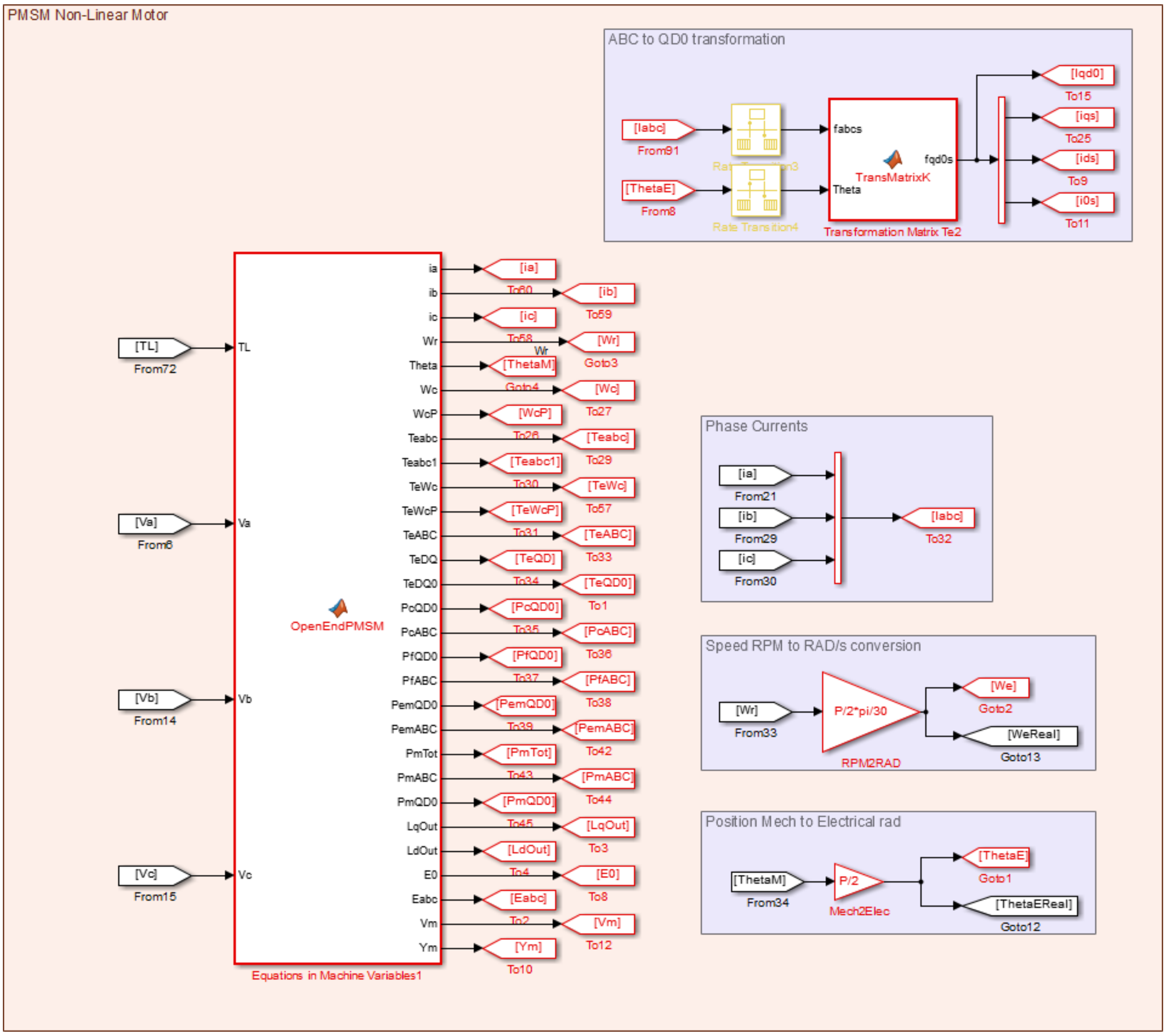

Fig. 4.7 – OEW PMSM Matlab/Simulink model for common DC link

4.1.3Inverter Simulation Design

The strategy of controlling each of the phases separately illustrated in Fig. 4.8was chosen. Giovanni Lo Calso explains this particular control technique in [97] well. The equations (4.10) and (4.11) show the duty cycles for each of the set of inverter legs.

$$d_{abcH} = \begin{cases} (d_{abcH} - 0.5) \cdot 2 & with \quad d_{abcH} \geq 0 \\ (d_{abcH} + 0.5) \cdot 2 & with \quad d_{abcH} < 0 \end{cases} \tag{4.10}$$

$$d_{abcL} = \begin{cases} 1 & with \quad d_{abcL} \geq 0 \\ -1 & with \quad d_{abcL} < 0 \end{cases} \tag{4.11}$$

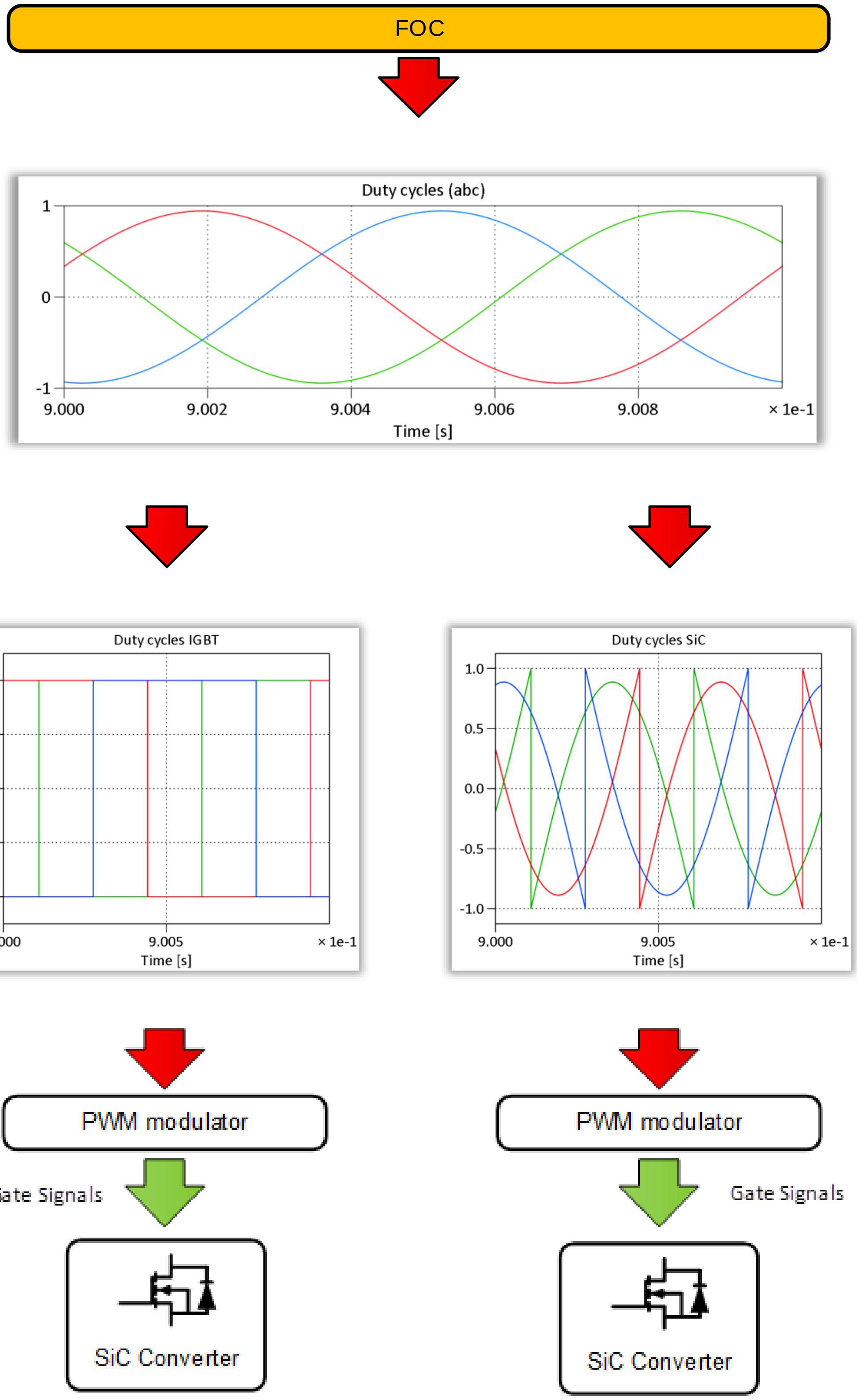

Fig. 4.8 – Modulation scheme for Open-End Winding PMSM control [97]

The reason why the duty cycles of two parts of the inverter d_{abcH} and d_{abcL} differ is because of the specifics of this inverter's cold plate. The water-cooled system is designed to work on one side only. So, the other side does not dissipate the heat at the same rate. Hence, the inverter on this side was chosen to be run at the fundamental frequency.

A Matlab simulation was designed to represent the 3D version of voltage vectors that could be used for the control, in Fig. 4.9. The particular voltage vectors for such a scheme are depicted in Fig. 4.10 in red. Thereby, the voltage limit for the voltage source converter (VSC) appears to be V_{DC} (magenta circle). This technique is explained by Luca Rovere in [57] [98] [99].

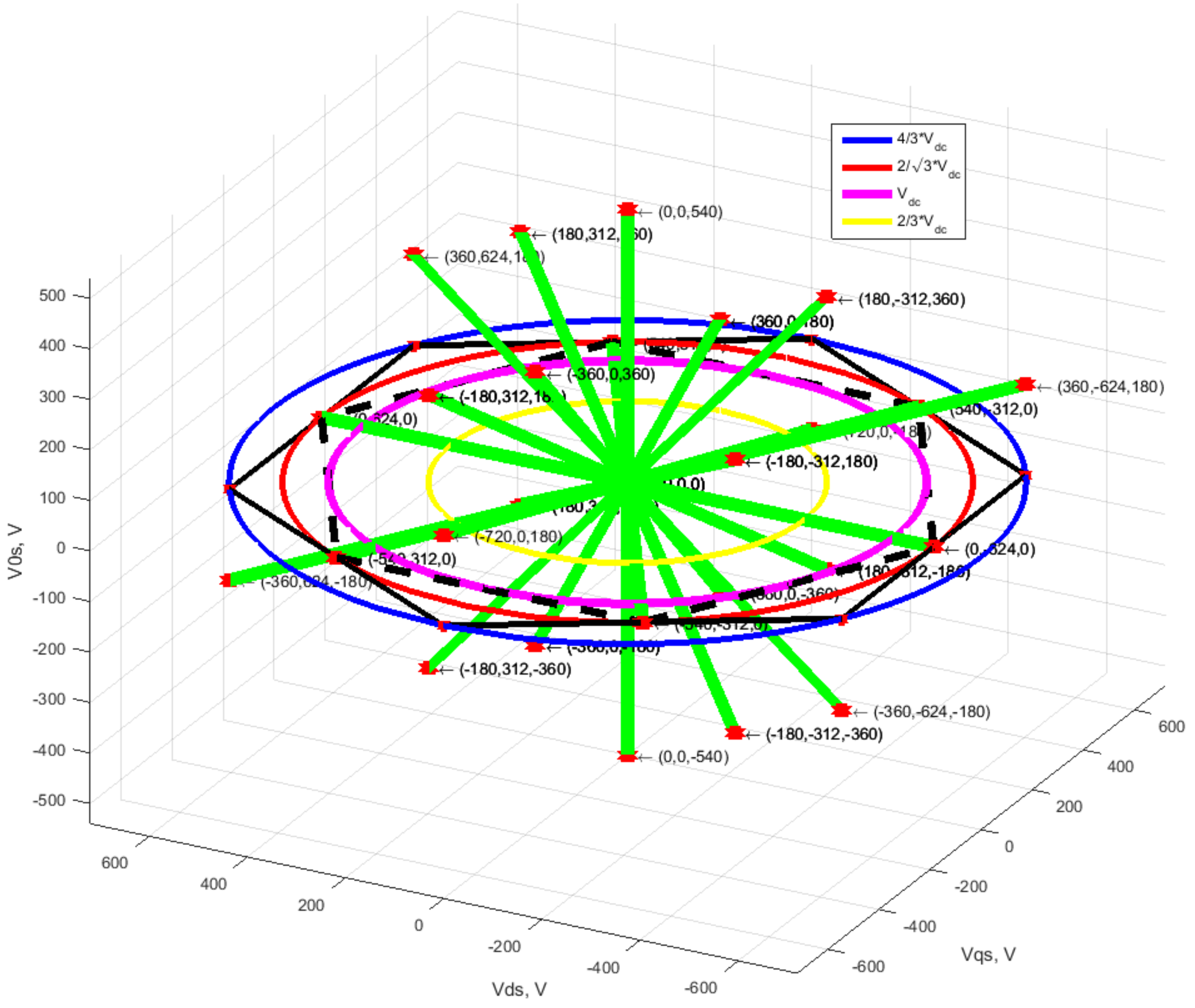

Fig. 4.9 – SVM diagram for the dual fed inverter in $qd0$ plane

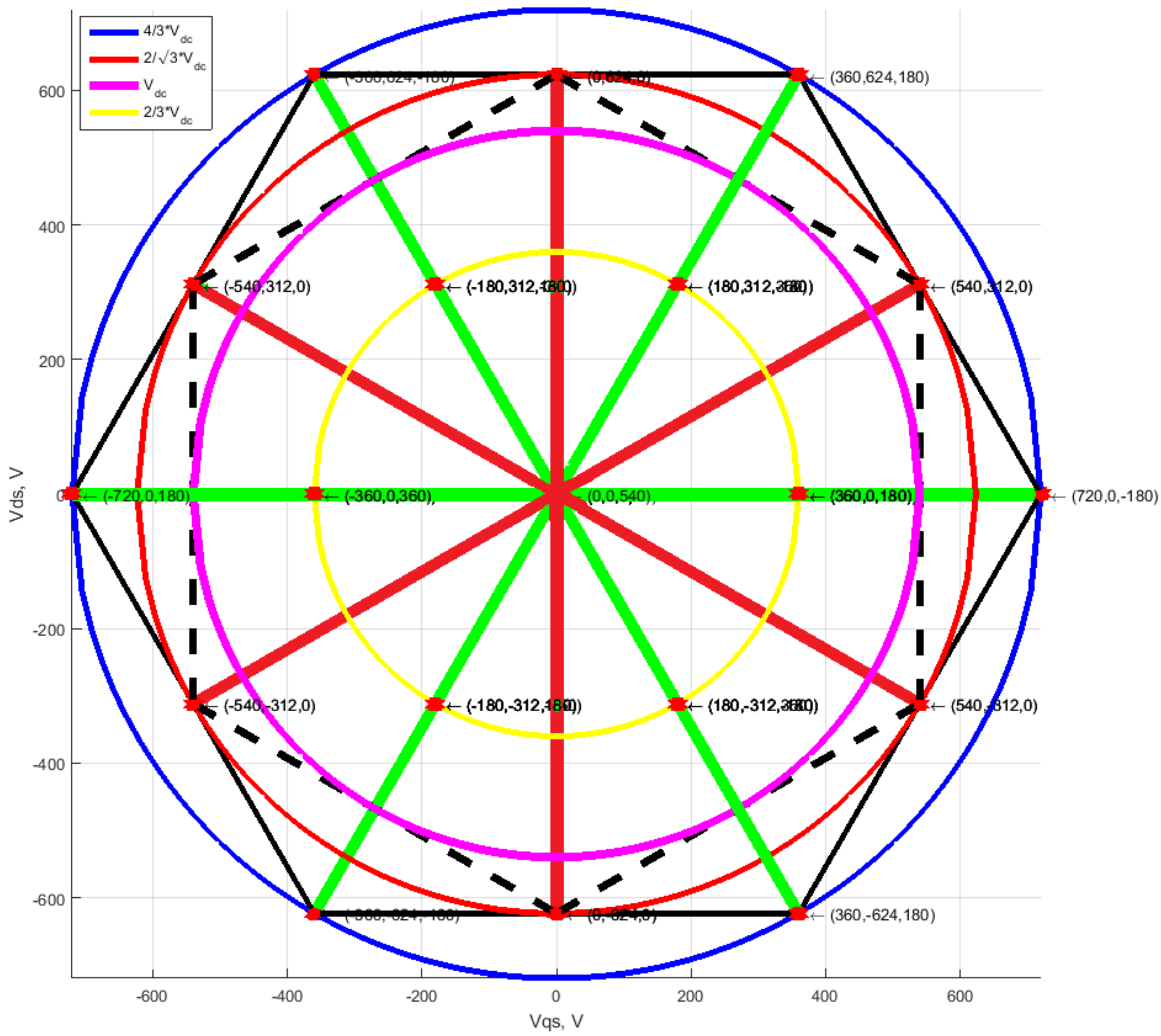

Fig. 4.10 – SVM diagram for the dual fed inverter in qd plane

4.2Experimental Test System

4.2.1Experimental SiC Inverter

A very promising [56] Dual Fed Open-End Winding 3-Phase Machine (DF-OEW3pM-MTD) topology that exploits SiC MOSFETs was chosen to prove the developed control strategies experimentally Fig. 4.11. SiC devices are especially used for high switching frequency inverters such as those used in the high-speed PMSM drives because the dead time approaches a very small value compared to IGBT modules. [100]

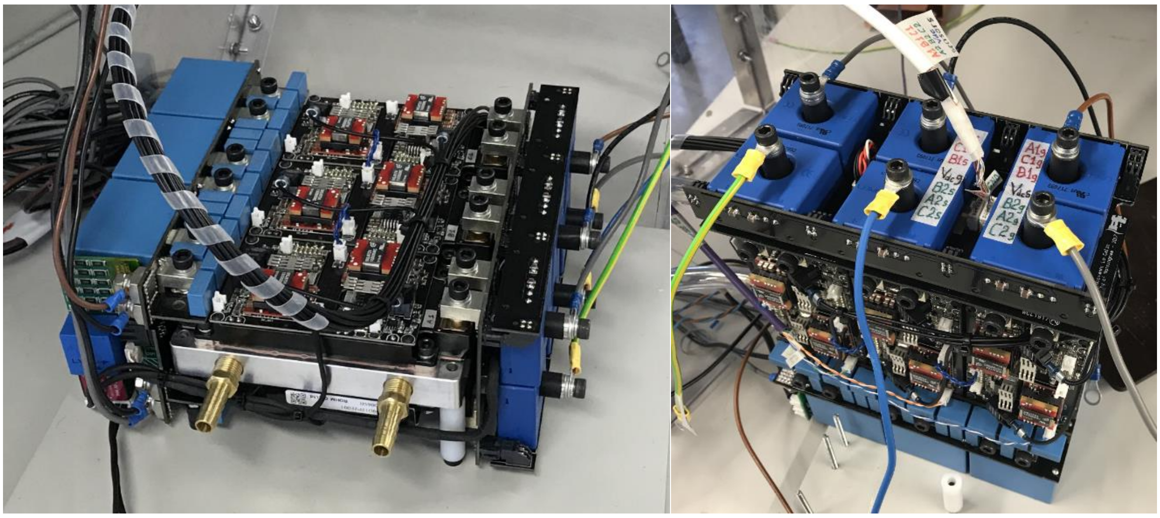

Fig. 4.11 – High power SiC Inveter for the OEW drive configuration

This inverter is a prototype developed by Dr Giovanni Lo Calzo from the University of Nottingham for an EPSRC project. The design is unique and very compact, meeting the current and voltage criteria of 150 A and 540 V, respectively. However, some modifications and a lot of high power testing had to be produced in order to ensure that the inverter is fit for the purpose.

4.2.2High-Speed High Power Density Open-End Winding Test Machine

The prototype machine the control is currently specified for is a High-Speed High-Power density three phase open-end winding PMSM that was designed by Dr Gaurang Vakil from the University of Nottingham according to the EPSRC specifications which included the rated power of 100 kW, rated speed of 20k RPM, maximum power operation speed range of 20k-40k RPM and a maximum operating speed of 36k RPM. The rest of the machine specification parameters are stated in TABLE I on page 67. The motor in discussion is shown in Fig. 4.12.

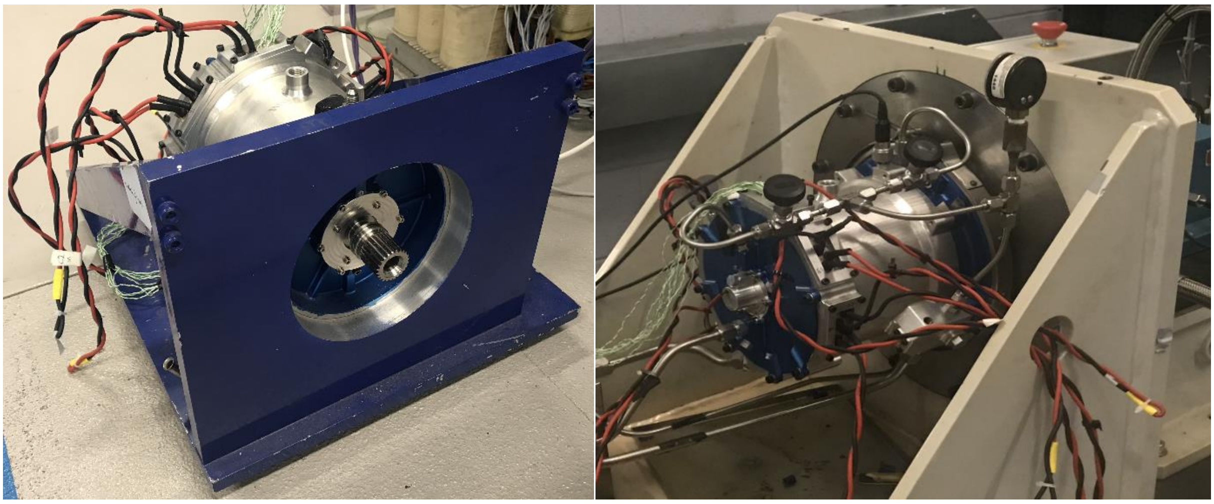

Fig. 4.12 – High-speed high torque machine

4.2.3Control Board

The following specially developed for the research at the University of Nottingham control platform [101] depicted in Fig. 4.13 is used for the implementation of the control techniques for the high-speed high power motor.

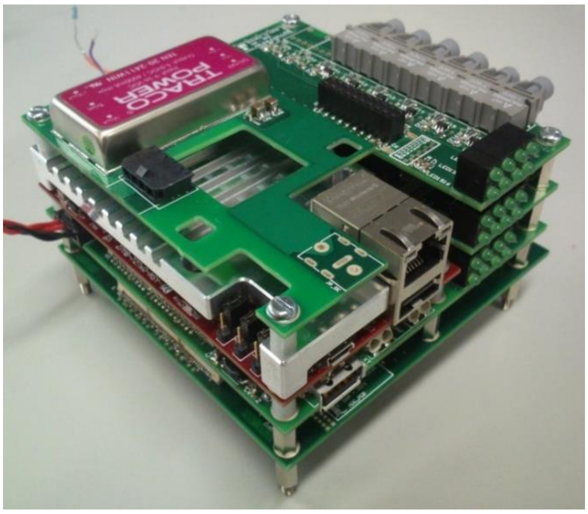

Fig. 4.13 – Control Platform based on ZynQ 7020 SoC

The control platform has the following features:

- Dual core ARM Cortex-A9 with NEON and FPU extensions 866MHz processor
    - CPU0
        - Linux
        - Communication with host PC
        - Scope functionality
        - Data logging
    - CPU1
        - Bare Metal control code
        - Receive data acquisition from FPGA and communicate back new reference value
        - AXI ACP communication between CPU1 and FPGA
- Onboard FPGA with:
    - 106,400 FlipFlops.
    - CPU1 interrupt generation
    - Encoders and resolver interfaces

    - ADC communication and digital filter (1MHz sampling frequency)
    - 3 PWM modulators
    - Fault handling
- 24 Fibre optics links
- Intrinsically isolated
- Each link configurable as output (power devices driving) or input (faults reading from power layer or system)
- Isolated CAN bus interface exploiting one of the two ARM CAN controller and a specific transceiver
- Power supplies for the FPGA fabric banks
- UART interface for sending and receiving data
- Isolated SPI controller, intended for possible external display

The ADC inputs of the control platform were slightly modified to fulfil the needs of the inverter's current sensors.

The overall setup was experimental. This means that there was no interface with the control board. The following contributions to the hardware were made as a result of the research:

- Current Sensors interface
- Voltage Sensor interface
- Temperature sensors interface
- Resolver interface.
- Various testing 3 phase inductor rigs
- Developed an easy Current and Voltage Sensors' calibration algorithm in Matlab for unknown inverters together with the testing programs.
- Developed an algorithm for the identification of the weak side of the inverter's cold plate.

4.2.4High-Speed Machines Testing Rig

The high-speed high power machines require a special testing rig that can withstand such speeds and powers. That is the reason why a 4-Quadrant starter/generator test rig depicted in Fig. 4.14 was used for the experimental validation.

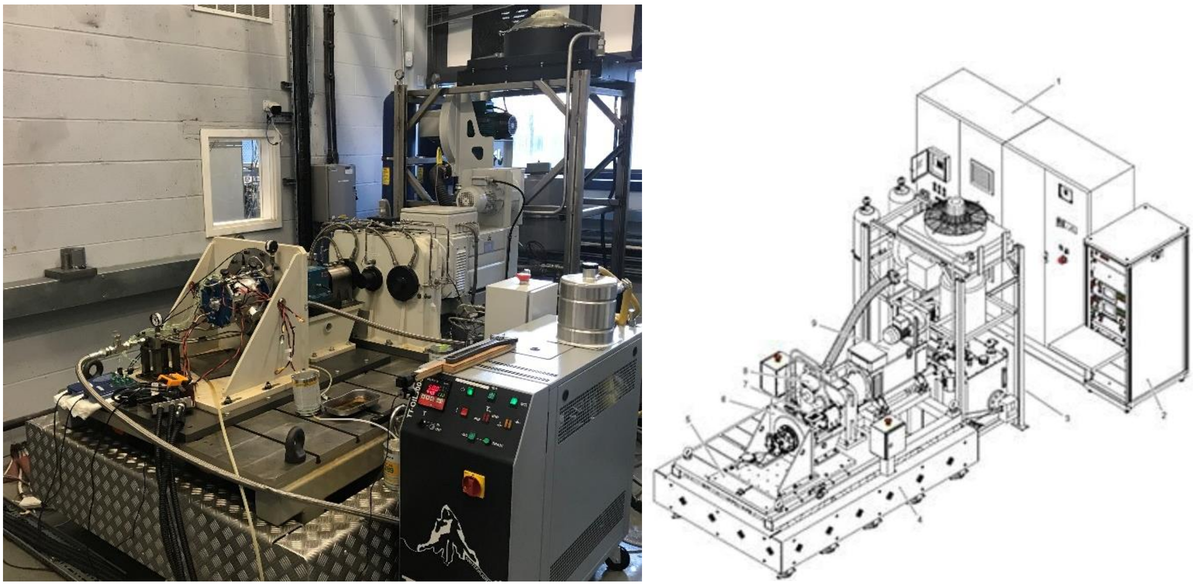

Fig. 4.14 – 4-Quadrant starter/generator test rig with schematic [102]

This experimental test rig was designed especially for the University of Nottingham and is rated to handle 150 kW of power at 35000 rpm. Key features of the installations include [102]:

- Complete test-rig system
- In-Line Torque measurement device
- Multiple torsion shafts for optimum accuracy at different application ratings
- Multiple output gearbox
- Very light-weight low mass overhang Tordisc Couplings
- Multi-purpose flexible test-cell
- Easy, repeatable installation and alignment of the test-article
- Accurate torque measurement
- Numerous performance envelopes

4.2.5The Experimental Setup Parameters Estimation

A system consisting of the experimental inverter described in 4.2.1 on page 77 and the OEW PMSM introduced in 4.2.2 on page 78 along with the control board shown in 4.2.3 on page 79 was connected together and then integrated into the high-speed high power starter/generator test rig shown in 4.2.4 on page 80. The parameters of the entire drive were estimated using the method of least squares [103] and recorded into

TABLE III. The values of the resistance R_s and the quadrature axis inductance L_q were estimated from the approximation of the quadrature current, shown in Fig. 4.15:

- Blue line – the quadrature current registered by the current sensors.
- Red line – the best approximation of the quadrature current that was derived using the least squares method.

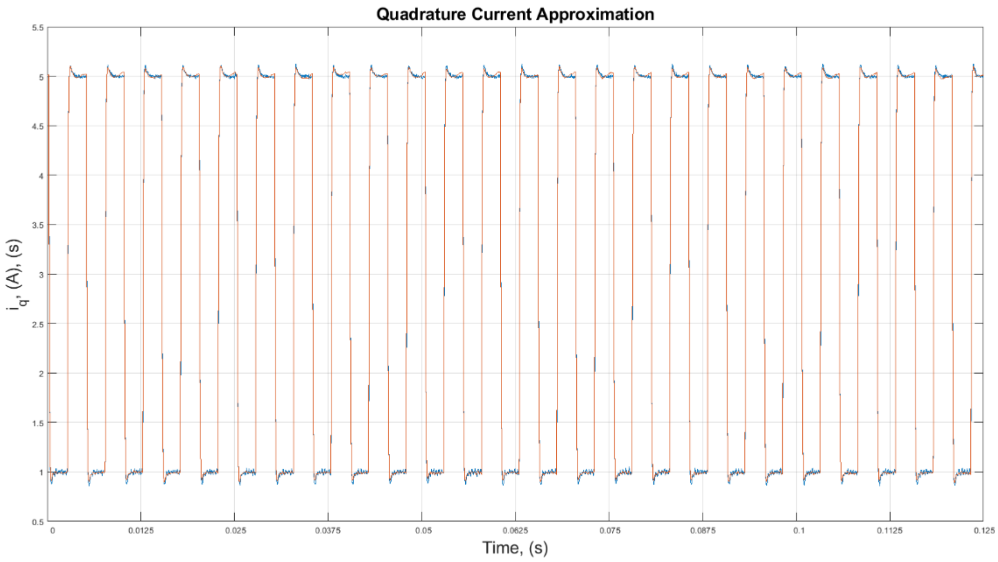

Fig. 4.15 – Comparison of quadrature current with its approximation

The values of the bearing friction coefficient B and the total inertia J were estimated driving the motor to rotate in a pattern shown in Fig. 4.16 at the top:

- Blue line – the speed of the motor registered by the position sensors.
- Red line – the best approximation of the speed of the motor that was derived using the least squares method.

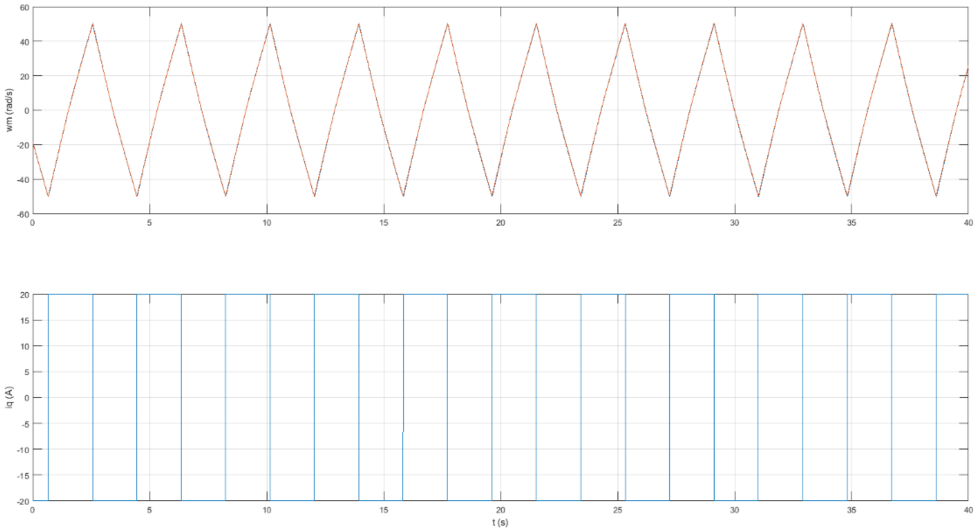

Fig. 4.16 – Comparison of the motor speed with its approximation

The flux linkage due to the permanent magnet as well as the third harmonic flux coefficient was estimated using the derived values of the back EMFs.

TABLE II - Flux coefficients estimation

Value	**Speed, (rpm)**	**Ea**	**Eb**	**Ec**	
$E_0, (V)$	**10000**	15.1600	13.4400	14.6400	**Mean**
	15000	21.9400	20.5200	21.6600	
$E_1, (V)$	**10000**	266.2000	260.1000	260.2000	
	15000	400.2000	390.5000	389.8000	
$\frac{E_0}{E_1}, (\%)$	**10000**	5.6950	5.1672	5.6264	
	15000	5.4823	5.2548	5.5567	
K_{pm3}	**10000**	0.0190	0.0172	0.0188	0.0182
	15000	0.0183	0.0175	0.0185	
$\lambda_{pm}, (Vs)$	**10000**	0.0847	0.0828	0.0828	0.0835
	15000	0.0849	0.0829	0.0827	

TABLE III 3-phase OEW PMSM Drive's Estimated Parameters

Parameter	Value
Rated Speed, $\omega_{r\,rated}$	20kRPM
Phase Resistance, R_s	1.44 Ω
q- and d-axis Inductance, $L_q = L_d$	403 μH
Leakage Inductance, L_0	132 μH
PM Flux Linkage, λ_{pm}	83.5 mVs
3rd Harmonic Flux Linkage coefficient, K_{pm3}	0.0182
Bearings friction coefficient, B	0.0117 Ns/rad
Total inertia, J	0.1795 kgm^2
Poles, P	6
Rated Current, I_{max}	150A
Rated Voltage, V_{DC}	540V

4.3 Discussion

This chapter developed a simulation model of an open-end winding permanent magnet synchronous motor drive with common DC bus for Simulink/Matlab incorporating the non-linear behaviour of the system due to the core saturation. Furthermore, this thesis is presented with the motor parameters that are used in all of the subsequent chapters to validate the proposed ideas.

In addition, the chapter describes the uniquely made for the University of Nottingham experimental high-speed testing rig and the experimental set up. The estimated parameters of the drive connected to this rig are also recorded. However, it was noticed that there is a discrepancy between the motor parameters for the simulation and the estimated parameters of the actual drive system. The resistance and the inductance of the phases appear to be greater for the experimental setup, hence, the leakage inductance is also much greater.

There are a couple of reasons accounting for the discrepancy in the intended machine parameters that can be found in TABLE I and the measured parameters recorded to TABLE III.

The high-speed machine testing rig shown in Fig. 4.14 and described in 4.2.4 on page 80 was situated in a special room separate from the control room. The experimental inverter and the control board described in 4.2.1 and 4.2.3, respectively, were not allowed to be put in. The inverter had to be placed in another room, the control room. Hence, it was necessary to connect the machine and the inverter with the long (~6 m) wires. In addition, the phases of the experimental starter/generator depicted in Fig. 4.12 on page 78 are divided into three sections that had to be connected in series using the sticking outside red and black wires as shown on the picture. Moreover, those wires were incorrectly chosen to be of a smaller diameter by the technicians.

It is likely that all of the mentioned facts resulted in a much higher phase resistance and inductance, hence, a considerably higher leakage inductance L_0.

The estimation of the flux linkage and the third harmonic flux linkage coefficient reveal a slight discrepancy between the theory and the real machine. These values appear to be slightly greater than the values given be the FEA.

The information revealed in this chapter is aimed to be the reference source for the proposed techniques introduced in the subsequent chapters of this thesis.

Chapter 5

5 Proposed Torque Quality Improvement Technique for an Open-End Winding PMSM

In this chapter a new closed-loop control strategy which improves the quality of the torque output of an open-end winding (OEW) permanent magnet synchronous motor (PMSM) with common DC bus is proposed. Such a configuration provides a path for the zero-sequence currents (ZSC) to flow in the windings. The analysis of the system revealed that these currents result in the electromagnetic torque oscillation. It has also been established that the zero-sequence currents are caused mainly by the third harmonic component of the back electromotive force (EMF). The research and a thorough analysis of the OEW PMSM showed that the existing methods of minimising the torque ripple cannot be applied when the leakage inductance of a machine is small, because the zero-sequence component can no longer be considered as one additional degree of freedom that can be managed. Therefore, a new control strategy presented in this chapter was proposed.

5.1 Modeling of the OEW PMSM Output Torque

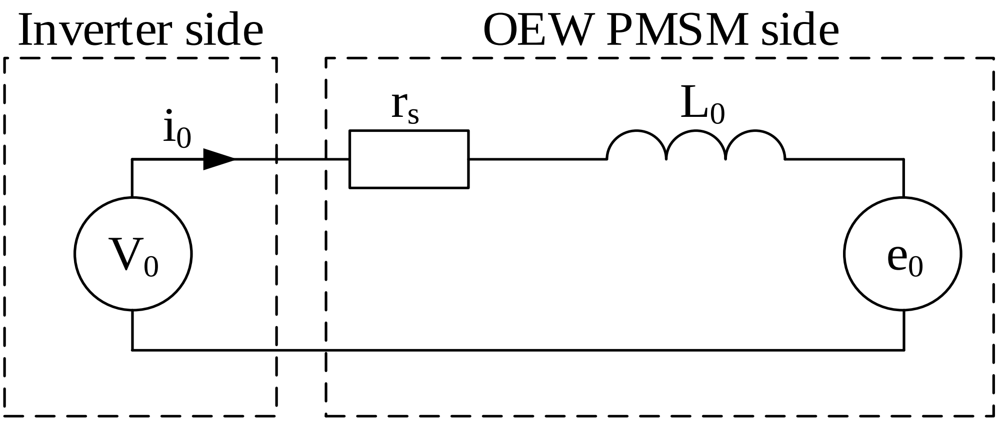

Fig. 5.1 – Equivalent circuit of zero-sequence component of OEW PMSM

The equivalent circuit of the zero-sequence component is shown in Fig. 5.1. In case of a high DC bus voltage and a low leakage inductance (L_0) an introduction of a pulse of ZSV (V_0) may result in unacceptable spikes of ZSC (i_0). Hence, the suppression of the ZSC by the means of the inverter's ZSV is not an option. It only remains to mitigate the influence of the ZSC due to the third harmonic back EMF (e_0) on the output torque quality. Thus, a new control technique was proposed in order to eliminate the variation of the torque due to the zero-sequence component without introducing V_0. According to the equation (3.71) on page 54 of chapter 3, the electromagnetic torque produced by the machine has an oscillation due to the cosine term which, in turn, is a result of both the back EMF 3rd harmonic and the zero-sequence current produced by the same harmonic.

$$T_e = \left(\frac{3}{2}\right)\left(\frac{P}{2}\right)\left[i_q\lambda_{pm} + i_q i_d\left(L_d - L_q\right) + 6i_0\lambda_{pm}K_{pm3}\cos(3\theta_e)\right] \qquad (5.1)$$

5.2Design of the Torque Ripple Compensator

Considering equation (5.3), if the oscillating term is compensated by one of the remaining terms the resultant torque must be free from this oscillation. Assuming i_d is zero, hence, the equation (5.1) above becomes:

$$T_e = \left(\frac{3}{2}\right)\left(\frac{P}{2}\right)\left[i_q\lambda_{pm} + 6i_0\lambda_{pm}K_{pm3}\cos(3\theta_e)\right] \tag{5.2}$$

Forcing i_q to be as shown in equation (5.3):

$$i_q{}^* = i_{qDC}{}^* - i_{qAC}{}^* \tag{5.3}$$

where, $i_{qDC}{}^*$ and $i_{qAC}{}^*$ are the constant and the alternating terms of the reference quadrature current $i_q{}^*$, respectively. The value $i_{qDC}{}^*$ is the main source of the average torque generation, whereas $i_{qAC}{}^*$ is the torque oscillation compensating term, denoted in (5.4).

$$i_{qAC}{}^* = 6i_0K_{pm3}\,cos(3\theta_e) \tag{5.4}$$

Combining (5.4) and (5.3), subsequently substituting the result into (5.2), the electromagnetic torque equation becomes the one show in (5.5).

$$\begin{aligned} T_e = \left(\frac{3}{2}\right)\left(\frac{P}{2}\right)\Big[&\left(i_{qDC}{}^*\right)\lambda_{pm} - 6i_0\lambda_{pm}K_{pm3}\cos(3\theta_e) \\ &+ 6i_0\lambda_{pm}K_{pm3}\cos(3\theta_e)\Big] \end{aligned} \tag{5.5}$$

The oscillating terms of (5.5) cancel out leaving the torque value to be as follows.

$$T_e = \left(\frac{3}{2}\right)\left(\frac{P}{2}\right)\left(i_{qDC}{}^{*}\right)\lambda_{pm} \tag{5.6}$$

According to (5.6) the oscillation due to the zero-sequence current is cancelled, hence, the value of the torque is no longer oscillatory. In order to implement the proposed control technique, a proportional integral plus resonant controller (PI+RC) is used for the quadrature current loop, the basic simulation diagram of which is shown in Fig. 5.2.

The process of derivation of i_0 is rather simple and does not involve the rotor position as per equation (5.7) below.

$$i_0 = \frac{i_a + i_b + i_c}{3} \tag{5.7}$$

According to the zero-sequence voltage equation of (3.39) in chapter 3, the zero-sequence current has a sinusoidal form, (5.8), if there is precisely zero ZSV applied to the motor.

$$i_0 = |i_0|\cos(3\theta_e + \gamma) \tag{5.8}$$

where, i_0 and $|i_0|$ are the zero-sequence current's instantaneous value and its amplitude, respectively, when the applied zero-sequence voltage is zero. $3\theta_e$ and γ are the angle and the phase of ZSC, respectively.

Substituting (5.8) into (5.4):

$$i_{qAC}{}^{*} = 6|i_0|K_{pm3}\cos(3\theta_e + \gamma)\,cos(3\theta_e) \tag{5.9}$$

Using trigonometric identity, the equation (5.9) becomes:

$$i_{qAC}^{*} = 3|i_0|K_{pm3}(\cos(6\theta_e + \gamma) + cos(\gamma)) \tag{5.10}$$

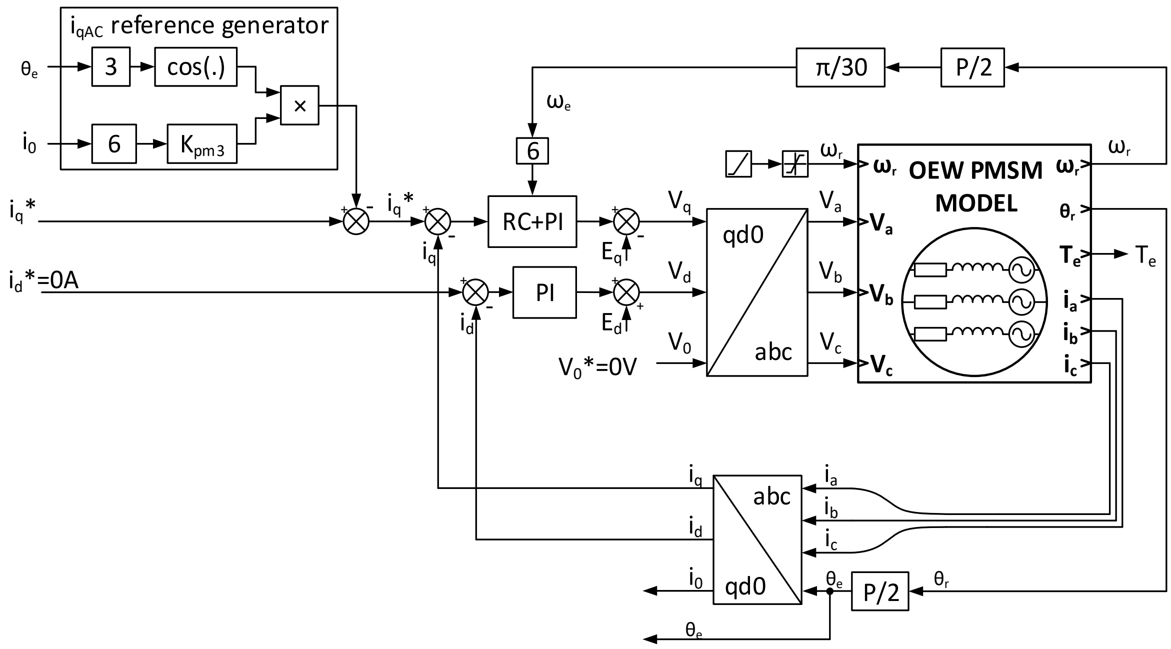

Fig. 5.2 – Basic Quadrature Current PI+RC simulation setup

According to equation (5.10) it is clear that the alternating part of the quadrature reference current has a frequency of six times the fundamental frequency. Hence, the RC, depicted in Fig. 5.2 is fed with the sixth harmonic electrical frequency $(6\omega_e)$.

In order to improve the current control the feed-forward E_q and E_d terms were introduced to compensate the cross coupling, as per Fig. 5.2.

A special form of a non-ideal adaptable resonant controller proposed in [104] is shown in equation (5.11).

$$G_{frc}(s) = \frac{2k_{ir}(\omega_{cr}s + \omega_{cr}^2)}{s^2 + 2\omega_{cr}s + \omega_{cr}^2 + \omega_0^2} \tag{5.11}$$

where, k_{ir} is the gain, ω_0 is the resonant frequency and ω_{cr} is the controller width. All of the derivations for the adaptable resonant controller can be found in [104]. Such a controller is used to maintain the AC reference of the quadrature current and a conventional PI is used in order to maintain the DC reference of the same current, Fig. 5.2. The following parameters were chosen for the RC: k_{ir} = 100, ω_{cr} = 0.9, ω_0 is the fed back electrical speed of the motor multiplied by six ($6\omega_e$) as discussed above. The Bode diagram of such a resonant controller is shown in Fig. 5.3. The peaks correspond to the particular value of the speed that ω_0 input takes.

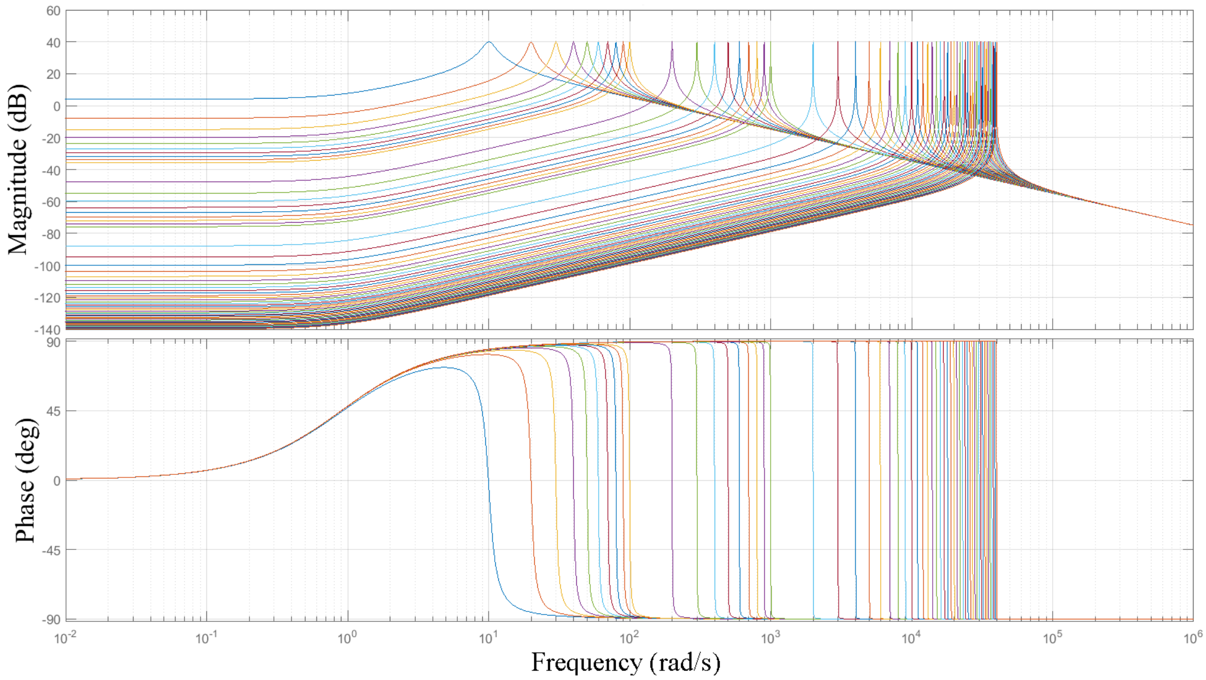

Fig. 5.3 – Bode diagram of the resonant controller according to the range of the input frequencies

The DC parts of the reference and feedback input signals of the RC does not affect its behaviour due to the nature of the RC. A properly tuned resonant controller responds to a particular resonant frequency only, considerably attenuating all of the other frequencies and especially DC value, as depicted in Fig. 5.3. In this case the resonant frequency is directly proportional to the speed of the rotor.

5.3Simulation Results

The basic performance of the proposed control concept shown in Fig. 5.2 was tested in Matlab/Simulink using the FEA parameters listed in TABLE I in chapter 4 on page 67.

The machine’s leakage inductance is around 5%, hence, introducing the 540V DC bus, even for as little as one microsecond, could result in a spike of the ZSC of approximately 30A. Such a behaviour is undesirable. Hence, the new control strategy presented in this chapter that does not introduce any ZSV on the inverter side is the appropriate solution to minimise the torque ripple output due to the third harmonic of the back EMF in such types of the machines.

5.3.1Ideal Simulation Case

According to the simulation outcome presented in Fig. 5.4 (top), the proposed control method resulted in the complete elimination of the torque ripple due to the third harmonic back EMF. The bottom graph shows that in order to achieve such a result the phase current was only slightly impacted.

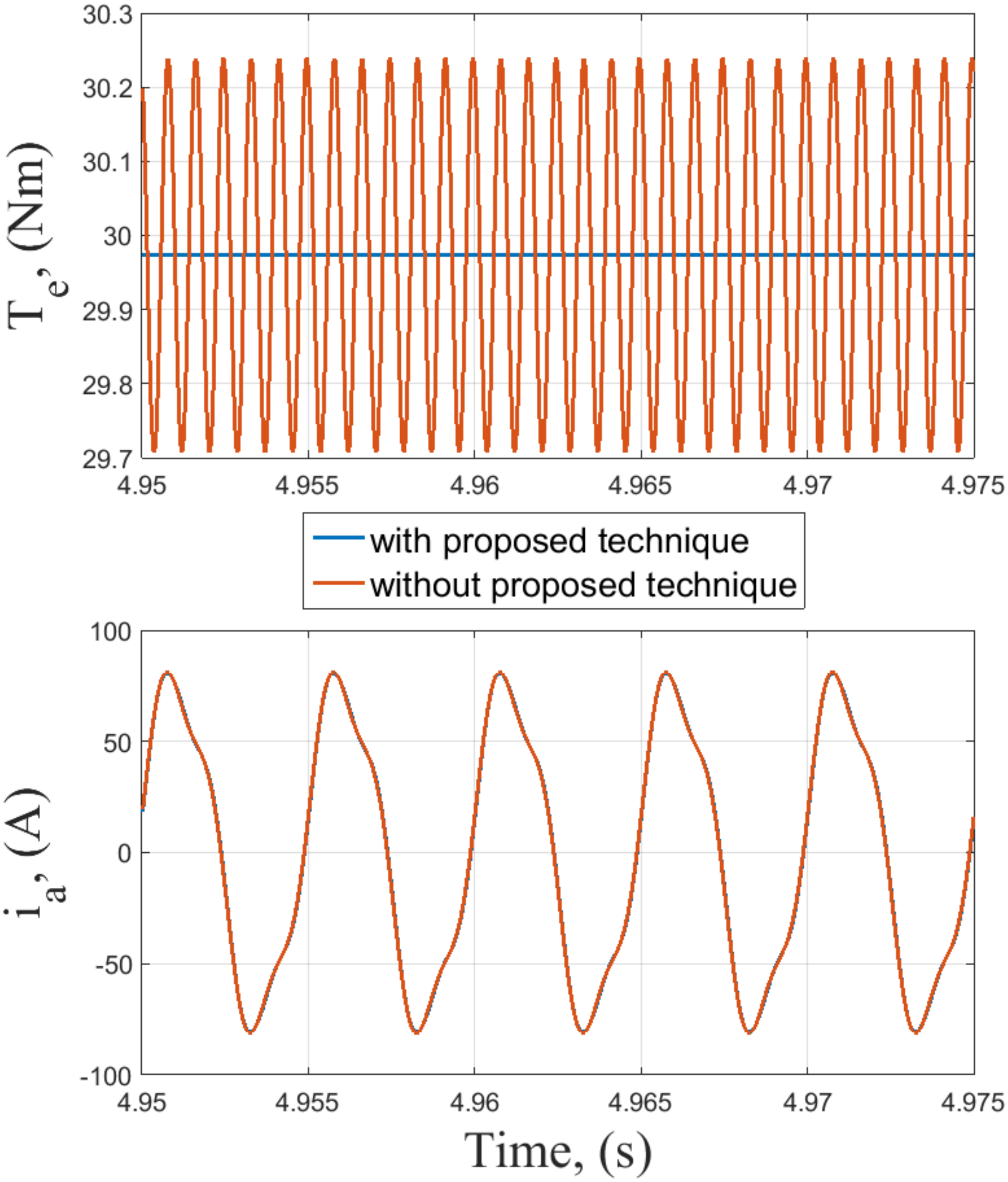

Fig. 5.4 – Electromagnetic torque (top) and phase current (bottom) at 200Hz electrical speed

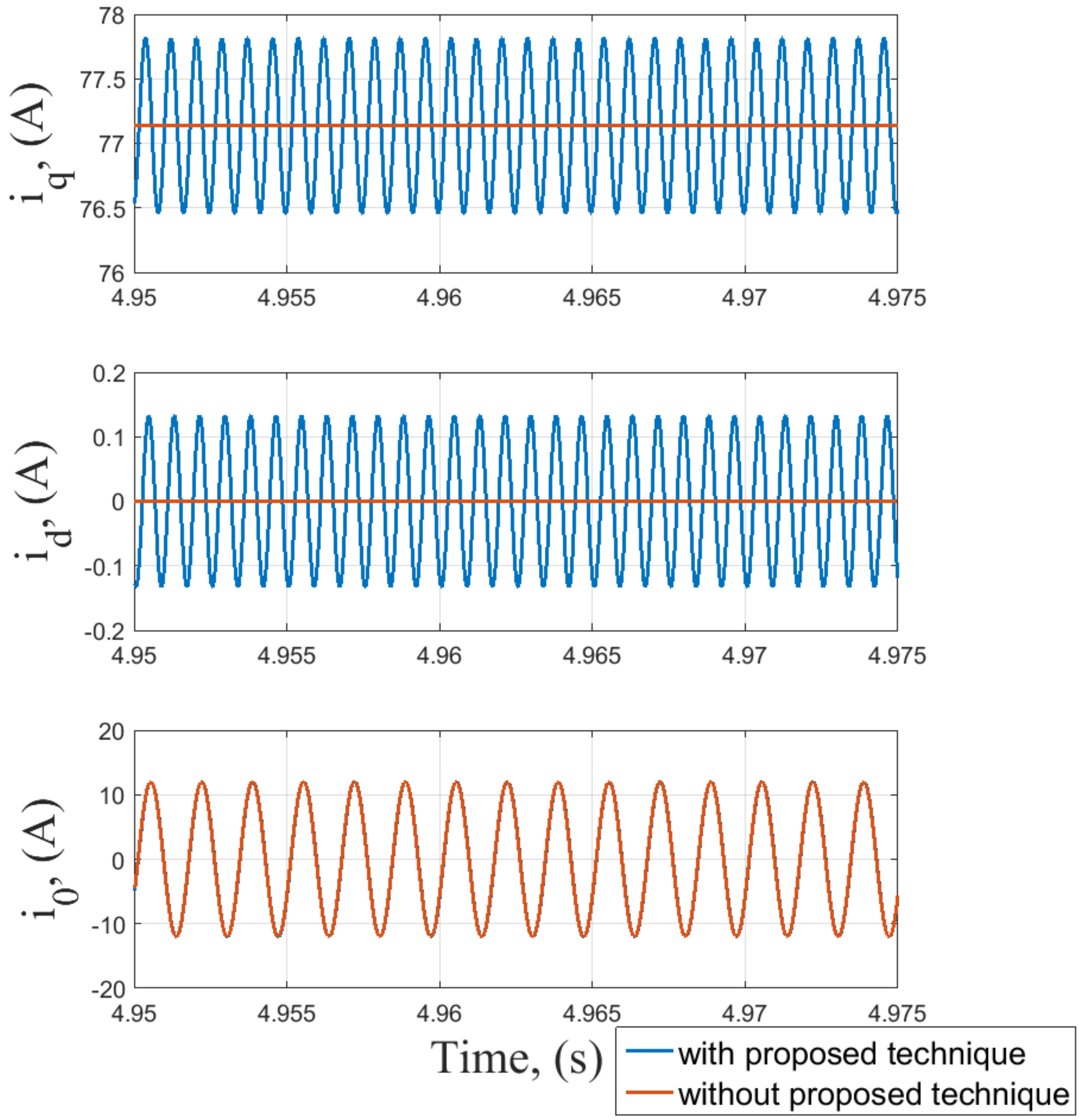

Fig. 5.5 – Quadrature, direct and zero currents (top, middle and bottom, respectively) at 200 Hz electrical speed

The quadrature, direct and zero axis currents are respectively shown in Fig. 5.5. The adaptable resonant controller made sure the oscillatory path is followed correctly in order to achieve smooth torque output. The zero-sequence current remained uncontrolled as expected. It can be noticed that it oscillates at the frequency of the third harmonic with an amplitude predicted by equation (3.74) from chapter 3. Even though the zero-sequence current is present in the system for the entire time of operation– the ability to increase the power output by using the OEW PMSM configuration could outweigh this drawback in some situations. Referring back to equations (5.4) and (5.5) along with the torque results in Fig. 5.4, it is very important to note that the torque ripple amplitude is independent of the average torque value. This amplitude is proportional to the ZSC amplitude which, in turn, is proportional to the speed of the machine. This means that such open-end winding machines will have a considerably large value of the torque ripple percentage particularly at the low average load torque. However, the basic simulation showed that the proposed method eliminated the ripple regardless of the average torque value.

5.3.2Non-Ideal Simulation Case

Although, mathematically the proposed method might seem as a good method to fully suppress the torque ripple, in reality the input phase voltages are modulated using switching inverters, which, in turn, induce an additional current noise due to the switching. Hence, a more accurate simulation method was introduced taking into account a special space vector voltage modulation technique (SVM) which eliminates the ZSV produced by the voltage source converter (VSC) by using only certain voltage vectors shown in Fig. 4.10 in chapter 4 on page 73 that do not produce ZSV [57].

A new simulation illustrated in Fig. 5.6 features a special modulation technique that is used in order to keep the ZSV always zero. The simulation clock frequency was set to be the same as the carrier counter of the actual modulator, 100MHz. Hence, the simulation very accurately mimics the behaviour of an FPGA based modulator that is used for the experimental testing.

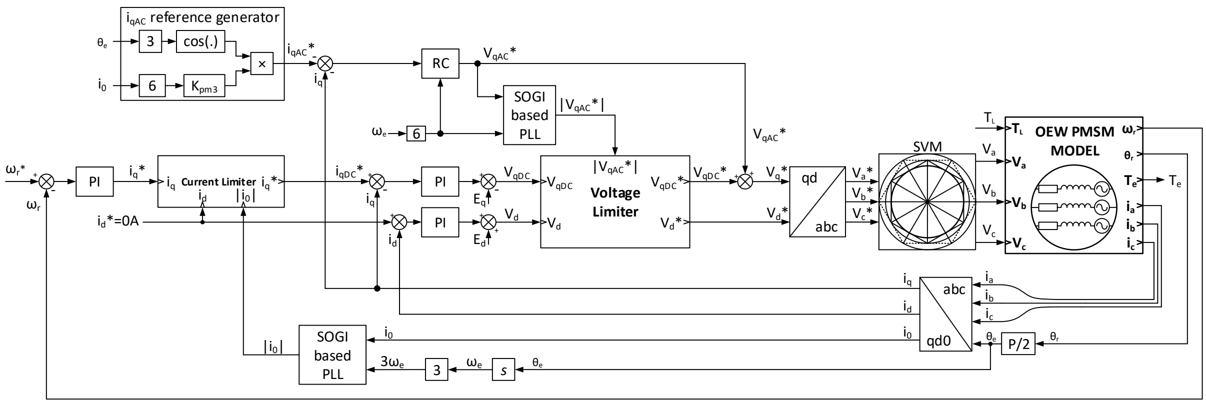

Fig. 5.6 – The full detailed simulation block diagram featuring voltage modulation

The sampling frequency of the controller was set to be 40 kHz to represent the actual switching frequency of a SiC inverter. The electrical rotor frequency was stabilised at 200 Hz. The output of the speed loop PI controller generates the DC reference for i_q. This current reference is limited by a special current limiter that takes into consideration the direct current and the amplitude of the ZSC in order to provide the machine with the maximum allowed RMS current. The RMS value of a signal is a square root of the squares of all of the harmonics RMS values that comprise the signal itself. The phase current of the considered OEW PMSM consists of the fundamental and the zero-sequence currents mainly.

$$i_{qDC\_lim} = \sqrt{2{I_{RMS\_lim}}^2 - {i_d}^2 - |i_0|^2} \tag{5.12}$$

The amplitude of the zero-sequence current is provided by the modified version of the second order generalised integrator (SOGI) based single phase Phase-Locked-Loop (PLL) (Fig. 5.6), explained in [105]. The modification added is the amplitude identification bit at the output of the mentioned PLL, as illustrated in Fig. 5.7.

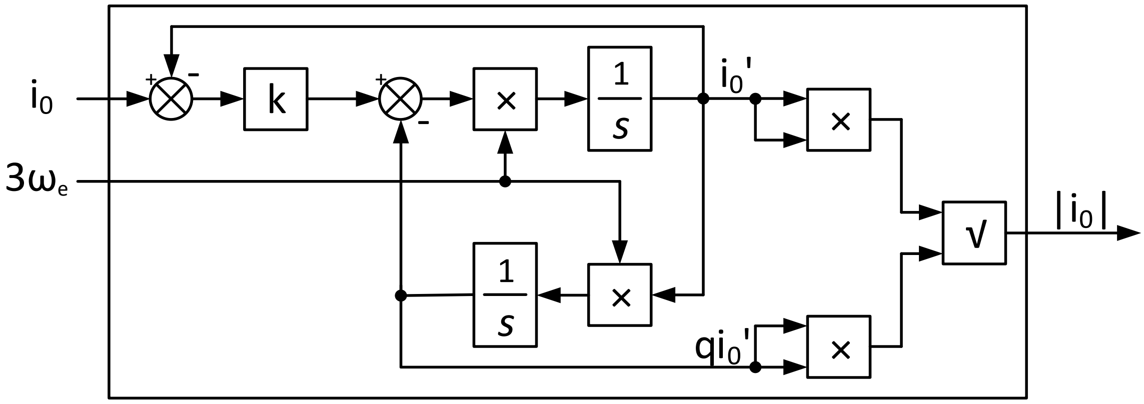

Fig. 5.7 – SOGI based single phase PLL amplitude estimator

The direct $i_0{}'$ and the quadrature $qi_0{}'$ output signals are used in the following formula to calculate the ZSC amplitude, $|i_0|$, for the current limiter.

$$|i_0| = \sqrt{(i_0{}'\,)^2 + (qi_0{}')^2} \tag{5.13}$$

The same SOGI based PLL block is used to identify the amplitude of the output of the resonant controller in order to be used in the voltage limiter to limit V_{qDC} reference value, according to the (5.15) derived from voltage limit equation (5.14).

$$V_{DC} = \sqrt{\left(V_{qDC\_lim} + \left|V_{qAC}{}^*\right|\right)^2 + V_d{}^2} \tag{5.14}$$

$$V_{qDC\_lim} = \sqrt{V_{DC}{}^2 - V_d{}^2} - \left|V_{qAC}{}^*\right| \tag{5.15}$$

where, V_{DC} is the bus voltage, V_{qDC_lim} is the limit value of the output of quadrature current loop PI, $\left|V_{qAC}{}^*\right|$ is the amplitude of the output oscillating signal of RC, and V_d is the quadrature voltage.

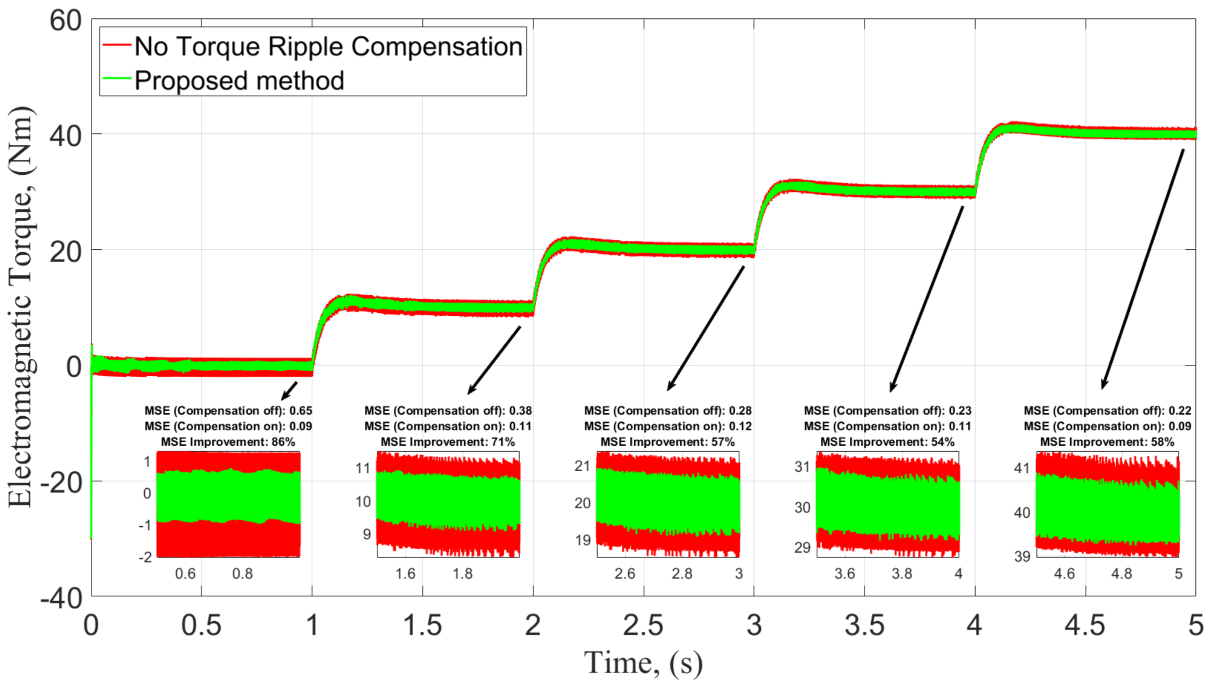

Fig. 5.8 – Electromagnetic torque comparison with MSE values

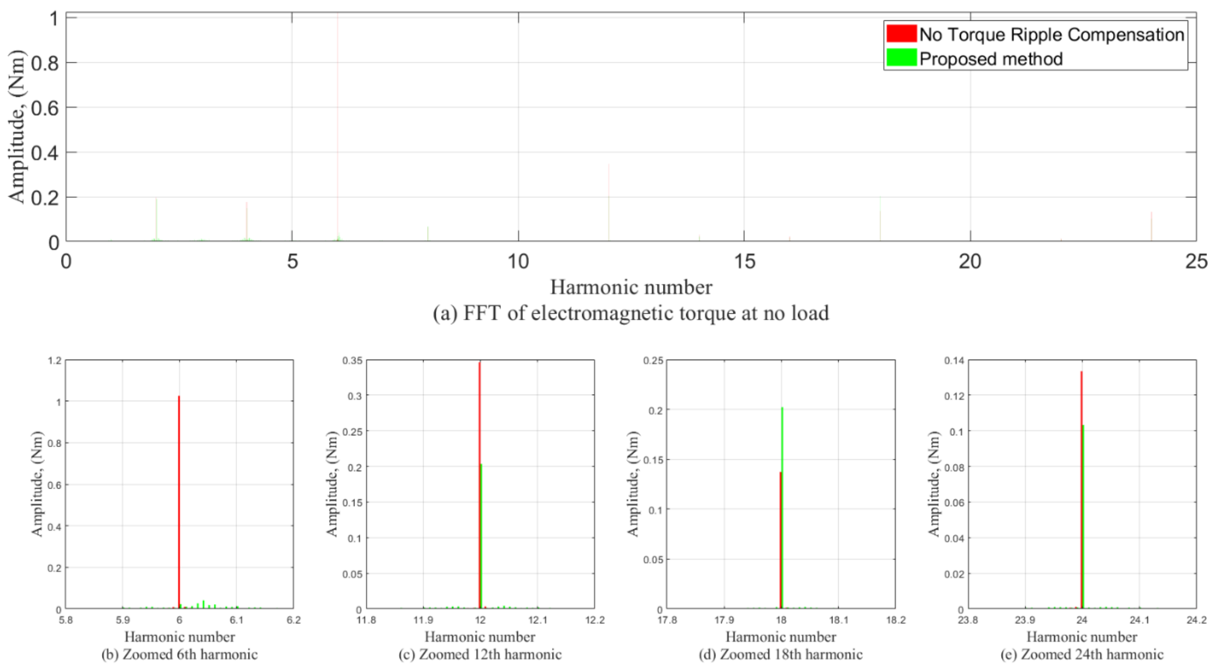

Fig. 5.9 – Electromagnetic torque FFT comparison (No load)

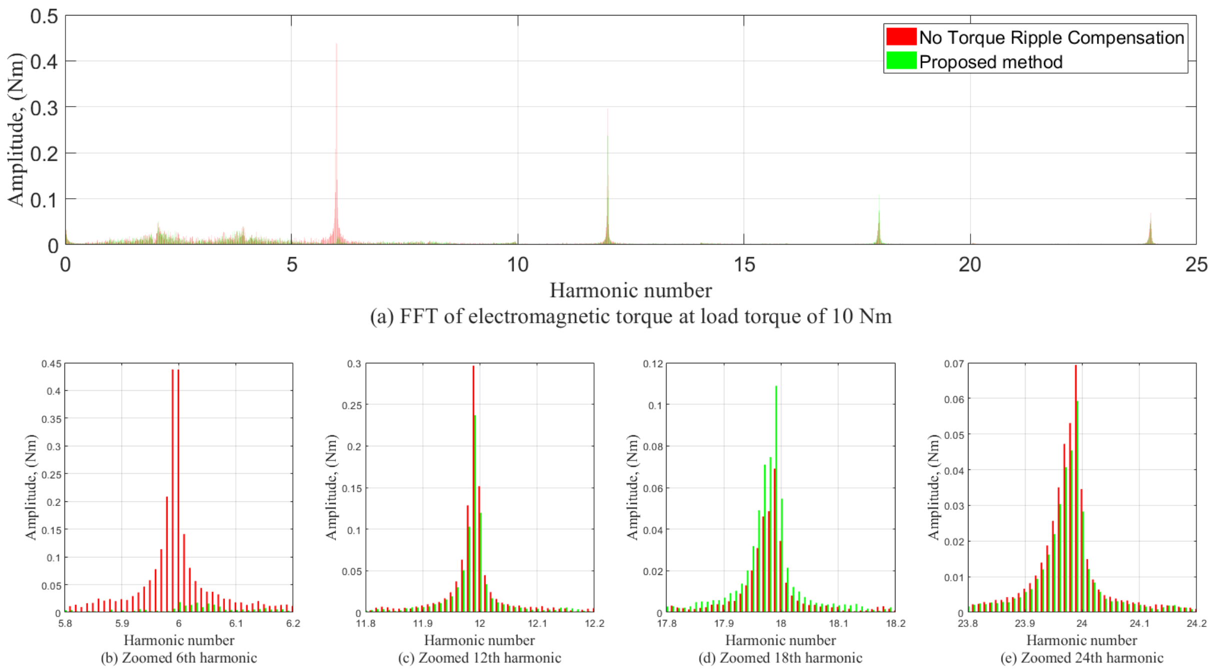

Fig. 5.10 – Electromagnetic torque FFT comparison (Load torque 10 Nm)

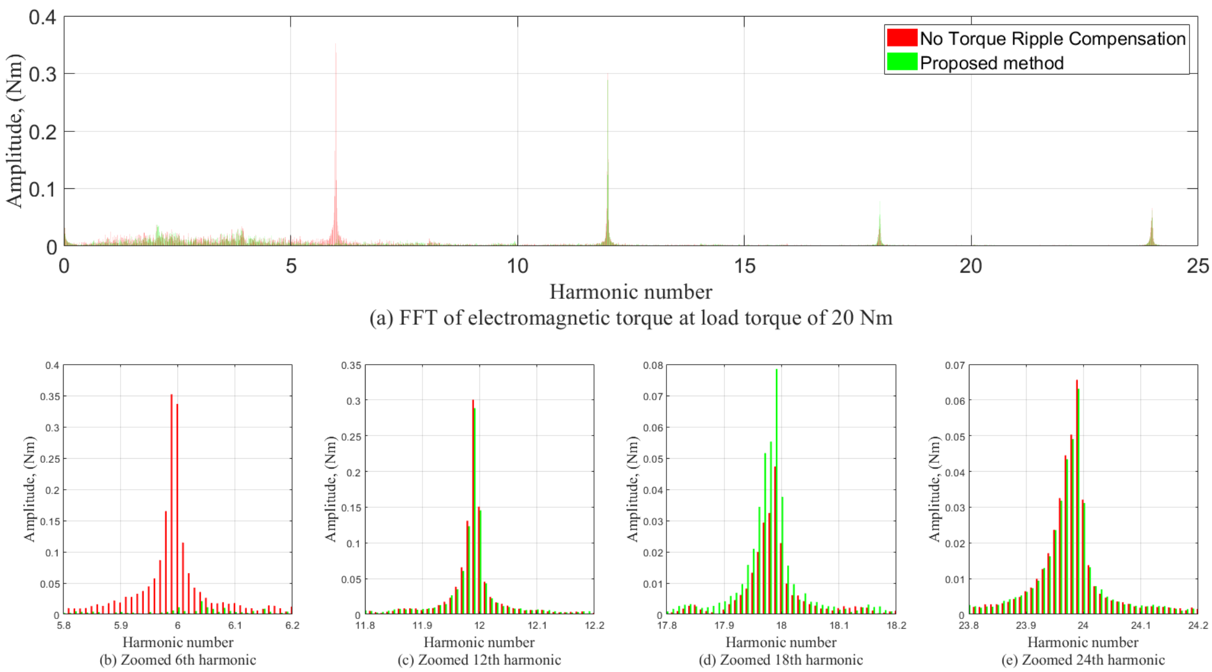

Fig. 5.11 – Electromagnetic torque FFT comparison (Load torque 20 Nm)

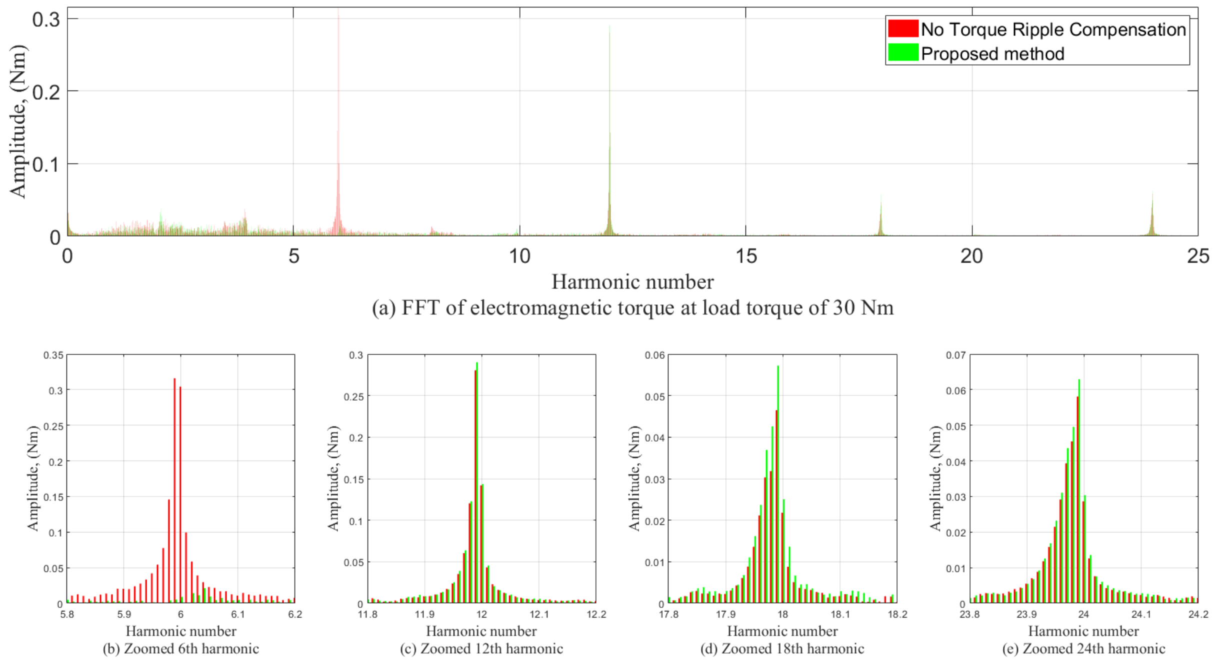

Fig. 5.12 – Electromagnetic torque FFT comparison (Load torque 30 Nm)

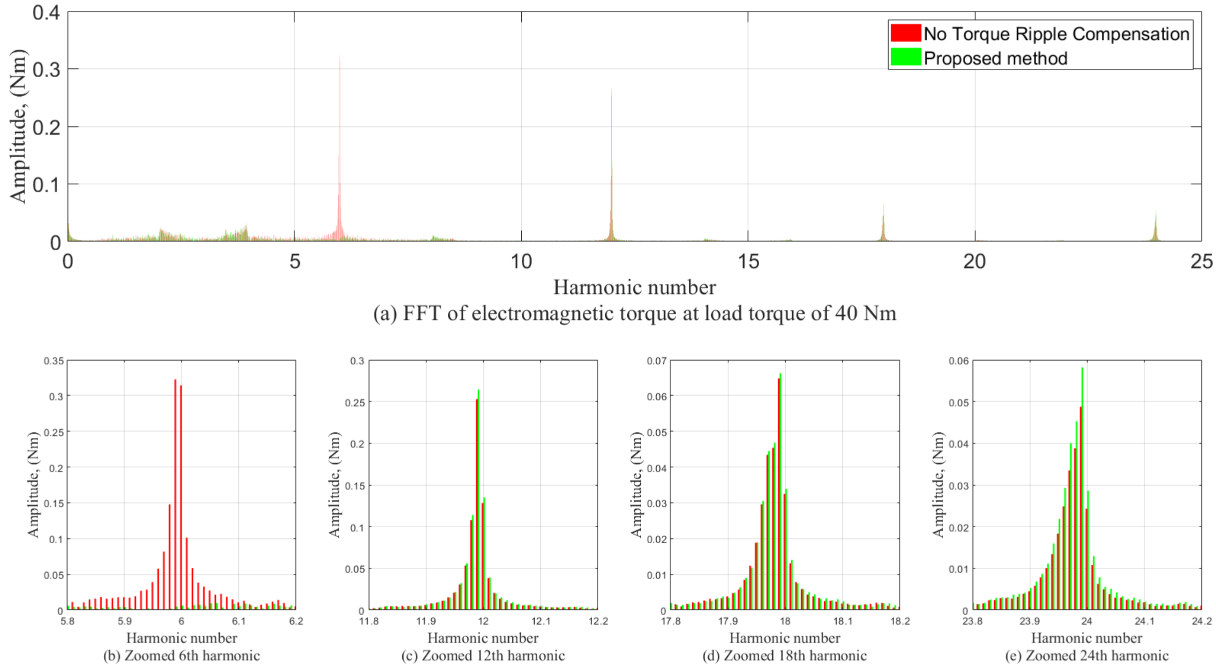

Fig. 5.13 – Electromagnetic torque FFT comparison (Load torque 40 Nm)

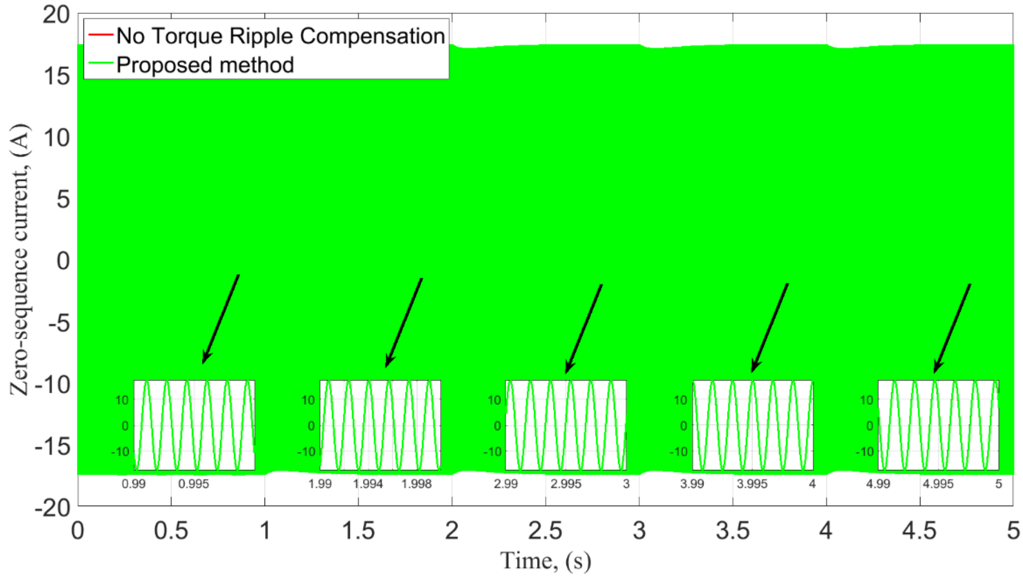

Fig. 5.14 – Zero-sequence current (i_0) comparison

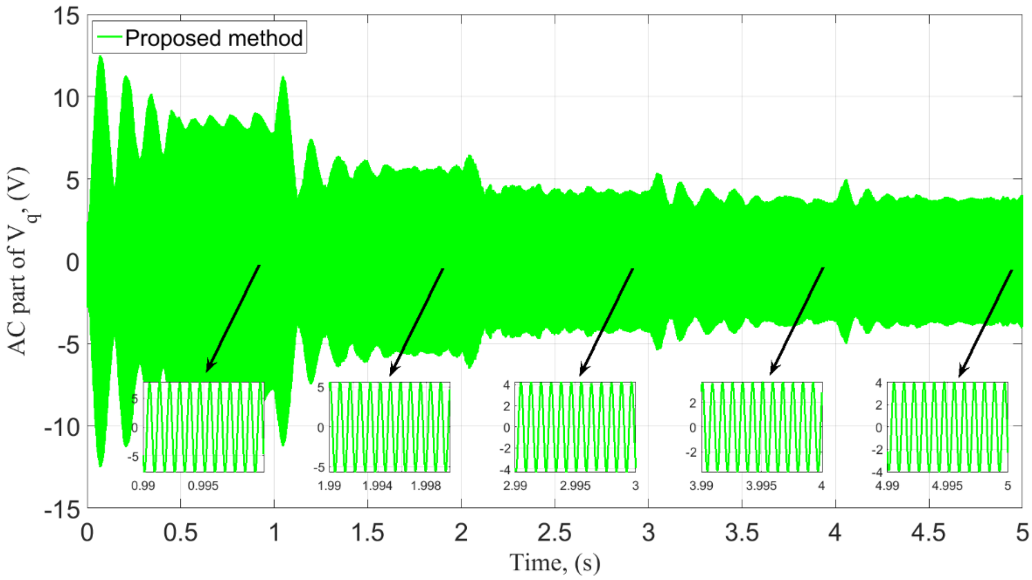

Fig. 5.15 – AC part of the quadrature axis voltage (V_{qAC})

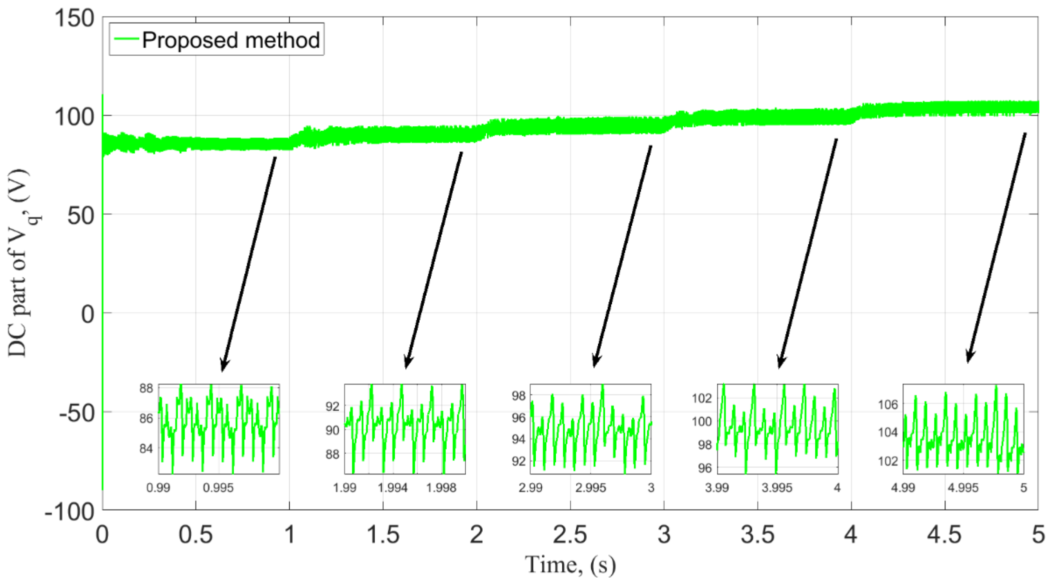

Fig. 5.16 – DC part of the quadrature axis voltage (V_{qDC})

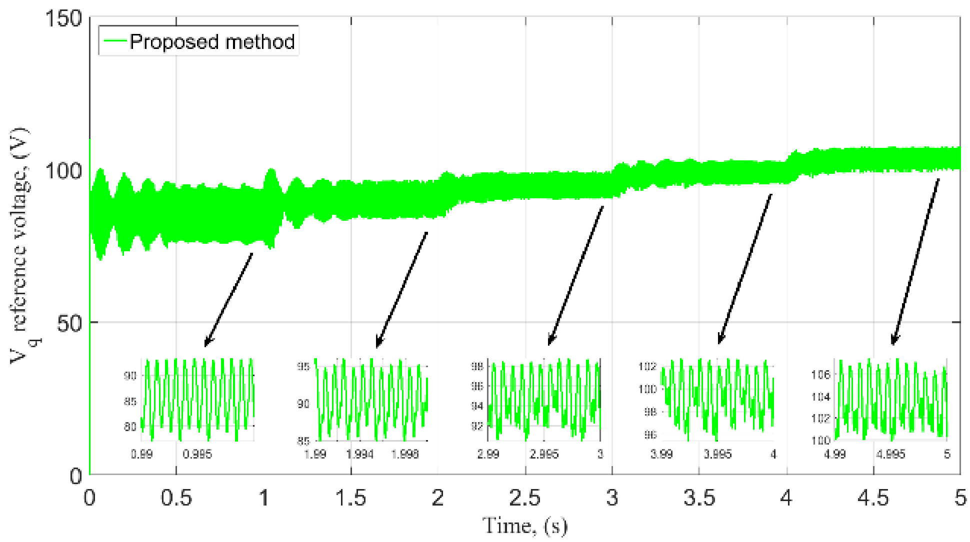

Fig. 5.17 – Quadrature axis voltage (V_q)

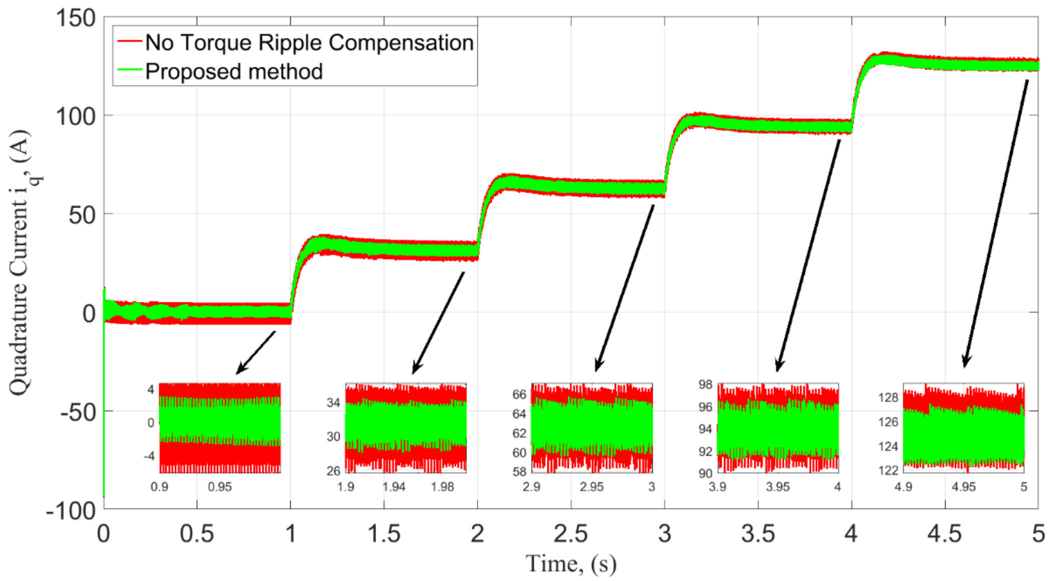

Fig. 5.18 – Quadrature axis current (i_q) comparison

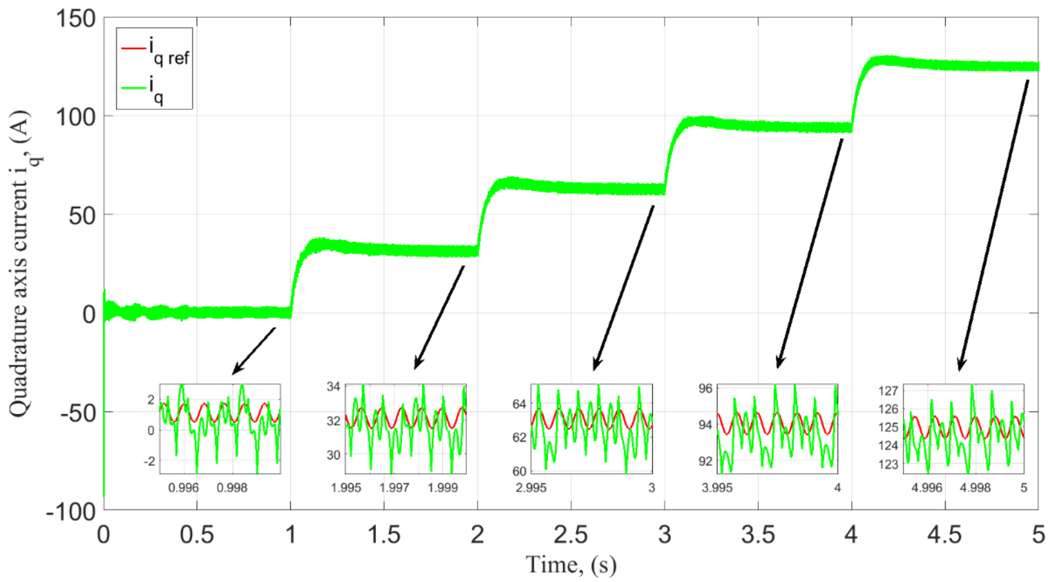

Fig. 5.19 – Quadrature axis current with reference (proposed control method)

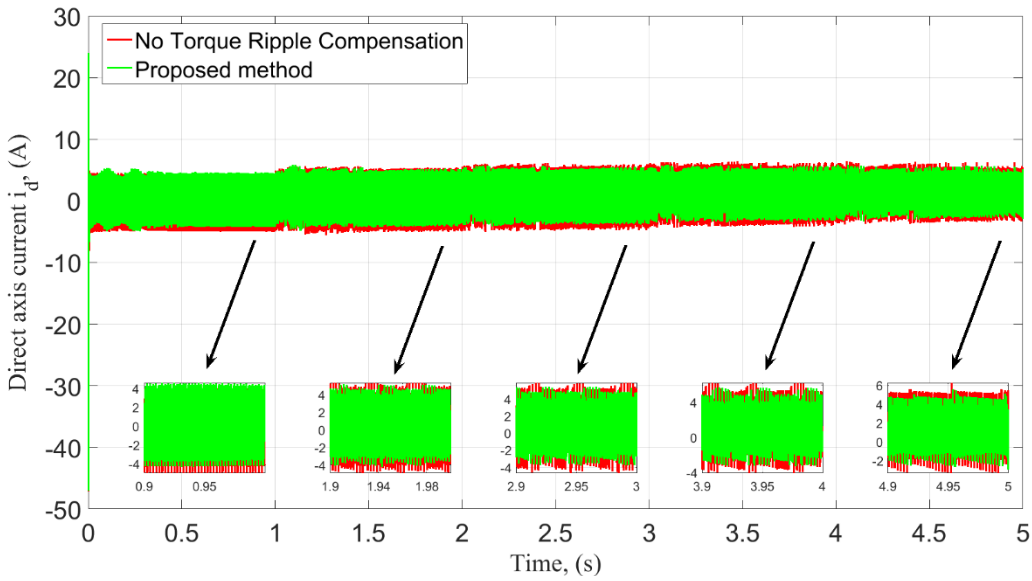

Fig. 5.20 – Direct axis current (i_d) comparison

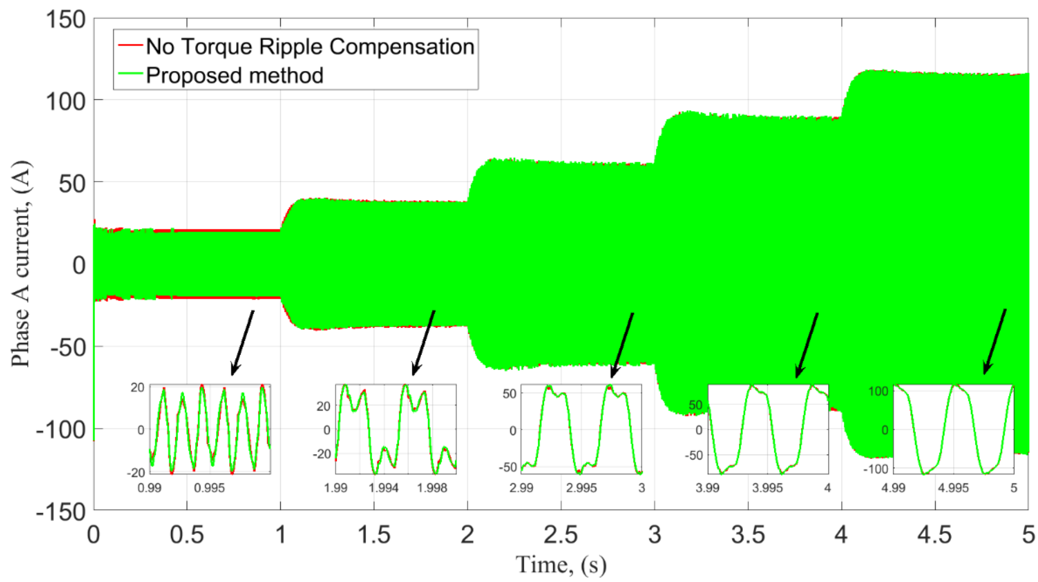

Fig. 5.21 – Phase A current (i_a) comparison

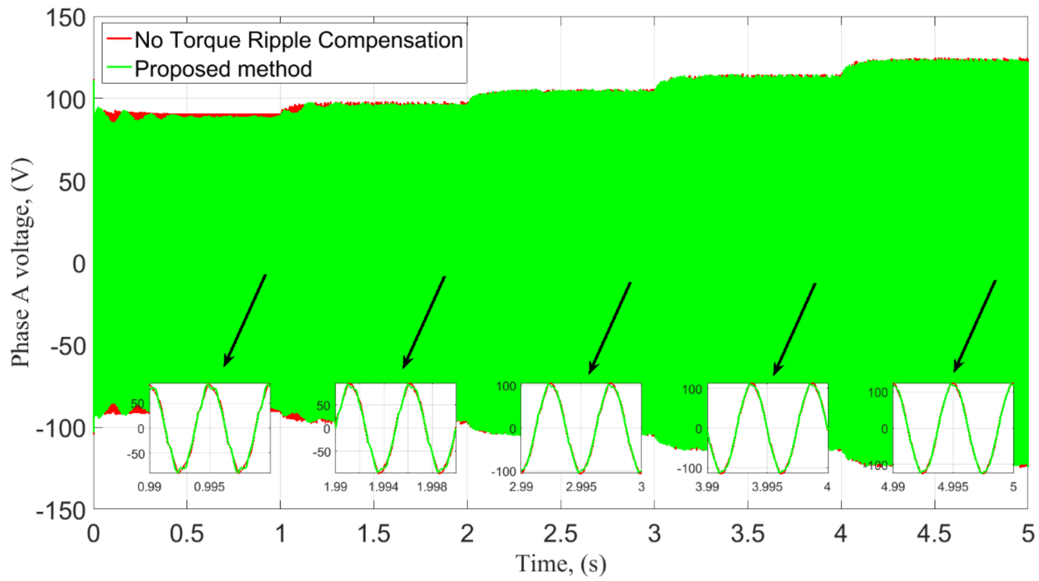

Fig. 5.22 – Phase A voltage (V_a) comparison

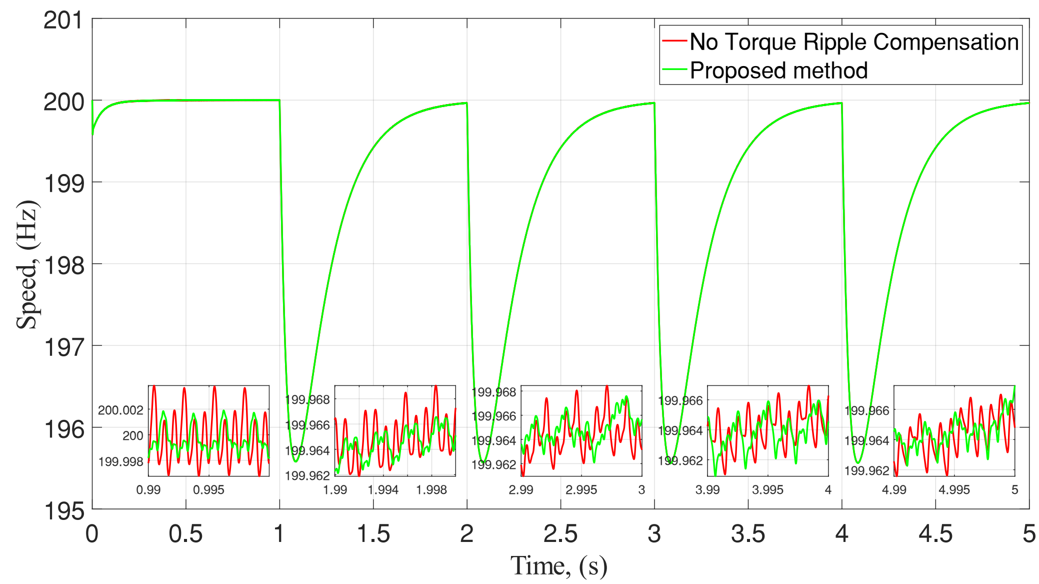

Fig. 5.23 – Electrical rotor speed during load transient

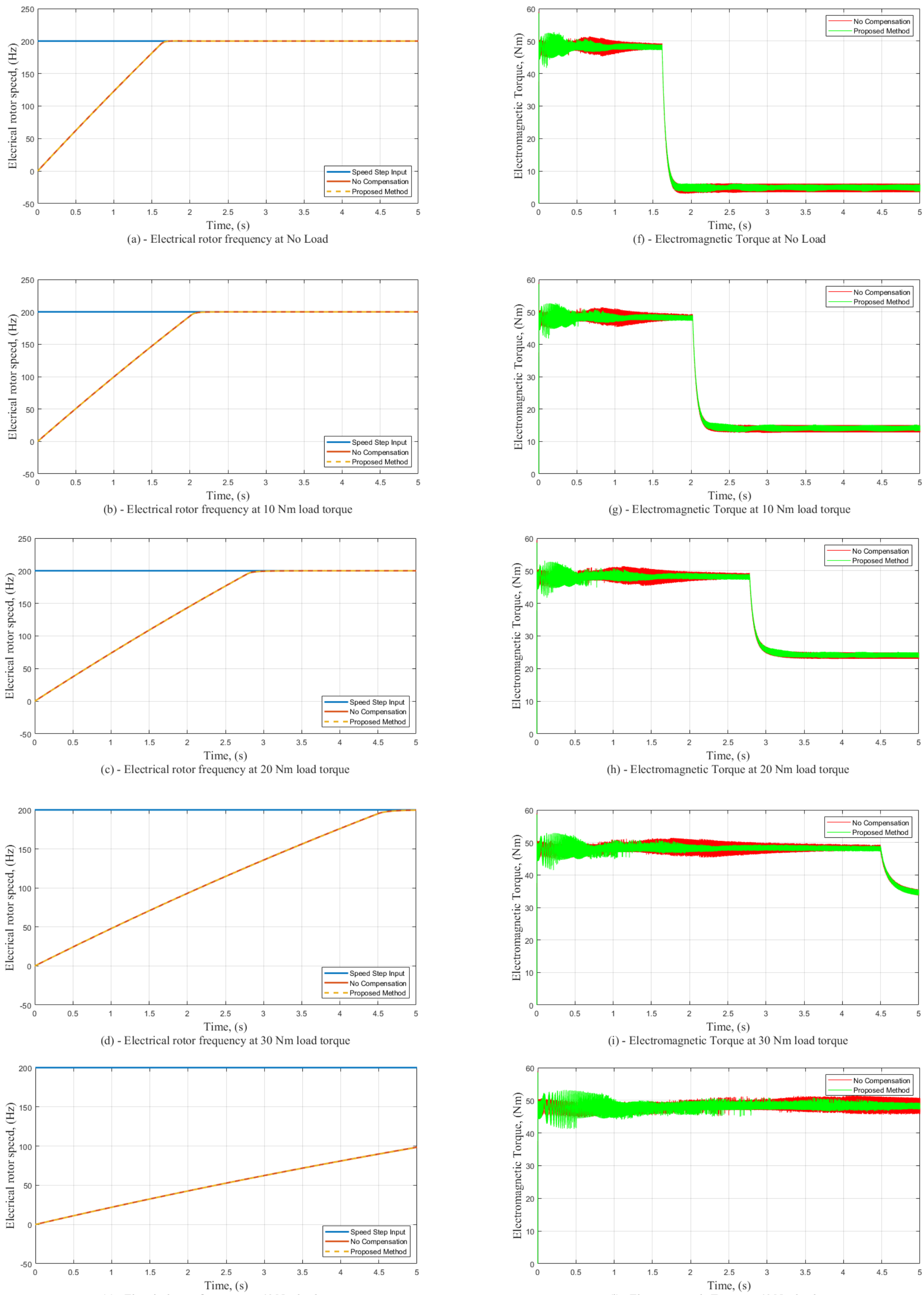

(a) - Electrical rotor frequency at No Load
(f) - Electromagnetic Torque at No Load
(b) - Electrical rotor frequency at 10 Nm load torque
(g) - Electromagnetic Torque at 10 Nm load torque
(c) - Electrical rotor frequency at 20 Nm load torque
(h) - Electromagnetic Torque at 20 Nm load torque
(d) - Electrical rotor frequency at 30 Nm load torque
(i) - Electromagnetic Torque at 30 Nm load torque
(e) - Electrical rotor frequency at 40 Nm load torque
(j) - Electromagnetic Torque at 40 Nm load torque

Fig. 5.24 – Electromagnetic torque during speed transient

During the simulation, the speed value was kept the same, at 200 Hz electrical frequency. The torque was increased in the following steps: 1, 10, 20, 30, and 40 Nm every second, respectively. The simulation results are shown in Fig. 5.8 - Fig. 5.22. It is clear that when the disturbance due to the inverter switching is introduced, the picture changes dramatically. The electrical torque ripple becomes considerably higher than the previously calculated value. Fig. 5.8 provides a comparative visual depiction of the electromagnetic torque output of the system shown in Fig. 5.6.

The proposed method is struggling to fully suppress the torque ripple, however, as it can be seen from the more accurate simulation results shown in Fig. 5.8 that there is still an improvement in the overall torque quality. The values of the absolute torque ripple were measured at each load torque step and recorder in TABLE IV.

TABLE IV Torque quality improvement – Peak-to-Peak (Simulation)

Load Torque, (Nm)	**Peak-to-Peak Torque Ripple, (Nm)**		**Improvement due to the Proposed Method, (%)**
	No Compensation	**Proposed Method**	
1	3.29	1.66	49.50
10	3.05	1.72	43.53
20	2.71	1.65	39.20
30	2.31	1.44	37.86
40	2.28	1.44	37.04

Considering the results shown in TABLE IV the proposed method still results in the improvement of the torque quality of up to 49.5%.

The current ripple of both the quadrature and the direct axis currents shown in Fig. 5.18 and Fig. 5.20 appears to be reduced as well. However, according to Fig. 5.19, it appears that the quadrature current is not following the reference, but, judging by the stability of the generated AC part of the quadrature axis voltage in Fig. 5.15 it can be concluded that the torque ripple harmonic due to the third harmonic back EMF that was subjected to be suppressed was, indeed, suppressed.

Mean Squared Error (MSE) values with respect to the average torque were calculated using the formular from Appendix C and recorded in TABLE V. The Improvement in MSE is up to 86%

TABLE V Torque quality improvement – MSE (Simulation)

Load Torque, (Nm)	**Mean Squared Error (MSE)**		**Improvement due to the Proposed Method, (%)**
	No Compensation	**Proposed Method**	
1	0.65	0.09	86
10	0.38	0.11	71
20	0.28	0.12	57
30	0.23	0.11	54
40	0.22	0.09	58

Fig. 5.23 shows that every change of the load value for the motor introduced the change of speed. The simulation showed that the speed returns to its original value within one second on every 10 Nm change. Fig. 5.24 show the behaviour of the controlled torque during the speed transient. The value of one second transient is confirmed through the speed step simulation. It can be seen from the simulation result that RC settles the torque value in around one second during the speed transient.

A synchronous controller could have been introduced to control the oscillations of the quadrature current such as the one proposed by Angelo Accetta, Marcello Pucci and others in [106]. This would have allowed to compare the transient behaviour of the controllers. However, the resonant controller used in the proposed control is not a regular resonant controller. It is an adaptive resonant controller. It has a bandwidth value in order to deal with the transients when the speed of the motor changes. In addition, the presented synchronous controller would require the actual value of the angle of the 6^{th} harmonic of the quadrature current. This includes the zero-sequence current phase shift which can be estimated using the values of the phase resistance, the zero-sequence inductance and the speed. Also, the response of the presented synchronous controller depends on the introduced high pass filters in order to separate the quadrature and direct current components from their DC values. This complicated the control further. As a whole, the adaptive resonant controller is a much simpler version that is less parameter dependent as well.

5.4Experimental Results

The experimental setup that was used to test the proposed method is described in chapter 4 on page 77. The switching frequency of the inverter was set to be 40 kHz through the control board described in chapter 4 on page 79. The experiment was conducted across the range of both the machine speeds from 500 rpm to 5500 rpm with a step of 500 rpm (Fig. 5.25-Fig. 5.35) and the load currents of the following values: 0 A (No Load), 10 A, 30 A, and 50 A. The electromagnetic torque was estimated, using the equation (3.46) derived in chapter 3 on page 47.

Considering the results in Fig. 5.25-Fig. 5.35, TQI is the torque quality improvement represented in percentage of the original peak to peak torque ripple value. The formula for this value along with a sample calculation of the presented torque quality improvement can be found in Appendix C.

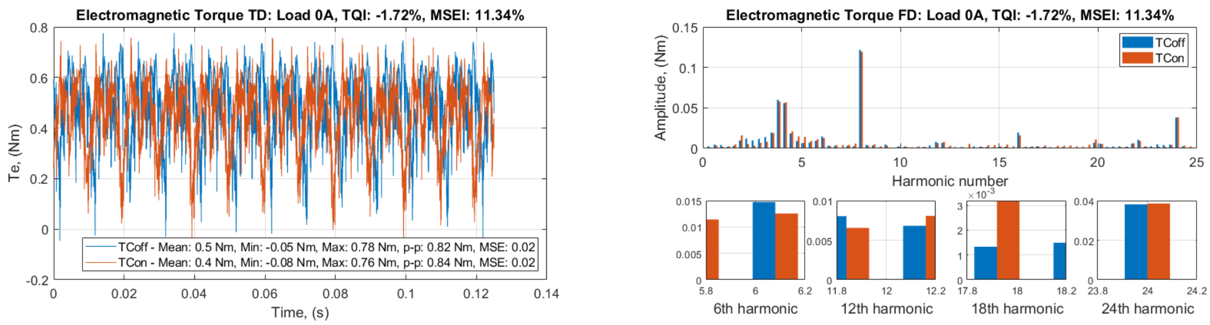

(a) Time Domain (TD) and Frequency Domain (FD) Electromagnetic Torque at Load Current of 0A

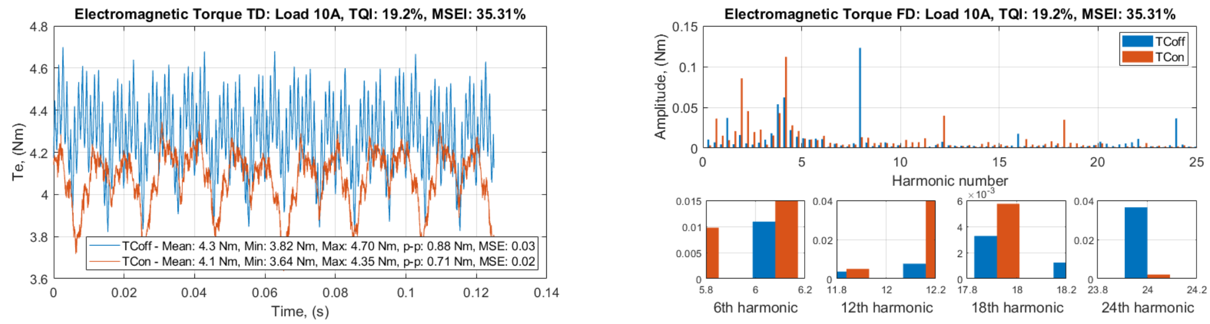

(b) Time Domain (TD) and Frequency Domain (FD) Electromagnetic Torque at Load Current of 10A

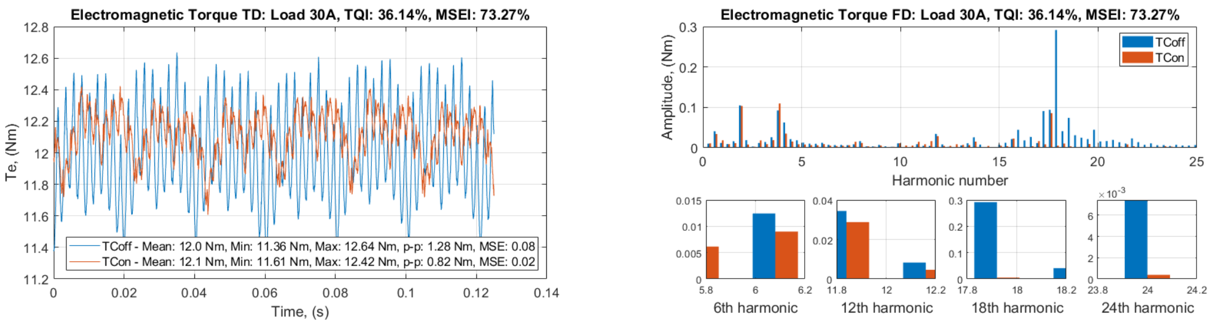

(c) Time Domain (TD) and Frequency Domain (FD) Electromagnetic Torque at Load Current of 30A

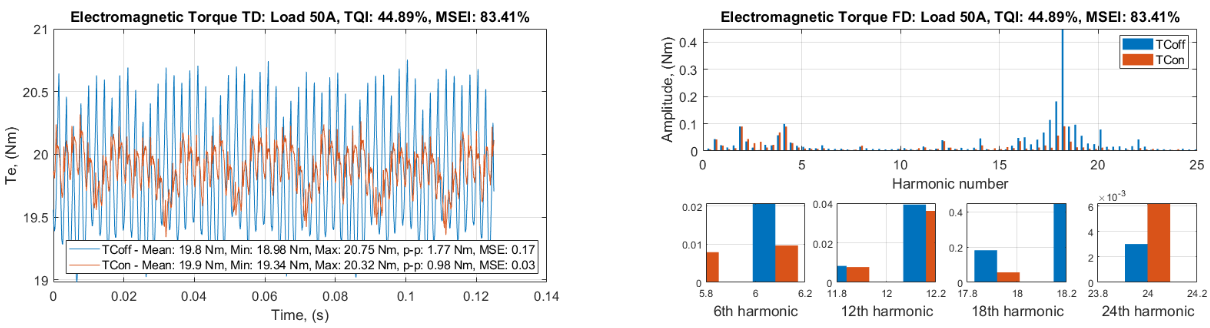

(d) Time Domain (TD) and Frequency Domain (FD) Electromagnetic Torque at Load Current of 50A

Fig. 5.25 – Torque comparison across the range of load currents at 500 rpm

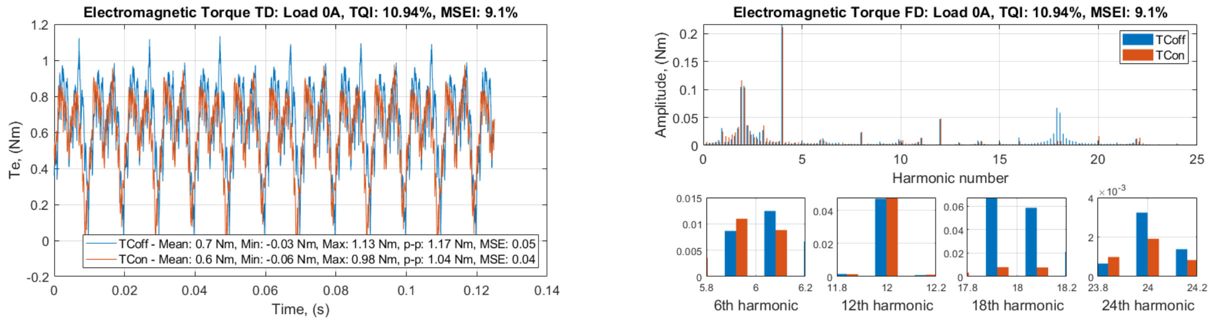

(a) Time Domain (TD) and Frequency Domain (FD) Electromagnetic Torque at Load Current of 0A

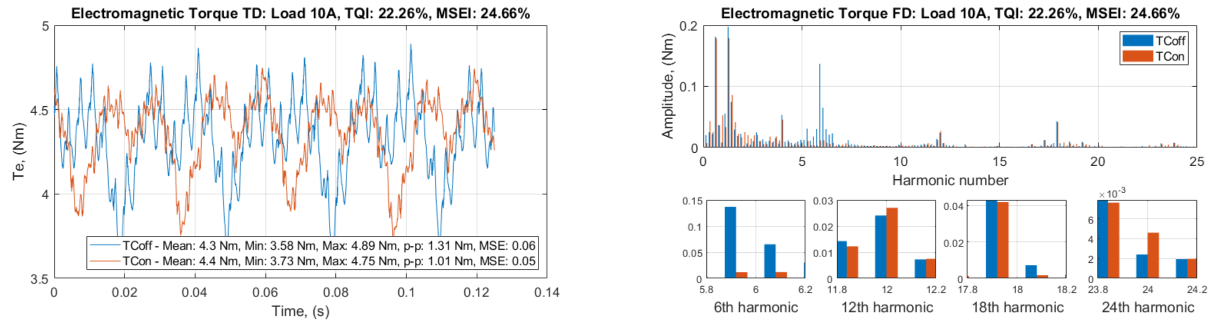

(b) Time Domain (TD) and Frequency Domain (FD) Electromagnetic Torque at Load Current of 10A

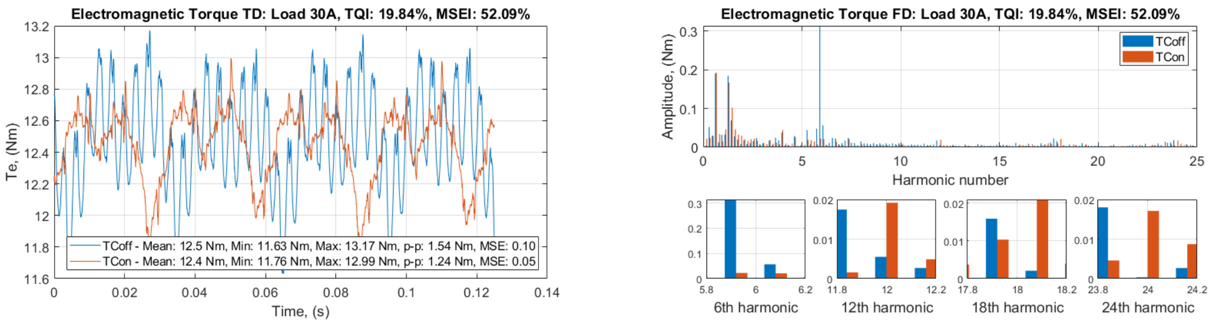

(c) Time Domain (TD) and Frequency Domain (FD) Electromagnetic Torque at Load Current of 30A

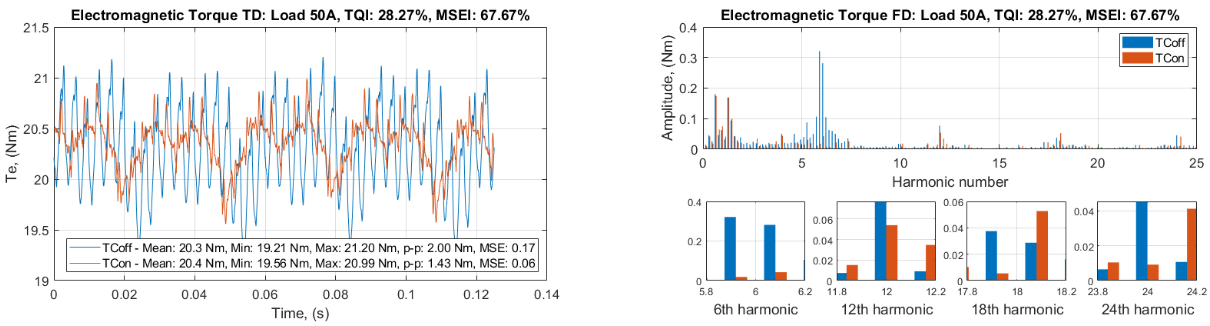

(d) Time Domain (TD) and Frequency Domain (FD) Electromagnetic Torque at Load Current of 50A

Fig. 5.26 – Torque comparison across the range of load currents at 1000 rpm

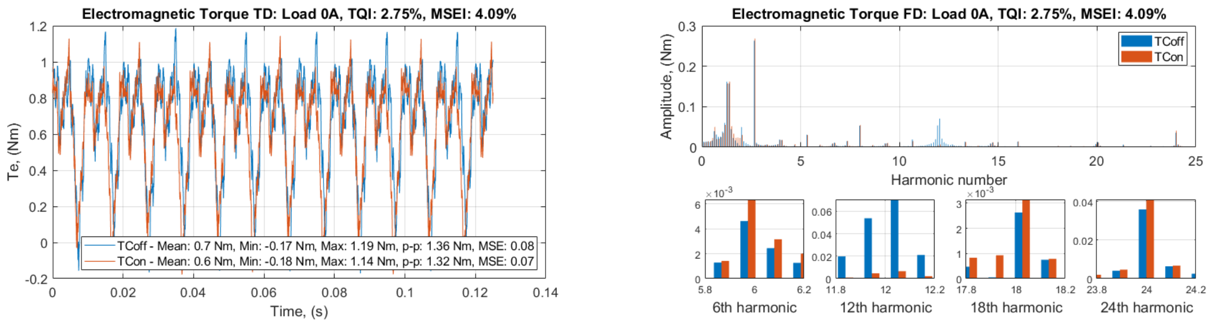

(a) Time Domain (TD) and Frequency Domain (FD) Electromagnetic Torque at Load Current of 0A

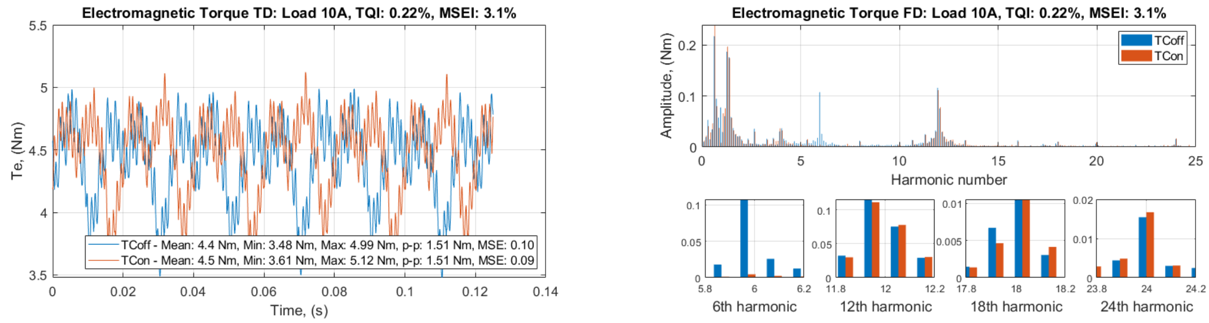

(b) Time Domain (TD) and Frequency Domain (FD) Electromagnetic Torque at Load Current of 10A

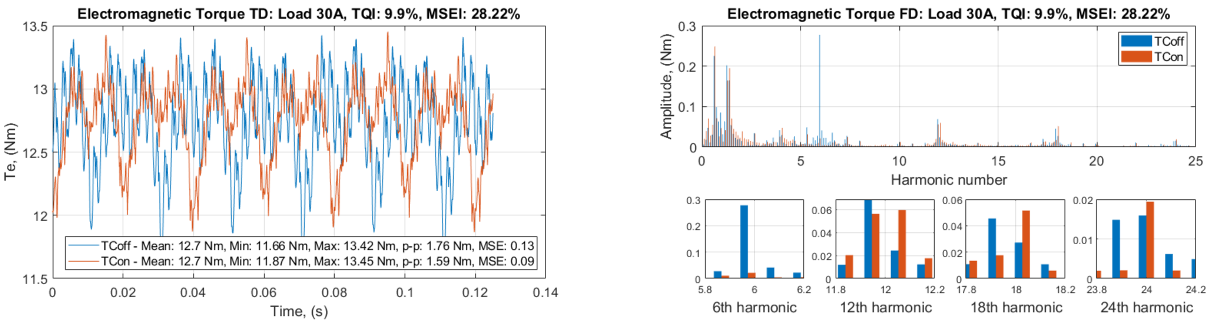

(c) Time Domain (TD) and Frequency Domain (FD) Electromagnetic Torque at Load Current of 30A

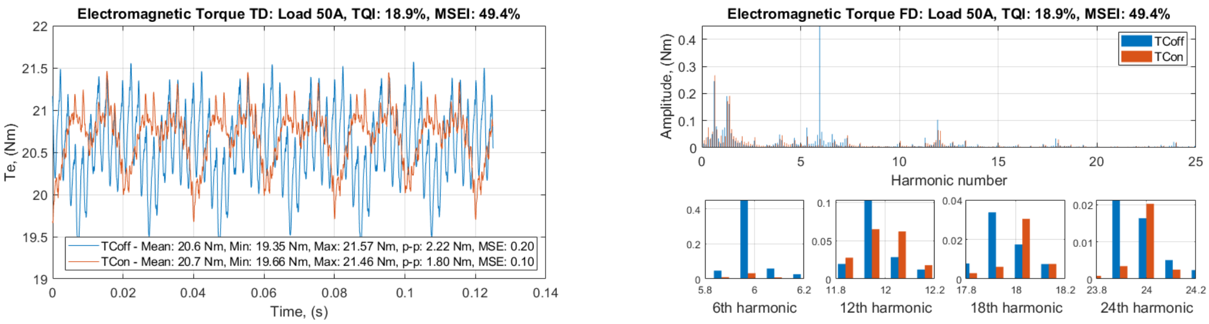

(d) Time Domain (TD) and Frequency Domain (FD) Electromagnetic Torque at Load Current of 50A

Fig. 5.27 – Torque comparison across the range of load currents at 1500 rpm

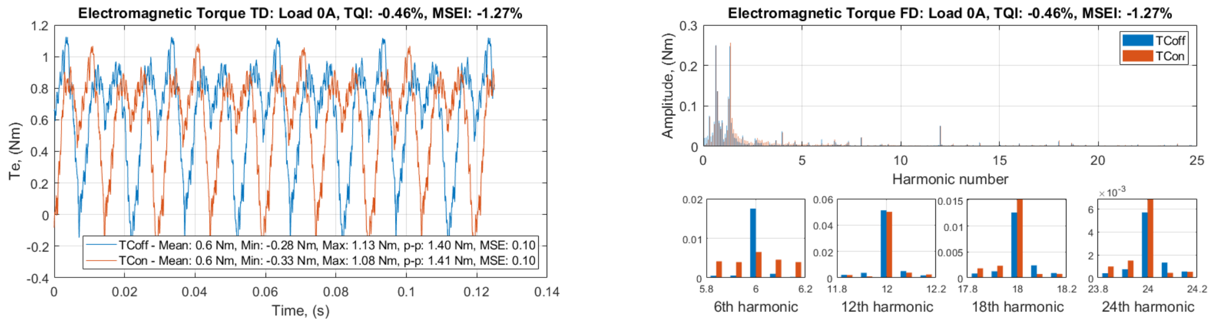

(a) Time Domain (TD) and Frequency Domain (FD) Electromagnetic Torque at Load Current of 0A

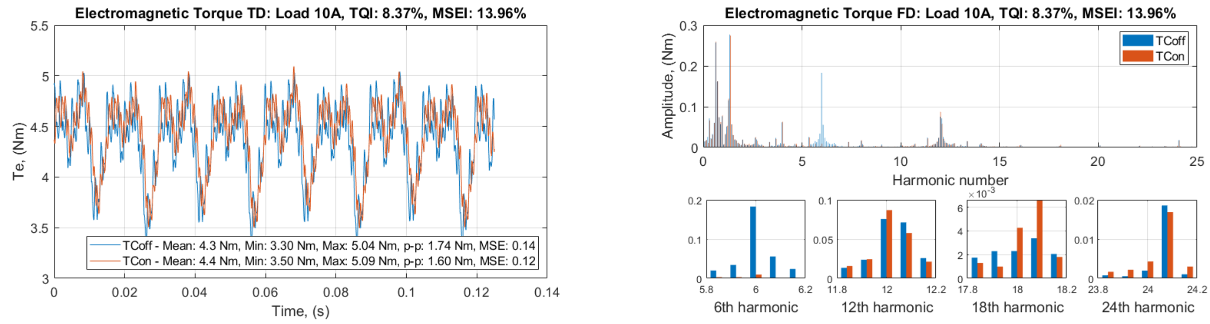

(b) Time Domain (TD) and Frequency Domain (FD) Electromagnetic Torque at Load Current of 10A

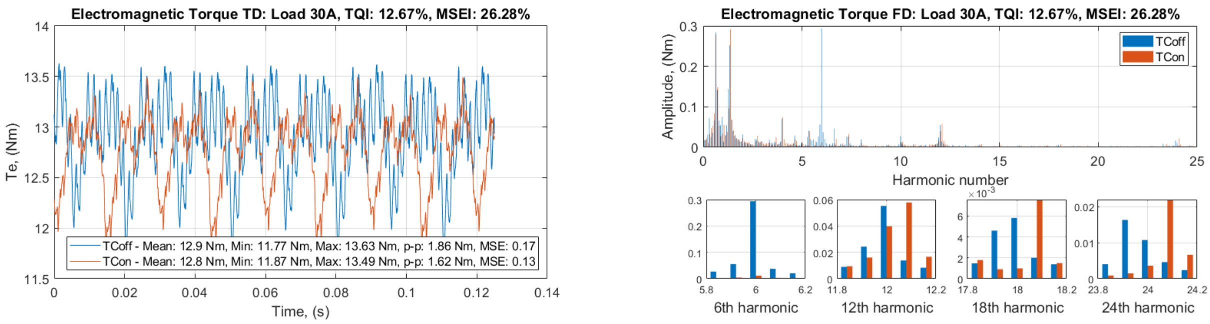

(c) Time Domain (TD) and Frequency Domain (FD) Electromagnetic Torque at Load Current of 30A

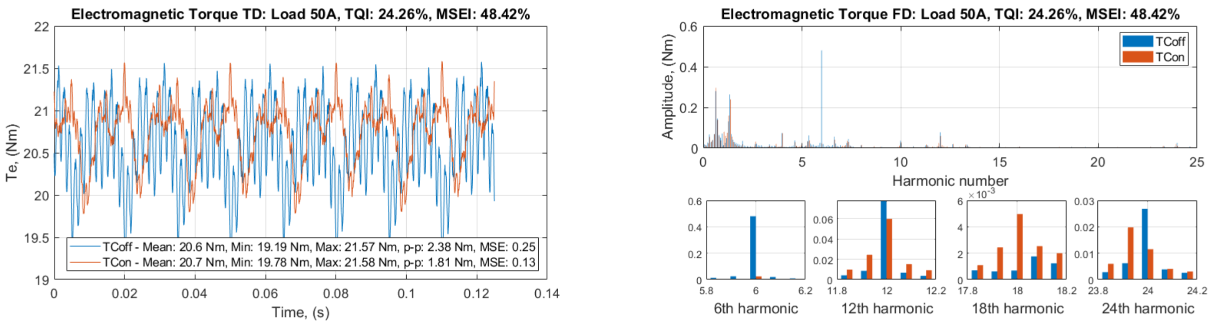

(d) Time Domain (TD) and Frequency Domain (FD) Electromagnetic Torque at Load Current of 50A

Fig. 5.28 – Torque comparison across the range of load currents at 2000 rpm

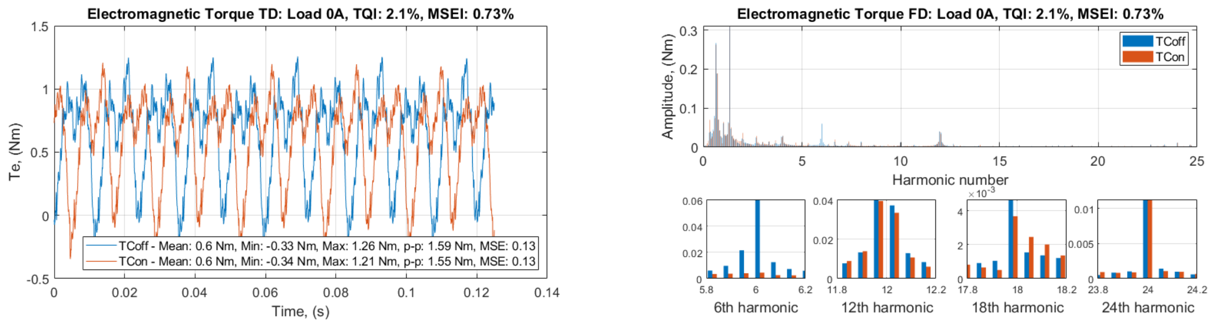

(a) Time Domain (TD) and Frequency Domain (FD) Electromagnetic Torque at Load Current of 0A

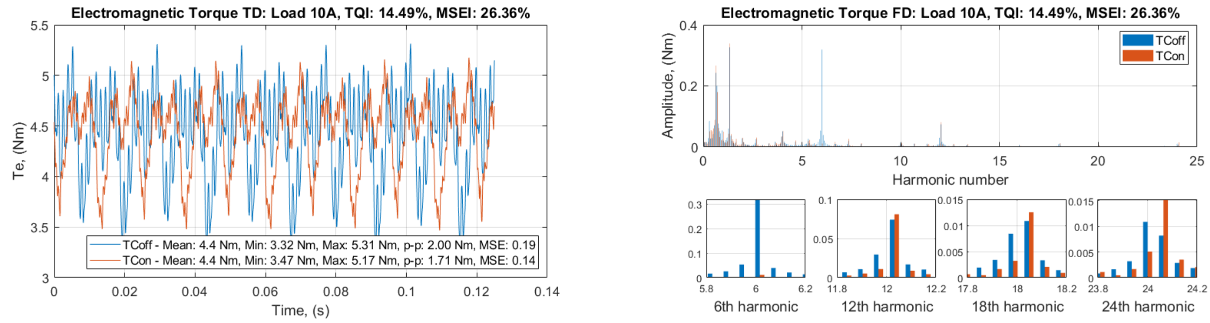

(b) Time Domain (TD) and Frequency Domain (FD) Electromagnetic Torque at Load Current of 10A

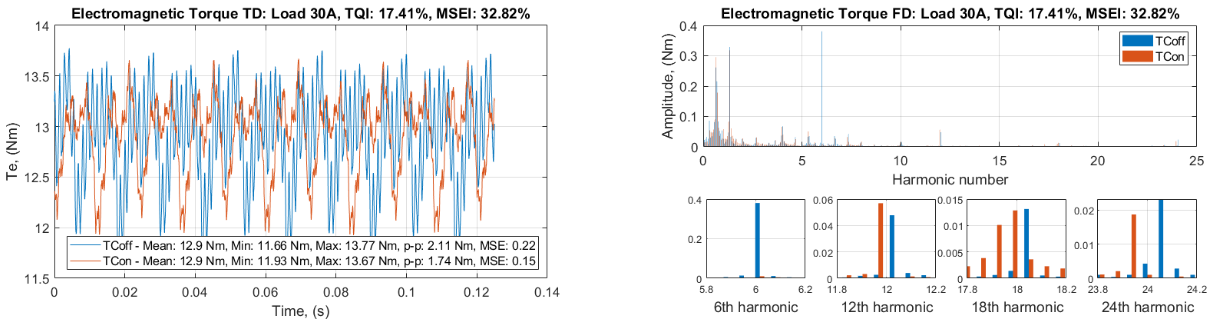

(c) Time Domain (TD) and Frequency Domain (FD) Electromagnetic Torque at Load Current of 30A

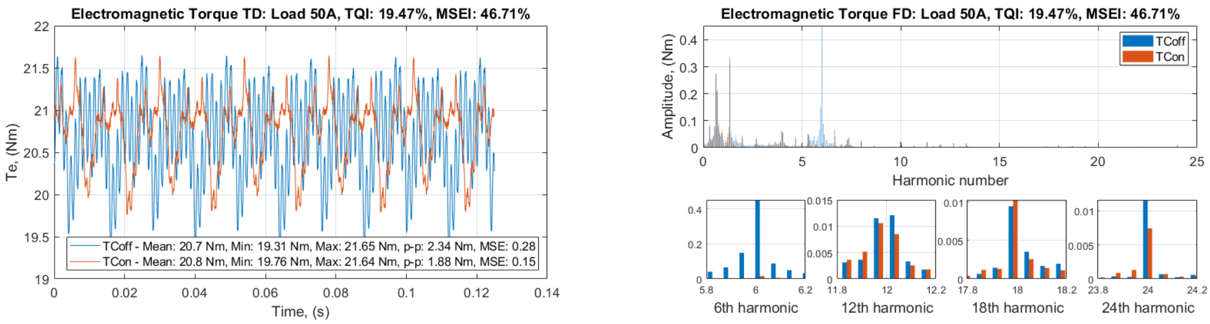

(d) Time Domain (TD) and Frequency Domain (FD) Electromagnetic Torque at Load Current of 50A

Fig. 5.29 – Torque comparison across the range of load currents at 2500 rpm

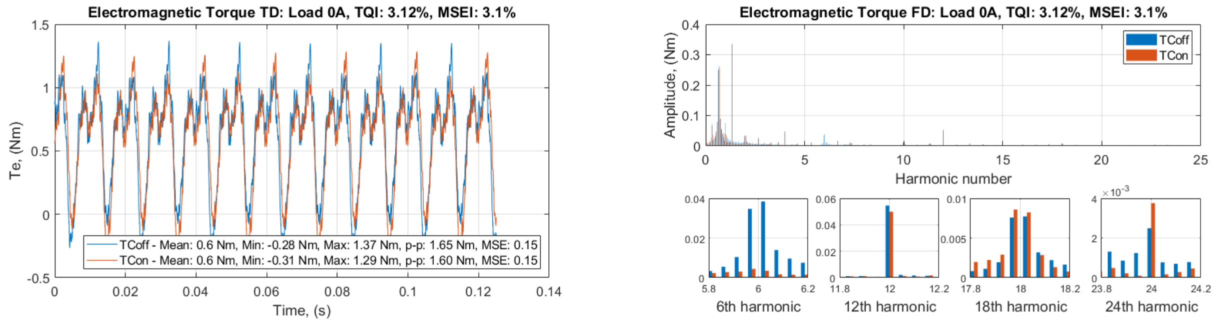

(a) Time Domain (TD) and Frequency Domain (FD) Electromagnetic Torque at Load Current of 0A

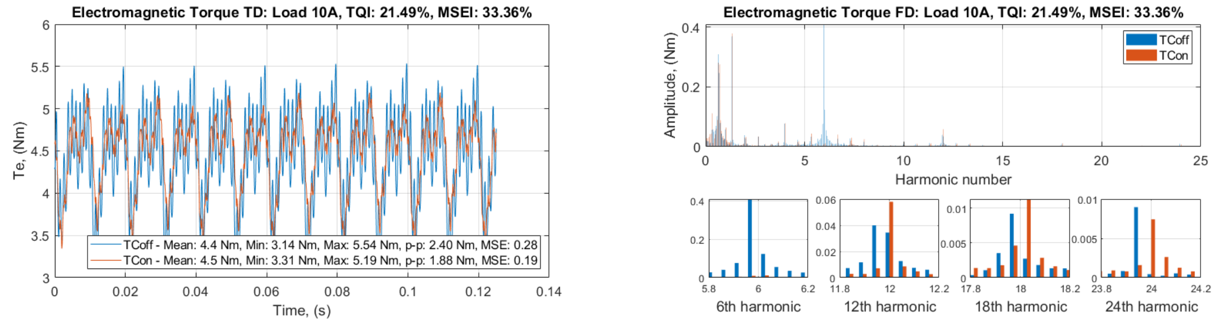

(b) Time Domain (TD) and Frequency Domain (FD) Electromagnetic Torque at Load Current of 10A

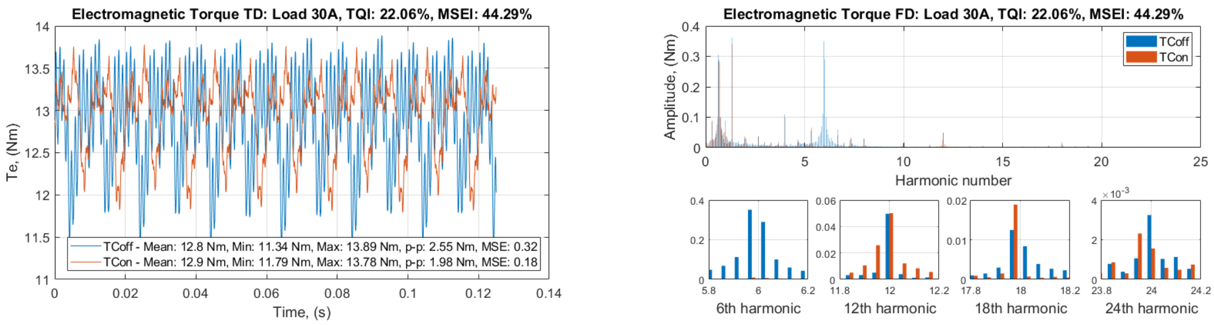

(c) Time Domain (TD) and Frequency Domain (FD) Electromagnetic Torque at Load Current of 30A

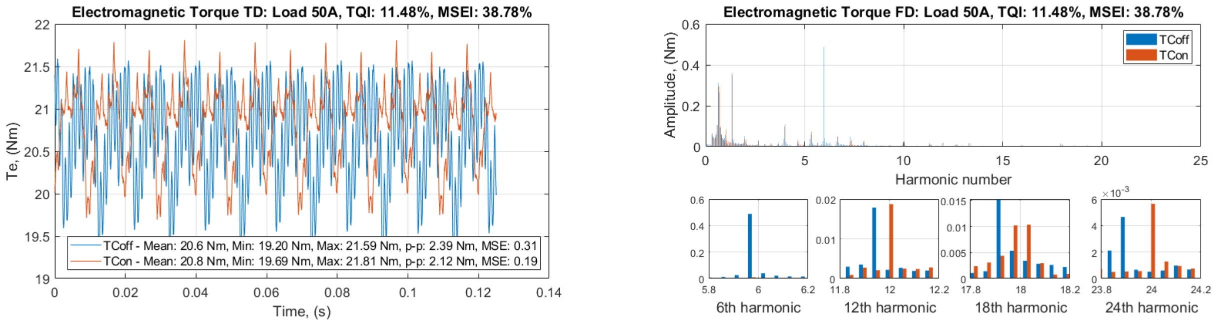

(d) Time Domain (TD) and Frequency Domain (FD) Electromagnetic Torque at Load Current of 50A

Fig. 5.30 – Torque comparison across the range of load currents at 3000 rpm

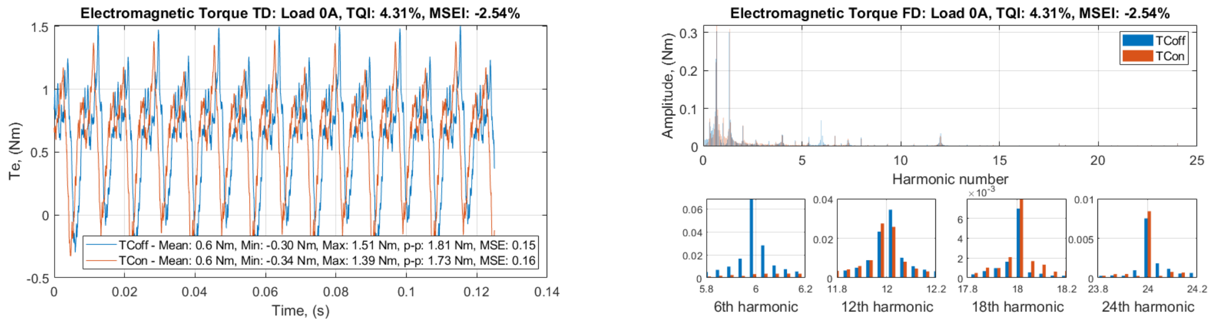

(a) Time Domain (TD) and Frequency Domain (FD) Electromagnetic Torque at Load Current of 0A

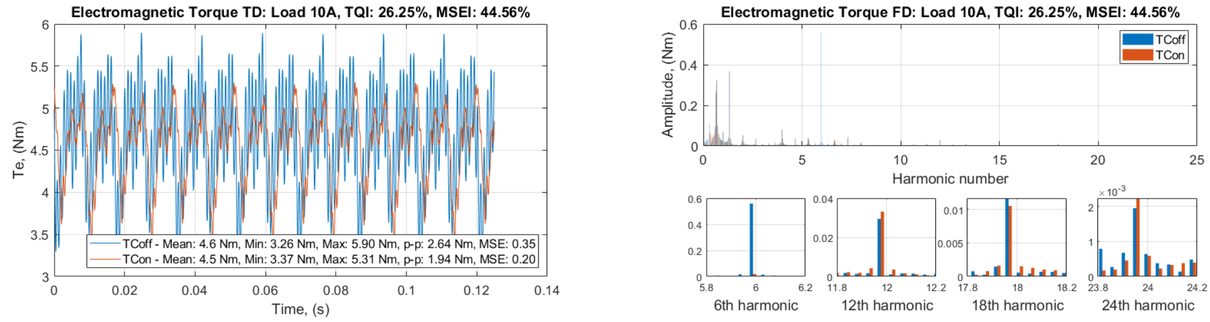

(b) Time Domain (TD) and Frequency Domain (FD) Electromagnetic Torque at Load Current of 10A

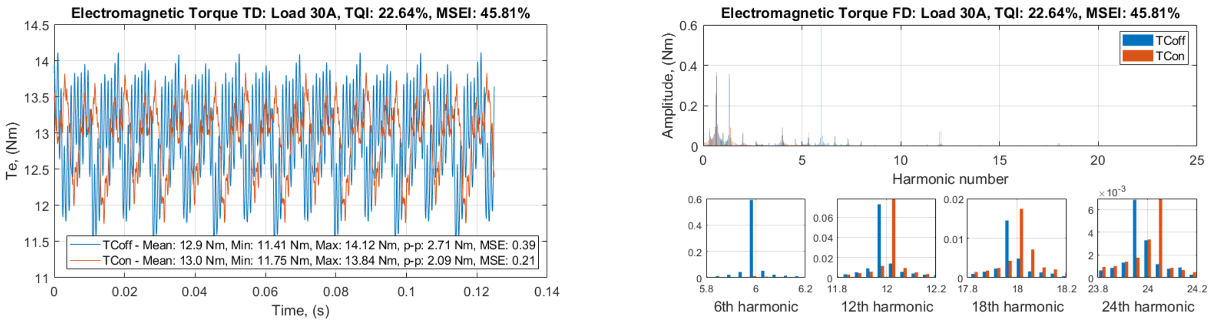

(c) Time Domain (TD) and Frequency Domain (FD) Electromagnetic Torque at Load Current of 30A

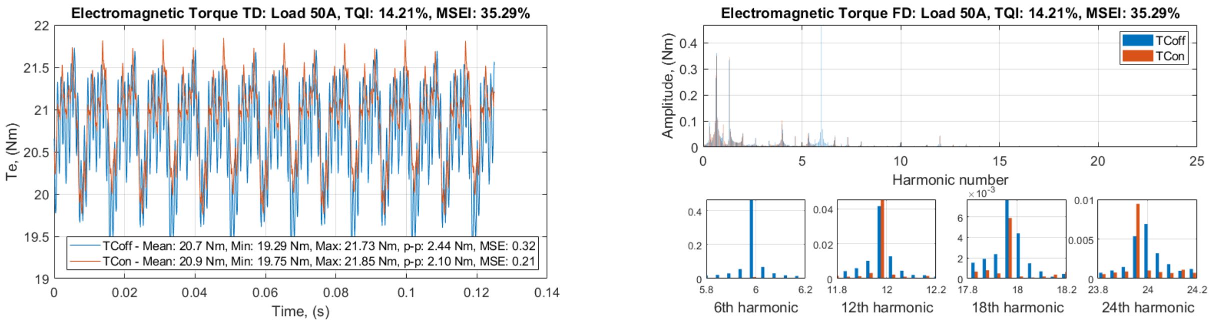

(d) Time Domain (TD) and Frequency Domain (FD) Electromagnetic Torque at Load Current of 50A

Fig. 5.31 – Torque comparison across the range of load currents at 3500 rpm

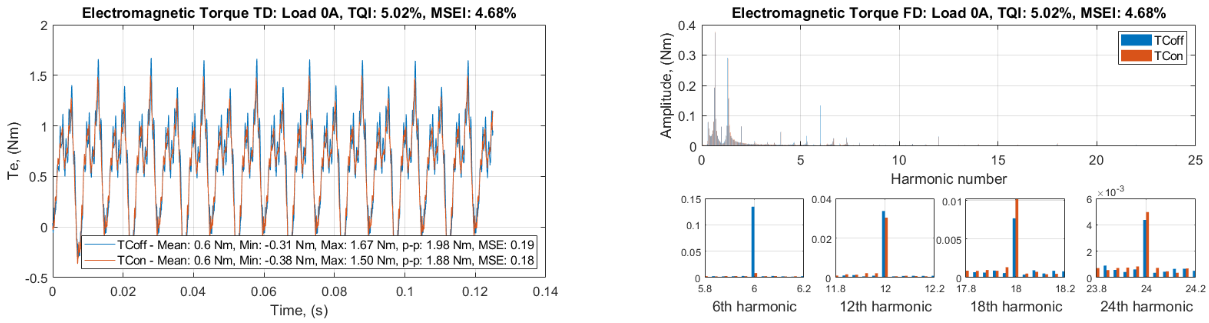

(a) Time Domain (TD) and Frequency Domain (FD) Electromagnetic Torque at Load Current of 0A

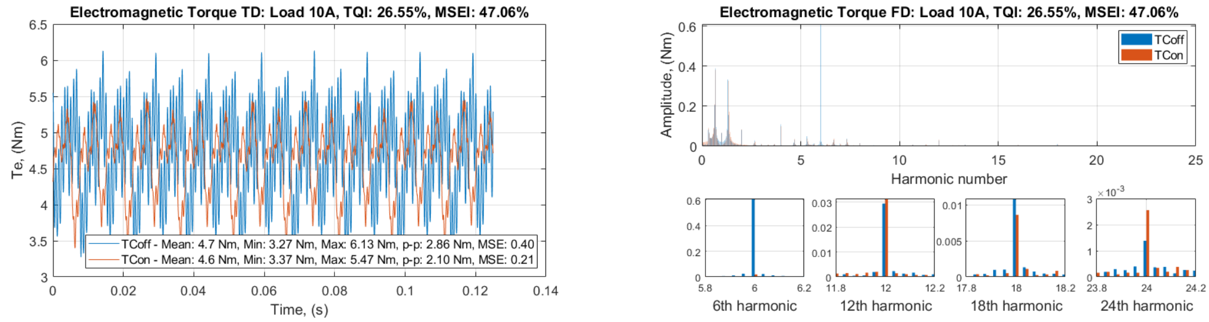

(b) Time Domain (TD) and Frequency Domain (FD) Electromagnetic Torque at Load Current of 10A

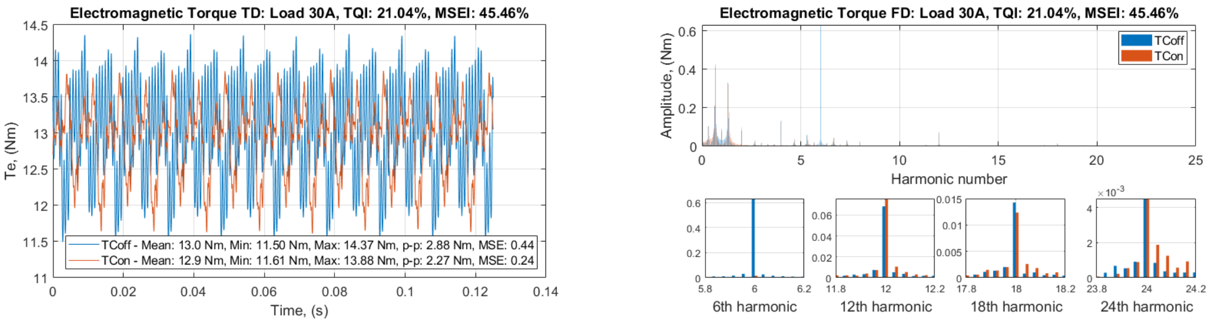

(c) Time Domain (TD) and Frequency Domain (FD) Electromagnetic Torque at Load Current of 30A

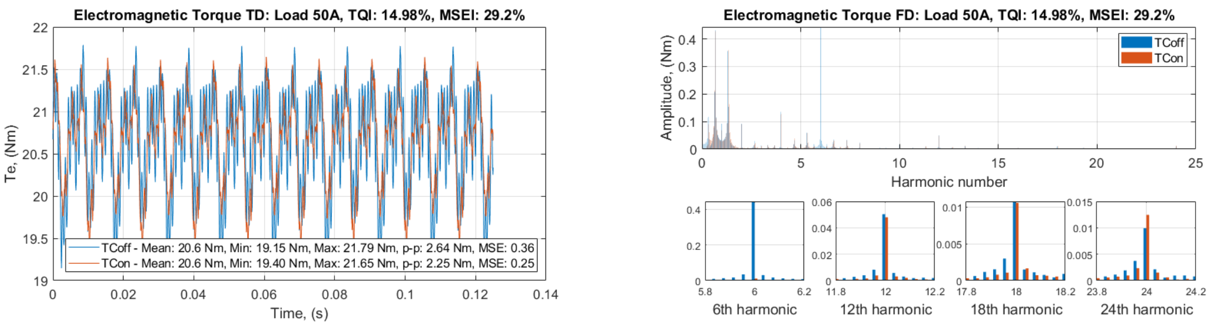

(d) Time Domain (TD) and Frequency Domain (FD) Electromagnetic Torque at Load Current of 50A

Fig. 5.32 – Torque comparison across the range of load currents at 4000 rpm

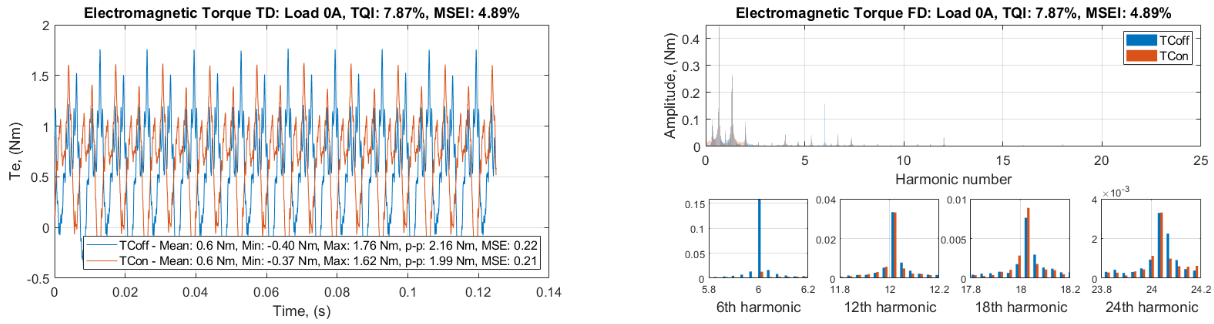

(a) Time Domain (TD) and Frequency Domain (FD) Electromagnetic Torque at Load Current of 0A

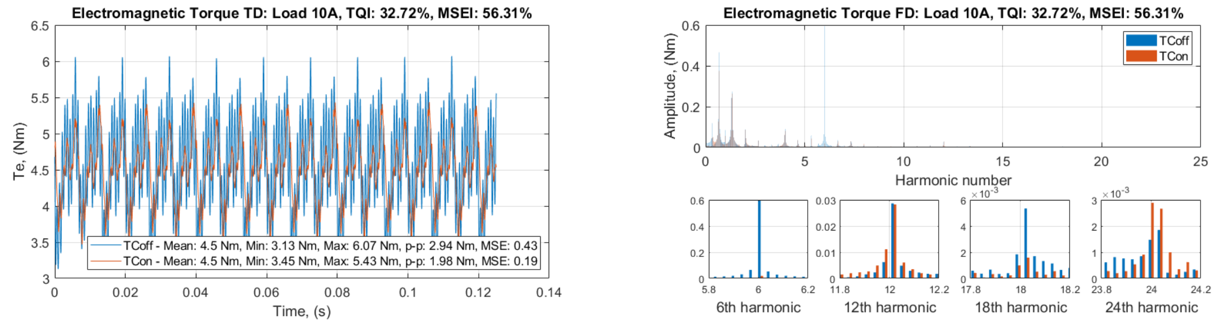

(b) Time Domain (TD) and Frequency Domain (FD) Electromagnetic Torque at Load Current of 10A

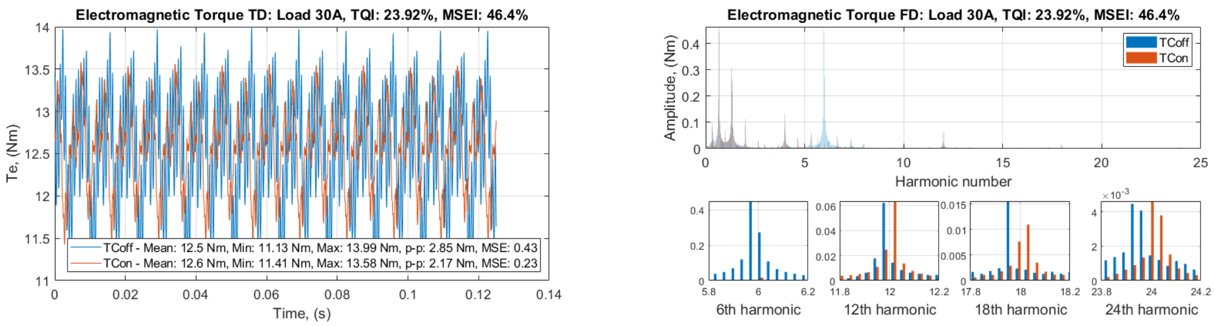

(c) Time Domain (TD) and Frequency Domain (FD) Electromagnetic Torque at Load Current of 30A

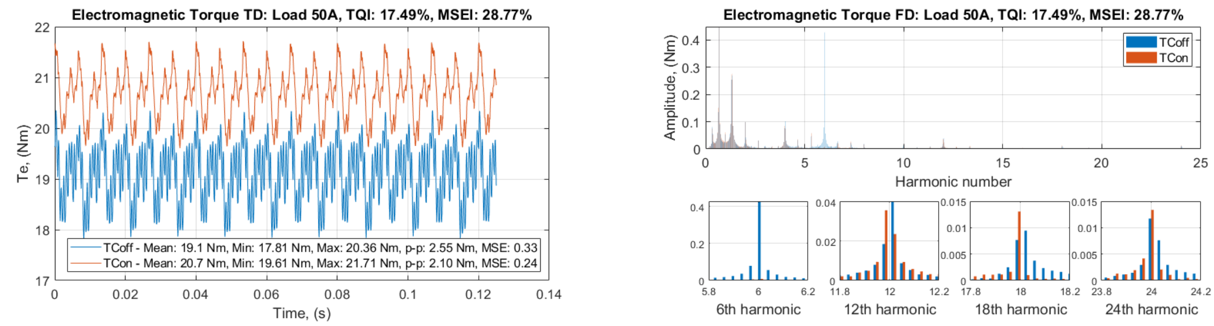

(d) Time Domain (TD) and Frequency Domain (FD) Electromagnetic Torque at Load Current of 50A

Fig. 5.33 – Torque comparison across the range of load currents at 4500 rpm

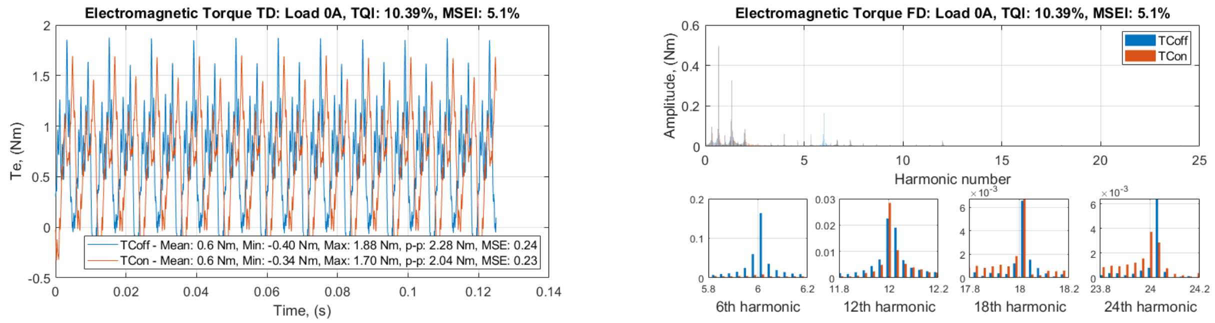

(a) Time Domain (TD) and Frequency Domain (FD) Electromagnetic Torque at Load Current of 0A

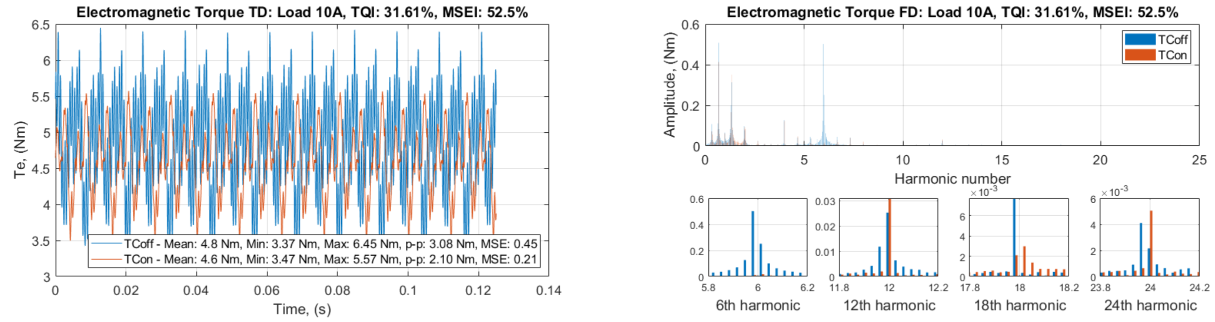

(b) Time Domain (TD) and Frequency Domain (FD) Electromagnetic Torque at Load Current of 10A

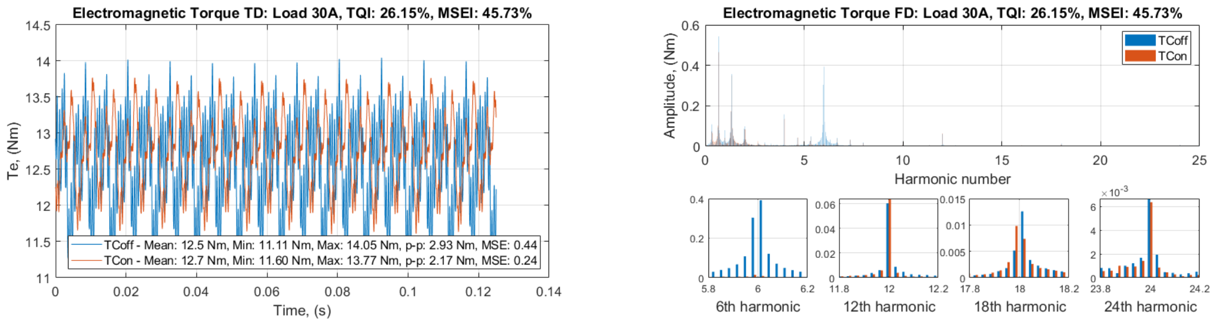

(c) Time Domain (TD) and Frequency Domain (FD) Electromagnetic Torque at Load Current of 30A

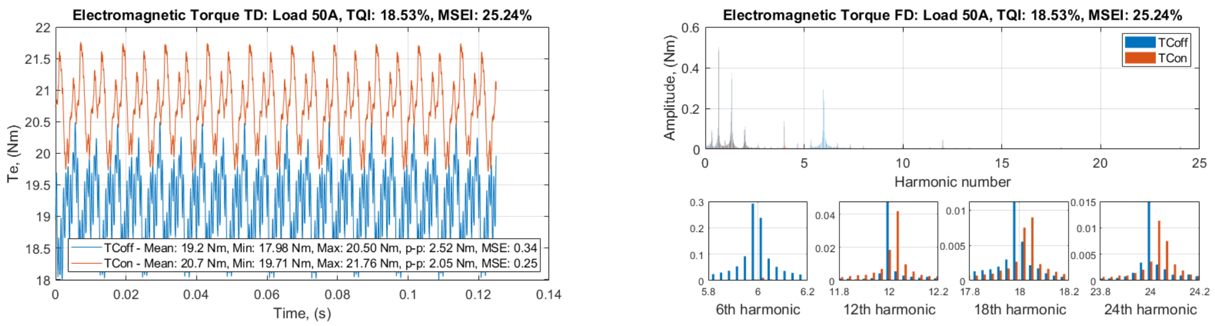

(d) Time Domain (TD) and Frequency Domain (FD) Electromagnetic Torque at Load Current of 50A

Fig. 5.34 – Torque comparison across the range of load currents at 5000 rpm

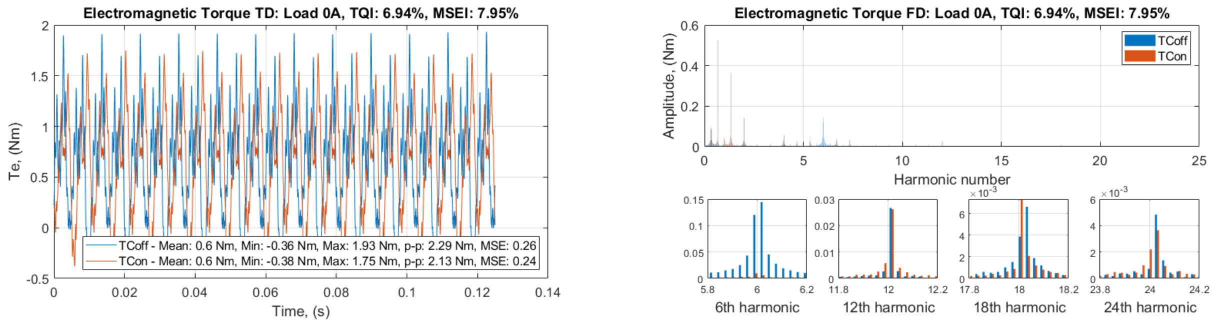

(a) Time Domain (TD) and Frequency Domain (FD) Electromagnetic Torque at Load Current of 0A

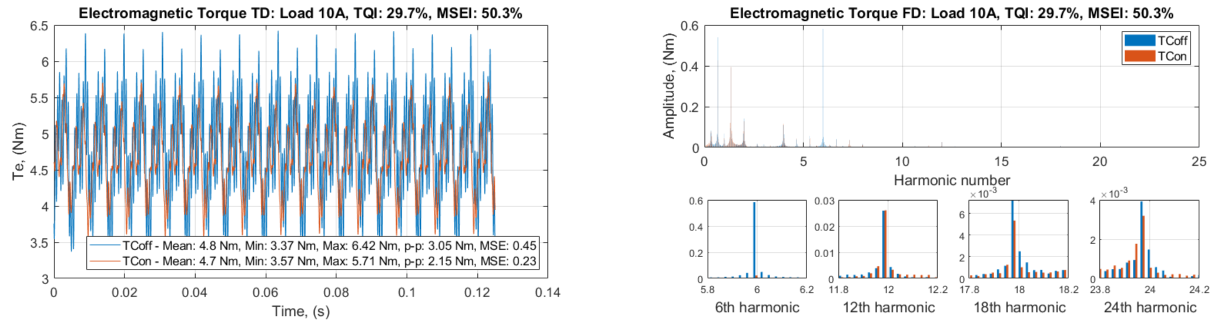

(b) Time Domain (TD) and Frequency Domain (FD) Electromagnetic Torque at Load Current of 10A

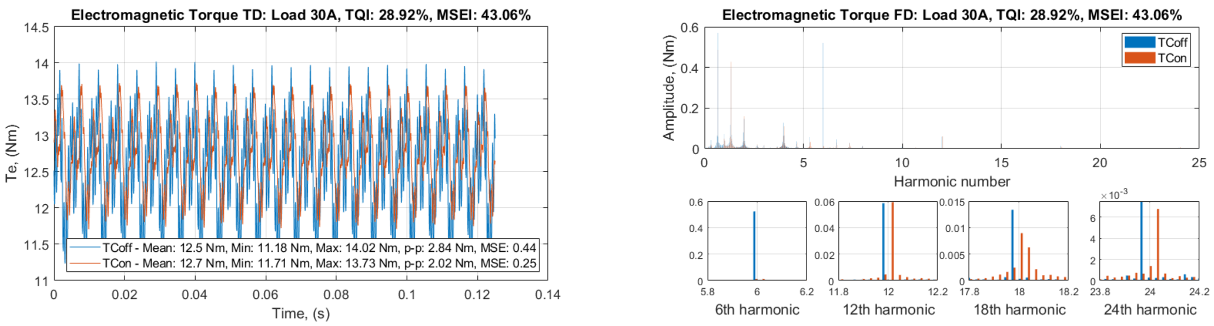

(c) Time Domain (TD) and Frequency Domain (FD) Electromagnetic Torque at Load Current of 30A

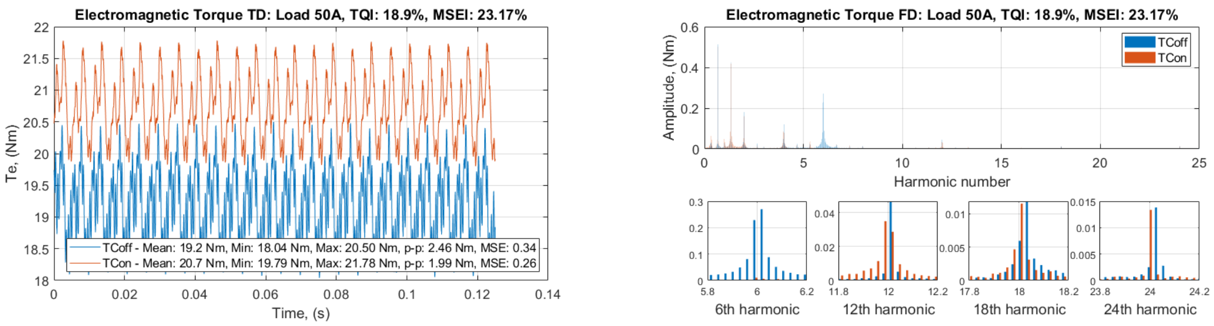

(d) Time Domain (TD) and Frequency Domain (FD) Electromagnetic Torque at Load Current of 50A

Fig. 5.35 – Torque comparison across the range of load currents at 5500 rpm

The torque quality improvement values presented in Fig. 5.25-Fig. 5.35 were recorded in TABLE VI - TABLE IX. Each of the tables represents different current i_q equivalent load.

TABLE VI Torque quality improvement – Experimental (No load)

Speed, RPM	**Peak-to-Peak Torque Ripple, (Nm)**		**Improvement due to the Proposed Method, (%)**
	No Compensation	**Proposed Method**	
500	0.82	0.84	-1.72
1000	1.17	1.04	10.94
1500	1.36	1.32	2.75
2000	1.40	1.41	-0.46
2500	1.59	1.55	2.10
3000	1.65	1.60	3.12
3500	1.81	1.73	4.31
4000	1.98	1.88	5.02
4500	2.16	1.99	7.87
5000	2.28	2.04	10.39
5500	2.29	2.13	6.94
		Average:	**4.66**

TABLE VII Torque quality improvement – Experimental (10 A load)

Speed, RPM	**Peak-to-Peak Torque Ripple, (Nm)**		**Improvement due to the Proposed Method, (%)**
	No Compensation	**Proposed Method**	
500	0.88	0.71	19.20
1000	1.31	1.01	22.26
1500	1.51	1.51	0.22
2000	1.74	1.60	8.37
2500	2.00	1.71	14.49
3000	2.40	1.88	21.49
3500	2.64	1.94	26.25
4000	2.86	2.10	26.55
4500	2.94	1.98	32.72
5000	3.08	2.10	31.61
5500	3.05	2.15	29.70
		Average:	**21.17**

TABLE VIII Torque quality improvement – Experimental (30 A load)

Speed, RPM	**Peak-to-Peak Torque Ripple, (Nm)**		**Improvement due to the Proposed Method, (%)**
	No Compensation	**Proposed Method**	
500	1.28	0.82	36.14
1000	1.54	1.24	19.84
1500	1.76	1.59	9.90
2000	1.86	1.62	12.67
2500	2.11	1.74	17.41
3000	2.55	1.98	22.06
3500	2.71	2.09	22.64
4000	2.88	2.27	21.04
4500	2.85	2.17	23.92
5000	2.93	2.17	26.15
5500	2.84	2.02	28.92
		Average:	**21.88**

TABLE IX Torque quality improvement – Experimental (50 A load)

Speed, RPM	**Peak-to-Peak Torque Ripple, (Nm)**		**Improvement due to the Proposed Method, (%)**
	No Compensation	**Proposed Method**	
500	1.77	0.98	44.89
1000	2.00	1.43	28.27
1500	2.22	1.80	18.90
2000	2.38	1.81	24.26
2500	2.34	1.88	19.47
3000	2.39	2.12	11.48
3500	2.44	2.10	14.21
4000	2.64	2.25	14.98
4500	2.55	2.10	17.49
5000	2.52	2.05	18.53
5500	2.46	1.99	18.90
		Average:	**21.03**

The data as to the improvement percentage of the torque quality was taken from TABLE VI - TABLE IX and represented as a surface plot in Fig. 5.36.

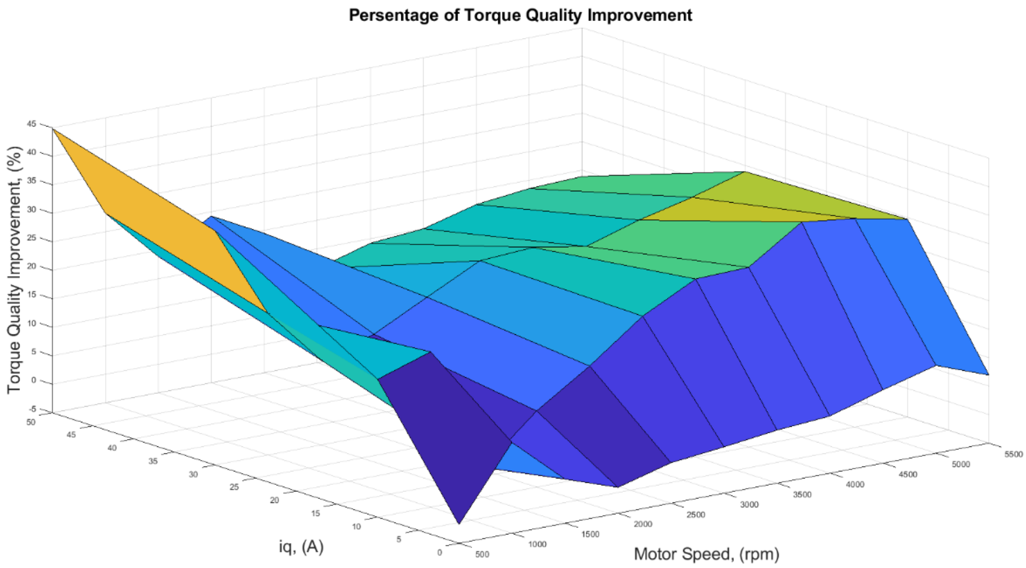

Fig. 5.36 – Torque quality improvement across the range of speeds and load currents

Fig. 5.36 shows the percentage improvement of the torque quality across the range of speeds and the range of loads represented as the i_q currents. It can be seen from Fig. 5.36 that the experimental results revealed that the proposed in this chapter method resulted in an improvement of the torque quality by up to 44.89%.

Considering the results presented in TABLE VI - TABLE IX, when a load is applied to the machine, the average improvement keeps its value on the level of around 21.36%. However, TABLE VI shows that the improvement is not as significant at no load operation, only up to 10.94%, averaging at 4.66%.

The MSE values were recorded in TABLE X - TABLE XIII.

TABLE X MSE improvement (MSEI) – Experimental (No load)

Speed, RPM	Mean Squared Error (MSE)		Improvement due to the Proposed Method, (%)
	No Compensation	Proposed Method	
500	0.02	0.02	11.34
1000	0.05	0.04	9.10
1500	0.08	0.07	4.09
2000	0.10	0.10	-1.27
2500	0.13	0.13	0.73
3000	0.15	0.15	3.10
3500	0.15	0.16	-2.54
4000	0.19	0.18	4.68
4500	0.22	0.21	4.89
5000	0.24	0.23	5.10
5500	0.26	0.24	7.95

TABLE XI MSE improvement (MSEI) – Experimental (10A load)

Speed, RPM	Mean Squared Error (MSE)		Improvement due to the Proposed Method, (%)
	No Compensation	Proposed Method	
500	0.03	0.02	35.31
1000	0.06	0.05	24.66
1500	0.10	0.09	3.10
2000	0.14	0.12	13.96
2500	0.19	0.14	26.36
3000	0.28	0.19	33.36
3500	0.35	0.20	44.56
4000	0.40	0.21	47.06
4500	0.43	0.19	56.31
5000	0.45	0.21	52.50
5500	0.45	0.23	50.30

TABLE XII MSE improvement (MSEI) – Experimental (30A load)

Speed, RPM	**Mean Squared Error (MSE)**		**Improvement due to the Proposed Method, (%)**
	No Compensation	**Proposed Method**	
500	0.08	0.02	73.27
1000	0.10	0.05	52.09
1500	0.13	0.09	28.22
2000	0.17	0.13	26.28
2500	0.22	0.15	32.82
3000	0.32	0.18	44.29
3500	0.39	0.21	45.81
4000	0.44	0.24	45.46
4500	0.43	0.23	46.40
5000	0.44	0.24	45.73
5500	0.44	0.25	43.06

TABLE XIII MSE improvement (MSEI) – Experimental (50A load)

Speed, RPM	**Mean Squared Error (MSE)**		**Improvement due to the Proposed Method, (%)**
	No Compensation	**Proposed Method**	
500	0.17	0.03	83.41
1000	0.17	0.06	67.67
1500	0.20	0.10	49.40
2000	0.25	0.13	48.42
2500	0.28	0.15	46.71
3000	0.31	0.19	38.78
3500	0.32	0.21	35.29
4000	0.36	0.25	29.20
4500	0.33	0.24	28.77
5000	0.34	0.25	25.24
5500	0.34	0.26	23.17

Fig. 5.37 – Mean Squared Error improvement (MSEI) of the torque across the range of speeds and load currents

The quadrature current i_q along with its reference are plotted according to the range of motor speeds and the different load conditions are show in Fig. 5.38 - Fig. 5.41. The graphs shown in the figures reveal how the quadrature current i_q follows its reference.

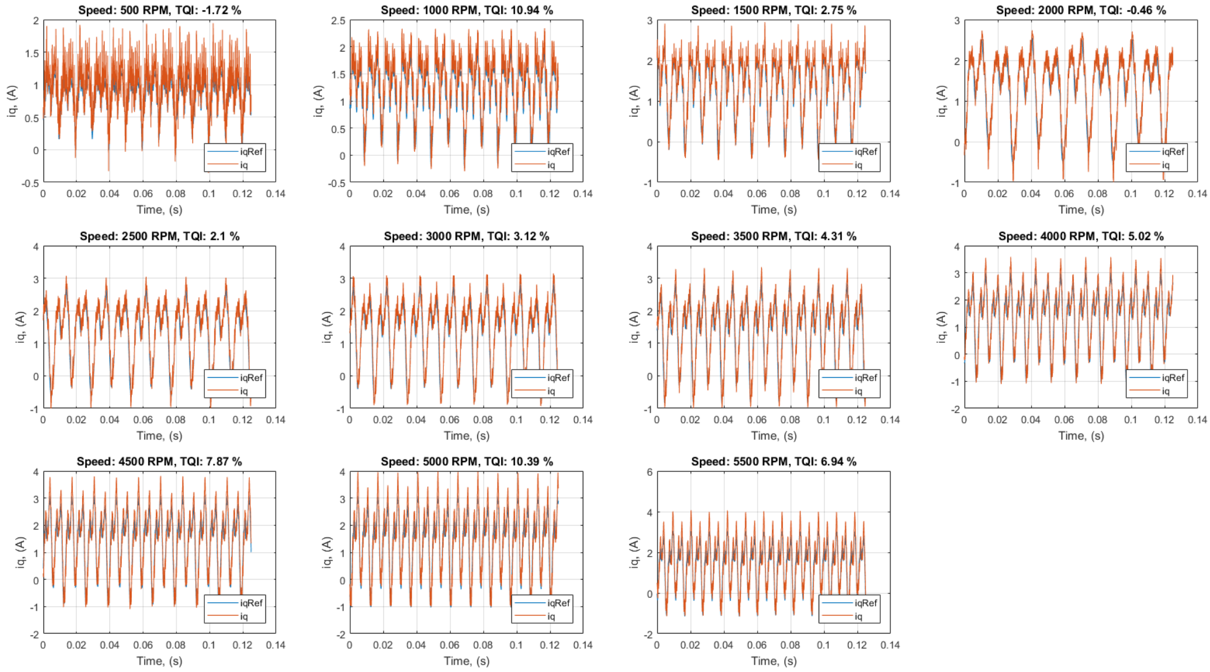

Fig. 5.38 – The quadrature current i_q at No Load condition

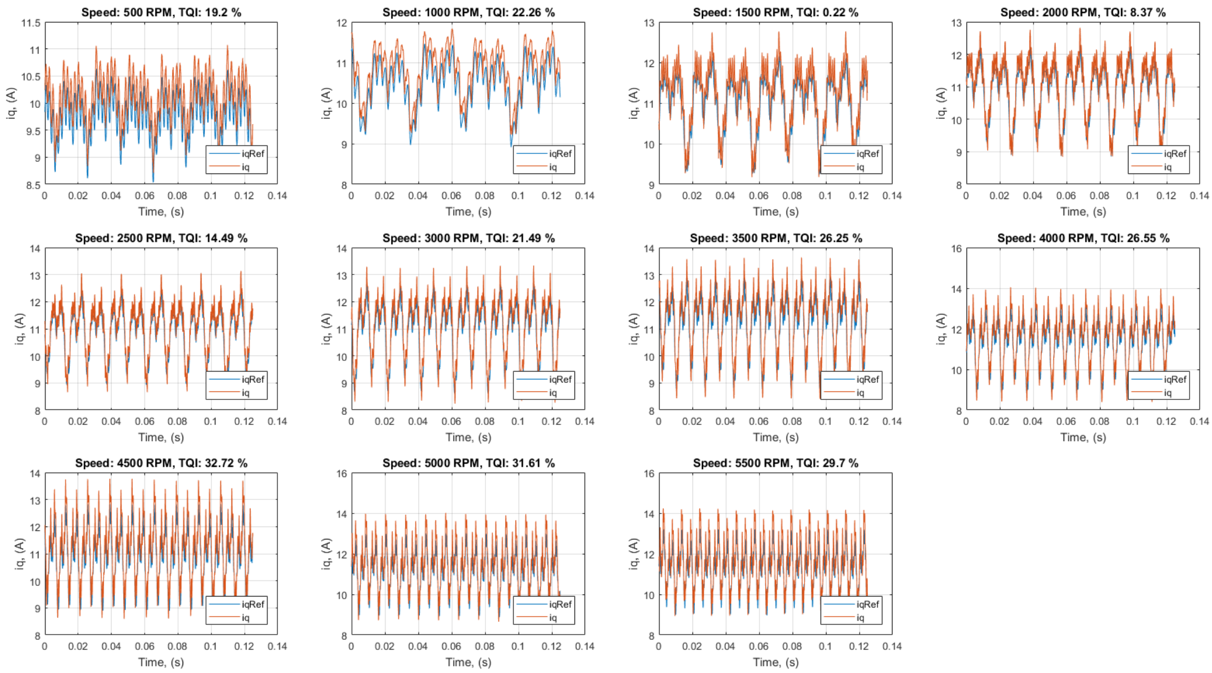

Fig. 5.39 – The quadrature current i_q at 10 A load condition

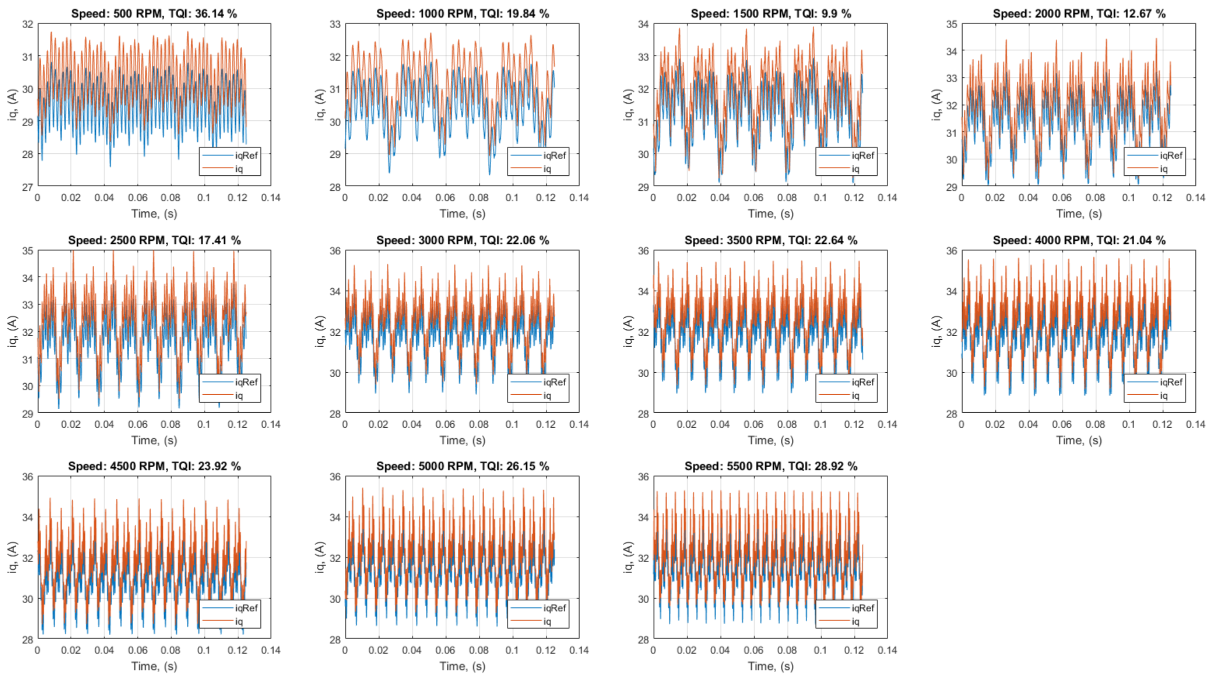

Fig. 5.40 – The quadrature current i_q at 30 A load condition

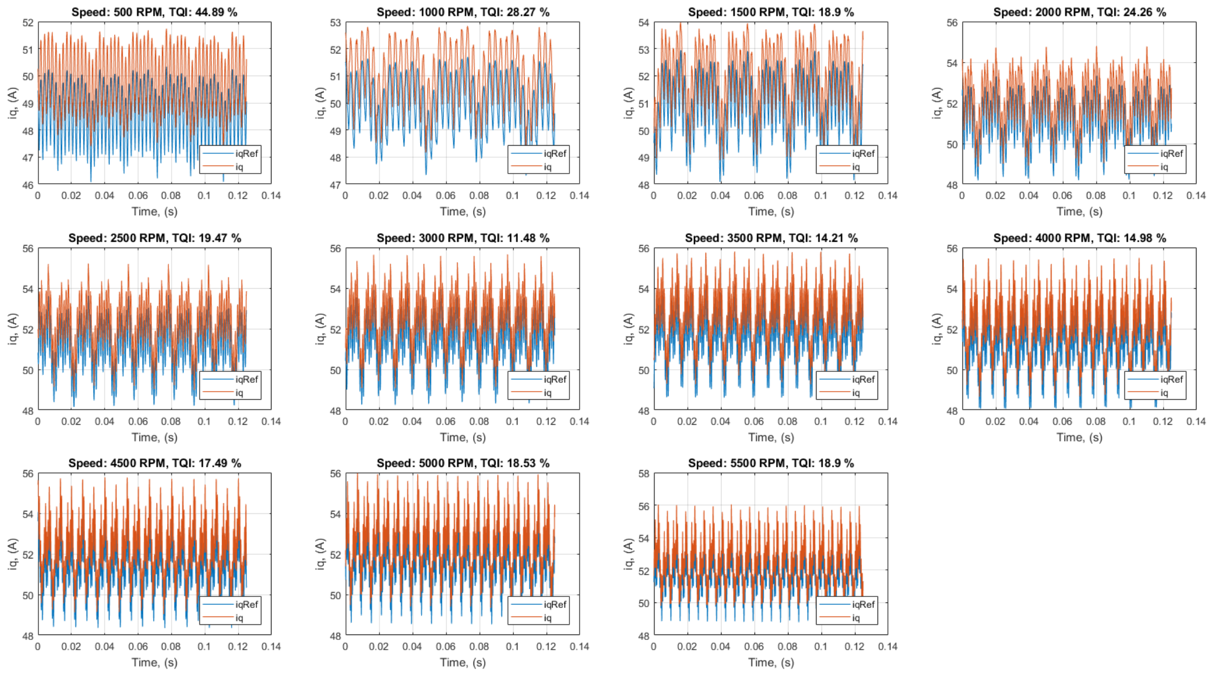

Fig. 5.41 – The quadrature current i_q at 50 A load condition

5.5Discussion

The third harmonic of the back EMF causes the zero-sequence currents to circulate in the OEW PMSM drives with common DC bus. This results in the degradation of the torque quality of such a system. The existing methods aimed at improving the torque quality cannot be used when a system with the low leakage inductance is introduced as under such condition it is hard to maintain the control of the zero-sequence component. This chapter proposed a control method that employs a proportional integral plus adaptive resonant controller for regulation of the quadrature current in order to compensate the torque ripple caused by the zero-sequence components.

The basic simulation of the proposed control showed a complete elimination of the torque ripple due to the zero-sequence component of the OEW PMSM without the need of introducing the zero-sequence voltage component. However, a more detailed simulation showed that due to the inverter switching the current noise substantially increased. Nevertheless, it was confirmed by the means of both simulation and experiment that the proposed method of improving the output torque quality of such machines results in an improvement of the overall torque quality even when the current noise due to the inverter switching was introduced.

In addition, the effect of the zero-sequence current during the experiment was not as pronounced because the physical layout of the experimental setup itself. The resistance and the leakage inductance of the drive increased due to the possible several reasons discussed in the discussion part of chapter 4 on page 85. This includes the introduction of long cables and wires that were erroneously chosen by the machine. The fact that the machine was specifically designed for the high-speed high power rig introduced in 4.2.4 on page 80 made it impossible to be flexible with the setup itself. It was impossible to place the inverter next to the motor which situated in another room. Hence, the long cables had to be used in order to deliver the power to the motor. The motor itself had long and nevertheless wrong diameter of the phase connections. All of this resulted in a high resistance and the high leakage inductance of the overall system. Introduction of other harmonics to the zero-sequence current could also influence the performance of the proposed control. It must be admitted that although the experimental results showed that the proposed technique is feasible as it improves the torque quality, it is still not as good as the theoretical predictions.

Chapter 6

6 Proposed Non-Intrusive Online Stator Temperature Estimation Technique for an Open-End Winding PMSM

In this chapter a new method for online identification of stator winding temperature for an open–end winding (OEW) permanent magnet synchronous motor (PMSM) is proposed. The method exploits the zero-sequence current (ZSC) due to the third harmonic back electromotive force (EMF) circulating in the system in order to estimate the phase resistance, which, in turn, is used to derive the winding temperature. In order to do this a proposed idea of maximum zero-sequence current amplitude along with the actual ZSC amplitude and the electrical speed of the motor is used. The temperature is estimated without any additional sensors in a wide operating speed range. A single synchronous phase-locked loop (PLL) is utilised in order to obtain the required parameters.

6.1Zero-Sequence Current Analysis

The zero-sequence component V_0 of equation (3.39) is shown below along with its equivalent circuit depicted in Fig. 6.1.

$$V_0 = r_s i_0 + L_0 \frac{di_0}{dt} + 3\omega_e \lambda_{pm} K_{pm3} \cos(3\theta_e) \tag{6.1}$$

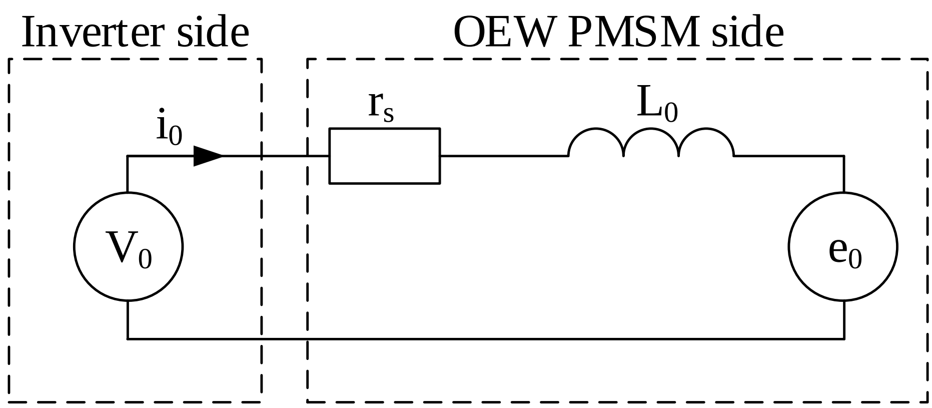

Fig. 6.1 – Equivalent circuit of zero-sequence component of OEW PMSM.

It can be seen that there are two causes of the zero-sequence current (ZSC): the third harmonic back EMF e_0 and the zero-sequence voltage (ZSV) from the inverter side V_0. This V_0 could be used to oppose e_0, thereby, suppressing the ZSC. However, in some cases when the DC bus voltage is large and the zero-sequence inductance L_0 is small the suppression of the ZSC by the means of the inverter's ZSV is not possible because introducing a modulated V_0 signal equal to a large DC bus value would result in a spike of i_0 as the value of L_0 is considerably low. In such a case it is more appropriate to let the i_0 due to e_0 to flow freely. Hence, V_0 is left 0V.

The steady state phasor form of ZSV equation (6.1) can be written as follows.

$$\tilde{V}_0 = r_s \tilde{I}_0 + jX_0 \tilde{I}_0 + \tilde{E}_0 \tag{6.2}$$

where, $\tilde{V}_0$ and $\tilde{I}_0$ are the zero-sequence voltage and current phasors, respectively, X_0 is the zero-sequence inductive reactance, $\tilde{E}_0$ is the zero-sequence back EMF phasor with a zero phase shift and the amplitude denoted as:

$$\left|\tilde{E}_0\right| = 3\omega_e \lambda_{pm} K_{pm3} \qquad\qquad X_0 = 3\omega_e L_0 \tag{6.3}$$

Simplifying equation (6.2) by setting V_0 to zero and substituting (6.3) into (6.2), rearranging the outcome in order to obtain the ZSC amplitude $\left|\tilde{I}_0\right|$:

$$\left|\tilde{I}_0\right| = \frac{3\omega_e \lambda_{pm} K_{pm3}}{\sqrt{{r_s}^2 + (3\omega_e L_0)^2}} \tag{6.4}$$

Introducing a concept of the maximum possible value that ZSC amplitude can achieve by taking the limit of (6.4) when the electrical rotor speed ω_e tends to infinity:

$$\left|\tilde{I}_0\right|_{max} = \lim_{\omega_e \to \infty}\left(\left|\tilde{I}_0\right|\right) = \lim_{\omega_e \to \infty}\left(\frac{3\omega_e \lambda_{pm} K_{pm3}}{\sqrt{{r_s}^2 + 9{\omega_e}^2 {L_0}^2}}\right) = \frac{\lambda_{pm} K_{pm3}}{L_0} \tag{6.5}$$

The maximum value of $\left|\tilde{I}_0\right|$ is a good indicator for the OEW PMSM that even if the rotor will experience an infinitely large change in position the ZSC will not exceed a certain maximum finite value. Moreover, substituting the concept of a maximum zero-sequence current of equation (6.5) into (6.4) the ZSC amplitude $\left|\tilde{I}_0\right|$ can now be written in terms of the maximum value $\left|\tilde{I}_0\right|_{max}$ and the electrical rotor speed ω_e:

$$\left|\tilde{I}_0\right| = \left|\tilde{I}_0\right|_{max} \frac{\omega_e}{\sqrt{{\sigma_0}^2 + {\omega_e}^2}} \tag{6.6}$$

where, σ_0 is a frequency constant that can be found using equation (6.7).

$$\sigma_0 = \frac{r_s}{3L_0} \tag{6.7}$$

Fig. 6.2 below shows the graph of equation (6.6) along a range of frequencies. It was noted that the multiples of the frequency constant from equation (6.7) correspond to the particular percentage values of the zero-sequence current amplitude with respect to the maximum ZSC amplitude concept, introduced in this chapter earlier.

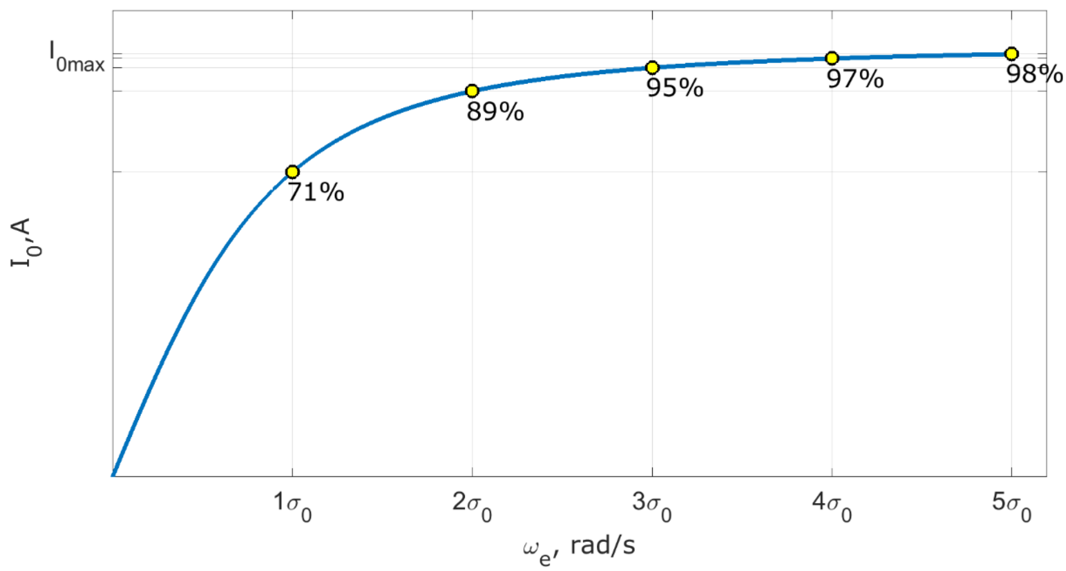

Fig. 6.2 – Relationship between the ZSC amplitude and the rotor electrical speed.

In order to determine a frequency that corresponds to a particular ZSC amplitude the frequency constant σ_0 must be multiplied by a frequency constant multiplier n:

$$\omega_e = n\sigma_0 \tag{6.8}$$

The frequency constant multiplier n, in turn, can be found using both the ZSC amplitude $|\tilde{I}_0|$ and the maximum ZSC amplitude value $|\tilde{I}_0|_{max}$:

$$n = \frac{|\tilde{I}_0|}{\sqrt{|\tilde{I}_0|_{max}^{\ 2} - |\tilde{I}_0|^2}} \tag{6.9}$$

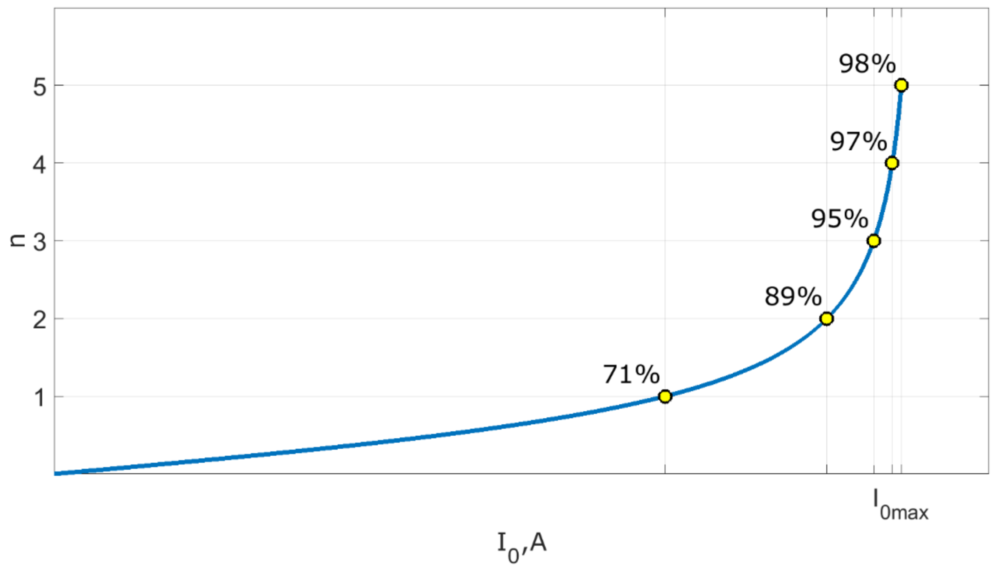

Fig. 6.3 – Relationship between the frequency constant multiplier and the ZSC amplitude.

The curve, derived from equation (6.9) is shown in Fig. 6.3. It can be observed that the frequency constant multiplier n corresponds to a particular percentage of the maximum ZSC.

6.2 Resistance and Temperature Estimation

6.2.1 Resistance Estimation

The amplitude of ZSC along with the electrical rotor speed contains the information about the phase resistance value through the frequency constant σ_0. Substituting equation (6.7) into (6.8) in order to obtain the phase resistance value:

$$r_s = 3L_0 \frac{\omega_e}{n} \tag{6.10}$$

According to equation (6.9), n is obtained using the maximum value of ZSC amplitude and the actual ZSC amplitude only which can be accurately estimated using a simple synchronous PLL algorithm. The electrical speed ω_e can be obtained precisely using a resolver or an encoder. Moreover, this speed could be estimated using a sensorless technique.

6.2.2 Temperature Estimation

The stator winding temperature estimation technique employs the fact that the resistivity of a metal is affected by the temperature. Whenever the temperature of the metal is raised the drift velocity of the electrons decreases. As a result, the temperature raise increases the metals resistivity according to the equation (6.11) below [107].

$$\rho_T = \rho_0[1 + \alpha(T - T_0)] \tag{6.11}$$

where, ρ_T is the metal resistivity at temperature T, ρ_0 is the resistivity at the reference temperature T_0 and α is the temperature coefficient of resistivity.

The relationship between the temperature T and resistivity ρ allows to exploit the phase resistance R to determine the winding temperature assuming that the length of the wire L and the cross sectional area A remain the same, hence $L_T = L_0$ and $A_T = A_0$, respectively.

$$R = \rho \frac{L}{A} \qquad \Longrightarrow \qquad \frac{R_T}{R_0} = \frac{\rho_T \frac{L_T}{A_T}}{\rho_0 \frac{L_0}{A_0}} \qquad \Longrightarrow \qquad \frac{R_T}{R_0} = \frac{\rho_T}{\rho_0} \tag{6.12}$$

Therefore, substituting (6.12) into (6.11):

$$R_T = R_0[1 + \alpha(T - T_0)] \tag{6.13}$$

Rearranging the equation and solving it for T:

$$T = \frac{1}{\alpha}\left(\frac{R_T}{R_0} - 1\right) + T_0 \tag{6.14}$$

where, R_T is the copper resistance at temperature T, R_0 is the resistance at the reference temperature T_0 and α is the temperature coefficient of copper resistivity. According to the standard values of temperature coefficient of annealed copper $\alpha = 0.0394/℃$ [108]. Using the derived equation of the temperature (6.14) and the estimated phase resistance R_T along with the temperature coefficient α and the measured beforehand phase resistance R_0 at the reference temperature T_0, the current winding temperature T can be estimated.

6.2.3 Implementation of Resistance and Temperature Estimation

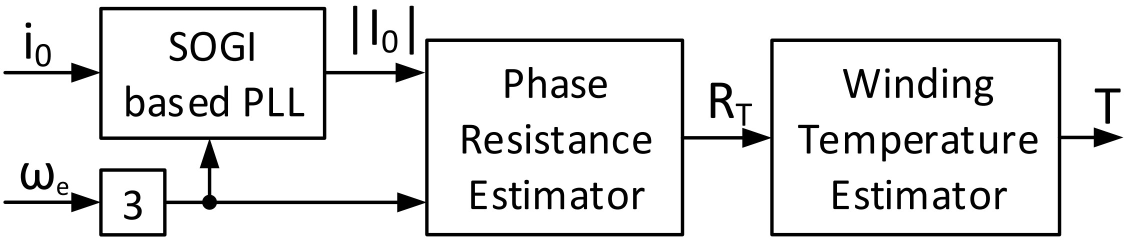

Fig. 6.4 – OEW PMSM temperature estimation block diagram.

Fig. 6.5 represents a combination of the resistance estimation technique derived in equation (6.10) and the temperature estimation in equation (6.13).

The process of derivation of i_0 is rather simple and does not involve the rotor position:

$$i_0 = \frac{i_a + i_b + i_c}{3} \tag{6.15}$$

The amplitude of the zero-sequence current is provided by the modified version of the second order generalised integrator (SOGI) based single phase Phase-Locked-Loop (PLL) (Fig. 6.4, Fig. 6.5 and Fig. 6.6) and explained in [105]. The modification added is the amplitude identification bit at the output of the mentioned PLL, as illustrated in Fig. 6.5.

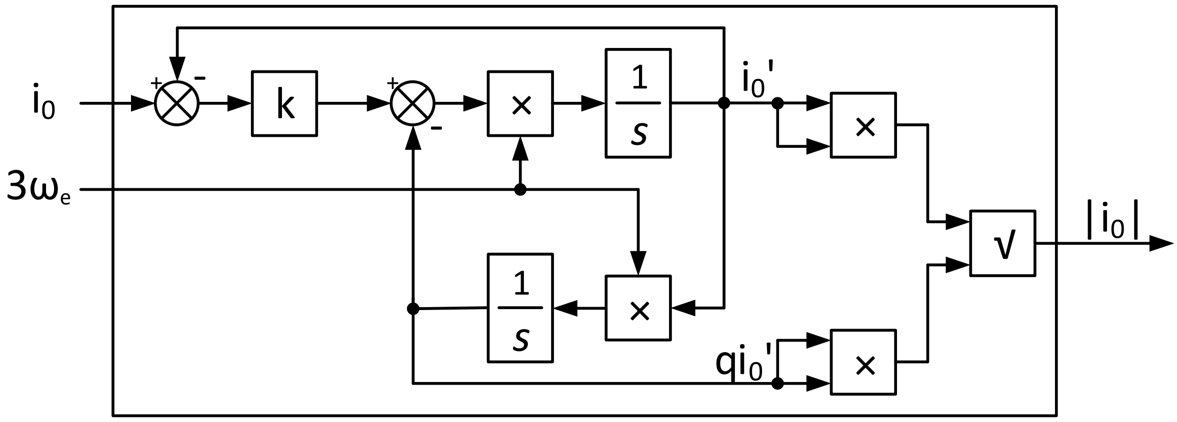

Fig. 6.5 – SOGI based single phase PLL amplitude estimator.

The direct $i_0{}'$ and the quadrature $qi_0{}'$ output signals are used in the following formula to calculate the ZSC amplitude $|i_0|$ for the current limiter.

$$|i_0| = \sqrt{(i_0{}'\,)^2 + (qi_0{}')^2} \tag{6.16}$$

The ZSC's amplitude is also used in the current reference limiter, shown in Fig. 6.6.

As it has been mentioned already, the introduction of the zero-sequence voltage for a machine with the parameters shown by the FEA in TABLE I on page 67 under consideration in this chapter is undesirable. In order to ensure that there is no ZSV produced by the modulation, a special space vector voltage modulation (SVM) technique is used. Such a modulation technique eliminates the ZSV produced by the voltage source converter (VSC). This is realised using only certain voltage vectors that do not produce ZSV. The particular voltage vectors are depicted in Fig. 4.10 in red in chapter 4 on page 76. Thereby, according to Fig. 4.10 the voltage limit for the VSC appears to be V_{DC} (magenta circle).

The simulation illustrated in Fig. 6.6 features the aforementioned special modulation technique that is used in order to keep the ZSV always zero. The simulation clock frequency was set to be the same as the carrier counter of the actual modulator, 100MHz. Hence, the simulation very accurately imitates the behaviour of an FPGA based modulator of the control platform described in [101] that was also used for the experimental validation in this thesis.

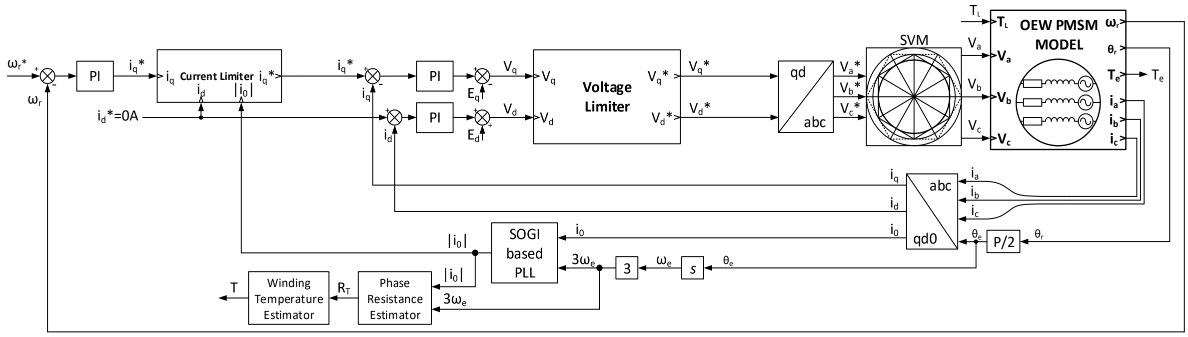

Fig. 6.6 – Temperature estimation simulation block diagram.

The sampling frequency of the controller was set to be 40 kHz to represent the actual switching frequency of a SiC inverter.

The variable parameters that are needed from the proposed method are the amplitude of ZSC and the electrical rotor speed. This information can be obtained with a virtually zero steady state estimation error by introducing the SOGI based PLL, Fig. 6.5, that has already been discussed above.

6.2.4Parameter Sensitivity Analysis

The estimation of both the resistance and, subsequently, the temperature rely on the third harmonic flux λ_{pm3} parameter (6.17) and the zero-sequence inductance L_0 parameter. These parameters are considered to have insignificant variations with the motor's allowed operating temperature. This makes the proposed method more robust.

$$\lambda_{pm3} = \lambda_{pm} K_{pm3} \tag{6.17}$$

Nonetheless, the produced parameter sensitivity analysis was set to be based upon an assumption that the third harmonic flux λ_{pm3} could vary by 5% and the zero-sequence inductance L_0 – by 10%. Thereby, the variation of the maximum zero-sequence current due to the third harmonic back EMF, $|\tilde{I}_0|_{max}$, that represents the ratio according to equation (6.5) can, in such a case, vary from -13.6% to +16.7%.

In order to represent the estimation error of resistance and temperature along a range of the machine's speeds the electrical speed was raised from 10 to 800 Hz in steps of 10 Hz. In addition, the two different temperatures: 45 ℃ and 100 ℃ were set as the actual constant temperatures of the phase winding.

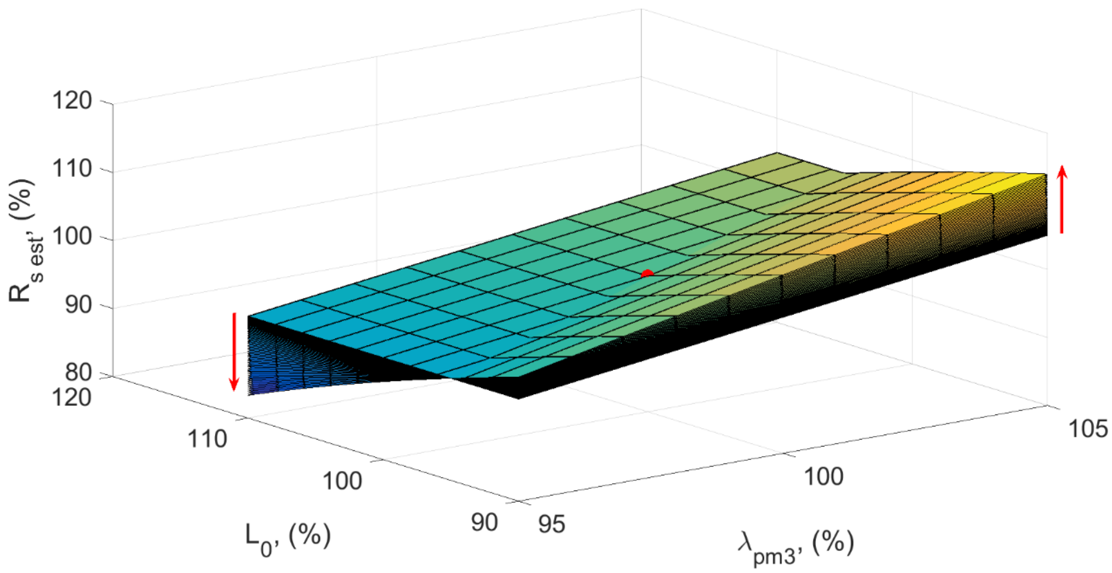

Fig. 6.7 – Resistance estimation parameter sensitivity with increasing electrical speed from 10 to 800 Hz at T = 45℃.

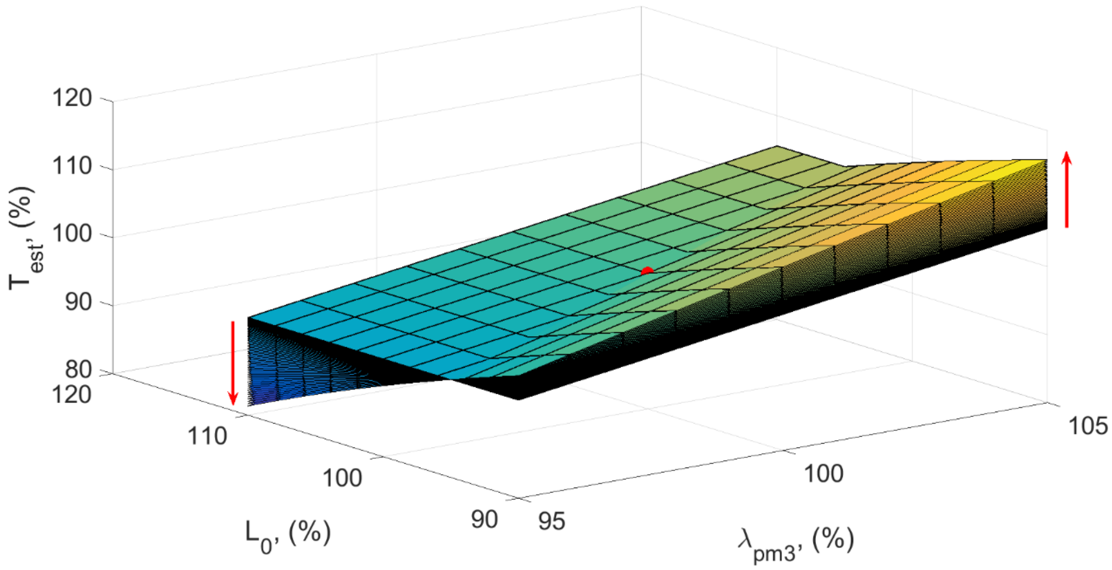

Fig. 6.8 – Temperature estimation parameter sensitivity with increasing electrical speed from 10 to 800 Hz at T = 45°C.

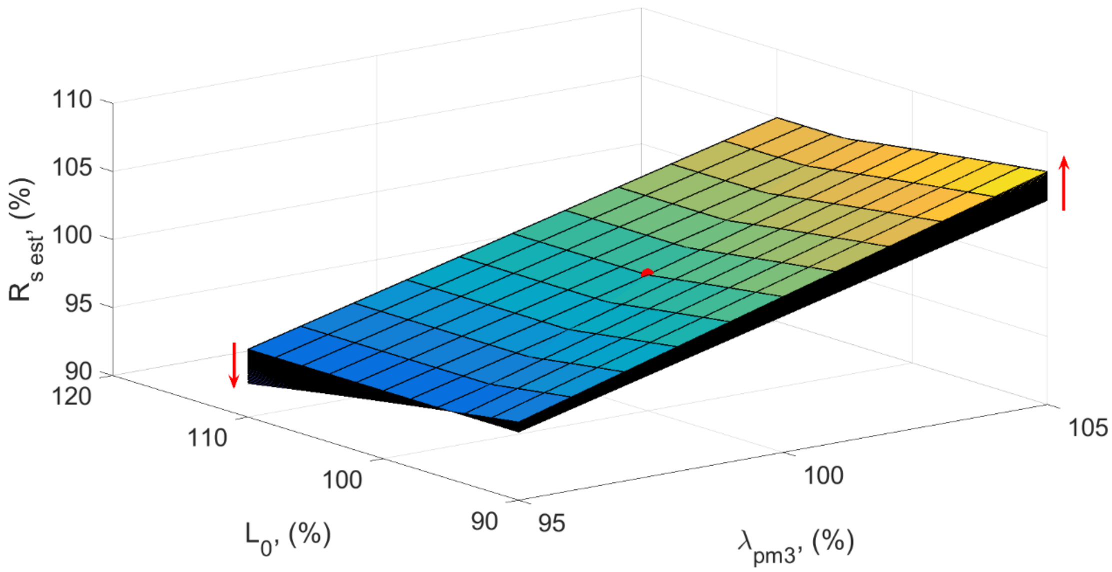

Fig. 6.9 – Resistance estimation parameter sensitivity with increasing electrical speed from 10 to 800 Hz at T = 100°C.

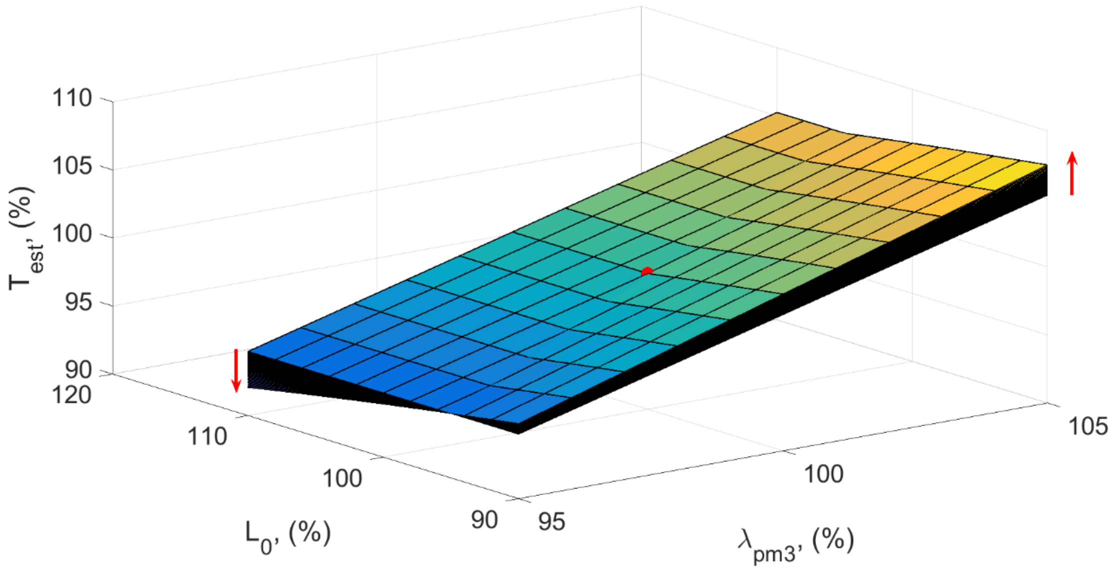

Fig. 6.10 – Temperature estimation parameter sensitivity with increasing electrical speed from 10 to 800 Hz at T = 100°C.

The parameter sensitivity analysis is shown in Fig. 6.7 and Fig. 6.8 for the phase winding temperature of 45 ℃ and in Fig. 6.9 and Fig. 6.10 for the phase winding temperature of 100 ℃. The red dot in the middle represents the correct parameter identification. The direction of the red arrows signify the direction of the error growth with increasing speed. The range of errors according to Fig. 6.7 to Fig. 6.10 were identified and recorded in TABLE XIV.

According to the results recorded in TABLE XIV, the estimation of the higher values of the phase winding temperature tends to be more robust to λ_{pm3} and L_0 parameters variations.

TABLE XIV ESTIMATION ERROR WITH $L_0 = \pm 5\%$ AND $\lambda_{pm3} = \pm 10\%$

Actual Temperature, (°C)	**Error range with increasing speed: 10 to 800 Hz**	
	Estimated Resistance, (%)	**Estimated Temperature, (%)**
45	-17 - +14	-19 - +16
100	-8 - +8	-8 - +8

6.3Simulation Results

The proposed winding temperature estimation method was tested in Matlab/Simulink using the machines parameters taken from the FEA listed in TABLE I in chapter 4 on page 67.

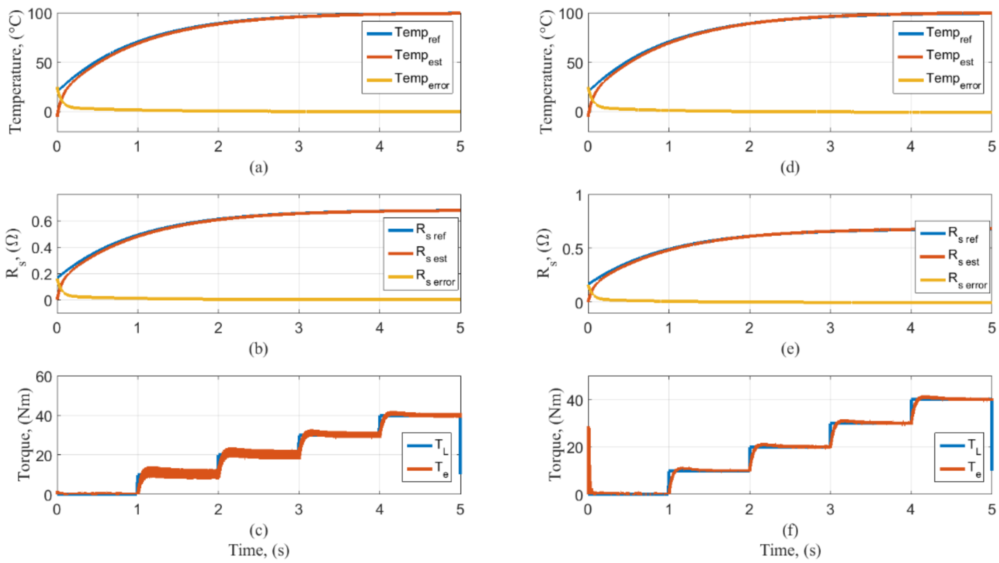

Fig. 6.11 – Simulation results: (a – stator winding temperature, b – phase resistance, c – electromagnetic torque) – 800Hz constant electrical speed, (d – stator winding temperature, e – phase resistance, f – electromagnetic torque) – 100Hz constant electrical speed

Considerably low leakage inductance prevents the suppression of ZSC in such a machine as an introduction of a 540V DC ZSV even for a short duration can result in a large ZSC spike. For example, the designed drive with the parameters produced by FEA introduces a 30A current spike if the ZSV equal to the DC bus voltage is applied even for as little as one microsecond. Hence, an obvious option for such types of drives would be to allow ZSC due to the third harmonic back EMF to flow freely in the system and ensure that there are no ZSV applied by the inverter. Although this would cause an additional loss, it creates an opportunity for estimation of the stator winding temperature.

During the simulation time, the OEW PMSM speed was set to be of a constant value: 100 Hz and 800Hz electrical for the two cases. Different load torque steps were applied: 1, 10, 20, 30, and 40 Nm every second. The reference temperature was increased exponentially from 20 to 100°C. The simulation results are shown in Fig. 6.11. The simulation has revealed that the estimated values of temperature and resistance tracks the actual values of the same parameters with an insignificant error in both cases: for 100Hz and 800Hz electrical speed.

6.4Discussion

The third harmonic of the back EMF causes the zero-sequence currents to circulate in the OEW PMSM drives with common DC bus. In case of a low leakage inductance it is impossible to suppress ZSC due to the third harmonic back EMF. Hence, this current is left flowing in the system. The new online temperature estimation method proposed in this thesis and validated through simulation benefits from the mentioned ZSC by using it to derive the information about the stator temperature. Thereby, it offers an alternative solution for the temperature monitoring of the OEW PMSM drives with common DC link.

The proposed method relies on the variable parameters such as the amplitude of ZSC and the rotor speed that can be estimated with virtually zero estimation error at steady state. Hence, the method could also be suitable for the sensorless control. Another advantage of the proposed method is that it does not require a high frequency injection, thereby, there is no additional acoustic noise and no additional torque ripple. The proposed method will be especially beneficial for a particular type of machines such as the one used in order to validate the proposed idea in simulation. The power density of that machine is achieved relying on an internal liquid cooling. Hence, the proposed method of the temperature estimation can improve the robustness of the overall system by introducing the system's protection mechanisms based on the stator temperature monitoring. It is especially beneficial when the ZSC is left flowing freely in the motor winding as it creates an additional power loss into heat that now can be monitored. Furthermore, this method can be used as a backup in case of a fault in the existing temperature monitoring system.

There is no need for a position sensor to be able to use the method, hence, the system's reliability can further be increased. The possibility of implementation of the proposed method together with a variety of different control techniques for OEW PMSM including the sensorless control such as that described in [28] is also one of the advantages. The proposed method is thought to work with any common DC bus voltage OEW PMSM control techniques that do not introduce the ZSV from the inverter side. The temperature estimation is run without interrupting the control process. The proposed new method involving the phase resistance estimator is also beneficial for online self-tuning of those controllers which are heavily dependent on the stator resistance value.

Due to the large value of the resistance and the additional inductance that the experimental testing facility and the rig itself introduced along with ill suppressed zero-sequence voltage, it was not possible to use such a rig for the experimental validation of the concept proposed in this chapter. These limitations are discussed in the discussion part of both chapter 4 on page 85 and chapter 5 on page 131. Ideally, the integrated drives discussed in 2.3 on page 36 would be the best option to test the developed algorithm due to short electrical connections, hence, the maintenance of the low leakage inductance and the low phase resistance.

Chapter 7

7 Further Improvements of the OEW PMSM control

A further investigation of the influence of the uncontrolled zero-sequence current on the power losses in conductor of an open-end winding permanent magnet synchronous drive with common DC link is produced in this chapter. This analysis gave birth to a novel technique of reduction of the power loss in conductor. In addition, not only did the mathematical analysis introduced in this chapter reveal that some of the concepts regarding the current limiting techniques from the literature appeared to be controversial, but also it enabled the proposal of a novel current limiting technique for an open-end winding PMSM configuration with common DC link.

7.1 Power Loss Reduction for OEW PMSM

When the proposed technique introduced in chapter 5 was validated experimentally, it was noticed that the overall estimated resistance of the open-end winding permanent magnet synchronous motor drive with common DC link described in 4.2 on page 77 appeared to be around 8.78 times greater than the one confirmed by Dr Gaurang Vakil from the FEA that he performed. The reasons for this discrepancy are discussed in the discussion part of both chapter 4 on page 85 and chapter 5 on page 131.

The increased resistance resulted in a smaller value of the zero-sequence current amplitude. According to the equation of the power loss in conductor (3.42) of chapter 3 on page 46, an open-end winding permanent magnet synchronous motor drive with common DC link could potentially benefit in terms of losses in conductor from having a low zero-sequence current.

If this phenomenon could be well understood, then the machine design engineers could take this knowledge into account when designing a permanent magnet synchronous machines to be used in an open-end winding configuration. This led the research towards an investigation of the influence of zero-sequence current on the power losses in conductor, presented in this chapter.

7.1.1 Power Loss due to the ZSC Analysis

7.1.1.1 Influence of the Internal Resistance on ZSC

The newly introduced concept of the maximum zero-sequence current $\left|\tilde{I}_0\right|_{max}$ (6.5) along with the new representation of its amplitude $\left|\tilde{I}_0\right|$ (6.6) involving the derived concept of a frequency constant σ_0 (6.7) in chapter 6 section 6.1 on page 134 reveals the steady state behaviour of the uncontrolled zero-sequence current in a range of frequencies, Fig. 6.2 on page 136 and, for convenience, also depicted in Fig. 7.1 below.

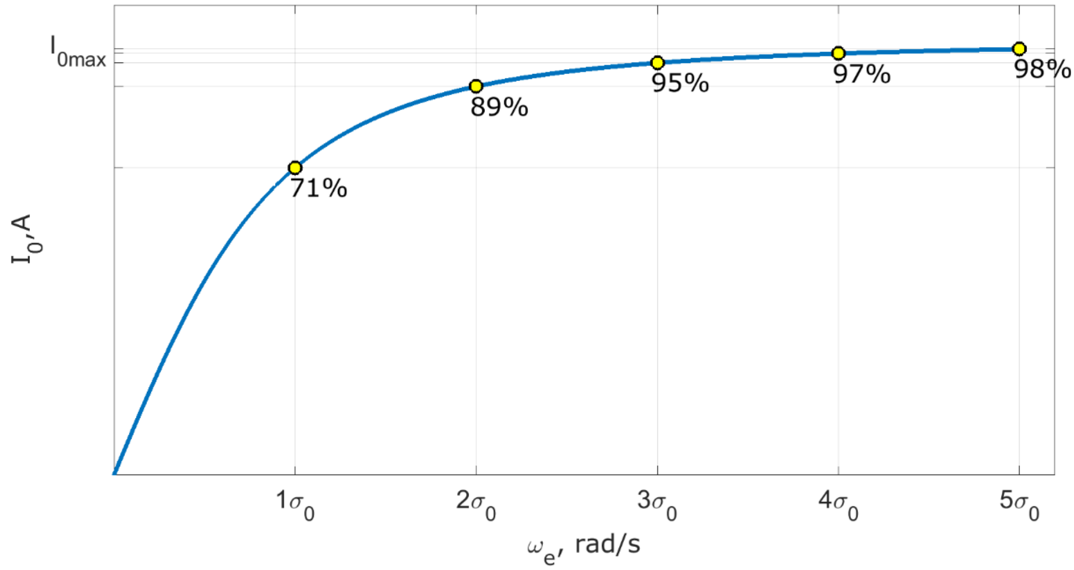

Fig. 7.1 – ZSC amplitude along a range of electrical angular speeds

The derivations for the equations which are used in order to plot the graph in Fig. 7.1 are taken from section 6.1 of chapter 6 and are shown in (7.1) and (7.2) for convenience.

$$|\tilde{I}_0| = |\tilde{I}_0|_{max} \frac{\omega_e}{\sqrt{{\sigma_0}^2 + {\omega_e}^2}} \tag{7.1}$$

where, ω_e is the angular frequency of the motor in radians and σ_0 is the already mentioned frequency constant that appears to be dependent on the phase resistance r_s as shown in both equation (6.7) in section 6.1 of chapter 6 and equation (7.2) below for convenience:

$$\sigma_0 = \frac{r_s}{3L_0} \tag{7.2}$$

Considering the equation (7.2), the value of the frequency constant σ_0 is directly proportional to the resistance r_s. It is not as intuitive to understand how the increasing value of the frequency constant σ_0 decreases the value of the amplitude of the zero-sequence current $|\tilde{I}_0|$ as the shape of the graph of Fig. 7.1 remains the same. The frequency constants multiples remain the same gap between them, resulting in the same percentage of the maximum zero-sequence current value: $1\sigma_0 \rightarrow 71\%,\ 2\sigma_0 \rightarrow 89\%,\ 3\sigma_0 \rightarrow 95\%$ and so on.

However, looking closely at Fig. 7.1, even though the percentage of maximum zero-sequence current remains the same, for example 71% at $1\sigma_0$, the actual value of σ_0 changes with changing resistance r_s: it increases with increase of the resistance and decreases with decrease of this resistance value. In the meantime, the base speed of the machine does not depend on the resistance. It always remains the same. Therefore, depending on the value of the resistance, the value of the frequency constant $1\sigma_0$ can appear before the base speed of the motor, as shown in Fig. 7.2, or after, as shown in Fig. 7.3.

Note, that the value of the maximum zero-sequence current does not change with resistance. Its derivation is shown in equation (6.5) of chapter 6 on page 135.

This gives a visual explanation of why the amplitude of the zero-sequence current $|\tilde{I}_0|$ decreases with increase of the resistance r_s and increases with decreasing value of the resistance.

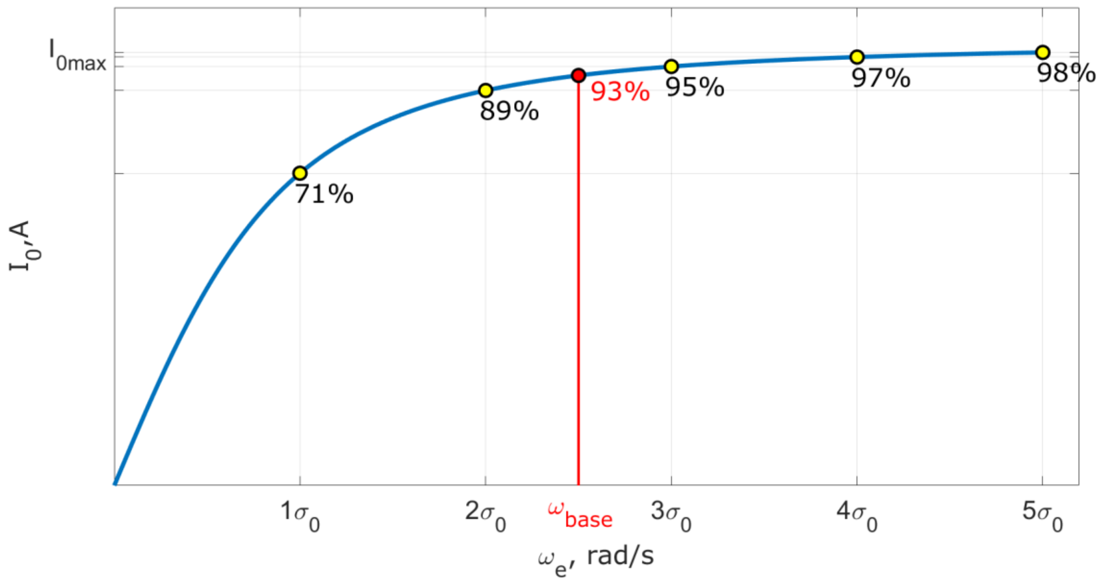

Fig. 7.2 – ZSC amplitude at constant base frequency (nominal r_s)

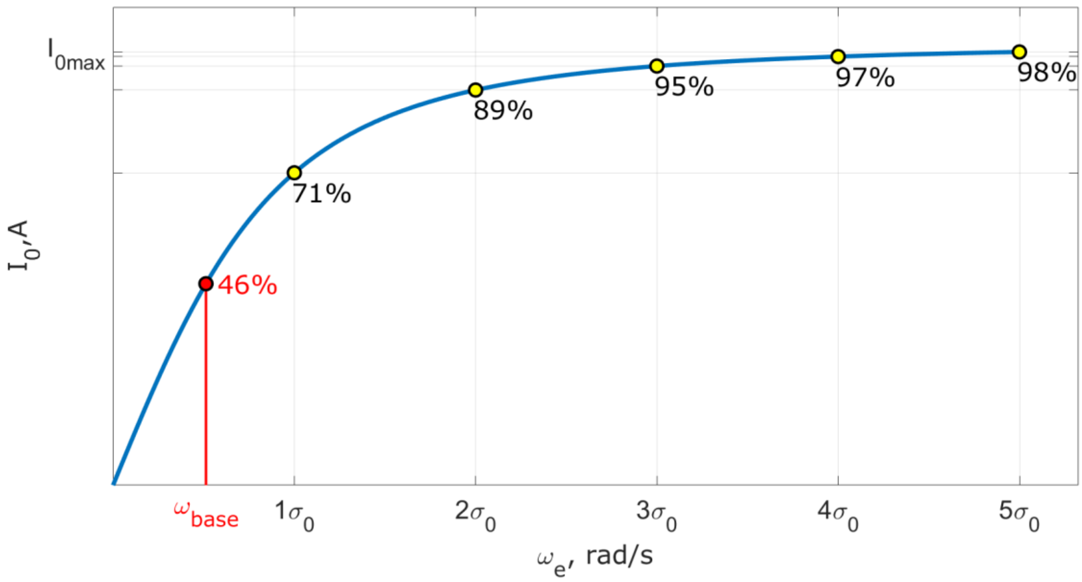

Fig. 7.3 – ZSC amplitude at constant base frequency (increased r_s)

In the first case, Fig. 7.2, the amplitude of the zero-sequence current is ranging from zero to 93% of the allowed maximum value of the zero-sequence current $|\tilde{I}_0|_{max}$ at the base speed ω_{base}. In the second case, when the value of the base speed remains the same, Fig. 7.3, the amplitude of the ZSC is ranging from zero to 46% of $|\tilde{I}_0|_{max}$ only, hence, it is indeed decreased.

In order to obtain a full picture of how the resistance influences the amplitude of the zero-sequence current, the parameters of the high-speed high power density starter/generator from TABLE I were used in equation (7.1) to construct a surface graph, illustrated in Fig. 7.4.

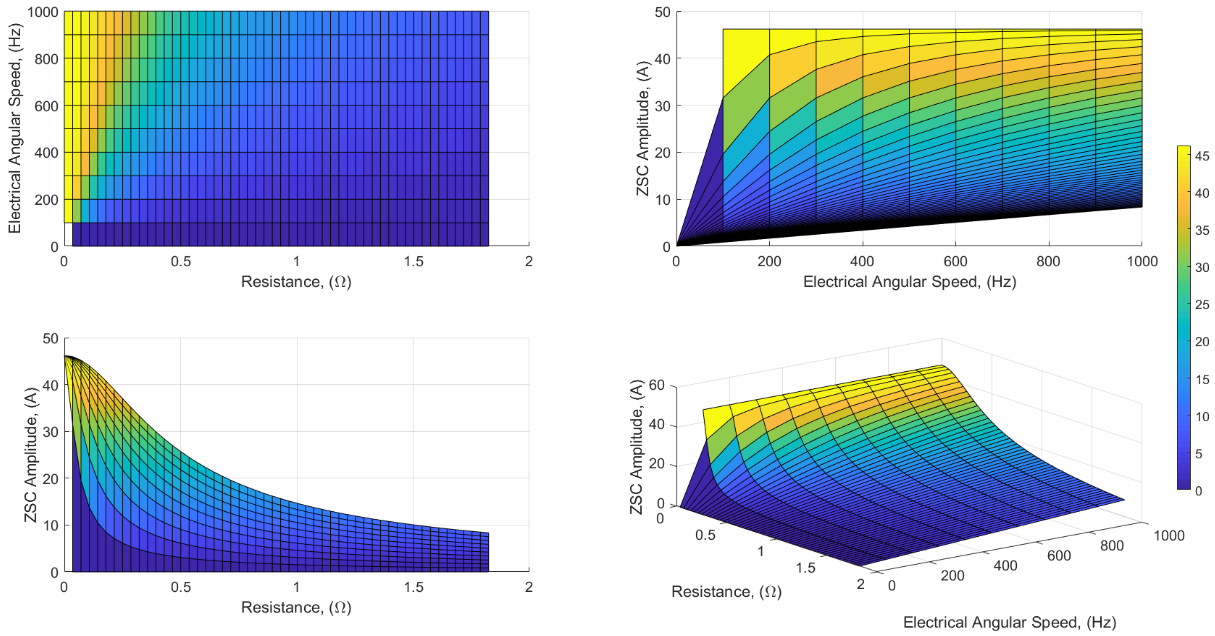

Fig. 7.4 – Amplitude of zero-sequence current

All of the four graphs presented in Fig. 7.4 illustrate a single surface plot of the amplitude of the zero-sequence current from different viewpoints.

The amplitude of ZSC is calculated across both the range of the electrical angular frequencies $(0 \rightarrow f_{base})$ and the range of resistances $(0 \rightarrow 1.825\ \Omega)$

It can be clearly seen from Fig. 7.4 how the amplitude of ZSC decays with increase of the resistance and grows non-linearly with the increase of the motor speed.

7.1.1.2 Influence of the Internal Resistance on Power Loss in Conductor

The power loss due to the zero-sequence current flowing in the system has already been discussed in chapter 3, sections 3.3, 3.4.1.2 and 3.4.2.2. This section aims at a further investigations of the influence of the uncontrolled zero-sequence current on the power loss in conductor when the phase resistance is changed.

The total instantaneous power loss due to the zero-sequence current s_0 can be found using the following formula:

$$s_0 = 3e_0 i_0 \tag{7.3}$$

The active instantaneous power p_0 could be found using the equation below:

$$p_0 = 3r_s {i_0}^2 \tag{7.4}$$

where, e_0 and i_0 are the instantaneous values of the zero-sequence back EMF and the zero-sequence current, respectively. r_s - is the phase resistance.

According to (3.61), the instantaneous value of the zero-sequence current can be found using the formula below.

$$i_0 = \left|\tilde{I}_0\right| \cos(3\theta_e + \gamma) \tag{7.5}$$

where, $\left|\tilde{I}_0\right|$ is the amplitude of the zero-sequence current, that could be found using equation (7.1). The variables θ_e and γ are the electrical phase angle and the phase shift, respectively. The phase shift γ can be found using equation (3.59) derived in chapter 3 on page 51.

Considering the derivation for equation (3.50) introduced in chapter 3 on page 48, the instantaneous value of the zero-sequence back EMF can be found using the equation below:

$$e_0 = |\tilde{E}_0| \cos(3\theta_e) \tag{7.6}$$

where, $|\tilde{E}_0|$ is the amplitude of the zero-sequence back EMF, that could be found using equation (3.51) from chapter 3 on page 49. θ_e is the electrical phase angle.

In order to visualise what is happening with the instantaneous values of the total power s_0 and active power p_0 along with the instantaneous values of the zero-sequence back EMF voltage e_0 and the zero-sequence current i_0, the equations (7.3) - (7.6) were plotted with the electrical angle as the domain: Fig. 7.5 - Fig. 7.24.

Each of the figures hold multiple plots corresponding to the different values of the motor speed expressed in the electrical frequency from zero to the base speed. The figures that share the same resistance value are grouped on a single page. TABLE XV was constructed in order to ease the navigation through the angle domain results.

TABLE XV Electrical angle domain plots

Quality	**Resistance r_s**				
	0.164 Ω	**0.597 Ω**	**1.031 Ω**	**1.464 Ω**	**2.000 Ω**
e_0	Fig. 7.5	Fig. 7.9	Fig. 7.13	Fig. 7.17	Fig. 7.21
i_0	Fig. 7.6	Fig. 7.10	Fig. 7.14	Fig. 7.18	Fig. 7.22
s_0	Fig. 7.7	Fig. 7.11	Fig. 7.15	Fig. 7.19	Fig. 7.23
p_0	Fig. 7.8	Fig. 7.12	Fig. 7.16	Fig. 7.20	Fig. 7.24

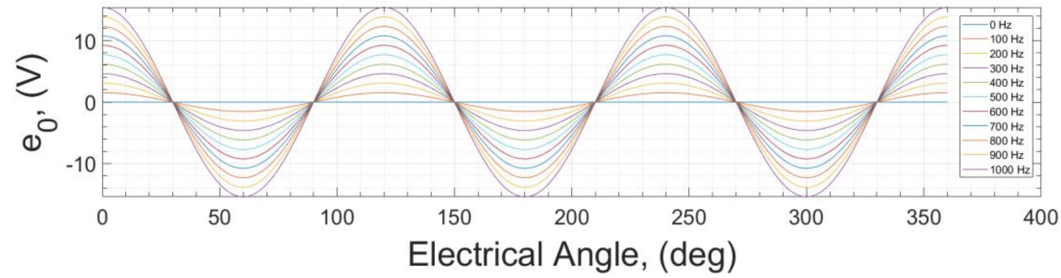

Fig. 7.5 – Zero-sequence back EMF ($r_s = 0.164\ \Omega$)

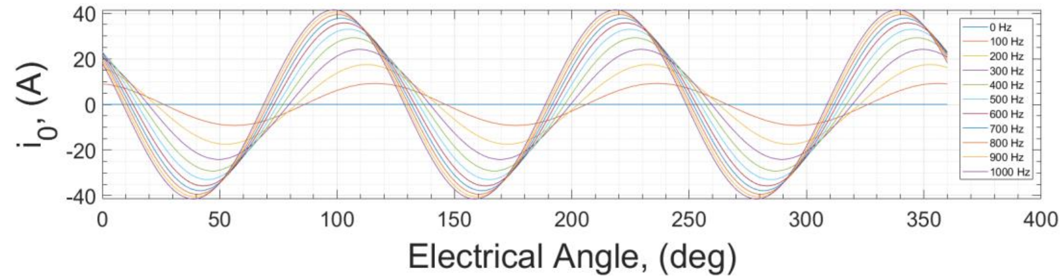

Fig. 7.6 – Zero-sequence current ($r_s = 0.164\ \Omega$)

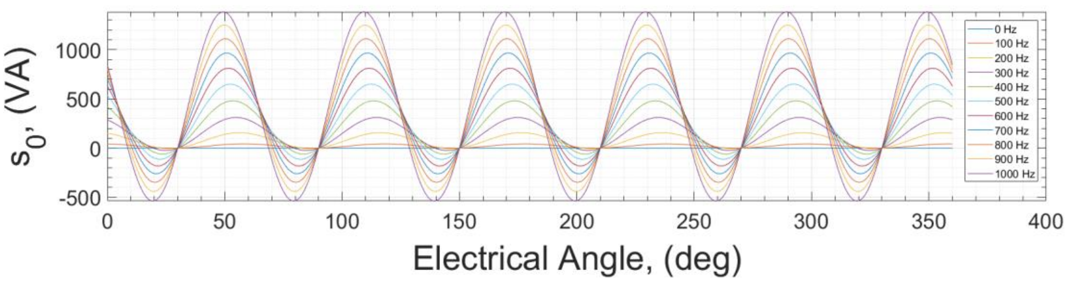

Fig. 7.7 – Total power loss due to zero-sequence component ($r_s = 0.164\ \Omega$)

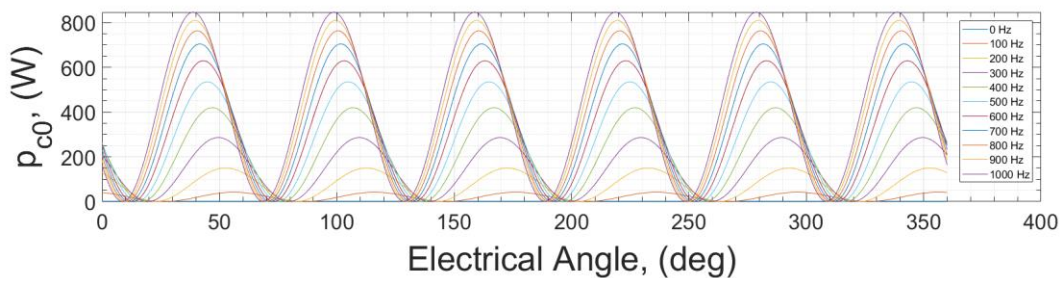

Fig. 7.8 – Power loss in conductor due to ZSC ($r_s = 0.164\ \Omega$)

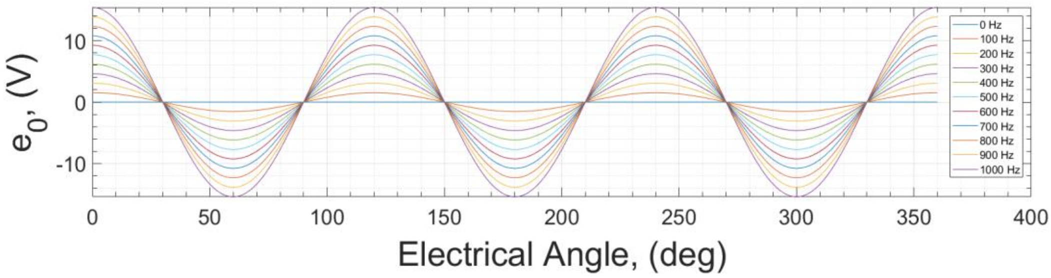

Fig. 7.9 – Zero-sequence back EMF ($r_s = 0.597\ \Omega$)

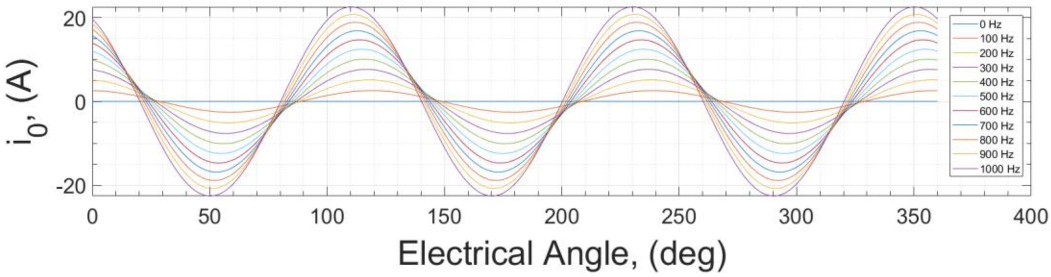

Fig. 7.10 – Zero-sequence current ($r_s = 0.597\ \Omega$)

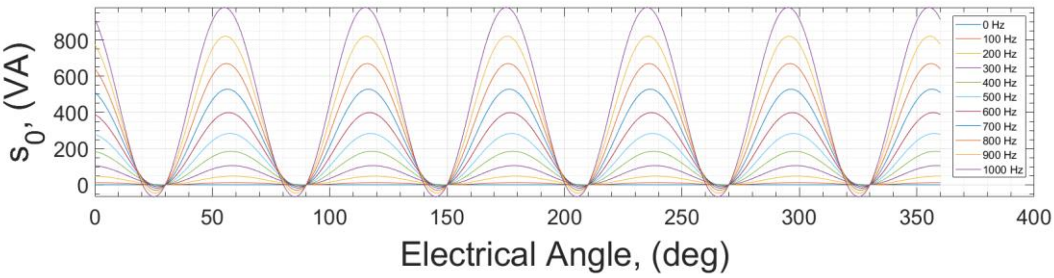

Fig. 7.11 – Total power loss due to zero-sequence component ($r_s = 0.597\ \Omega$)

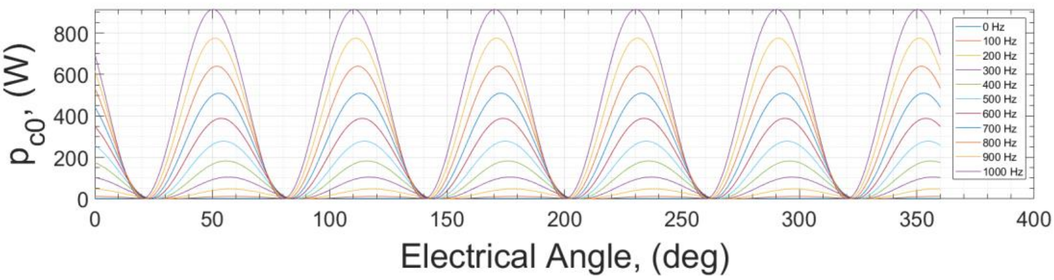

Fig. 7.12 – Power loss in conductor due to ZSC ($r_s = 0.597\ \Omega$)

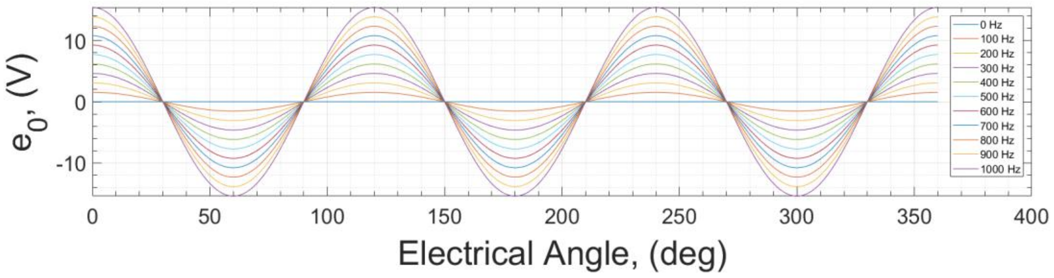

Fig. 7.13 – Zero-sequence back EMF ($r_s = 1.031\ \Omega$)

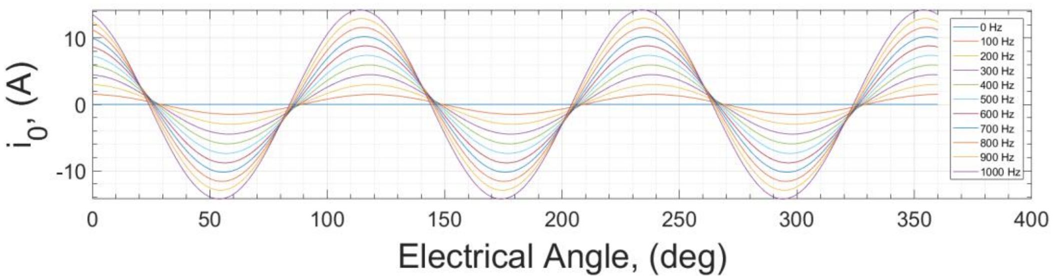

Fig. 7.14 – Zero-sequence current ($r_s = 1.031\ \Omega$)

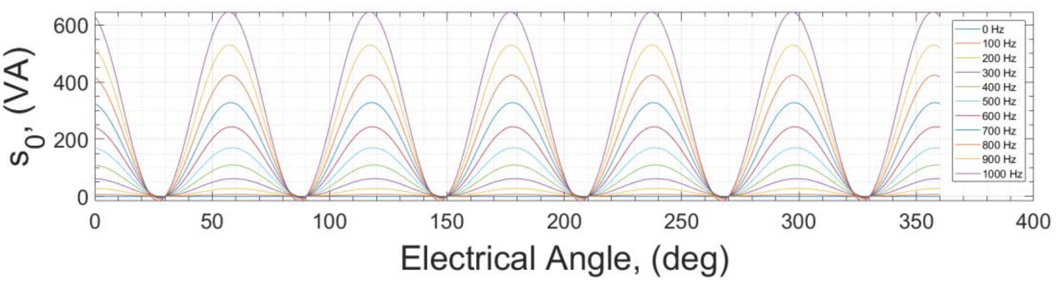

Fig. 7.15 – Total power loss due to zero-sequence component ($r_s = 1.031\ \Omega$)

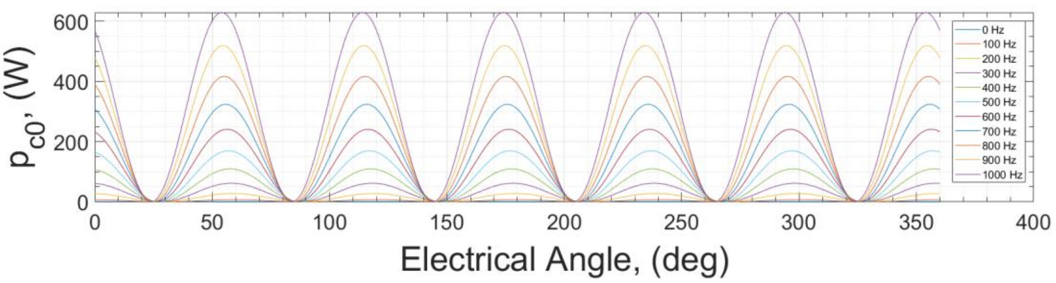

Fig. 7.16 – Power loss in conductor due to ZSC ($r_s = 1.031\ \Omega$)

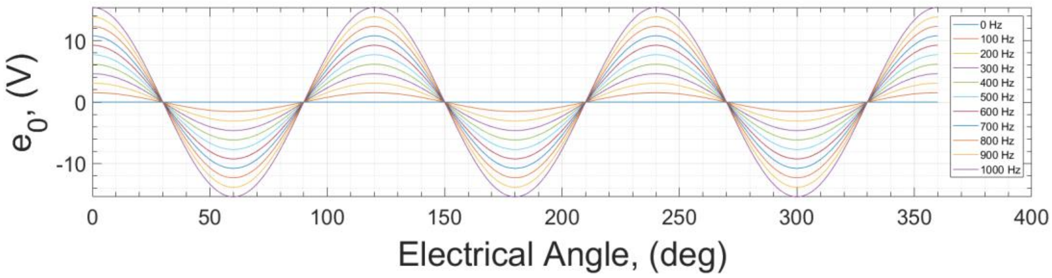

Fig. 7.17 – Zero-sequence back EMF ($r_s = 1.464\ \Omega$)

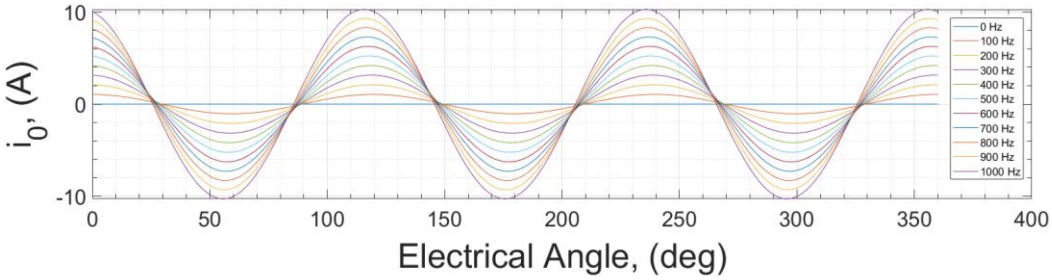

Fig. 7.18 – Zero-sequence current ($r_s = 1.464\ \Omega$)

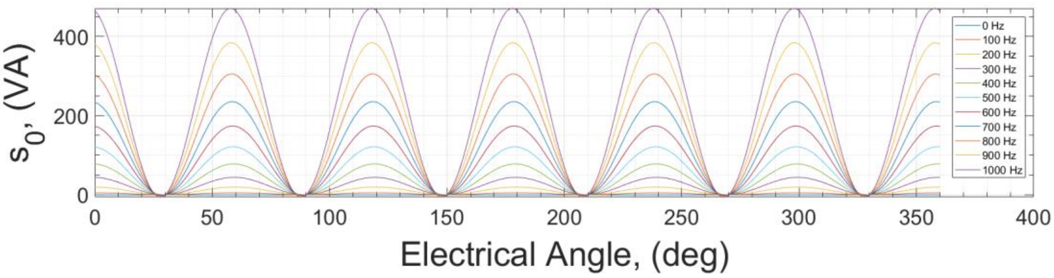

Fig. 7.19 – Total power loss due to zero-sequence component ($r_s = 1.464\ \Omega$)

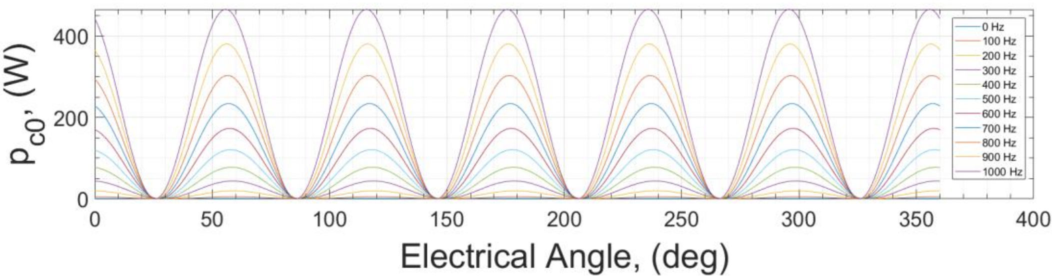

Fig. 7.20 – Power loss in conductor due to ZSC ($r_s = 1.464\ \Omega$)

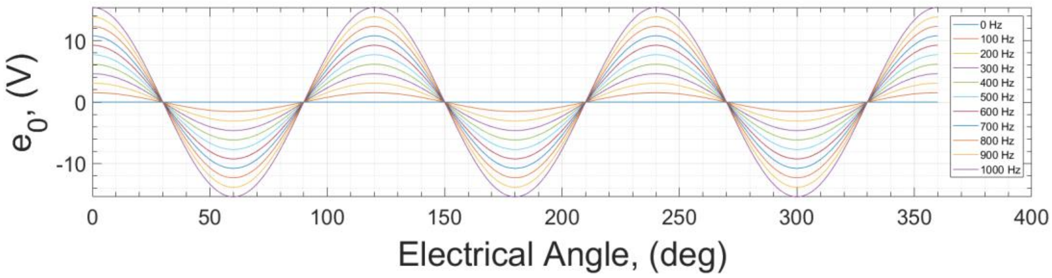

Fig. 7.21 – Zero-sequence back EMF ($r_s = 2\,\Omega$)

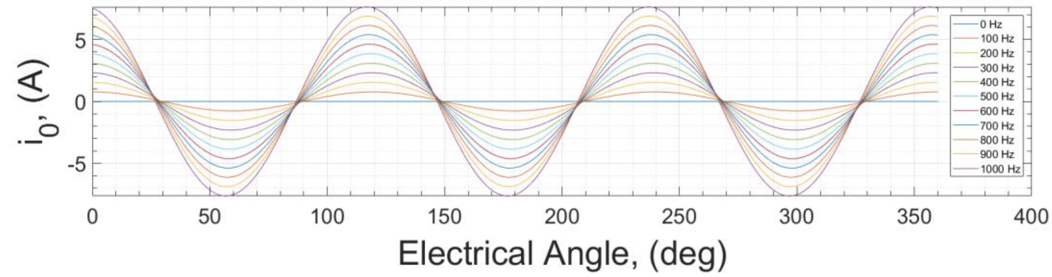

Fig. 7.22 – Zero-sequence current ($r_s = 2\,\Omega$)

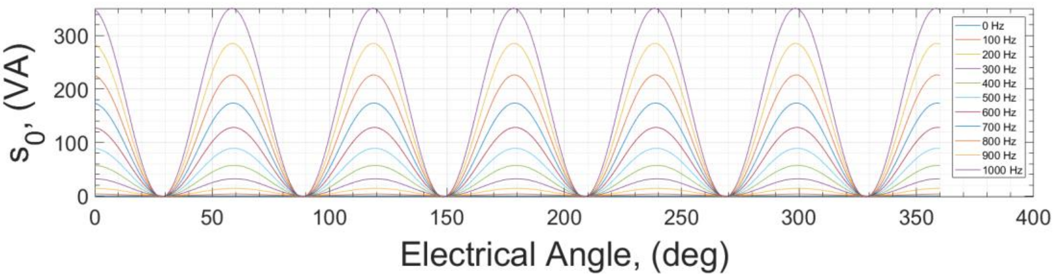

Fig. 7.23 – Total power loss due to zero-sequence component ($r_s = 2\,\Omega$)

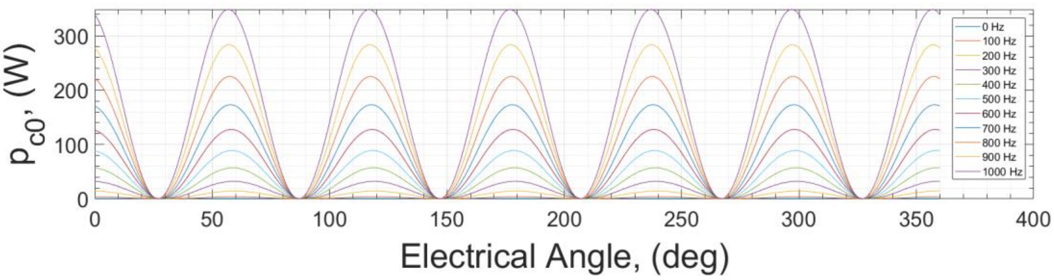

Fig. 7.24 – Power loss in conductor due to ZSC ($r_s = 2\,\Omega$)

It can be deduced from the figures the reference for which is introduced in TABLE XV that the speed of the motor and the phase resistance influences the behaviour of the zero-sequence components' qualities.

The phase shift of the zero-sequence current i_0 is more pronounced at a higher frequency when the resistance is low. Therefore, it is seen from the representation of the instantaneous total zero-sequence power s_0 that there is a lot of zero-sequence reactive power introduced in the system looking at the negative component of it, Fig. 7.7. This behaviour is not seen when the resistance is kept high: Fig. 7.11, Fig. 7.15, Fig. 7.19 and Fig. 7.23.

In order to better the understanding of the zero-sequence components qualities introduced in Fig. 7.5 - Fig. 7.24, their amplitudes have been plotted along the electrical frequencies: Fig. 7.25 - Fig. 7.28. The multiple graphs on a single plot represent the values at different phase resistances, stated in the legend in each of the figures.

The behaviour of the steady state zero-sequence back EMF voltage, Fig. 7.25, and the zero-sequence current, Fig. 7.26, are as expected and already discussed. The linear dependency of $|\tilde{E}_0|$ is well pronounced and independent of the phase resistance, as shown in Fig. 7.25.

Fig. 7.27 and Fig. 7.28 represent a constant growth of the power loss with increasing rotor speed for a single chosen phase resistance.

The rate of change of the total power loss due to the zero-sequence component increases with the smaller values of resistance r_r.

Considering the active power loss in Fig. 7.28 at 1000 Hz, despite of the general trend the increase of the resistance results in the greater power loss. The general trend represents a decay of the power loss with decreasing resistance. However, this situation is rather odd. Hence, more investigation was required to fully understand what is happening in the system.

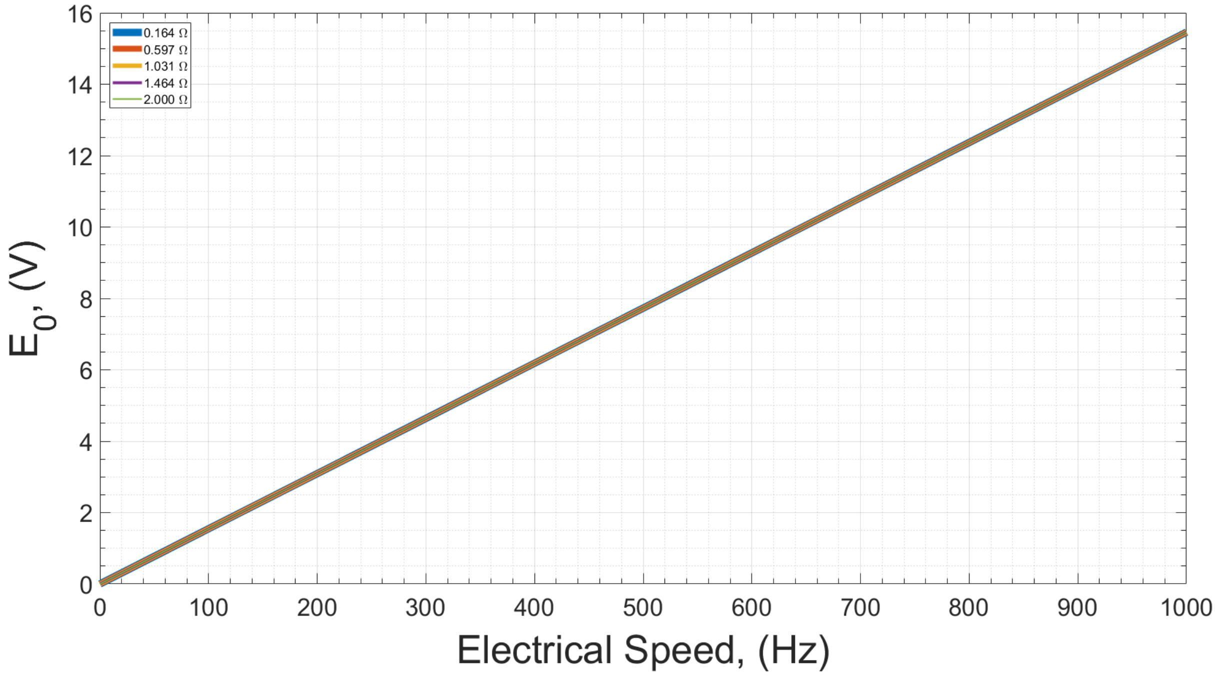

Fig. 7.25 – Steady state zero-sequence back EMF

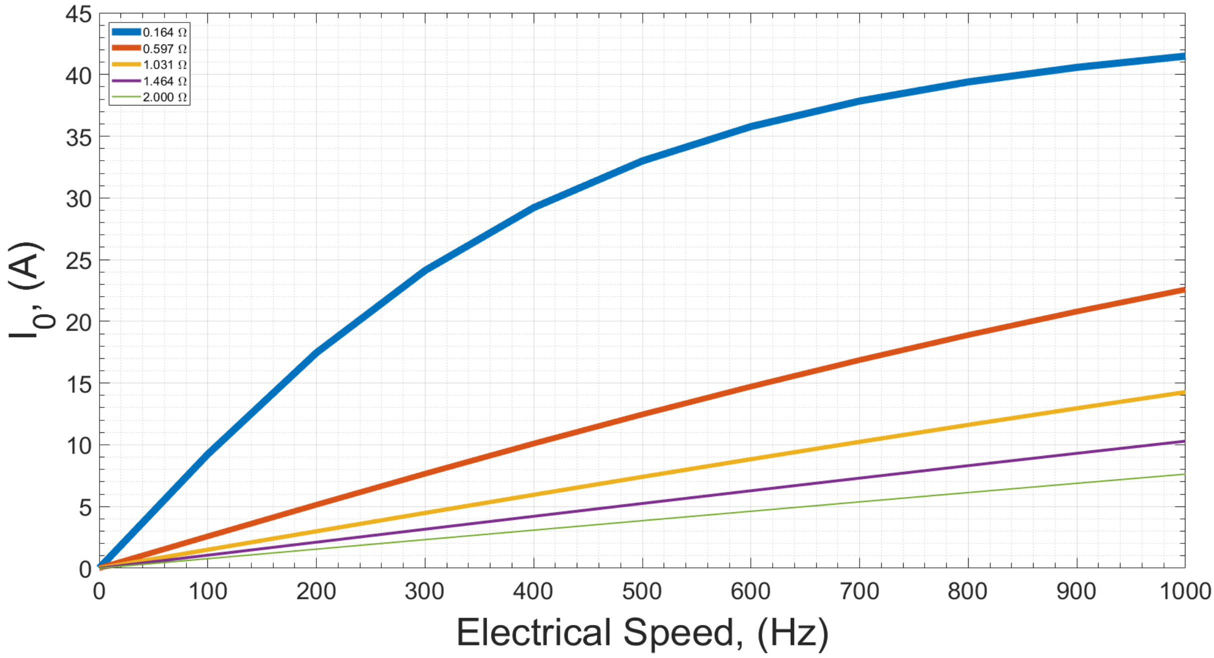

Fig. 7.26 – Steady state zero-sequence current

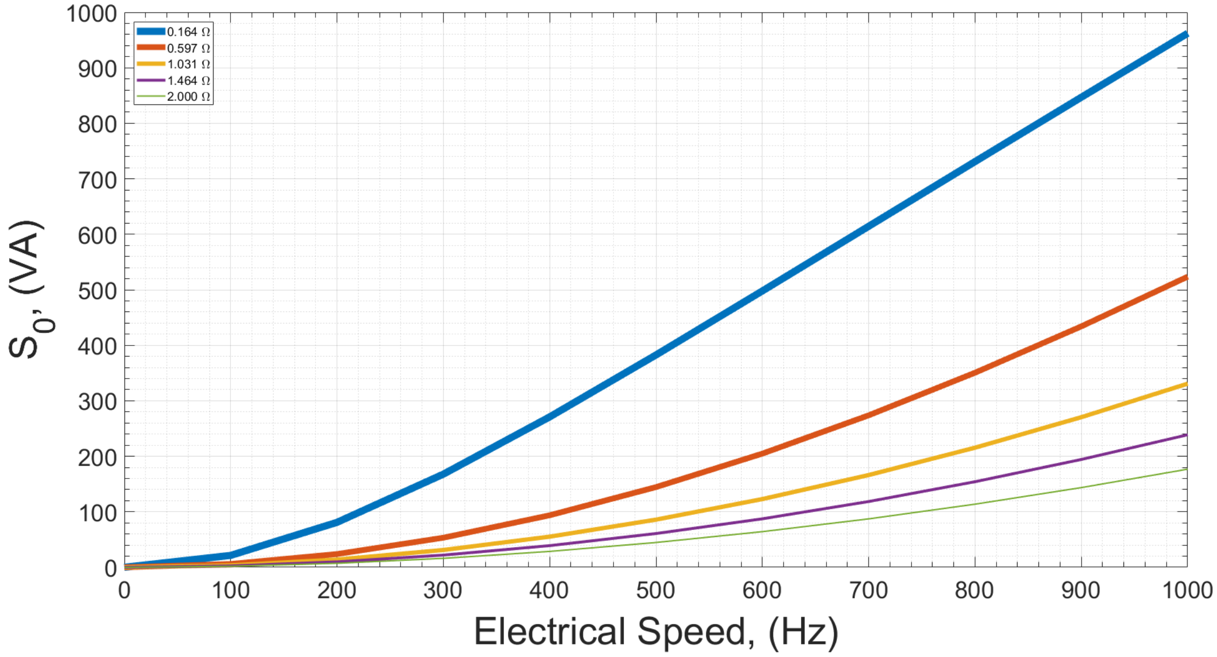

Fig. 7.27 – Steady state total power loss due to zero-sequence component

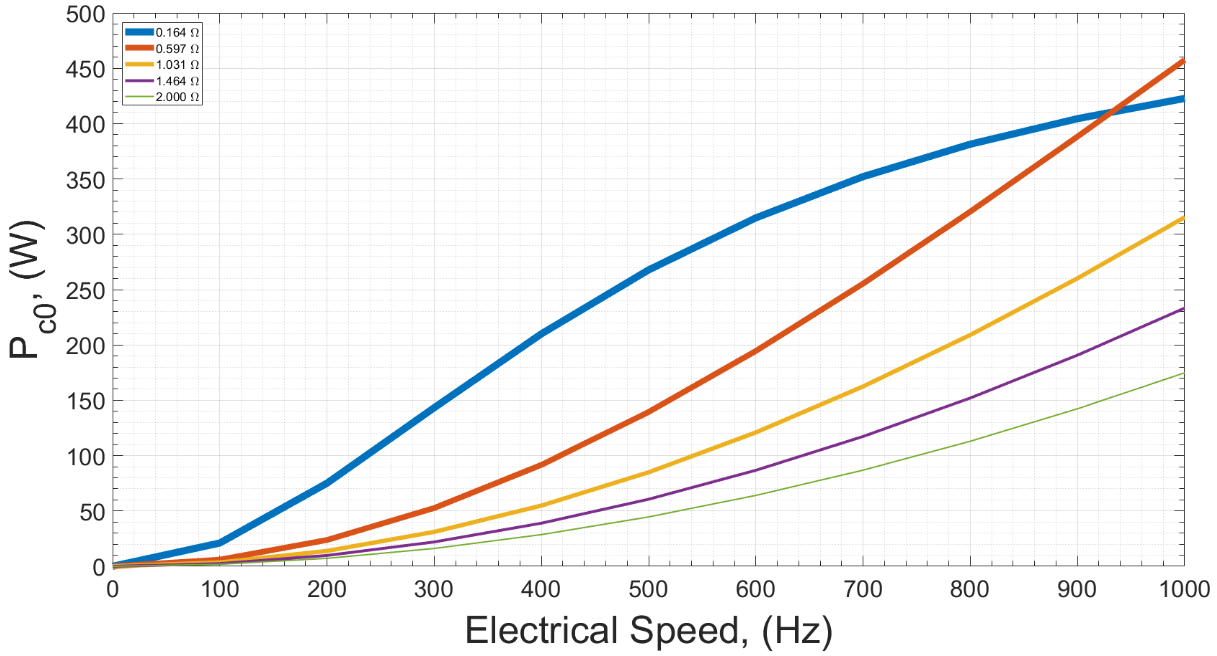

Fig. 7.28 – Steady state power loss in conductor due to ZSC

To make the analysis consistent, active P_0, reactive Q_0 and total S_0 power losses due to the zero-sequence component were plotted on the same graph along the range of the motor's electrical speeds and the changing value of the resistance, Fig. 7.29.

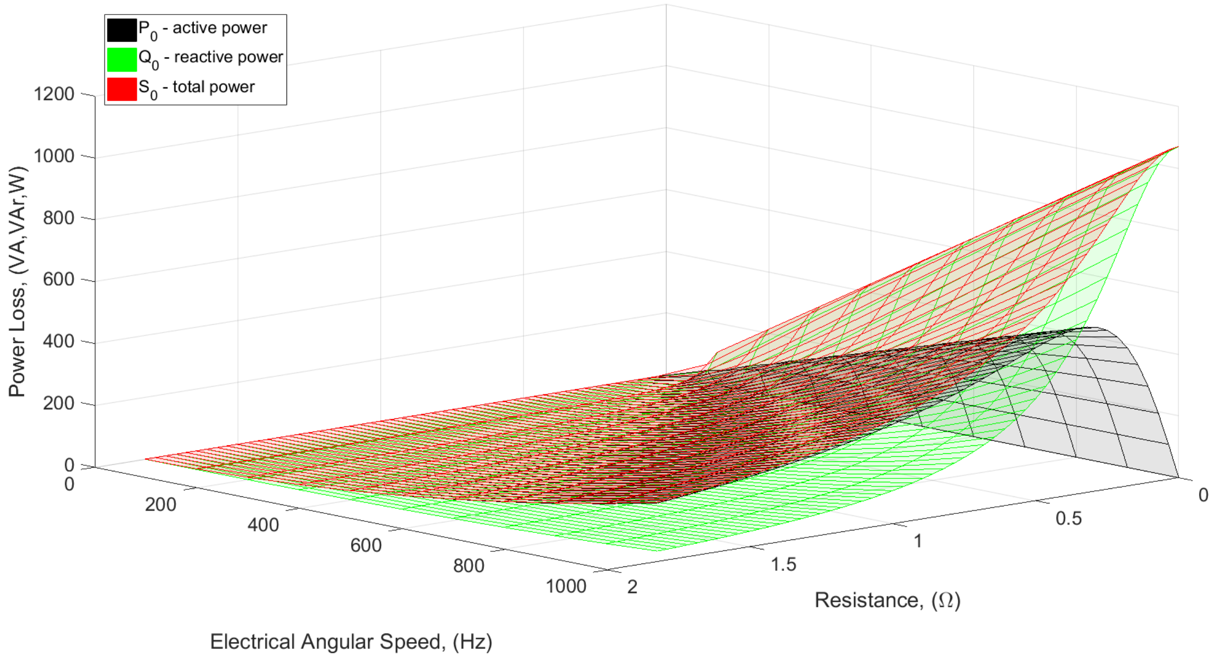

Fig. 7.29 – Components of power loss due to ZSC

The formulae used to construct the surfaces of Fig. 7.29 are as follows.

Active power P_0:

$$P_0 = \frac{3}{2}|\tilde{E}_0||\tilde{I}_0|\cos(\gamma) \tag{7.7}$$

where, $|\tilde{E}_0|$ is the zero-sequence back EMF, $|\tilde{I}_0|$ is the zero-sequence current and γ is the phase shift of the zero-sequence current.

Reactive power Q_0:

$$Q_0 = \frac{3}{2}|\tilde{E}_0||\tilde{I}_0|\sin(\gamma) \tag{7.8}$$

Total power S_0:

$$S_0 = \sqrt{{P_0}^2 + {Q_0}^2} \tag{7.9}$$

Fig. 7.29 shows the behaviour of all of the zero-sequence power components. The reactive component dominates at a lower resistance and the active power component dominates at a higher resistance. The crossing points are right at the maximum values of the active power component along the range of the motor speeds. This happens when the active and reactive impedances of the zero-sequence power components match, i.e. $r_s = 3\omega_e L_0$. At this point the active power is at its maximum value shown with magenta markers in Fig. 7.30.

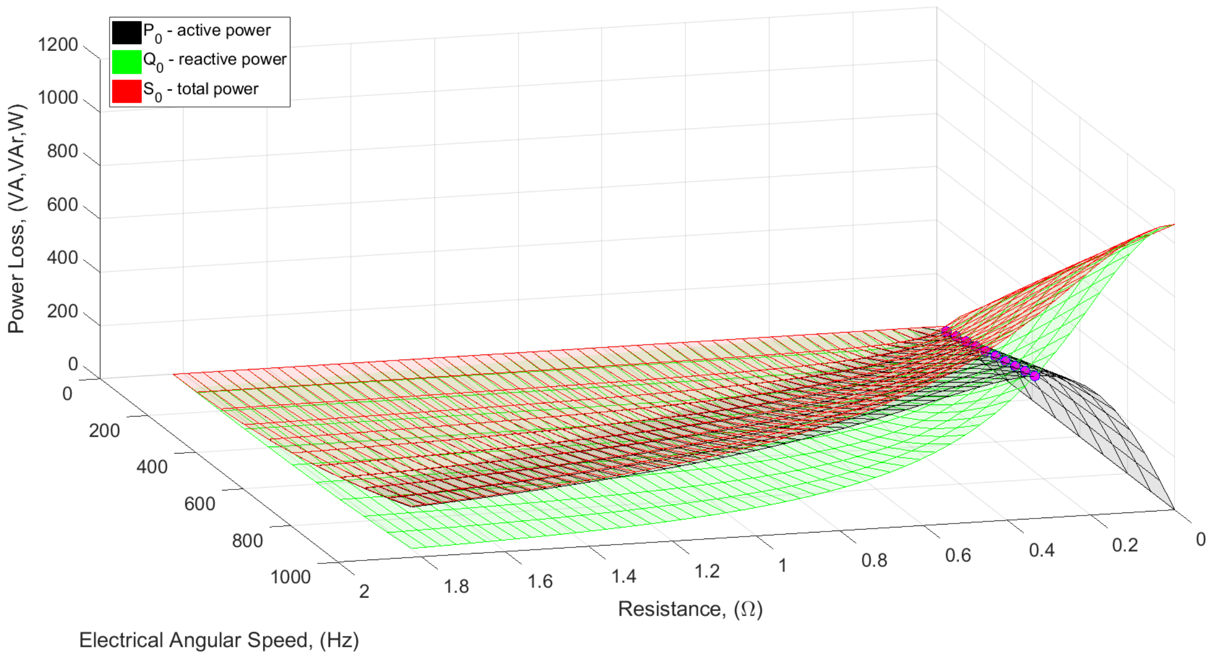

Fig. 7.30 – Power loss in conductor due to ZSC with crossing active and reactive planes points.

The presented active power P_0 also represents the power loss in conductor due to the zero-sequence current P_{c0}, shown in equation (7.14).

During the constant torque operation region of a permanent magnet synchronous motor, the value of the direct axis current i_d is controlled to remain zero. Therefore, the term with this current in the equation of power loss in conductor (3.42) introduced in chapter 3 on page 46 can be ignored. The new equation would look as follows.

$$P_c = \frac{3}{2}\left(r_s i_q{}^2 + 2 r_s i_0{}^2\right) \tag{7.10}$$

Substituting the RMS value of the zero-sequence current $\frac{|\tilde{I}_0|}{\sqrt{2}}$ instead of its instantaneous value i_0, the equation of the power loss in conductor (7.10) becomes:

$$P_c = \frac{3}{2}\left(r_s i_q{}^2 + r_s \left|\tilde{I}_0\right|^2\right) \tag{7.11}$$

where, i_q is the quadrature axis current, controlled to meet the torque demands of an OEW PMSM with common DC link, $\left|\tilde{I}_0\right|$ is the amplitude value of zero-sequence current and r_s is the phase resistance.

As per equation (7.11), the power loss in conductor is comprised of two parts (7.12): the power loss in conductor due to the torque producing current P_{cq}.(7.13) and the power loss in conductor due to the zero-sequence current P_{c0} (7.14).

$$P_c = P_{cq} + P_{c0} \tag{7.12}$$

where,

$$P_{cq} = \frac{3}{2} r_s i_q{}^2 \tag{7.13}$$

and

$$P_{c0} = \frac{3}{2} r_s \left|\tilde{I}_0\right|^2 \tag{7.14}$$

It can be deduced from equation (7.13) that the power loss in conductor due to the torque producing current is independent of the frequency of the motor. This power loss component P_{cq} can be represented as a function of the resistance r_s and the quadrature axis current i_q as shown in Fig. 7.31.

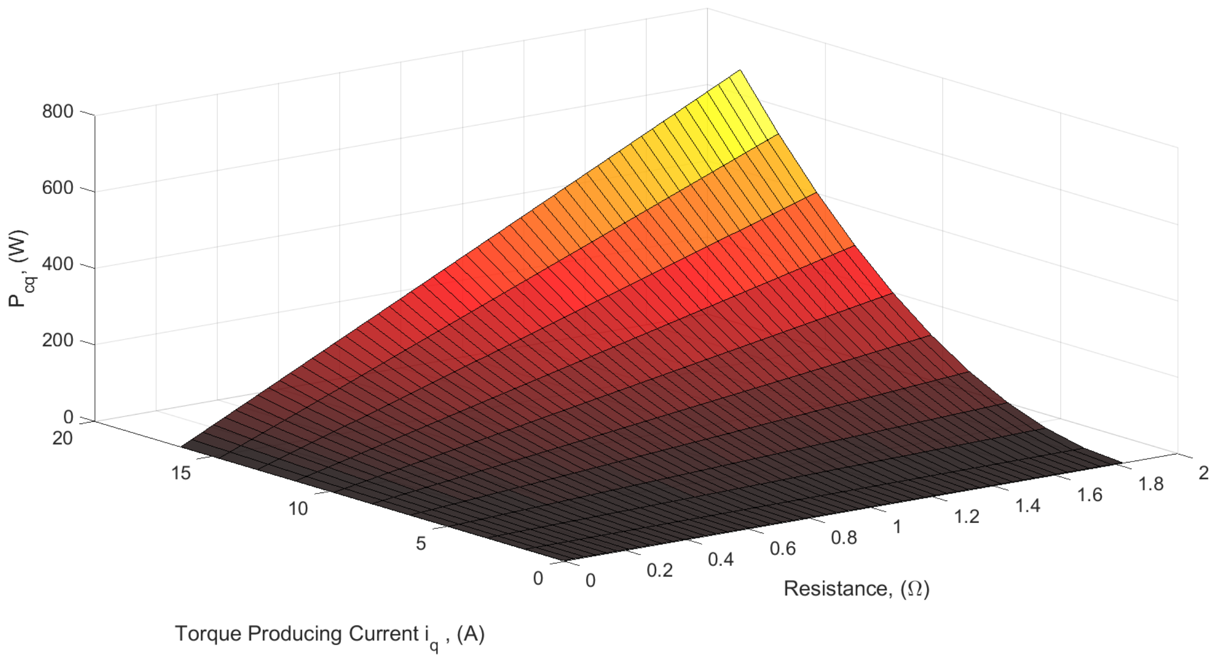

Fig. 7.31 – Power loss in conductor due to the torque producing current i_q

Considering the power loss in conductor due to the zero-sequence current, presented in equation (7.14), not only does this power component depend on the resistance r_s, but also it becomes a function of the electrical frequency ω_e, as per the equation (7.1). Hence, substituting the equation (7.1) into (7.14), the power loss in conductor due to the zero-sequence current becomes as stated in equation (7.15).

$$P_{c0} = \frac{3}{2} r_s \left(\left| \tilde{I}_0 \right|_{max} \frac{\omega_e}{\sqrt{{\sigma_0}^2 + {\omega_e}^2}} \right)^2 = \frac{3}{2} r_s \left| \tilde{I}_0 \right|_{max}^2 \frac{{\omega_e}^2}{{\sigma_0}^2 + {\omega_e}^2} \tag{7.15}$$

where, ω_e is the angular frequency of the motor in radians, σ_0 is the already mentioned frequency constant that appears to be dependent on the phase resistance r_s as shown in (7.2) and $\left| \tilde{I}_0 \right|_{max}$ is the introduced concept of a maximum value of the zero-sequence current flowing in an open-end winding machine drive with common DC link under the uncontrolled ZSC condition, described in 3.4.2.

Substituting the equation of the frequency constant σ_0 (7.2) into (7.15), the equation (7.16) is obtained:

$$P_{c0} = \frac{3}{2} r_s \left| \tilde{I}_0 \right|_{max}^2 \frac{{\omega_e}^2}{\left(\frac{r_s}{3L_0} \right)^2 + {\omega_e}^2} \tag{7.16}$$

where, L_0 is the leakage inductance.

It is also worth noting that with the increasing speed, the power loss due to the zero-sequence current will not grow to infinity. Instead, it will tend to a particular value that is calculated in (7.17) by taking the limit of (7.16) when the angular electrical frequency ω_e tends to infinity:

$$P_{c0\,max} = \lim_{\omega_e \to \infty} \left(\frac{3}{2} r_s \left| \tilde{I}_0 \right|_{max}^2 \frac{{\omega_e}^2}{\left(\frac{r_s}{3L_0} \right)^2 + {\omega_e}^2} \right) = \frac{3}{2} r_s \left| \tilde{I}_0 \right|_{max}^2 \tag{7.17}$$

Equation (7.17) shows that regardless of the speed value, the power loss in copper due to the zero-sequence current will never exceed $\frac{3}{2} r_s \left| \tilde{I}_0 \right|_{max}^2$ watt.

The equation (7.16) of the zero-sequence component P_{c0} of the power loss in conductor P_c was represented as a function of both the angular frequency ω_e and the phase resistance r_s, thereby plotted as a surface graph shown in Fig. 7.32.

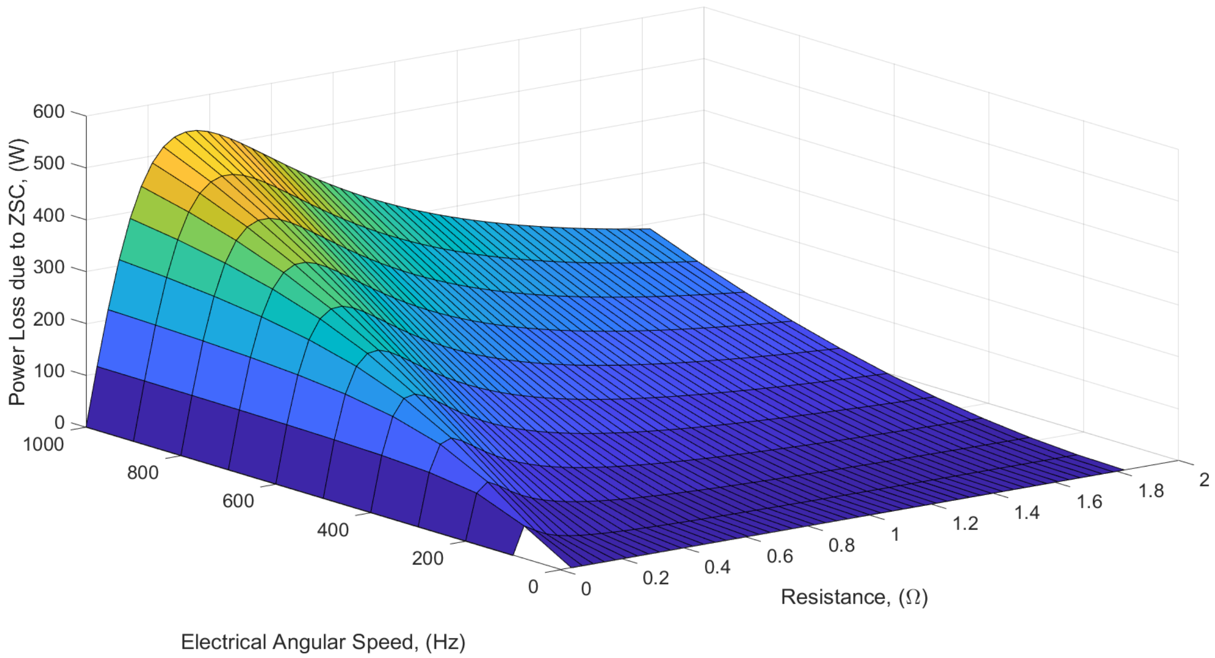

Fig. 7.32 – Power loss in conductor due to zero-sequence current

Considering Fig. 7.32, the lines along the resistance axis represent a constant value of the motor's speed. It can be seen that the power loss in conductor due to the zero-sequence current increases with increasing phase resistance to a certain maximum point and then decreases with increasing resistance afterwards. These maximum points of power loss in conductor due to the zero-sequence current can be found at a particular operating frequency using a special mathematical procedure described below.

In order to find the points of interest, the derivative of (7.16) is taken and equated to zero:

$$\frac{dP_{c0}}{dr_s} = \frac{27}{2}\left|\tilde{I}_0\right|_{max}^2 {L_0}^2{\omega_e}^2 \frac{{r_s}^2 - 9{L_0}^2{\omega_e}^2}{{r_s}^2 + 9{L_0}^2{\omega_e}^2} = 0 \tag{7.18}$$

The solution for (7.18) with respect to r_s:

$$r_s = \begin{cases} 3\omega_e L_0, & for\ \omega_e > 0 \\ -3\omega_e L_0, & for\ \omega_e < 0 \end{cases} \qquad (7.19)$$

Taking the second derivative of (7.16):

$$\frac{d^2 P_{c0}}{d{r_s}^2} = 27 r_s \left|\tilde{I}_0\right|_{max}^2 {L_0}^2 {\omega_e}^2 \frac{{r_s}^2 - 27{L_0}^2{\omega_e}^2}{\left({r_s}^2 + 9{L_0}^2{\omega_e}^2\right)^3} \qquad (7.20)$$

Substituting (7.19) into (7.20) to identify whether the point of interest is a local maximum or minimum:

$$\frac{d^2 P_{c0}}{d{r_s}^2} = \begin{cases} -\frac{\left|\tilde{I}_0\right|_{max}^2}{4\omega_e L_0}, when\ \omega_e > 0 \Rightarrow \frac{d^2 P_{c0}}{d{r_s}^2} < 0 \Rightarrow local\ maximum \\ \frac{\left|\tilde{I}_0\right|_{max}^2}{4\omega_e L_0}, when\ \omega_e < 0 \Rightarrow \frac{d^2 P_{c0}}{d{r_s}^2} < 0 \Rightarrow local\ maximum \end{cases} \qquad (7.21)$$

According to (7.21) with incorporated (7.19), the value of the resistance that results in the maximum power loss in conductor due to the zero-sequence current when the rotor speed is positive can be presented as follows.

$$r_s = 3\omega_e L_0 \qquad (7.22)$$

Substituting the solution (7.22) into equation (7.16), the peak power loss in conductor at a particular speed of the motor can be determined:

$$P_{c0\,peak} = \frac{9}{4}\omega_e L_0 \left|\tilde{I}_0\right|_{max}^2 \qquad (7.23)$$

The equation for the peak value of the power loss in conductor due to the zero-sequence current (7.23) along with the equation for the resistance (7.22) were used to plot the peak points on the top in the surface plot depicted in Fig. 7.32. The side view of the resulting plot is shown in Fig. 7.33.

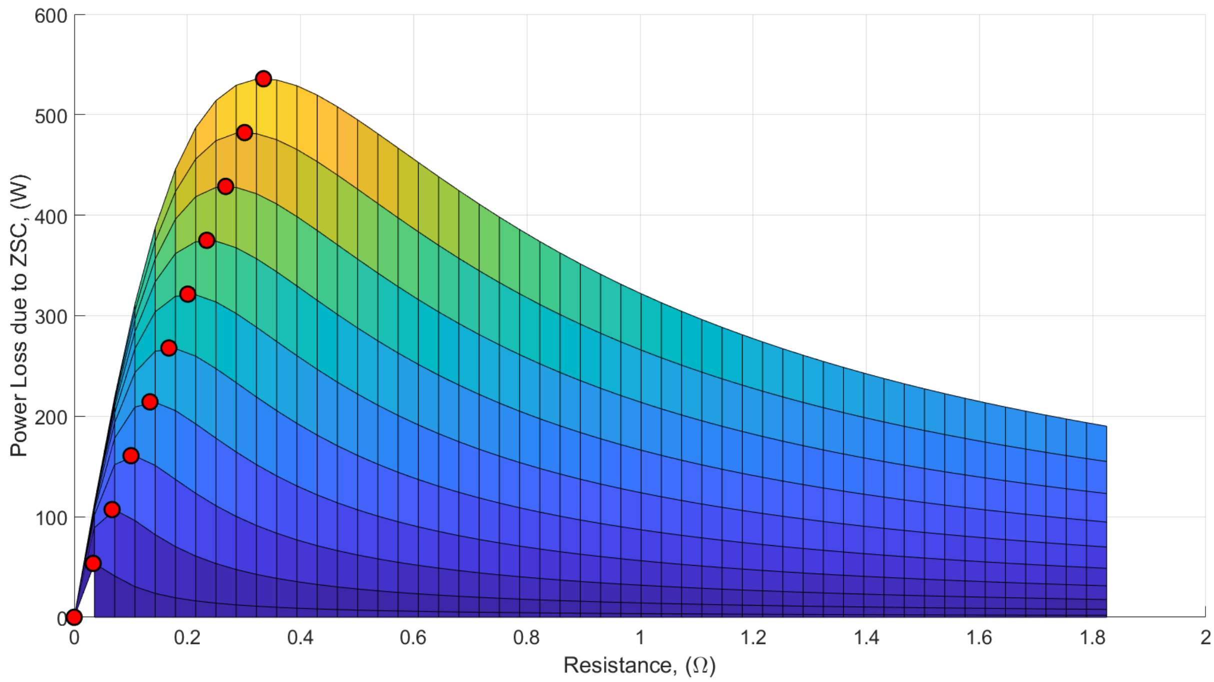

Fig. 7.33 – Power loss in conductor due to ZSC (resistance domain)

The red markers indicate the maximum value of the power loss in conductor due to the zero-sequence current at a particular drive operating speed.

It has already been mentioned that the power loss in conductor due to the torque producing current i_q does not depend on the speed of the motor unlike the power loss in conductor due to the zero-sequence current. However, in order to combine these two power loss components as per equation (7.12), the power loss due to the torque producing current i_q (7.13) has to be expressed in terms of the operational speed of the OEW PMSM motor considered in this thesis. Thereby, using equation (7.13) a set of surfaces was produced showing how the power loss due to the torque producing current changes with the value of the phase resistance, Fig. 7.34.

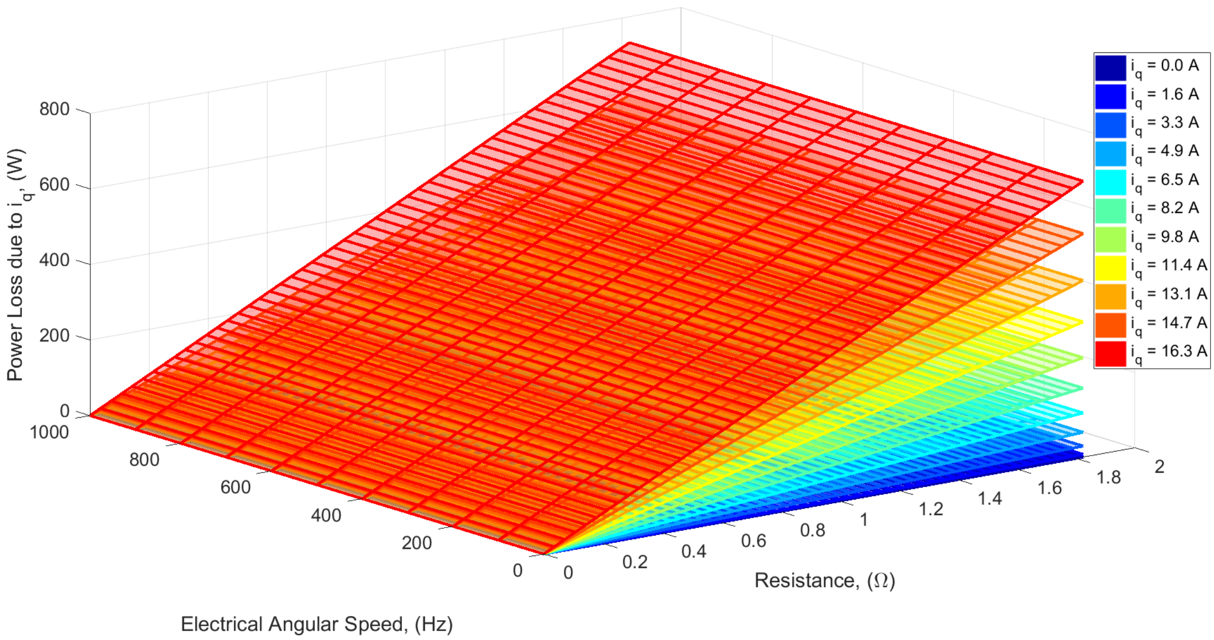

Fig. 7.34 – Power loss in conductor due to i_q

One of the planes representing the power loss in conductor due to the torque producing current from Fig. 7.34 was plotted on the same axes with the power loss in conductor due to the zero-sequence current. This combination is illustrated in Fig. 7.32.

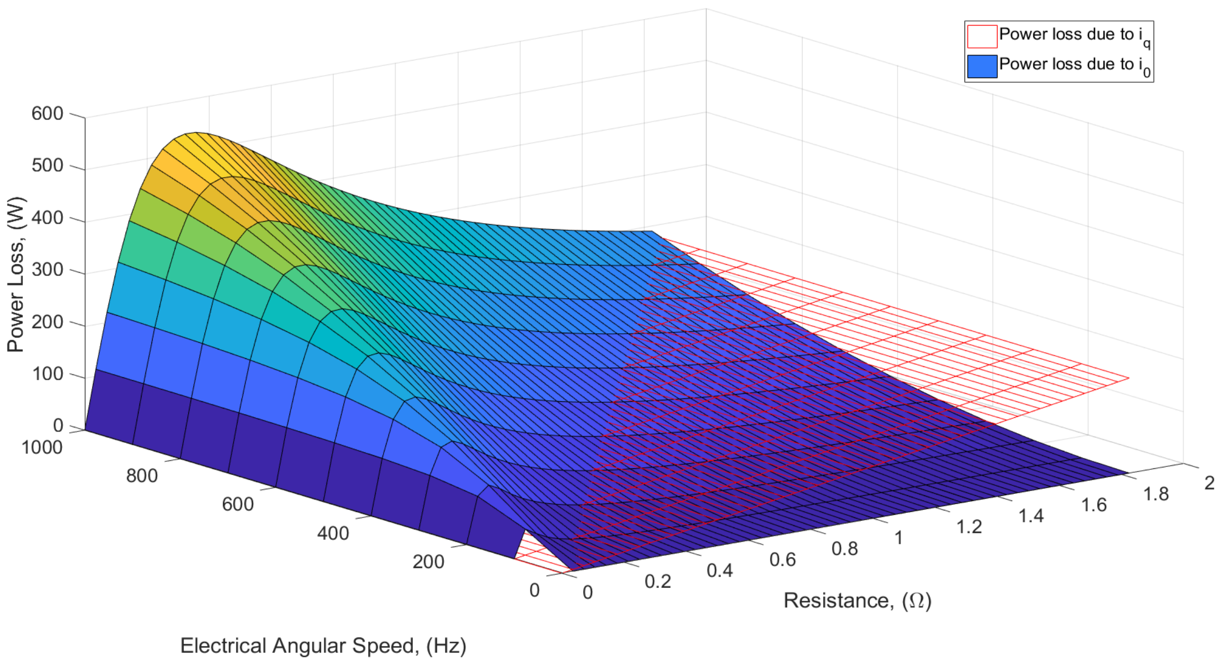

Fig. 7.35 – Components of the power loss in conductor

The two graphs of Fig. 7.35 were then combined together according the equation of the total power loss in conductor (7.12) and the result of this combination can be observed in Fig. 7.36.

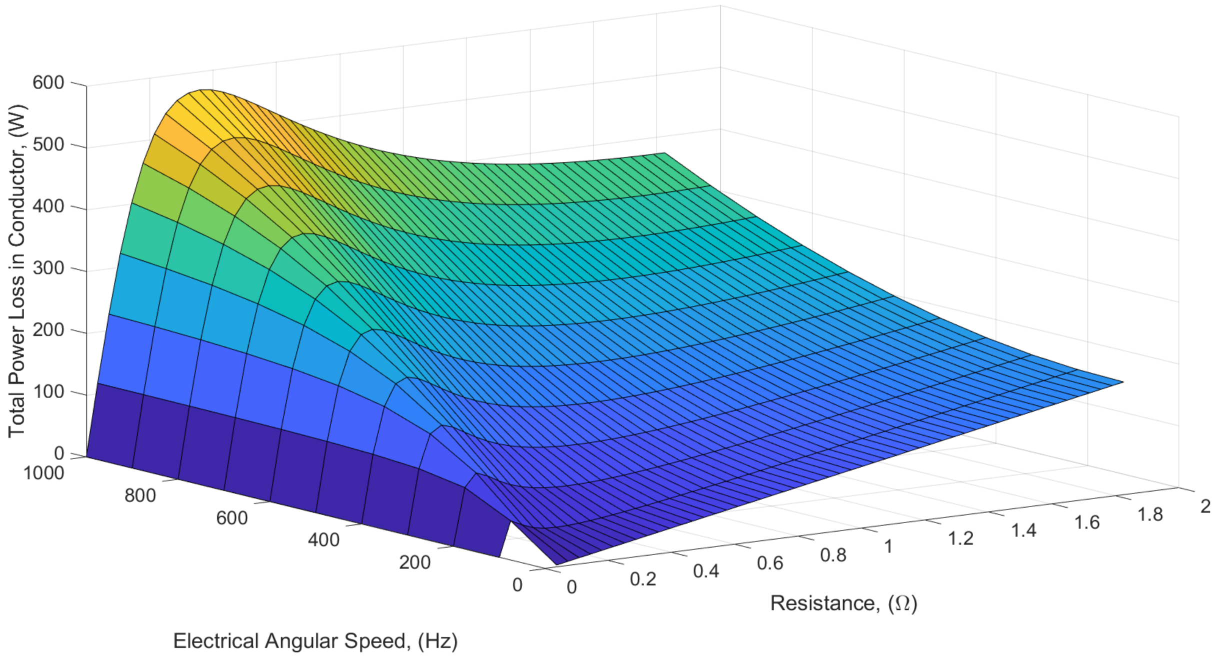

Fig. 7.36 – Total power loss in conductor

7.1.2Proposed Power Loss in Conductor Reduction Technique

Consider the total power loss in conductor, represented in Fig. 7.36. The equation for this plot is a combination of the power loss in conductor due to both the zero-sequence current and the torque producing current as discussed in the previous section. Obtaining the side view of the surface graph in Fig. 7.36, the resistance - power loss in conductor relationship is revealed, Fig. 7.37.

Looking closely at the resistance – power loss relationship of Fig. 7.37, it can be noticed that unlike the graph of the power loss due to the zero-sequence current shown in Fig. 7.33, the current plot has the local minimum point as well as the maximum point.

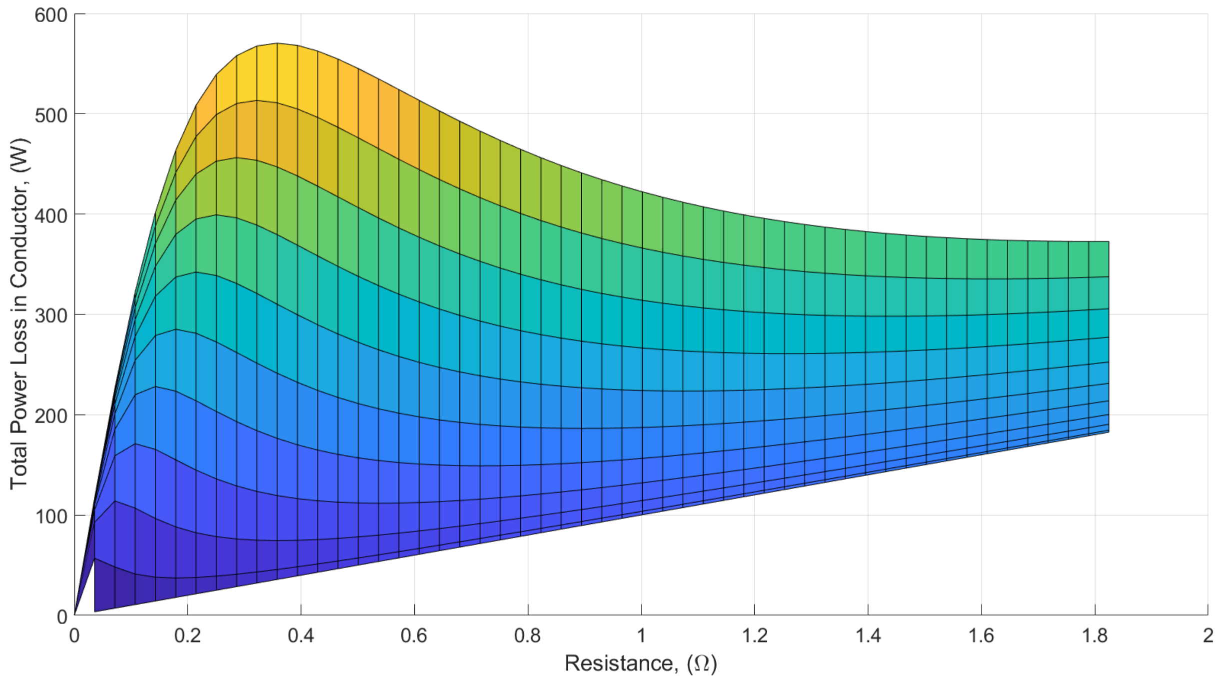

Fig. 7.37 – Total power loss in conductor (resistance domain)

Therefore, for each of the values of the rotor speeds there is a minimum value of power loss for the higher resistance value that is determined by the phase resistance at a particular value of the torque producing current.

Substituting the equation of the power loss in conductor due to the torque producing current (7.13) and the equation of the power loss in conductor due to the zero-sequence current (7.16) into (7.12), the total power loss in conductor P_c becomes:

$$P_c = \frac{3}{2}\left(r_s {i_q}^2 + r_s \left|\tilde{I}_0\right|_{max}^2 \frac{{\omega_e}^2}{\left(\frac{r_s}{3L_0}\right)^2 + {\omega_e}^2} \right) \tag{7.24}$$

In order to determine the minimum and the maximum points of the total power loss in conductor, first, the derivative of equation (7.24) with respect to the phase resistance r_s must be taken. Equation (7.25) shows the derivative of (7.24).

$$\frac{dP_c}{dr_s} = \frac{3}{2}\left({i_q}^2 + \left|\tilde{I}_0\right|_{max}^2 \frac{{\omega_e}^2}{\left(\frac{r_s}{3L_0}\right)^2 + {\omega_e}^2} \right) - \frac{{r_s}^2}{3{L_0}^2}\left|\tilde{I}_0\right|_{max}^2 \frac{{\omega_e}^2}{\left(\left(\frac{r_s}{3L_0}\right)^2 + {\omega_e}^2\right)^2} \qquad (7.25)$$

Equating (7.25) to zero and solving it for the phase resistance value r_s:

$$\frac{3}{2}\left({i_q}^2 + \left|\tilde{I}_0\right|_{max}^2 \frac{{\omega_e}^2}{\left(\frac{r_s}{3L_0}\right)^2 + {\omega_e}^2} \right) - \frac{{r_s}^2}{3{L_0}^2}\left|\tilde{I}_0\right|_{max}^2 \frac{{\omega_e}^2}{\left(\left(\frac{r_s}{3L_0}\right)^2 + {\omega_e}^2\right)^2} = 0 \qquad (7.26)$$

The solutions to (7.26) appear to be as follows.

$$r_s = \begin{cases} \frac{3\sqrt{2}}{2}\frac{\omega_e L_0}{i_q}\sqrt{\left|\tilde{I}_0\right|_{max}^2 + \left|\tilde{I}_0\right|_{max}\sqrt{\left|\tilde{I}_0\right|_{max}^2 - 8{i_q}^2} - 2{i_q}^2}, & for\ \omega_e > 0 \\ -\frac{3\sqrt{2}}{2}\frac{\omega_e L_0}{i_q}\sqrt{\left|\tilde{I}_0\right|_{max}^2 + \left|\tilde{I}_0\right|_{max}\sqrt{\left|\tilde{I}_0\right|_{max}^2 - 8{i_q}^2} - 2{i_q}^2}, & for\ \omega_e < 0 \\ \frac{3\sqrt{2}}{2}\frac{\omega_e L_0}{i_q}\sqrt{\left|\tilde{I}_0\right|_{max}^2 - \left|\tilde{I}_0\right|_{max}\sqrt{\left|\tilde{I}_0\right|_{max}^2 - 8{i_q}^2} - 2{i_q}^2}, & for\ \omega_e > 0 \\ -\frac{3\sqrt{2}}{2}\frac{\omega_e L_0}{i_q}\sqrt{\left|\tilde{I}_0\right|_{max}^2 - \left|\tilde{I}_0\right|_{max}\sqrt{\left|\tilde{I}_0\right|_{max}^2 - 8{i_q}^2} - 2{i_q}^2}, & for\ \omega_e < 0 \end{cases} \qquad (7.27)$$

where, the values of $\left|\tilde{I}_0\right|_{max}$, i_q and L_0 are real and positive. In addition, a condition in (7.28) must be satisfied.

$$0 \leq i_q \leq \frac{\sqrt{2}}{4}\left|\tilde{I}_0\right|_{max} \qquad (7.28)$$

Taking the second derivative of (7.24):

$$\frac{d^2P_c}{dr_s{}^2} = 27r_s\left|\tilde{I}_0\right|_{max}^2 L_0{}^2\omega_e{}^2 \frac{r_s{}^2 - 27L_0{}^2\omega_e{}^2}{\left(r_s{}^2 + 9L_0{}^2\omega_e{}^2\right)^3} \tag{7.29}$$

Substituting the first solution $r_s(1)$ of equation (7.27) into (7.29):

$$\frac{d^2P_c}{dr_s{}^2} = \sqrt{2}\frac{\left|\tilde{I}_0\right|_{max}^2}{\omega_e L_0}\kappa_1 \tag{7.30}$$

where, the coefficient κ_1 is presented as follows.

$$\kappa_1 = \frac{3}{2}\frac{\sqrt{\sigma_1}}{i_q\left(1 + \frac{\sigma_1}{2i_q{}^2}\right)^2} - \frac{\sqrt{\sigma_1{}^3}}{i_q{}^3\left(1 + \frac{\sigma_1}{2i_q{}^2}\right)^2} \tag{7.31}$$

where,

$$\sigma_1 = \left|\tilde{I}_0\right|_{max}^2 + \left|\tilde{I}_0\right|_{max}\sqrt{\left|\tilde{I}_0\right|_{max}^2 - 8i_q{}^2} - 2i_q{}^2 \tag{7.32}$$

The coefficient κ_1 is positive when the values of $\left|\tilde{I}_0\right|_{max}$ and i_q are real and positive. Also as per equation (7.32), the condition in (7.28) must be satisfied.

Substituting the second solution $r_s(2)$ of equation (7.27) into (7.29):

$$\frac{d^2P_c}{dr_s{}^2} = -\sqrt{2}\frac{\left|\tilde{I}_0\right|_{max}^2}{\omega_e L_0}\kappa_1 \tag{7.33}$$

Substituting the third solution $r_s(3)$ of equation (7.27) into (7.29):

$$\frac{d^2 P_c}{d{r_s}^2} = -\sqrt{2}\frac{\left|\tilde{I}_0\right|_{max}^2}{\omega_e L_0}\kappa_2 \tag{7.34}$$

where, the coefficient κ_2 has the following function.

$$\kappa_2 = \left(\frac{3}{2}\frac{\sqrt{\sigma_2}}{i_q\left(1+\frac{\sigma_2}{2{i_q}^2}\right)^2} - \frac{\sqrt{{\sigma_2}^3}}{{i_q}^3\left(1+\frac{\sigma_2}{2{i_q}^2}\right)^3}\right) \tag{7.35}$$

where,

$$\sigma_2 = \left|\tilde{I}_0\right|_{max}^2 - \left|\tilde{I}_0\right|_{max}\sqrt{\left|\tilde{I}_0\right|_{max}^2 - 8{i_q}^2} - 2{i_q}^2 \tag{7.36}$$

The coefficient κ_2 is positive when the values of $\left|\tilde{I}_0\right|_{max}$ and i_q are real and positive. Furthermore, as per equation (7.36), the condition in (7.28) must be satisfied.

Substituting the fourth solution $r_s(4)$ of equation (7.27) into (7.29):

$$\frac{d^2 P_c}{d{r_s}^2} = \sqrt{2}\frac{\left|\tilde{I}_0\right|_{max}^2}{\omega_e L_0}\kappa_2 \tag{7.37}$$

In order to identify whether the point of interest is a local maximum or minimum when the values of $\left|\tilde{I}_0\right|_{max}$, i_q and L_0 are real and positive and the condition stated in equation (7.28) is satisfied, the following conditions stated in (7.38) were applied to (7.30), (7.33), (7.34) and (7.37).

$$\frac{d^2P_c}{dr_s{}^2} = \begin{bmatrix} \sqrt{2}\frac{\left|\tilde{I}_0\right|_{max}^2}{\omega_e L_0}\kappa_1, & when\ \omega_e > 0 \Rightarrow \frac{d^2P_{c0}}{dr_s{}^2} > 0 \ \Rightarrow local\ minimum \\ -\sqrt{2}\frac{\left|\tilde{I}_0\right|_{max}^2}{\omega_e L_0}\kappa_1, & when\ \omega_e < 0 \Rightarrow \frac{d^2P_{c0}}{dr_s{}^2} > 0 \ \Rightarrow local\ minimum \\ -\sqrt{2}\frac{\left|\tilde{I}_0\right|_{max}^2}{\omega_e L_0}\kappa_2, & when\ \omega_e > 0 \Rightarrow \frac{d^2P_{c0}}{dr_s{}^2} < 0 \ \Rightarrow local\ maximum \\ \sqrt{2}\frac{\left|\tilde{I}_0\right|_{max}^2}{\omega_e L_0}\kappa_2, & when\ \omega_e < 0 \Rightarrow \frac{d^2P_{c0}}{dr_s{}^2} < 0 \ \Rightarrow local\ maximum \end{bmatrix} \tag{7.38}$$

According to the analysis presented in (7.38) along with the solutions shown in (7.27), the value of the resistance that results in the maximum power loss in conductor due to the zero-sequence current when the rotor speed is positive can be estimated at a particular frequency ω_e and a particular value of the torque producing current i_q as follows.

$$r_{s\,\max loss} = \frac{3\sqrt{2}}{2}\frac{\omega_e L_0}{i_q}\sqrt{\left|\tilde{I}_0\right|_{max}^2 - \left|\tilde{I}_0\right|_{max}\sqrt{\left|\tilde{I}_0\right|_{max}^2 - 8i_q{}^2} - 2i_q{}^2} \tag{7.39}$$

Besides, considering (7.38) and (7.27), the value of the resistance that results in the minimum power loss in conductor due to the zero-sequence current when the rotor speed is positive can be estimated at a particular frequency ω_e and a particular value of the torque producing current i_q as per equation (7.40) below.

$$r_{s\,\min loss} = \frac{3\sqrt{2}}{2}\frac{\omega_e L_0}{i_q}\sqrt{\left|\tilde{I}_0\right|_{max}^2 + \left|\tilde{I}_0\right|_{max}\sqrt{\left|\tilde{I}_0\right|_{max}^2 - 8i_q{}^2} - 2i_q{}^2} \tag{7.40}$$

It must be emphasised that the real positive solutions of (7.39) and (7.40) exist only when the values of $|\tilde{I}_0|_{max}$, i_q and L_0 are real and positive and the condition stated in equation (7.28) is satisfied.

Substituting the solution (7.39) into equation (7.24), the peak power loss in conductor $P_{c\,max}$ at a particular electrical speed of the motor ω_e and a particular torque producing current i_q can be determined either using equation (7.41) or its expanded version (7.42).

$$P_{c\,max} = \frac{3}{2} r_{s\,\max loss} \left({i_q}^2 + |\tilde{I}_0|_{max}^2 \frac{{\omega_e}^2}{\left(\frac{r_s}{3L_0}\right)^2 + {\omega_e}^2} \right) \tag{7.41}$$

$$P_{c\,max} = \frac{9\sqrt{2}}{4} L_0 \omega_e \frac{i_q \left(3|\tilde{I}_0|_{max} - \sqrt{|\tilde{I}_0|_{max}^2 - 8{i_q}^2} \right) \sqrt{|\tilde{I}_0|_{max}^2 - |\tilde{I}_0|_{max} \sqrt{|\tilde{I}_0|_{max}^2 - 8{i_q}^2} - 2{i_q}^2}}{|\tilde{I}_0|_{max} - \sqrt{|\tilde{I}_0|_{max}^2 - 8{i_q}^2}} \tag{7.42}$$

Substituting the solution (7.40) into equation (7.24), the minimum power loss in conductor at the higher resistance values $P_{c\,min}$ at a particular speed of the motor ω_e and a particular torque producing current i_q can be determined either using equation (7.43) or its expanded version (7.44).

$$P_{c\,min} = \frac{3}{2} r_{s\,\min loss} \left({i_q}^2 + |\tilde{I}_0|_{max}^2 \frac{{\omega_e}^2}{\left(\frac{r_s}{3L_0}\right)^2 + {\omega_e}^2} \right) \tag{7.43}$$

$$P_{c\,min} = \frac{9\sqrt{2}}{4} L_0 \omega_e \frac{i_q \left(3|\tilde{I}_0|_{max} + \sqrt{|\tilde{I}_0|_{max}^2 - 8{i_q}^2} \right) \sqrt{|\tilde{I}_0|_{max}^2 + |\tilde{I}_0|_{max} \sqrt{|\tilde{I}_0|_{max}^2 - 8{i_q}^2} - 2{i_q}^2}}{|\tilde{I}_0|_{max} + \sqrt{|\tilde{I}_0|_{max}^2 - 8{i_q}^2}} \tag{7.44}$$

Considering the equations for the maximum power loss in conductor (7.42) and the minimum power loss in conductor (7.44), it is clear that these quantities become independent of the value of the resistance and depend solely on the two changing quantities: the electrical operational speed of the motor ω_e and the torque producing current i_q.

The maximum value of the torque producing current i_q allowed for the operating point to be considered for a potential improvement can be derived from the condition introduced in (7.28). It states that the current i_q must not exceed the value of $\frac{\sqrt{2}}{4}\left|\tilde{I}_0\right|_{max}$. Hence, the maximum torque producing current for the potential minimisation of the power loss in conductor can be found from equation (7.45) below.

$$i_{q\,max} = \frac{\sqrt{2}}{4}\left|\tilde{I}_0\right|_{max} \tag{7.45}$$

Having the derived equations of the maximum power loss in conductor $P_{c\,max}$ and the minimum power loss in conductor $P_{c\,min}$ stated in (7.42) and (7.44), respectively, along with the total power loss in conductor P_c, the graph depicted in Fig. 7.37 was redrawn featuring the maximum power loss in conductor points (red) and the minimum power loss in conductor points at higher resistance (green) in Fig. 7.38 and Fig. 7.39.

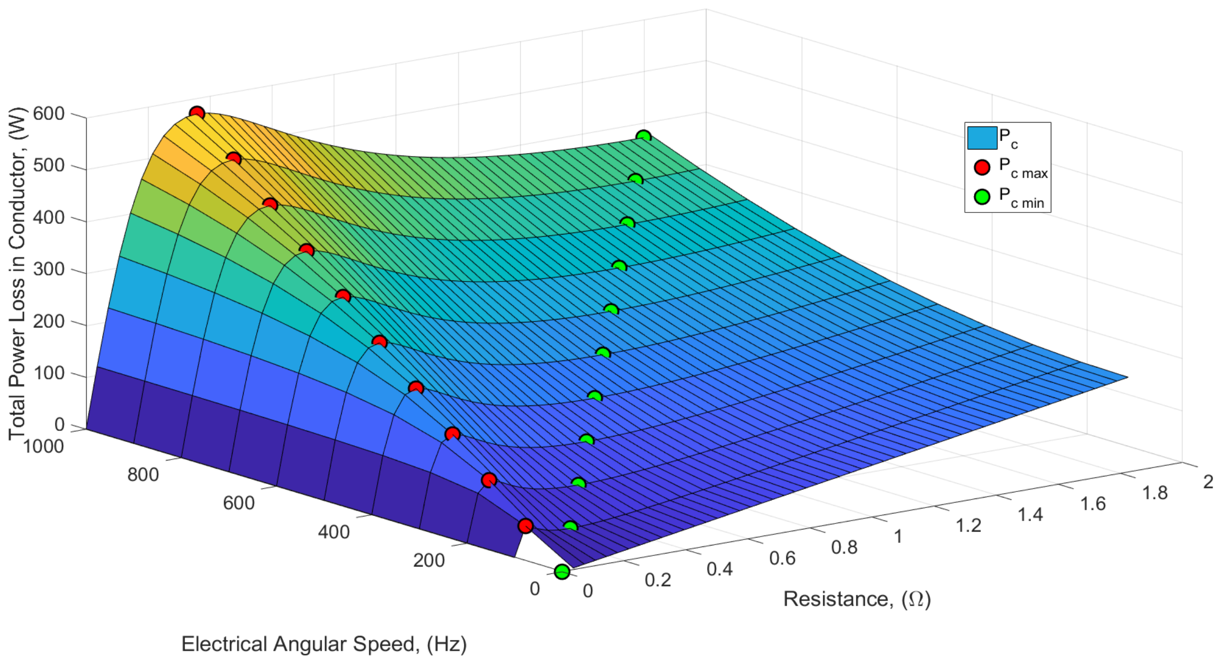

Fig. 7.38 – Total power loss in conductor with max/min points

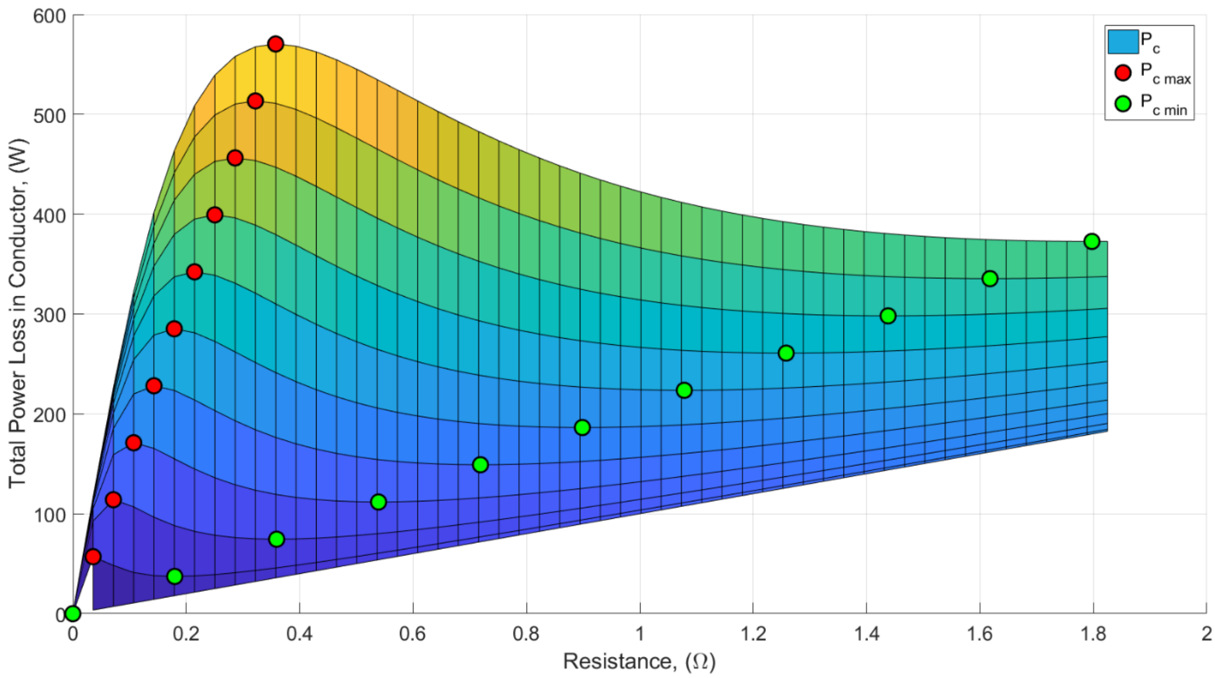

Fig. 7.39 – Max/min power loss in conductor points (resistance domain)

Fig. 7.39 shows the side view of the surface plot of Fig. 7.38 where the domain now is the phase resistance. Each of the horizontal lines represent a single operating frequency of the motor with the top one appearing to be the maximum frequency (the base frequency in this case) and the bottom ones representing the lowest frequency of the frequency range. It can be deducted from the representation of the equations for the power loss in conductor in Fig. 7.39 that if the phase resistance would have been increased leaving the motor to operate at a particular frequency, the overall power loss in conductor would decrease its value. Also it was noticed that for the certain operational frequencies and the resistance values, the power loss decrease due to a change of resistance could be substantial.

For the further analysis, equation (7.42) was used to construct the maximum power loss in conductor $P_{c\,max}$ surface plot (red) and equation (7.44) was used to construct the minimum power loss in conductor $P_{c\,min}$ surface plot (green). Both of the plots feature the electrical frequency domain along with the torque producing current domain as shown in Fig. 7.40.

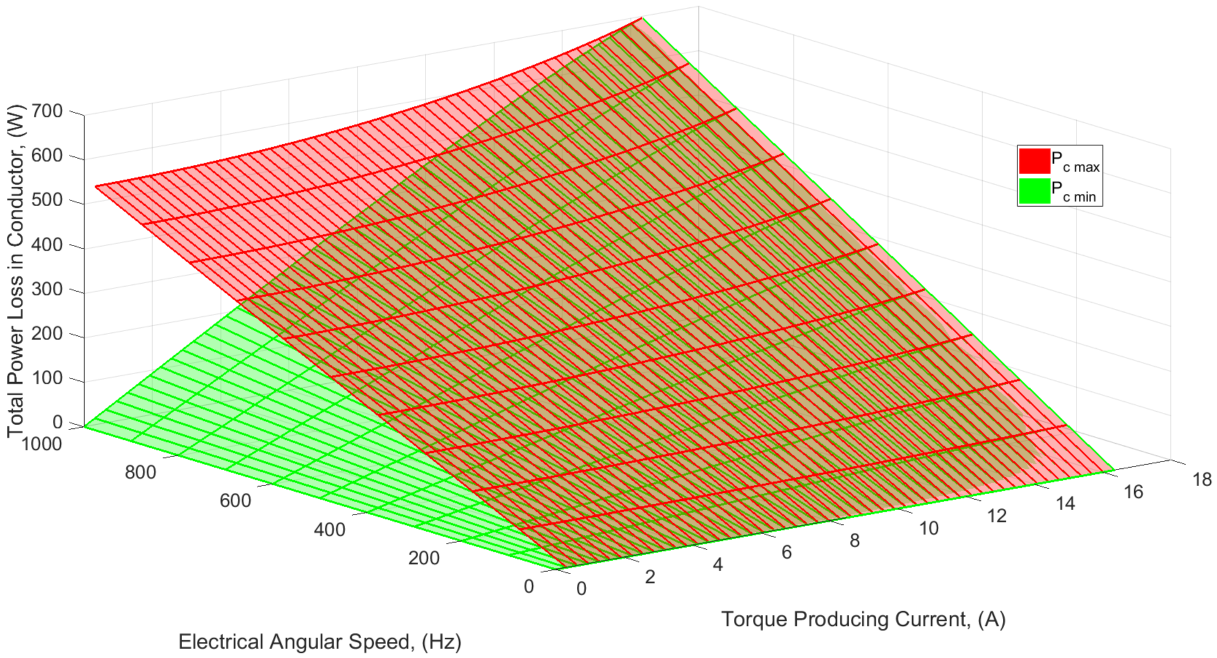

Fig. 7.40 – Total maximum and minimum power loss in conductor

Absolute value of the maximum potential reduction of power loss in conductor can be found using (7.46).

$$PLR_{\max} = P_{c\,max} - P_{c\,min} \tag{7.46}$$

Relative value for the maximum reduction of power loss in conductor $PLR_{\max\%}$ can be calculated either by using the equation involving maximum (7.42) and minimum (7.44) power loss formulae, shown in (7.47) or using the equations of the resistance required for the maximum (7.39) and minimum (7.40) power loss, shown in (7.48).

$$PLR_{\max\%} = \frac{P_{c\,max} - P_{c\,min}}{P_{c\,max}} \cdot 100\% \tag{7.47}$$

$$PLR_{max\,\%} = \frac{r_{s\,\max loss} - r_{s\,\min loss}}{r_{s\,\max loss}} \cdot 100\% \tag{7.48}$$

The absolute (Fig. 7.41) and relative (Fig. 7.42) values of the maximum reduction of the power loss in conductor according to the equations (7.46) and (7.47), respectively, were plotted along the range of electrical motor speeds and the torque producing currents.

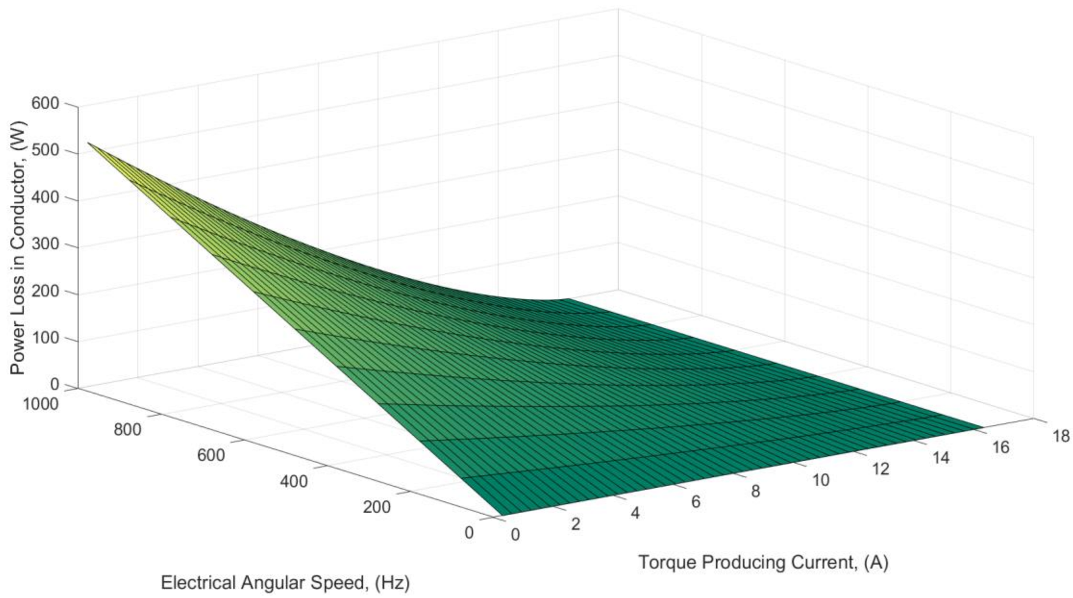

Fig. 7.41 – Absolute maximum reduction of power loss in conductor

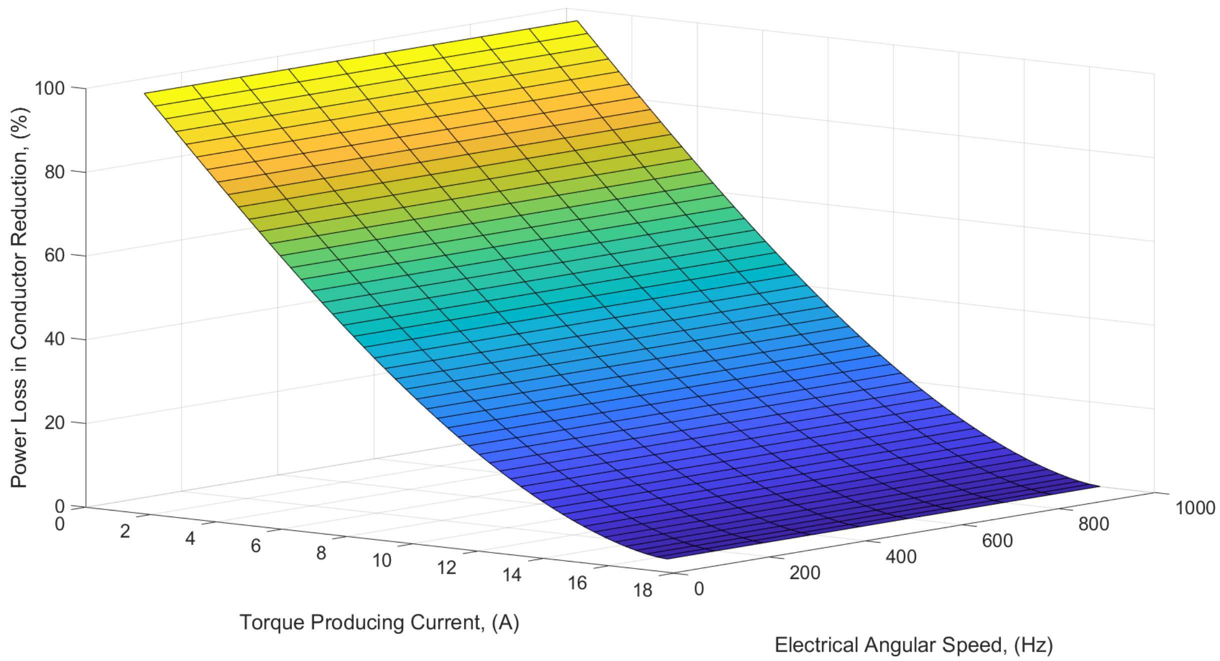

Fig. 7.42 – Relative maximum reduction of power loss in conductor

When both of the equations for the maximum (7.42) and the minimum (7.44) power loss in conductor are substituted into the equation (7.47), the resultant formula appears to be the same as when both of the equations for the maximum (7.39) and (7.40) minimum power loss in conductor resistances are substituted into the equation (7.48). Those manipulations result in the equation for the relative value of the maximum reduction of power loss in conductor $PLR_{\max\%}$, shown below in (7.49).

$$PLR_{\max\%} = 1 - \frac{\sqrt{\left|\tilde{I}_0\right|_{max}^2 + \left|\tilde{I}_0\right|_{max}\sqrt{\left|\tilde{I}_0\right|_{max}^2 - 8{i_q}^2} - 2{i_q}^2}}{\sqrt{\left|\tilde{I}_0\right|_{max}^2 - \left|\tilde{I}_0\right|_{max}\sqrt{\left|\tilde{I}_0\right|_{max}^2 - 8{i_q}^2} - 2{i_q}^2}} \tag{7.49}$$

Although the absolute power loss in conductor reduction depends on the speed of the machine, the relative value of the maximum reduction of power loss in conductor appears to be independent on the speed of the motor (as per equation (7.49)). The relative value depends on the value of the torque producing current only. Hence, the graph of $PLR_{\max\%}$ has only one dimension as illustrated in Fig. 7.43 below.

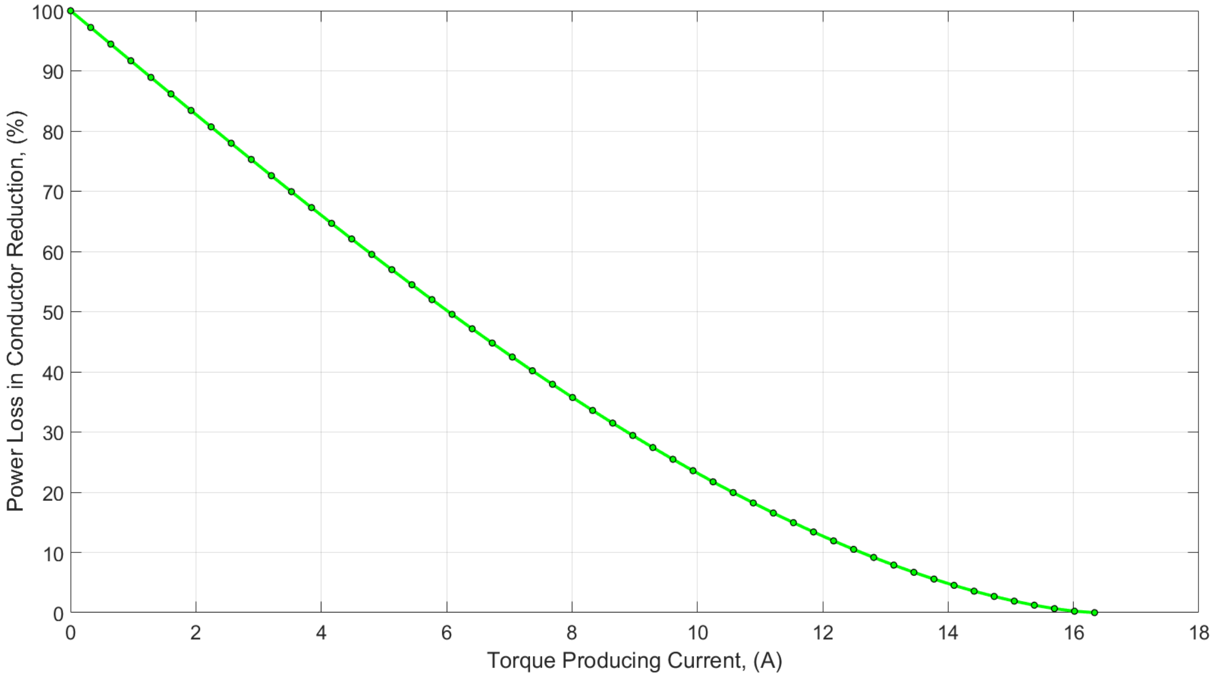

Fig. 7.43 – Maximum relative reduction of power loss in conductor

It can be seen from Fig. 7.43 that the proposed method of changing the phase resistance of a machine has a potential to reduce the power loss in conductor that tends up to 100% relative reduction of the power losses

The equation (7.50) was used to construct a graph in Fig. 7.44 that shows the behaviour of the potential reduction of power loss in conductor across a range of operating speeds and a particular torque producing current. The current was taken from the following operating point:

- Speed ω_{rpm} (f_e): 17500 rpm (875 Hz)
- Current i_q: 8.17 A ($\frac{i_{q\,max}}{2}$ as per (7.45))

$$PLR_{\%} = \frac{P_c - P_{c\,min}}{P_c} \cdot 100\% \qquad (7.50)$$

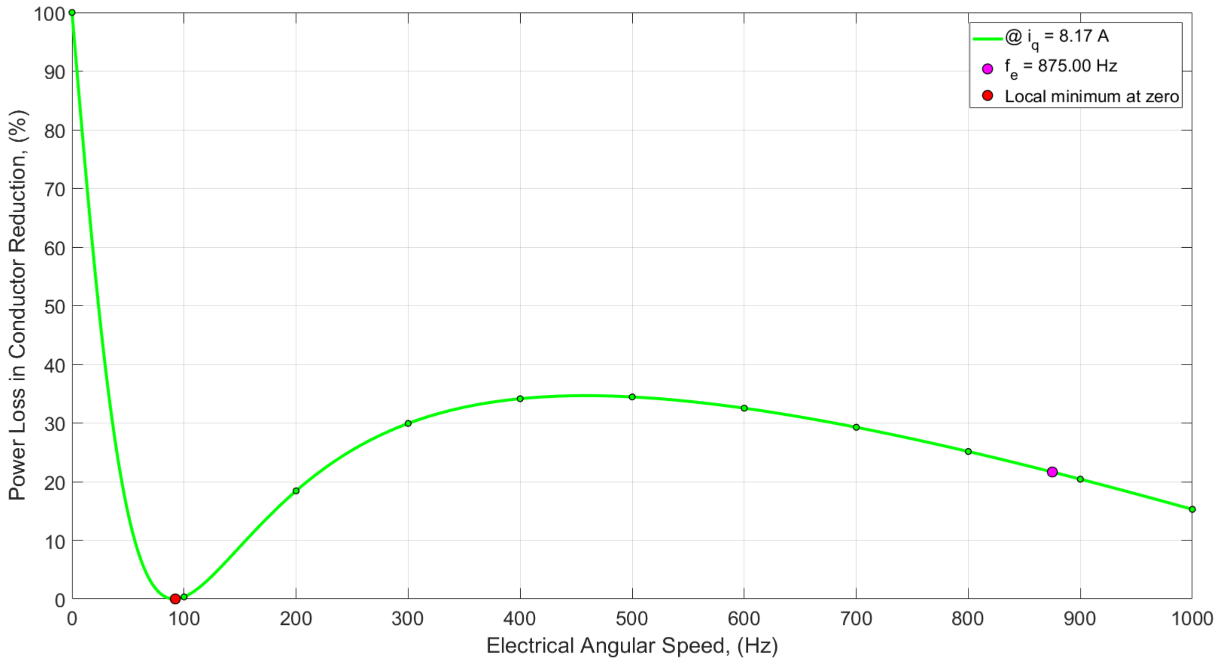

Fig. 7.44 – Potential reduction of power loss in conductor at $\frac{i_{q\,max}}{2}$

Considering Fig. 7.44, the magenta point indicates the operating point and the red point – the point of local minimum at zero point. This local minimum at zero point reveals that there is a specific motor speed that is already resulting in the minimum power loss in conductor with the current motor parameters and the torque producing current.

It is also worth mentioning that the top point of the graph in Fig. 7.44 after the local minimum at zero is the maximum available improvement that is independent of the speed of the motor, it depends entirely on the torque producing current i_q as per (7.49)

It was then decided to check the behaviour of a number of plots of equation (7.50) in a range of the torque producing currents from 1 A up to the maximum allowed current stated in equation (7.45) to observe whether it exerts a similar kind of behaviour. The result is depicted in Fig. 7.45.

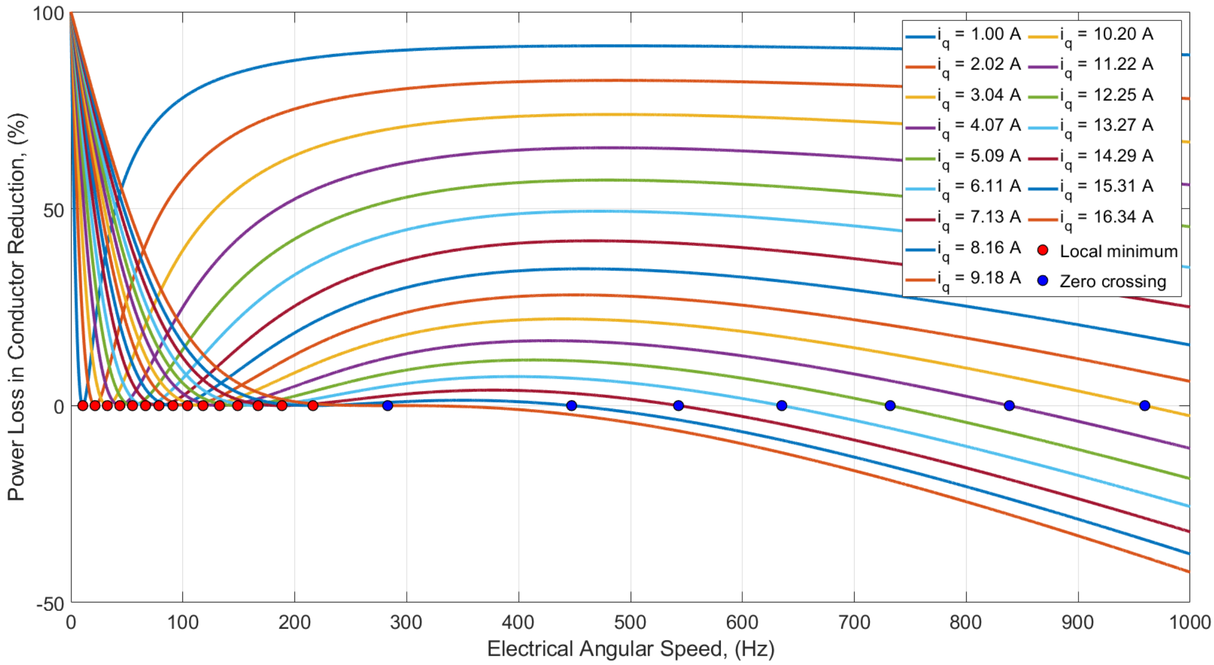

Fig. 7.45 – Potential reduction of power loss in conductor (f_e domain)

Analysing the results presented in Fig. 7.45, it was noticed that for each torque producing current i_q value there is a value of the motor's speed exists that results in the zero percent potential reduction of the power loss in conductor, as this particular operation point is already situated at the spot of the minimum power loss in conductor. Therefore, a range of particular operational speeds of a motor could be identified where there will be no need to increase the resistance in order to reduce the power loss in conductor.

Considering Fig. 7.45, equation (7.51) must be solved for the angular electrical frequency ω_e in order to identify the mentioned points at zero power loss improvement shown in Fig. 7.45.

$$PLR_{\%} = \frac{P_c - P_{c\,min}}{P_c} \cdot 100\% = 0 \tag{7.51}$$

According to equation (7.51), the following equation must be true.

$$P_c - P_{c\,min} = 0 \tag{7.52}$$

Substituting the general equation for power loss in conductor (7.24) and the equation for minimum power loss in conductor (7.43) into (7.52):

$$r_s\left(i_q{}^2 + \left|\tilde{I}_0\right|_{max}^2 \frac{\omega_e{}^2}{\left(\frac{r_s}{3L_0}\right)^2 + \omega_e{}^2}\right) = r_{s\min loss}\left(i_q{}^2 + \left|\tilde{I}_0\right|_{max}^2 \frac{\omega_e{}^2}{\left(\frac{r_{s\min loss}}{3L_0}\right)^2 + \omega_e{}^2}\right) \tag{7.53}$$

The goal is to find the operating points of the torque producing current i_q and the corresponding electrical angular speed ω_e at a particular value of the phase resistance r_s. It is clear from the visual inspection of equation (7.53) that one of the solutions can be found when the phase resistances r_s and $r_{s\min loss}$ are the same:

$$r_s = r_{s\min loss} \tag{7.54}$$

Substituting the equation of the resistance $r_{s\min loss}$ that results in the minimum power loss in conductor (7.40) into (7.54), the equation (7.55) can be obtained.

$$r_s = \frac{3\sqrt{2}}{2}\frac{\omega_e L_0}{i_q}\sqrt{\left|\tilde{I}_0\right|_{max}^2 + \left|\tilde{I}_0\right|_{max}\sqrt{\left|\tilde{I}_0\right|_{max}^2 - 8i_q{}^2} - 2i_q{}^2} \tag{7.55}$$

Solving (7.55) for the angular electrical speed ω_e:

$$\omega_e = \frac{\sqrt{2}}{3} \frac{r_s i_q}{L_0 \sqrt{\left|\tilde{I}_0\right|_{max}^2 + \left|\tilde{I}_0\right|_{max} \sqrt{\left|\tilde{I}_0\right|_{max}^2 - 8{i_q}^2} - 2{i_q}^2}} \tag{7.56}$$

It has to be noted that in order to find the solutions using the equation (7.56), the condition (7.28) must be satisfied, hence, the torque producing current i_q must be lower than or equal to the maximum current shown in (7.45). The equation (7.56) represents the local minimum points at zero, marked as red circles in Fig. 7.45.

Substituting the equation for the maximum torque producing current i_q (7.45) into the solution shown in (7.56), the maximum angular electrical frequency ω_e for this solution can be obtained:

$$\omega_e = \frac{r_s}{3\sqrt{3}L_0} \tag{7.57}$$

Hence, the solution (7.56) is valid in the range of electrical speeds that satisfy the condition (7.58).

$$0 \leq \omega_e \leq \frac{r_s}{3\sqrt{3}L_0} \tag{7.58}$$

The potential reduction of power loss in conductor along a range of electrical angular frequencies plots, depicted in Fig. 7.45, have the second solution as well. This second solution can be observed when the line crosses the zero point for the second time at the higher frequencies (blue circles). Those zero crossing points are hard to obtain analytically from equation (7.53) as even the analytical tool of *Matlab R2020a* could not compute a solution. However, after a series of manipulations, the solution was eventually found.

The series of manipulations started with solving equation (7.53) for the torque producing current i_q first. The obtained solutions are shown in the set of equations of (7.59).

$$i_q = \begin{bmatrix} 3\omega_e L_0 |\tilde{I}_0|_{max} \dfrac{\sqrt{{r_s}^2 - (3\omega_e L_0)^2}}{(3\omega_e L_0)^2 + {r_s}^2} \\ -3\omega_e L_0 |\tilde{I}_0|_{max} \dfrac{\sqrt{{r_s}^2 - (3\omega_e L_0)^2}}{(3\omega_e L_0)^2 + {r_s}^2} \\ \dfrac{\sqrt{6}}{2} \dfrac{|\tilde{I}_0|_{max}}{r_s} \left(3\omega_e L_0 + \sqrt{(3\omega_e L_0)^2 + {r_s}^2}\right) \sqrt{\dfrac{\omega_e L_0 \left(3\omega_e L_0 - \sqrt{(3\omega_e L_0)^2 + {r_s}^2}\right)}{(3\omega_e L_0)^2 + {r_s}^2}} \\ -\dfrac{\sqrt{6}}{2} \dfrac{|\tilde{I}_0|_{max}}{r_s} \left(3\omega_e L_0 + \sqrt{(3\omega_e L_0)^2 + {r_s}^2}\right) \sqrt{\dfrac{\omega_e L_0 \left(3\omega_e L_0 - \sqrt{(3\omega_e L_0)^2 + {r_s}^2}\right)}{(3\omega_e L_0)^2 + {r_s}^2}} \\ \dfrac{\sqrt{6}}{2} \dfrac{|\tilde{I}_0|_{max}}{r_s} \left(3\omega_e L_0 - \sqrt{(3\omega_e L_0)^2 + {r_s}^2}\right) \sqrt{\dfrac{\omega_e L_0 \left(3\omega_e L_0 + \sqrt{(3\omega_e L_0)^2 + {r_s}^2}\right)}{(3\omega_e L_0)^2 + {r_s}^2}} \\ -\dfrac{\sqrt{6}}{2} \dfrac{|\tilde{I}_0|_{max}}{r_s} \left(3\omega_e L_0 - \sqrt{(3\omega_e L_0)^2 + {r_s}^2}\right) \sqrt{\dfrac{\omega_e L_0 \left(3\omega_e L_0 + \sqrt{(3\omega_e L_0)^2 + {r_s}^2}\right)}{(3\omega_e L_0)^2 + {r_s}^2}} \end{bmatrix} \quad (7.59)$$

The set of solutions presented in (7.59) was considered when the angular speed ω_e, the zero-sequence inductance L_0, the phase resistance r_s, the maximum amplitude of the zero-sequence current $|\tilde{I}_0|_{max}$ and the torque producing current i_q are all positive real numbers.

Drawing attention to the first equation $i_q(1)$ of the set of solutions in (7.59), it can be seen that this solution gives a positive value of the torque producing current i_q. In addition, it appears to be the same as the already found solution shown in equation (7.56) when it is solved for the electrical angular frequency ω_e. Hence, the first equation of (7.59) is indeed the true solution that can be used to determine the operating point of the minimum power loss in conductor. It has already been discussed that this solution is valid in the range of electrical frequencies stated in (7.58).

The second equation $i_q(2)$ of the set of the solutions in (7.59) is similar to the first one that has just been considered, however, introducing the positive electrical angular frequency ω_e results in a negative value of the torque producing current i_q. Therefore, this equation is not considered as the possible solution of (7.53).

Considering the third $i_q(3)$ and the fourth $i_q(4)$ equations of (7.59), it can be concluded that the numerator $\omega_e L_0\left(3\omega_e L_0 - \sqrt{(3\omega_e L_0)^2 + r_s{}^2}\right)$ under the square root is always going to be negative when the electrical angular frequency ω_e and the zero-sequence inductance L_0 are positive. Hence, the torque producing current i_q is always going to be a complex number under the stated conditions. Thereby, the equations $i_q(3)$ and $i_q(4)$ of (7.59) cannot be considered the solutions of (7.53).

The fifth equation $i_q(5)$ of (7.59) is going to always be negative under the stated conditions, as $\left(3\omega_e L_0 - \sqrt{(3\omega_e L_0)^2 + r_s{}^2}\right)$ is going to be negative. Therefore, it cannot be considered the solution of (7.53).

Equation six $i_q(6)$ of the set of equations presented in (7.59) results in a positive real value of the torque producing current i_q under the specified conditions. Hence, it could be considered to be the second solution of (7.53). The analysis showed that the domain of this solution (7.60) is a continuation of the domain of the first solution shown in (7.58).

$$\omega_e > \frac{r_s}{3\sqrt{3}L_0} \tag{7.60}$$

Therefore, the operating points which result in the minimum power loss in conductor at a particular value of the phase resistance r_s can be found using the set of equations shown in (7.61).

$$i_q = \begin{cases} 3\omega_e L_0 \left|\tilde{I}_0\right|_{max} \dfrac{\sqrt{{r_s}^2 - (3\omega_e L_0)^2}}{(3\omega_e L_0)^2 + {r_s}^2} \\ -\dfrac{\sqrt{6}}{2} \dfrac{\left|\tilde{I}_0\right|_{max}}{r_s} \left(3\omega_e L_0 - \sqrt{(3\omega_e L_0)^2 + {r_s}^2}\right) \sqrt{\dfrac{\omega_e L_0 \left(3\omega_e L_0 + \sqrt{(3\omega_e L_0)^2 + {r_s}^2}\right)}{(3\omega_e L_0)^2 + {r_s}^2}} \end{cases} \tag{7.61}$$

where, the domain of (7.61) is described in (7.62) below

$$i_q = \begin{cases} i_q(1), & for \quad 0 \leq \omega_e \leq \dfrac{r_s}{3\sqrt{3}L_0} \\ i_q(2), & for \quad \omega_e > \dfrac{r_s}{3\sqrt{3}L_0} \end{cases} \tag{7.62}$$

Solving the second equation $i_q(2)$ of (7.61) for the electrical angular speed of the motor, an alternative method can be obtained in order to construct the operational point for the minimum power loss in conductor operation, shown in (7.63).

$$\omega_e = \begin{cases} -\dfrac{\sqrt{2}}{24} \dfrac{r_s}{L_0 i_q} \left(\left|\tilde{I}_0\right|_{max} - \sqrt{\left|\tilde{I}_0\right|_{max}^2 - 8{i_q}^2}\right) \dfrac{\sqrt{\left|\tilde{I}_0\right|_{max}^2 - \left|\tilde{I}_0\right|_{max} \sqrt{\left|\tilde{I}_0\right|_{max}^2 - 8{i_q}^2} + 4{i_q}^2}}{\sqrt{\left|\tilde{I}_0\right|_{max}^2 + {i_q}^2}} \\ \dfrac{\sqrt{2}}{24} \dfrac{r_s}{L_0 i_q} \left(\left|\tilde{I}_0\right|_{max} - \sqrt{\left|\tilde{I}_0\right|_{max}^2 - 8{i_q}^2}\right) \dfrac{\sqrt{\left|\tilde{I}_0\right|_{max}^2 - \left|\tilde{I}_0\right|_{max} \sqrt{\left|\tilde{I}_0\right|_{max}^2 - 8{i_q}^2} + 4{i_q}^2}}{\sqrt{\left|\tilde{I}_0\right|_{max}^2 + {i_q}^2}} \\ -\dfrac{\sqrt{2}}{24} \dfrac{r_s}{L_0 i_q} \left(\left|\tilde{I}_0\right|_{max} + \sqrt{\left|\tilde{I}_0\right|_{max}^2 - 8{i_q}^2}\right) \dfrac{\sqrt{\left|\tilde{I}_0\right|_{max}^2 + \left|\tilde{I}_0\right|_{max} \sqrt{\left|\tilde{I}_0\right|_{max}^2 - 8{i_q}^2} + 4{i_q}^2}}{\sqrt{\left|\tilde{I}_0\right|_{max}^2 + {i_q}^2}} \\ \dfrac{\sqrt{2}}{24} \dfrac{r_s}{L_0 i_q} \left(\left|\tilde{I}_0\right|_{max} + \sqrt{\left|\tilde{I}_0\right|_{max}^2 - 8{i_q}^2}\right) \dfrac{\sqrt{\left|\tilde{I}_0\right|_{max}^2 + \left|\tilde{I}_0\right|_{max} \sqrt{\left|\tilde{I}_0\right|_{max}^2 - 8{i_q}^2} + 4{i_q}^2}}{\sqrt{\left|\tilde{I}_0\right|_{max}^2 + {i_q}^2}} \end{cases} \tag{7.63}$$

Both the first equation $\omega_e(1)$ and the third equation $\omega_e(3)$ of (7.63) will produce the negative values only under the stated conditions, hence, cannot be considered to be the solutions.

The second equation $\omega_e(2)$ of (7.63) works in the range of the electrical angular speeds stated in the condition (7.58) only, when the current range of (7.28) is applied. This range is already covered by the solution shown in (7.56). Thereby, this equation is not considered to be the true practical solution.

The fourth solution $\omega_e(4)$ of (7.63), however, has the same range as the domain of equation $i_q(2)$ of (7.61) and is real and positive when the current range of (7.28) is applied. Hence, $\omega_e(4)$ of (7.63) can be considered the solution of $i_q(2)$ from the set of equations shown in (7.61).

Therefore, the corresponding alternative method of finding the solutions of (7.43) can be found using the set of equations of (7.64).

$$\omega_e = \begin{bmatrix} \dfrac{\sqrt{2}}{3}\dfrac{r_s i_q}{L_0\sqrt{\left|\tilde{I}_0\right|_{max}^2 + \left|\tilde{I}_0\right|_{max}\sqrt{\left|\tilde{I}_0\right|_{max}^2 - 8{i_q}^2} - 2{i_q}^2}} \\ \dfrac{\sqrt{2}}{24}\dfrac{r_s}{L_0 i_q}\left(\left|\tilde{I}_0\right|_{max} + \sqrt{\left|\tilde{I}_0\right|_{max}^2 - 8{i_q}^2}\right)\dfrac{\sqrt{\left|\tilde{I}_0\right|_{max}^2 + \left|\tilde{I}_0\right|_{max}\sqrt{\left|\tilde{I}_0\right|_{max}^2 - 8{i_q}^2} + 4{i_q}^2}}{\sqrt{\left|\tilde{I}_0\right|_{max}^2 + {i_q}^2}} \end{bmatrix} \tag{7.64}$$

where, the first solution $\omega_e(1)$ is taken from equation (7.56) and the second one $\omega_e(2)$ – from the fourth equation of (7.63).

The domain and range of (7.64) are stated in (7.65) below.

$$\omega_e = \begin{bmatrix} \omega_e(1), & for \quad 0 \le i_q \le \dfrac{\sqrt{2}}{4}\left|\tilde{I}_0\right|_{max} & \& \quad 0 \le \omega_e \le \dfrac{r_s}{3\sqrt{3}L_0} \\ \omega_e(2), & for \quad 0 \le i_q \le \dfrac{\sqrt{2}}{4}\left|\tilde{I}_0\right|_{max} & \& \quad \omega_e > \dfrac{r_s}{3\sqrt{3}L_0} \end{bmatrix} \tag{7.65}$$

According to (7.64) and (7.65), the local minimum (red circles) and the zero crossing points (blue circles) of Fig. 7.45 could be found using $\omega_e(1)$ and $\omega_e(2)$ of (7.64), respectively.

The set of equations of (7.61) along with their corresponding domain shown in (7.62) were used in order to construct the graph depicted in Fig. 7.46.

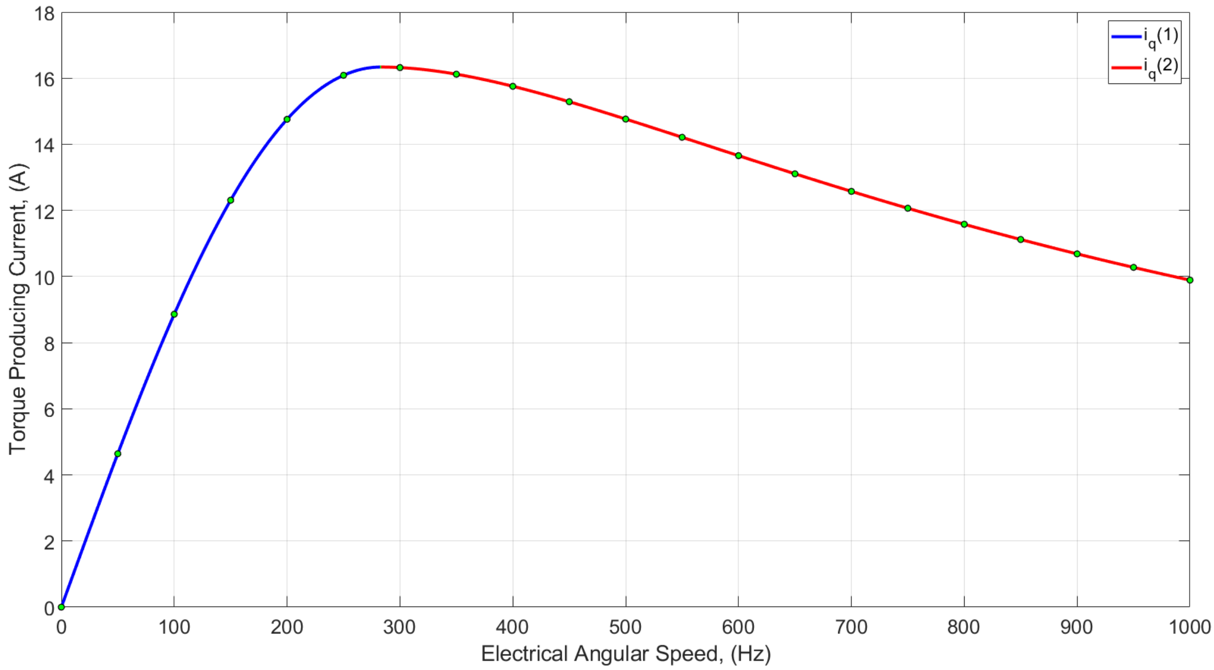

Fig. 7.46 – Operational points for the minimum power loss in conductor

The operating points could be found for every individual value of the phase resistance. The one presented in Fig. 7.46 corresponds to the value of phase resistance of 0.164 Ω. It is also seen that the function is piecewise as per the equations of (7.61). These operating points over the ranges of ω_e and corresponding i_q of a motor at a particular value of the existing phase resistance r_s result in a minimum power loss in conductor operation.

This means that if the machine is operating at the operating points presented in Fig. 7.46, there is no need to apply the technique of increasing its phase resistance, as the machine will be operating at the minimum power loss in conductor already.

Furthermore, the equation (7.50) was used to plot a graph depicted in Fig. 7.47 that shows the behaviour of the potential reduction of power loss in conductor across a range of torque producing currents when the speed is fixed at the operating point.

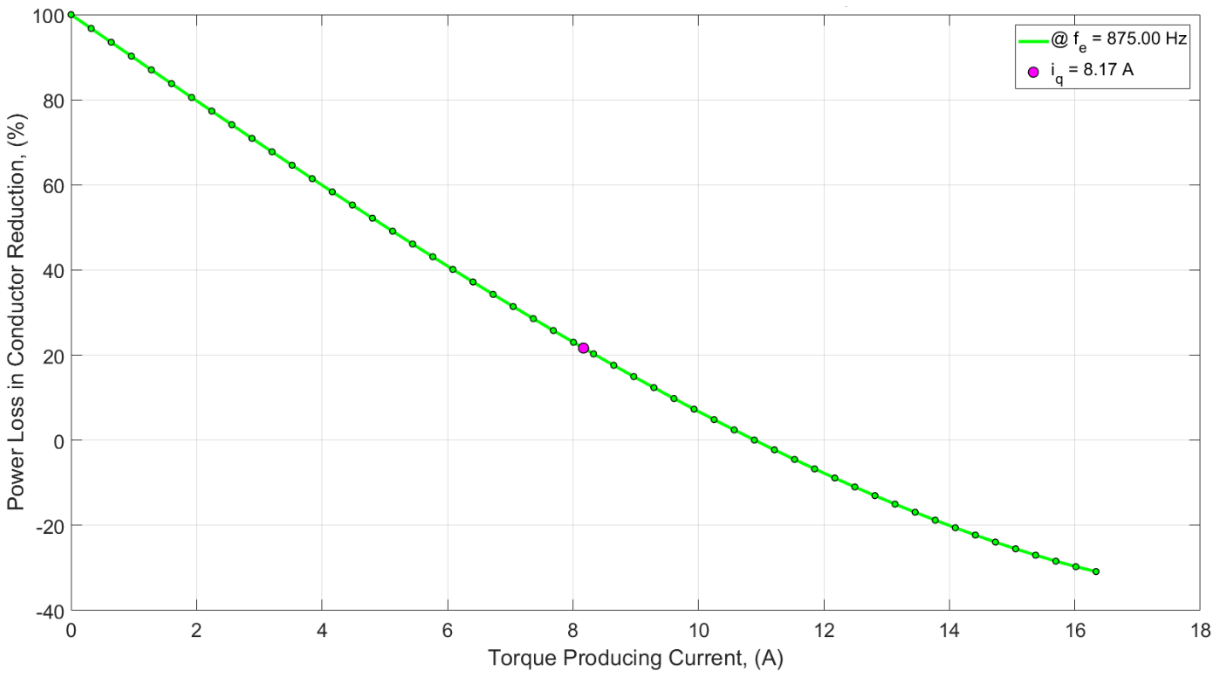

Fig. 7.47 – Potential reduction of power loss in conductor at $f_{e\ o/p}$

Fig. 7.47 gives an understanding that the chosen operating point $i_q = 8.17\ A$ at the chosen frequency of 875 Hz could be improved by around 21% if it would have been possible to increase the phase resistance. Besides, the figure also shows that if one was to choose another value of the torque producing current, the potential for the reduction of the power loss in conductor could be increased or decreased depending on where the operating point (magenta dot) is on the line. The general trend is: the lower the value of the torque producing current i_q the higher the potential reduction of the power loss in conductor by the means of increasing the phase resistance.

The same equation (7.50) was also used to show an expanded version of the behaviour of the potential reduction of the power loss in conductor, Fig. 7.48.

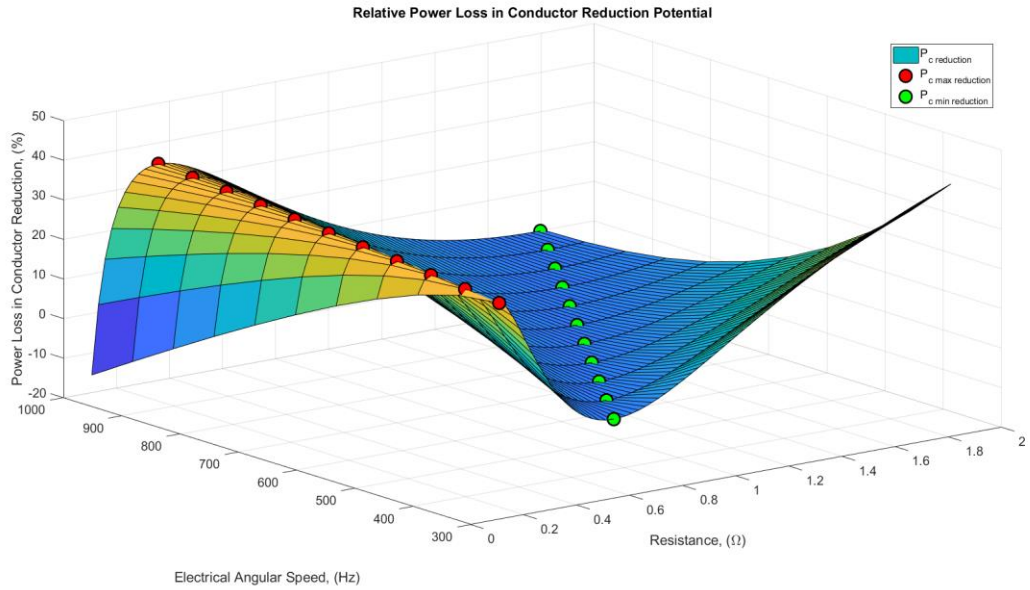

Fig. 7.48 – Surface of potential reduction of power loss in conductor

Not only does Fig. 7.48 provide an information on the potential reduction of the power loss in conductor across the range of speeds as Fig. 7.44 does, but also it gives an estimate of the resistance that is required to be used in order to achieve the specified reduction in power loss in conductor.

7.1.3Discussion

It is clear from Fig. 7.43 that the maximum possible potential mitigation of power loss in conductor is consistent along all of the frequencies with the maximum relative improvement closer to 100%. This means that for some certain motor operational points there is a potential to decrease the power losses in conductor by increasing the phase resistance. This is, of course, counterintuitive, as the general idea of a method to reduce power losses in conductor would involve either reducing the current or decreasing the resistance. However, the outcome of this research showed, that for an open-end winding permanent magnet synchronous motor drive with common DC bus there are some operational cases exist when it will be beneficial to increase the phase resistance in order to reduce the power losses in conductor. The percentage of the improvement does, however, depend on the value of the torque producing current. The greater the value of the torque producing current, the lower the potential maximum reduction of the power losses in conductor.

A useful concept of the maximum possible power loss in conductor due to the uncontrolled zero-sequence current was introduced. This concept states that regardless of the value of the speed of the machine, the power losses in conductor due to the zero-sequence current will never exceed $\frac{3}{2} r_s \left|\tilde{I}_0\right|_{max}^2$ Watts. This concept can be used as a quick reference check for an open-end winding permanent magnet synchronous machine drive with a common DC link that is going to be operated under an uncontrolled current condition.

The obtained analysis of the power loss in conductor proposed a technique to reduce the power loss by increasing the phase resistance. The proposed method resulted from the thorough analysis that could be used for an algorithm that has a potential to aid the machine design and control engineers.

In case the reduction of the power loss in conductor is possible by increasing the resistance, it is up to an engineer how this resistance increase will be implemented. Below are just some of the examples of the options available:

- Adding physical resistance component
- Using longer and/or thinner cables
- Increasing the temperature of operation

The advantage of the proposed method are the reduced power losses in conductor of up to closer to 100%, depending on the operating point determined by the speed of operation and the amount of the torque producing current. The disadvantages are the limited current range of the proposed method and, for the best result, the machine has to have a single operating point. However, the method can be expanded to include the selection of the value of the phase resistance depending on the optimal power loss reduction across a range of speeds or a range of torque producing currents rather than for a specific operating point.

7.2 Current Limit of OEW PMSM with common DC Link

It has already been established that the uncontrolled zero-sequence current due to the machine side of on open-end winding permanent magnet synchronous motor with common DC link influences the overall system by adding an additional stress that does not produce any useful rotational motion. This section analyses what happens in an OEW PMSM with common DC link systems when the phase current reaches its current limit.

7.2.1 RMS Current Limiter for OEW PMSM

The analysis performed in this section revealed that the equations of the current limit presented in some research papers [71] [109] is incorrect. In fact, limiting the current the way that is suggested in some literature could be dangerous. A more accurate current limiting strategy has been developed and presented in this section.

7.2.1.1 Proposed RMS Current Limiter

The phase current i_a of an open-end winding PMSM with common DC link is as follows.

$$i_a = I_{a1}\cos(\theta_e) + I_{a3}\cos(3\theta_e + \gamma) \tag{7.66}$$

where, I_{a1} is the fundamental, I_{a3} is the third harmonic current, θ_e is the phase angle and γ is the phase shift of the third harmonic current.

Fundamental component of i_a can be written in terms of i_{qd} currents as:

$$I_{a1} = \left|\sqrt{{i_q}^2 + {i_d}^2}\right| \tag{7.67}$$

where, i_q and i_d are the quadrature and direct current components in the rotor reference frame.

Using the equation (7.67) the RMS of the fundamental current component is:

$$I_{a1\,RMS} = \frac{I_{a1}}{\sqrt{2}} = \frac{\left|\sqrt{{i_q}^2 + {i_d}^2}\right|}{\sqrt{2}} \tag{7.68}$$

The third harmonic I_{a3} can be written in terms of i_0 as per:

$$I_{a3} = |i_0| \tag{7.69}$$

The third harmonic RMS value can be found from the peak value of the wave and using (7.69) can also be written as:

$$I_{a3\,RMS} = \frac{I_{a3}}{\sqrt{2}} = \frac{|i_0|}{\sqrt{2}} \tag{7.70}$$

Substituting equations (7.67) and (7.69) into (7.66), the phase current i_a could be written in terms of i_{qd0} currents:

$$i_a = \left|\sqrt{{i_q}^2 + {i_d}^2}\right| \cos(\theta_e) + |i_0| \cos(3\theta_e + \gamma) \tag{7.71}$$

The total RMS value of a signal is a square root of the squares of all of the RMS harmonics values that comprise the signal itself. The phase current of the considered OEW PMSM consists of the fundamental and the zero-sequence currents mainly. Hence, the following equation appears to be an appropriate limit for the phase current:

$$I_{a\,RMS} = \sqrt{I_{a1\,RMS}^2 + I_{a3\,RMS}^2} \tag{7.72}$$

where., $I_{a\,RMS}$ is the RMS limit for the phase current I_a.

Substituting equations (7.68) and (7.69) into (7.72), the RMS can be represented in terms of i_{qd0} currents:

$$I_{a\,RMS} = \sqrt{\left(\frac{\left|\sqrt{{i_q}^2 + {i_d}^2}\right|}{\sqrt{2}}\right)^2 + \left(\frac{|i_0|}{\sqrt{2}}\right)^2} \tag{7.73}$$

Simplifying the equation (7.73):

$$I_{a\,RMS} = \sqrt{\frac{{i_q}^2 + {i_d}^2 + |i_0|^2}{2}} \tag{7.74}$$

Simply the equation (7.74) even further to get rid of the square root:

$$2{I_{a\,RMS}}^2 = {i_q}^2 + {i_d}^2 + |i_0|^2 \tag{7.75}$$

Solving the equation (7.75) for i_q:

$$i_q = \sqrt{2{I_{a\,RMS}}^2 - {i_d}^2 - |i_0|^2} \tag{7.76}$$

The new limit for the quadrature axis current can be implemented according to (7.77).

$$i_{q\_Lim} = \sqrt{2{I_{RMS\,Lim}}^2 - {i_d}^2 - |i_0|^2} \tag{7.77}$$

This special current limiter takes into consideration the direct current and the amplitude of the ZSC in order to provide the machine with the maximum allowed RMS current has to be introduced when controlling an open-end winding permanent magnet synchronous motor drive with common DC link.

7.2.1.2Comparison between the Existing RMS Current Limiting Technique and the Proposed One

This section provides a comparison between the existing current limiting technique and the proposed one.

The formula for the current limit introduced in [71] and denoted as (8):

$$I_q^{**} = \sqrt{\left(I_q^*\right)^2 - (I_d^*)^2 - I_{0,rms}^2} \tag{7.78}$$

The formula for the current limit introduced in [109] and denoted as (17):

$$I_q^* = \sqrt{I_{dq,max}^2 - {I_d^*}^2 - I_{0\,RMS}^2} \tag{7.79}$$

$$I_q^* = \sqrt{\sqrt{\frac{3}{2}}I_{peak} - {I_d^*}^2 - I_{0\,RMS}^2} \tag{7.80}$$

The formula for the current limit derived in this chapter:

$$i_{q\_Lim} = \sqrt{2I_{RMS\,Lim}{}^{2} - i_d{}^{2} - |i_0|^2} \tag{7.81}$$

7.2.1.3Discussion

It can be seen from the visual comparison of the derived equation for the RMS limit and the one proposed in the papers that the one proposed in papers results in a higher value of the reference current. The proposed current limit uses the peak value of ZSC and the one in the paper – RMS.

7.2.2Peak Current Limiter

Although the machine current limit is defined by the RMS value, the inverter components limit could be defined by the peak current values. Due to the phase shift of the zero-sequence current that depends on the speed of a motor, the estimation of the peak of the phase current becomes a non-trivial task. This section addresses the mentioned issue.

7.2.2.1Proposed idea

A method of dealing with this issue was proposed in order to keep the phase current peak at its maximum value. Consider the equation of the phase current when the zero-sequence current is left to flow freely in the system:

$$i_a = I_{a1}\cos(\theta_e) + I_{a3}\cos(3\theta_e + \gamma) \tag{7.82}$$

where, i_a is the phase current, I_{a1} is the amplitude of the fundamental frequency, I_{a3} is the amplitude of the 3rd harmonic or the zero-sequence current component, θ_e is the electrical angle of the rotor and γ is the phase shift of the zero-sequence current component as described in Fig. 3.4 and Fig. 3.5 of chapter 3 on page 51.

Knowing that I_{a1} is controlled by the average of i_q and I_{a3} is the amplitude of the zero-sequence current $|\tilde{I}_0|$, the equation (7.82) can be rewritten as:

$$i_a = |i_q|\cos(\theta_e) + |\tilde{I}_0|\cos(3\theta_e + \gamma) \tag{7.83}$$

If the fundamental current i_a is to be kept at some particular peak value I_{peak}, the equation (7.83) becomes:

$$I_{peak} = |i_q|\cos(\theta_e) + |\tilde{I}_0|\cos(3\theta_e + \gamma) \tag{7.84}$$

In order to keep the phase current at a particular peak value I_{peak}, $|i_q|$ could be used to control the amplitude of the fundamental current component. According to (7.84) an iterative process was proposed in order to determine the minimum value of the peak of the fundamental of the phase current:

$$|i_q|^* = min\left(\frac{I_{peak} - |\tilde{I}_0|\cos(3\theta + \gamma)}{\cos(\theta)}\right) \tag{7.85}$$

Where θ is an array of the values from 0 to -50 degrees. It was also determined through simulation that the number of iterations can be as little as 10. The equation (7.85) was used as the core for the block presented in Fig. 7.49.

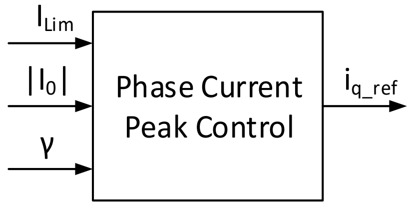

Fig. 7.49 – Phase current peak control block

7.2.2.2Simulation and results

The following graphs represent different values if I_{a1} across the range of speeds in order to maintain the overall phase current at a desired value. This value is represented by $I_{Lim} = 150\ A$.

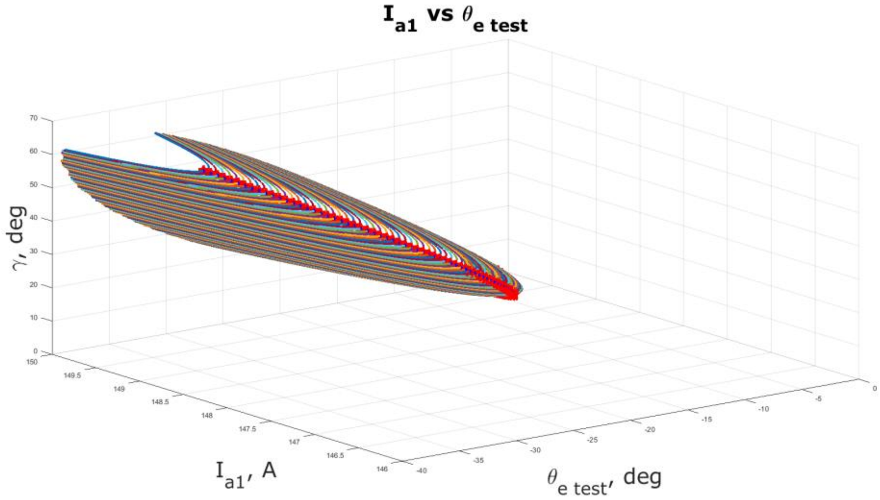

Fig. 7.50 – Minimum of the peak fundamentals at various γ 3D

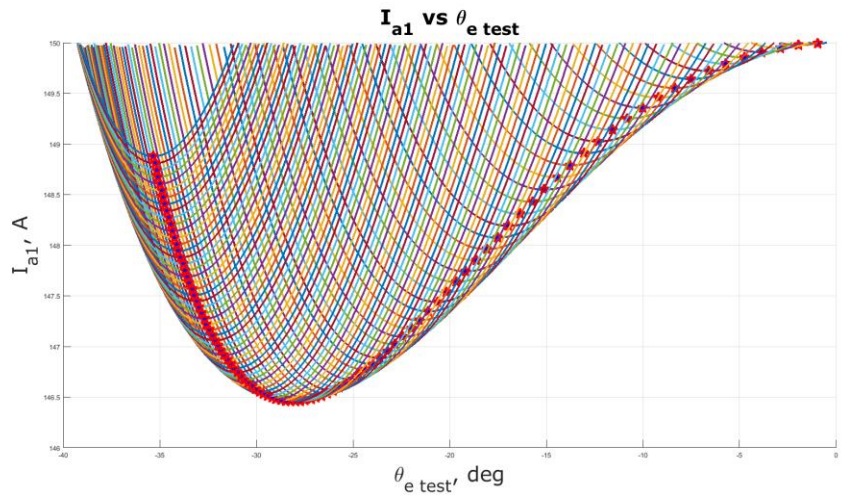

Fig. 7.51 – Minimum of the peak fundamentals at various γ 2D

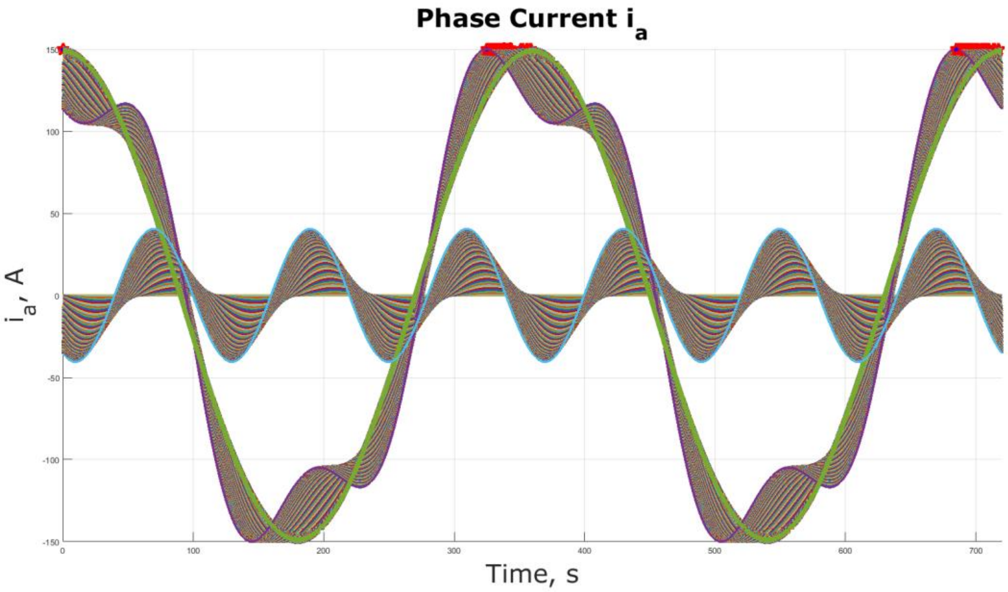

Fig. 7.52 – Fundamental, 3rd Harmonic and Phase Current

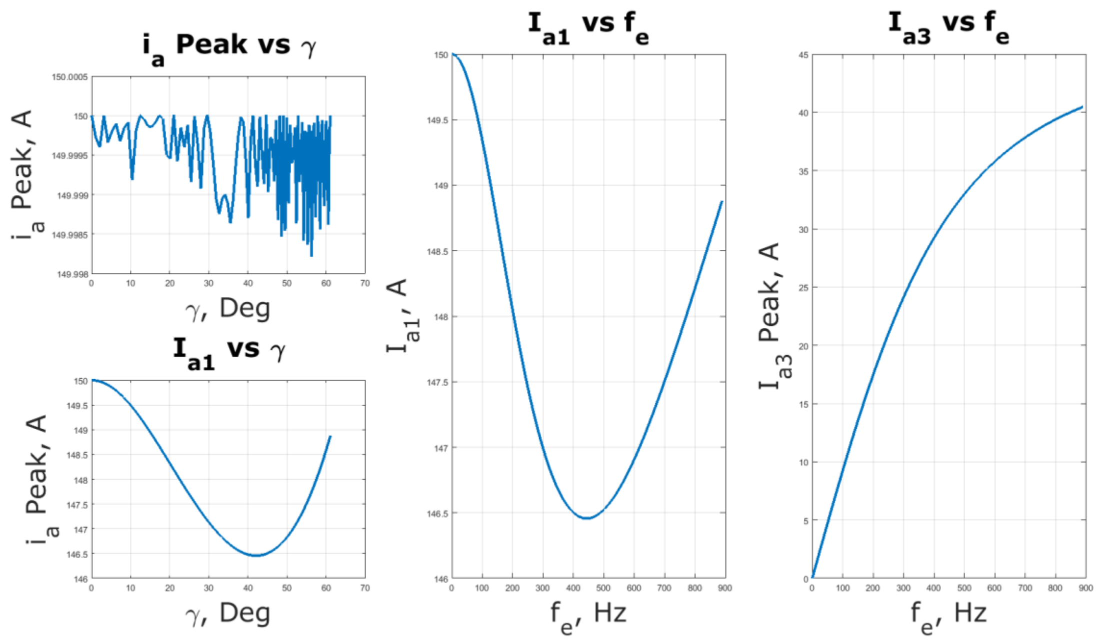

Fig. 7.53 – Phase current peak according to change in Ia1 and Ia3

7.2.2.3Discussion

The simulation showed that the proposed method results in the quadrature reference current generation of a particular value so that the peak of the phase current remained at the same constant level.

7.3Development of a Design Aid Algorithm for OEW PMSM with Common DC Link

The analysis performed in sections 7.1 and 7.2 revealed some crucial information an engineer should be aware of when designing or operating an open-end winding permanent magnet synchronous motor drive with common DC link under the uncontrolled zero-sequence current operation.

7.3.1Power Loss Reduction Aid

A separate algorithm and an application were designed using Matlab in order to incorporate the findings and proposed ideas of chapter 7.1.

7.3.1.1Power Loss Reduction Aid Algorithm

The designed algorithm provides the user with the visualisation of the power loss in conductor for an OEW PMSM with common DC link and feeds back the estimated value of the phase resistance that has to be increased in order to make sure that the motor is operating with the minimum possible power loss in conductor. The developed Matlab algorithm can be found in Appendix D.

The inputs of the algorithm:

```
% === Motor parameters ===
Rs = 164e-3;             % Phase Resistance
L0 = 17.75e-6;           % Leakage inductance
Ypm = 0.07147648494;     % Fundamental flux linkage
Kpm3 = 0.0114748014533; % Perm. Magn. 3rd harmonic flux coef.
P = 6;                   % Number of poles
RatedSpeedRPM = 20000;   % Rated speed in RPM
% ========================

% === User's Operating Point ===
OperatingSpeedRPM = 17500;  % Rotor speed in RPM
LoadCurrent = 8.1684;       % Load current iq
% ==============================
```

Output of the program:

```
Power Loss in Conductor Reduction Calculator
Operating load current must not exceed 16.34 A
Load current of 8.17 A is lower than the maximum allowed.
Operating point can be considered for reduction of Power Loss in Conductor!
Operating speed is 17500 RPM (875.00 Hz electrical)

21.65% Reduction of Power Loss in Conductor is possible.

The resistance is too low.
The resistance must be 1.573 Ohm.
Current resistance value: 0.164 Ohm.
Additional resistance required: 1.409 Ohm.
```

Fig. 7.54 – Text output of the developed Matlab algorithm

Along this the text output of the developed program, the user is presented with some visual aid for a better understanding on the machines behaviour: Fig. 7.55 - Fig. 7.61.

Equation (7.25) along with (7.42) and (7.44) were used to plot the surface depicted in Fig. 7.55. It shows the range of power loss in conductor points according to the value of phase resistances and speeds at a particular torque producing current. It features the minimum and maximum total power loss in conductor points as well as the users operating point.

Fig. 7.56, in turn, shows the surface with maximum and minimum potential reduction of the total power loss in conductor. It also features the potential reduction of the power loss in conductor at the users chosen operating point.

Moreover, the algorithm provides the user with representation of components of the power loss in conductor due to the zero-sequence current along with the marked chosen operating point. This feature is illustrated in Fig. 7.57. It is clear how the power loss due to the zero-sequence current varies with the phase resistance.

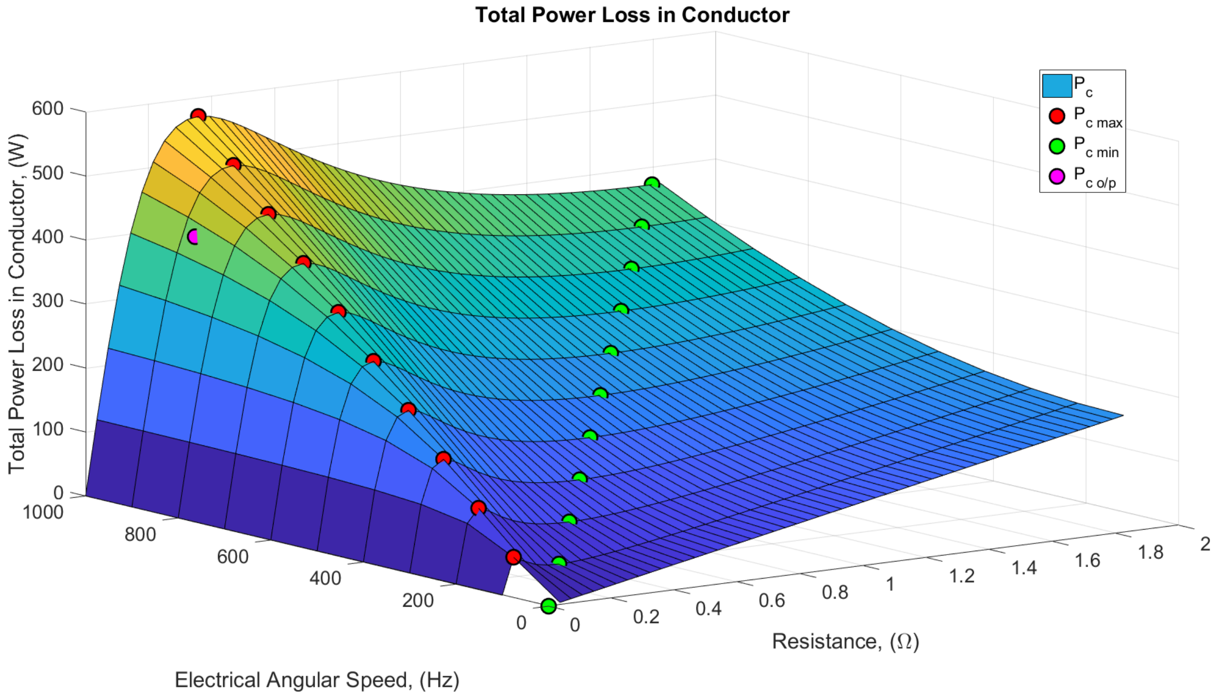

Fig. 7.55 – Total power loss in conductor with max/min points and the user's operating point

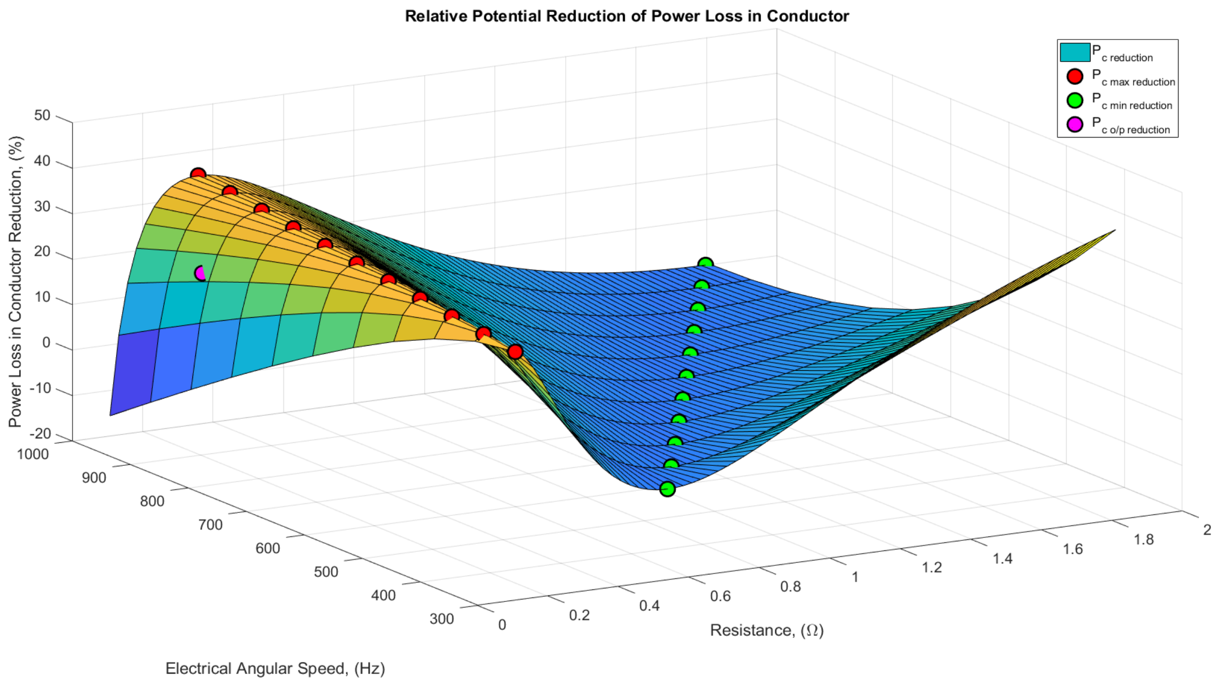

Fig. 7.56 – Potential reduction of power loss in conductor with the user's operating point

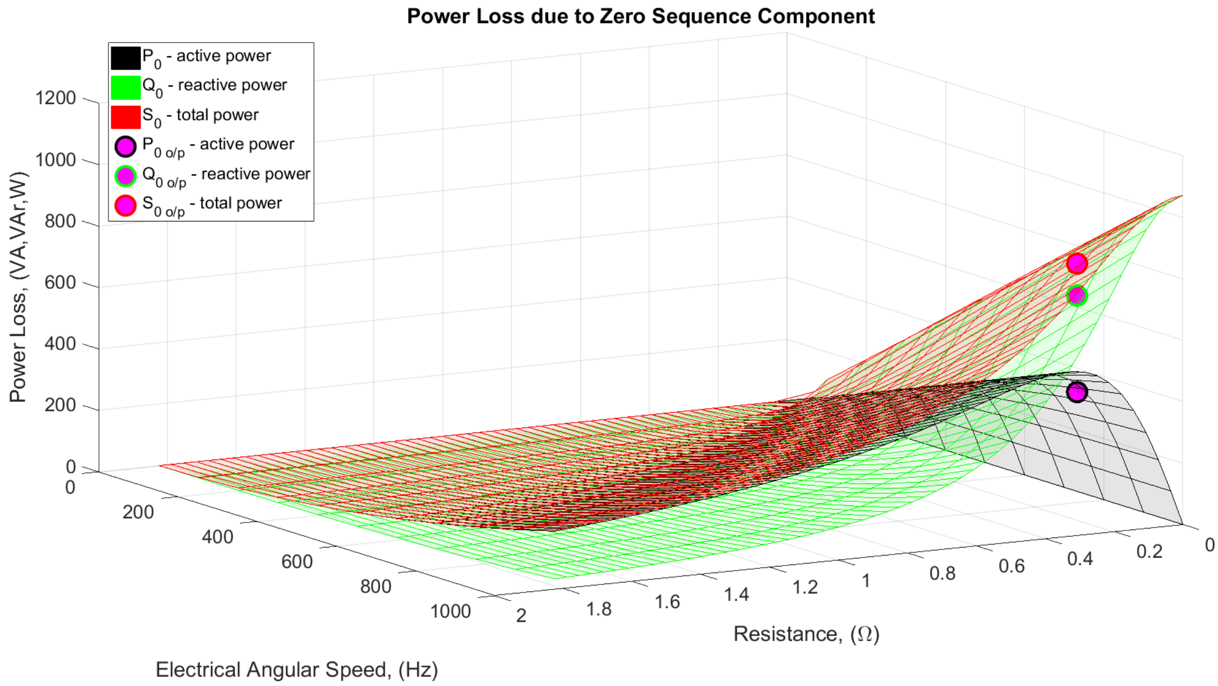

Fig. 7.57 – Power loss due to the zero-sequence component with the user's operating point

In order to explore the potential of reduction of the power loss in conductor along a range of speeds of the motor at a particular chosen torque producing current, the user is provided with the graph, shown in Fig. 7.58

In addition, the user is provided with a graph of the potential reduction of the power loss in conductor along a range of torque producing currents i_q at a particular chosen operating point frequency. An example of this plot is shown in Fig. 7.59.

Moreover, as it was revealed in 7.1, the existing motor parameters already have a set of operating points where the motor will be controlled at the minimum power loss in conductor. This set of points is also provided to the user to identify whether any of them will be useful for a particular application - Fig. 7.60. Furthermore, the algorithms present a new set of operating points (Fig. 7.61) derived from the suggested value of the resistance shown in Fig. 7.54.

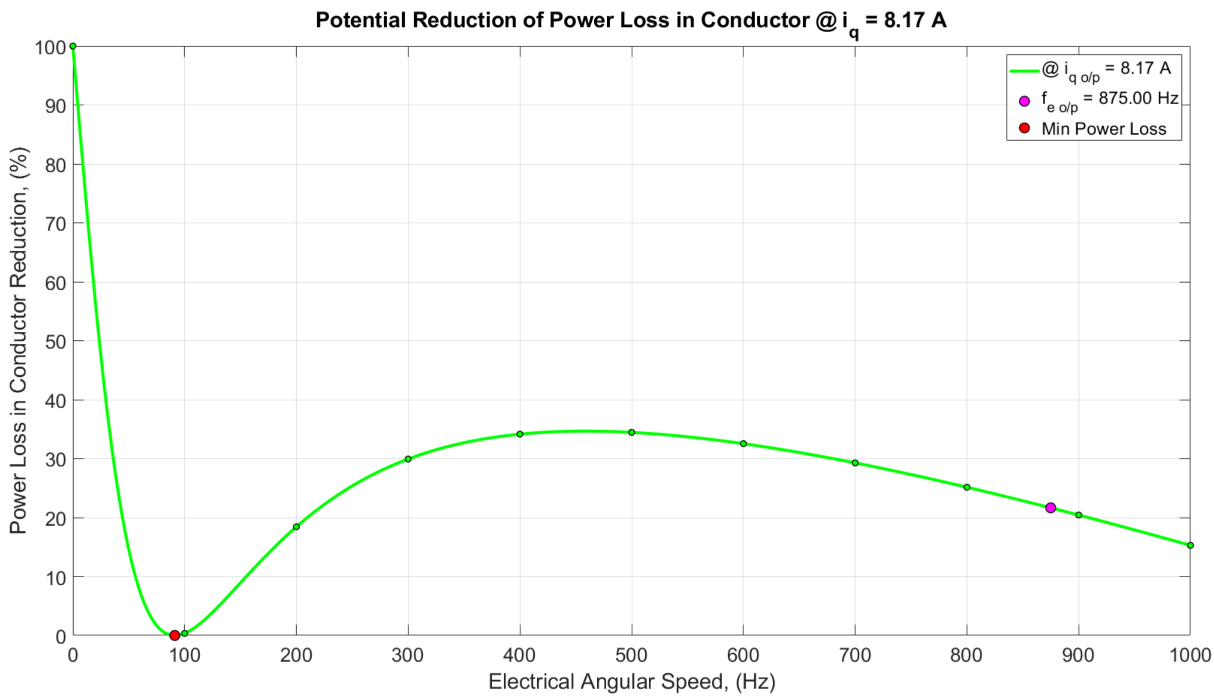

Fig. 7.58 – Potential reduction of power loss in conductor at $i_{q\ o/p}$ with the user's operating point

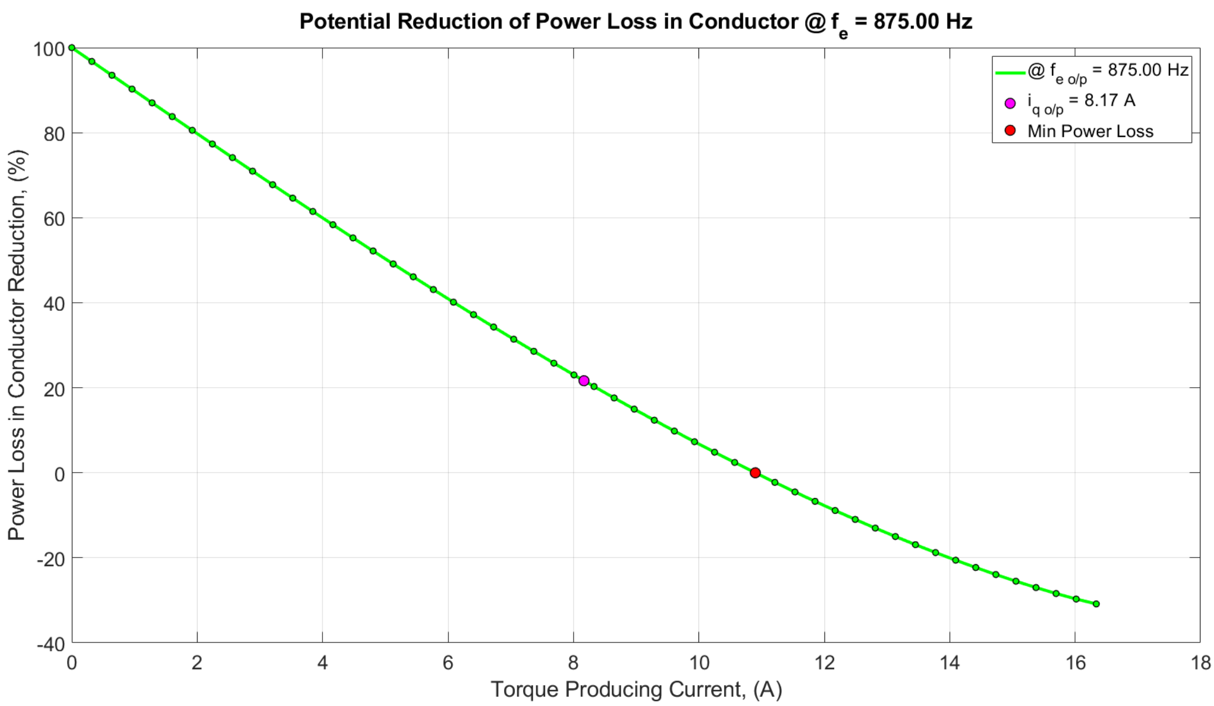

Fig. 7.59 – Potential reduction of power loss in conductor at $f_{e\ o/p}$ with the user's operating point

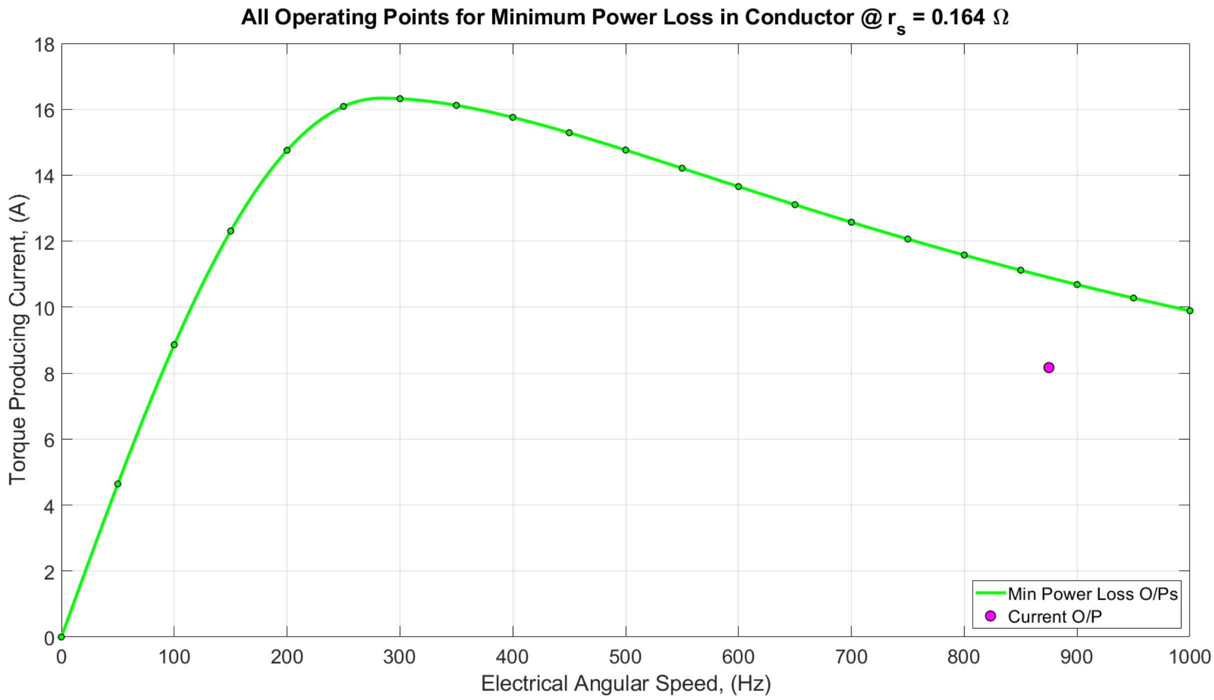

Fig. 7.60 – Operational points for the minimum power loss in conductor at the current resistance value

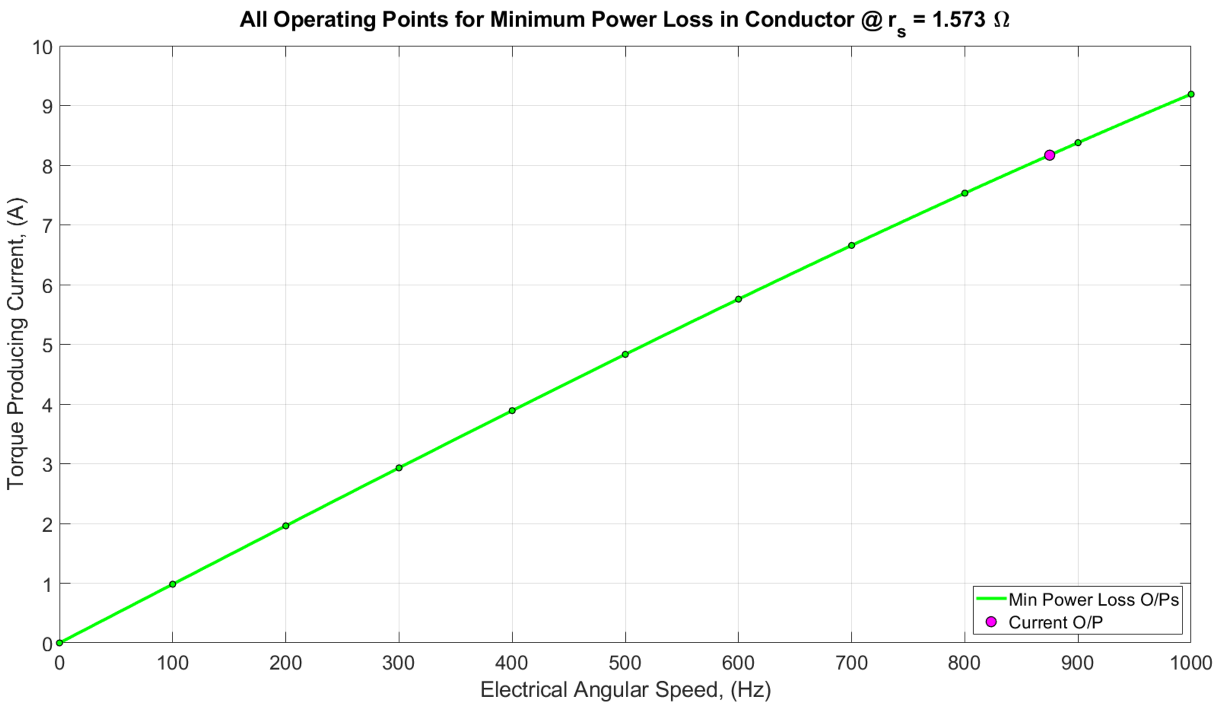

Fig. 7.61 – Operational points for the minimum power loss in conductor at the suggested resistance value

7.3.1.2 Power Loss Reduction Application

Along with the algorithm mentioned in 7.3.1.1 a Matlab application called "Power Loss in Conductor Calculator" was developed for the ease of use of the proposed power loss reduction technique for the open-end winding permanent magnet synchronous motor with common DC link. The application's graphical user interface (GUI) is shown in Fig. 7.62 and the code for the app is attached as Appendix E.

The top left corner of the GUI features the "Input" field that has the text boxes for the necessary machine variables. All of the input boxes have annotations and units associated with them.

The application is written in such a way that it is easily expandable. This is why an "Additional Input" tab is made for the program extension and introduction of the new futures.

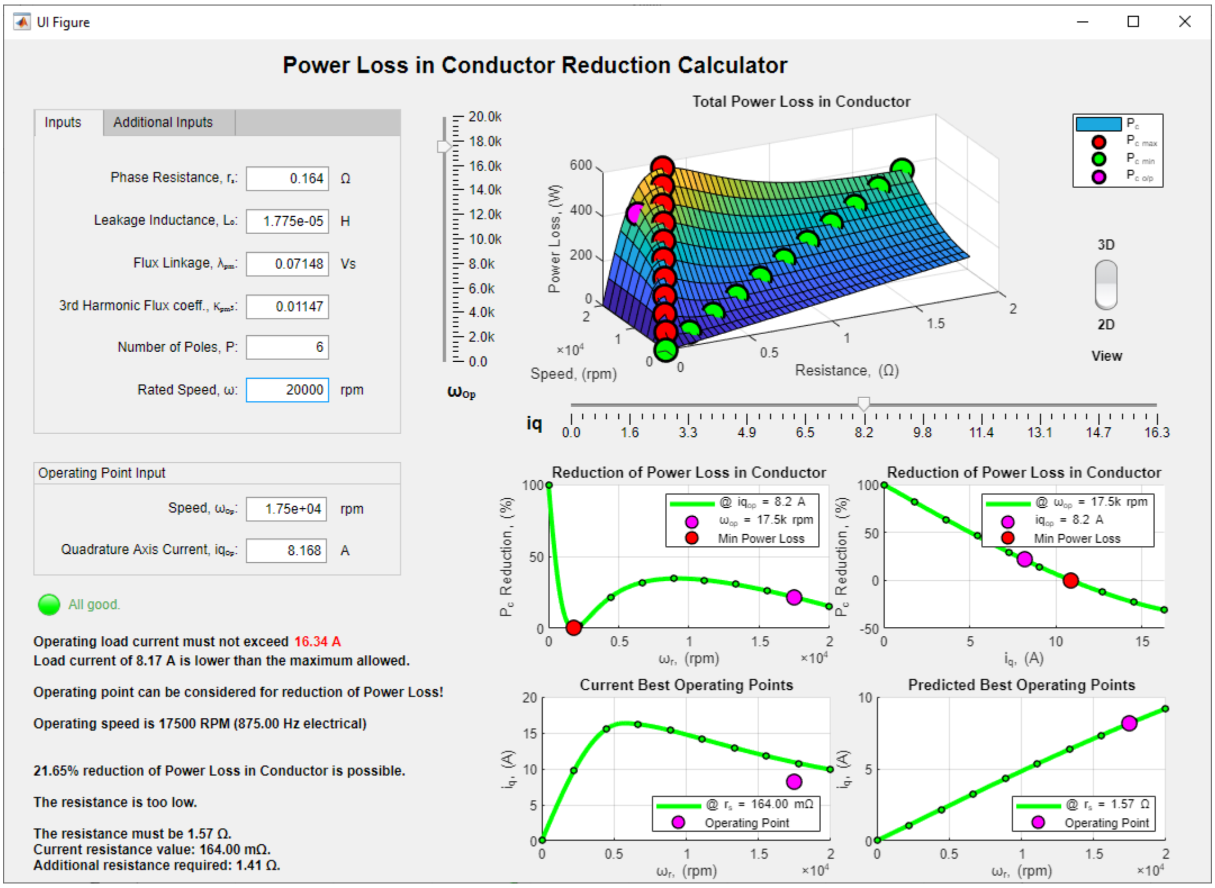

Fig. 7.62 – Power Loss in Conductor Reduction Calculator app (3D view)

The machine's operating point can be set either in the "Operating Point Input" field just below the "Input" field or by setting the values using the vertical and the horizontal sliders, corresponding to the operating speed ω_{op} in RPM and the operating torque producing current i_q in ampers, respectively. The vertical slider is situated by the left hand side of the "Total Power Loss in Conductor" graph. It represents the motor's operating speed with the already calculated minimum and maximum limits. The horizontal slider that represents the machine's operating torque producing current is situated at the bottom of the "Total Power Loss in Conductor" graph. The user is able to change the operating current by changing the slider's position within the automatically calculated current limits according to the motor parameters.

The bottom left corner of the GUI depicted in Fig. 7.62 is reserved for the text output that provides the user with the information on the possible reduction of total power loss in conductor along with the calculation of the phase resistance required to achieve the estimated reduction as also shown in Fig. 7.63. The green indicator above the text is signalling that there is no errors in the inputs and the information given is consistent. The text output in this particular case indicates that the reduction of the power loss by the means of increasing the conductor resistance is possible.

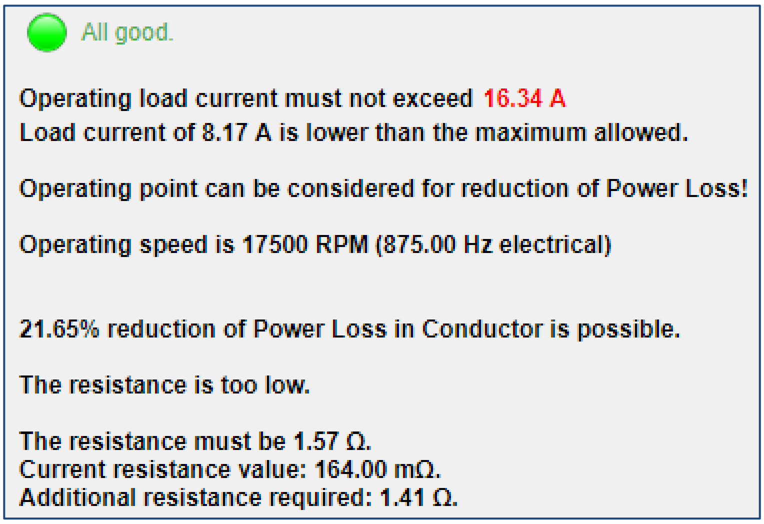

Fig. 7.63 – Text output of the application

Along with the text output the developed application displays a surface plot of the "Total Power Loss in Conductor" along the range of motor's speeds and the phase resistances. There are the maximum and the minimum points shown on the graph as well the particular operating point.

The application also features a "View" switch that could be used to toggle the 3D/2D view. The 2D view gives a clearer picture of how the operating point moves through the surface of the total power loss in conductor points as the operating speed and the operating currents are changed, Fig. 7.64.

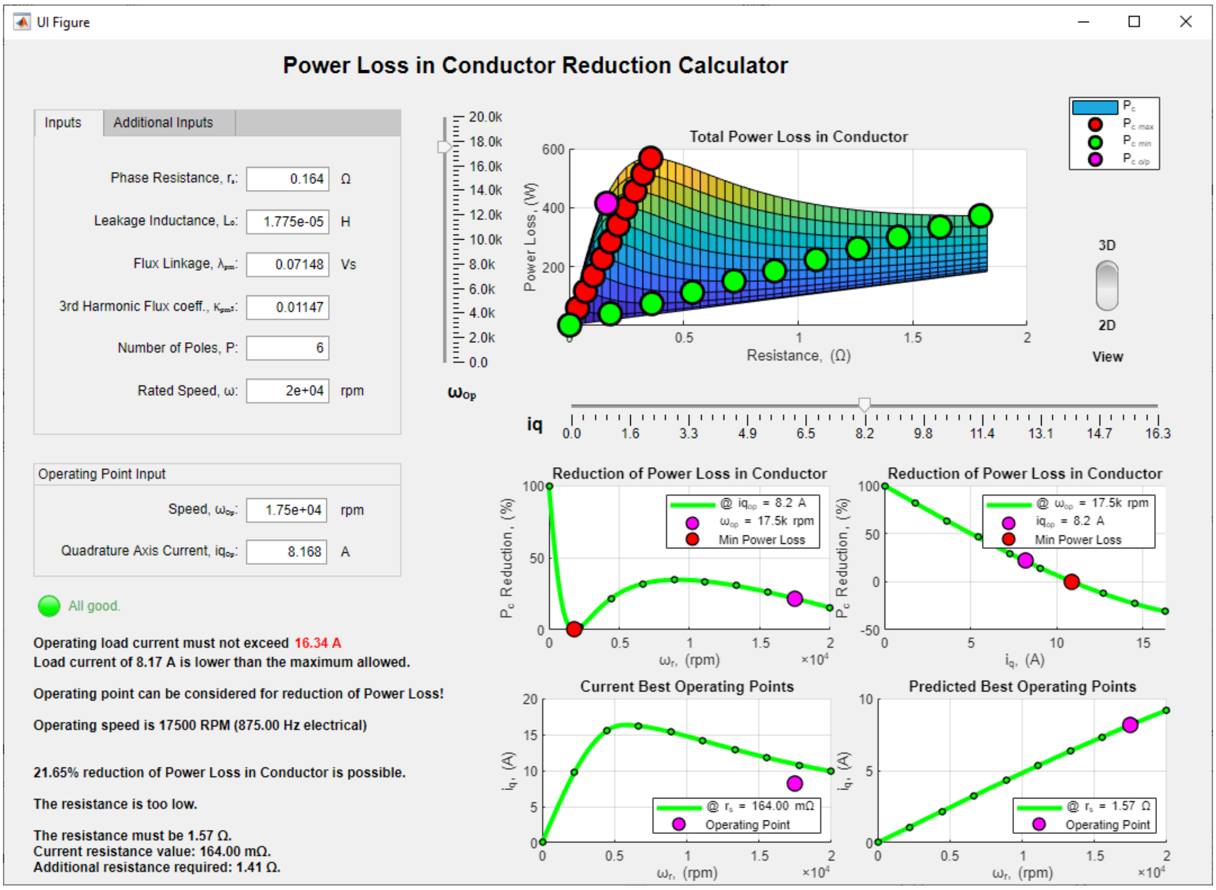

Fig. 7.64 – Power Loss in Conductor Reduction Calculator App (2D view)

Moreover, the application provides four additional 1D graphs in the bottom right corner shown in Fig. 7.65. The two top ones are the potential reduction of power loss in conductor with respect to the motor's speed and with respect to the torque inducing current. The two bottom ones are the minimum power loss operating points with the user defined resistance and the same graph, but with the estimated resistance suggested by the program. All four of them feature the current user defined operating point.

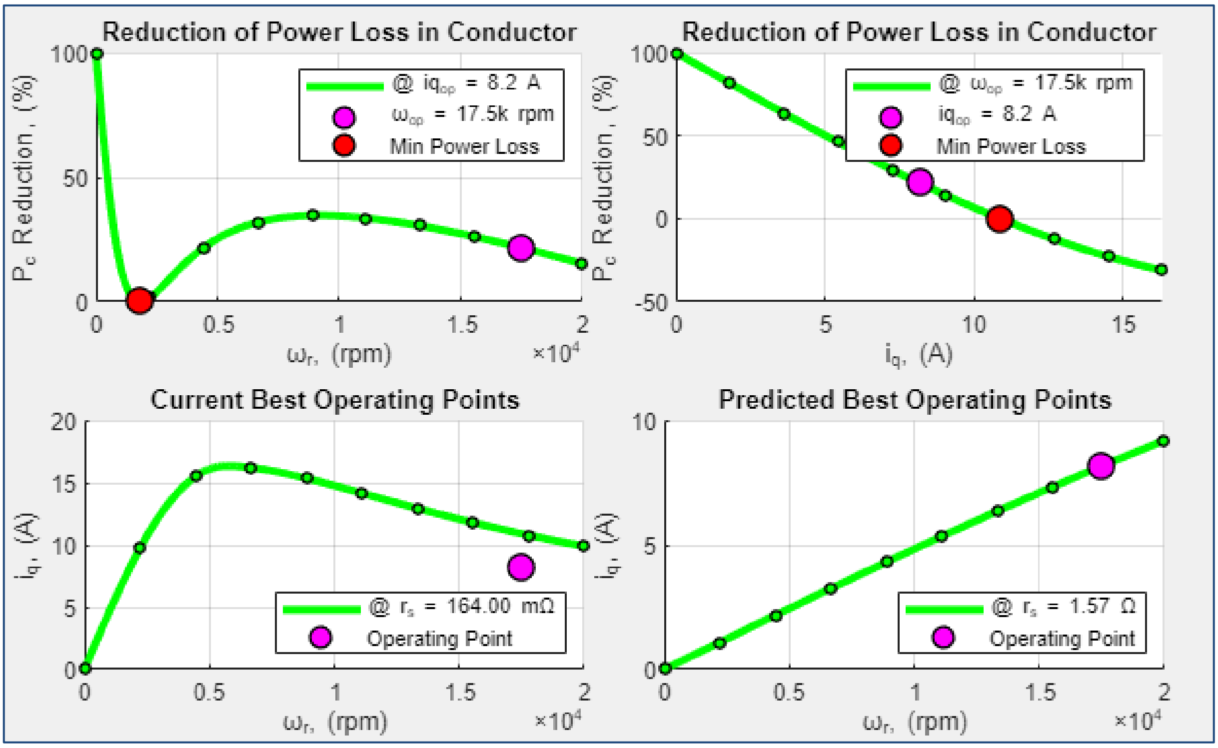

Fig. 7.65 – Graphical 1D outputs of the application

All of the graphs presented in the GUI are updating with every change of the slider values or the input variables on the left hand side, giving a better understanding of what is happening in the system when the user varies the parameters.

There could also be a case when the operating point is already placed in the minimum total power loss in conductor region or the decrease of the total power loss in conductor is impossible by using the introduced in this thesis method of increasing the phase resistance. In such a case the "Predicted Best Operating Points" graph will disappear as per the bottom right corner of the GUI presented in Fig. 7.66. This plot will no longer be displayed because there is no need for the increase of the phase resistance. The rest of the plots will remain to show the current condition of the system.

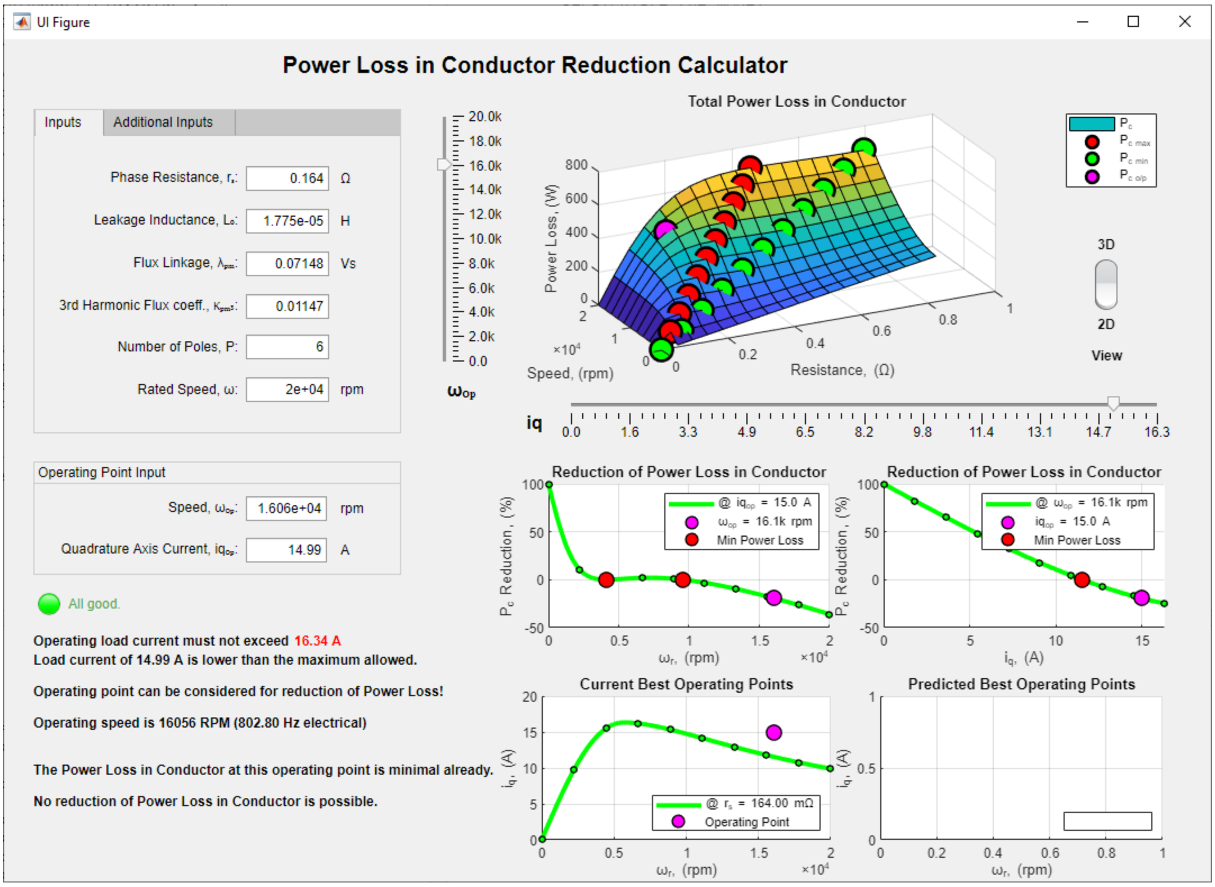

Fig. 7.66 – Power loss in conductor is already at minimum GUI (3D view)

Once it is established to be impossible to apply the developed power loss reduction technique for the particular motor specification or for the specific operating point, the application will show the appropriate message in the text field as depicted in the snippet of the GUI presented in Fig. 7.67 below.

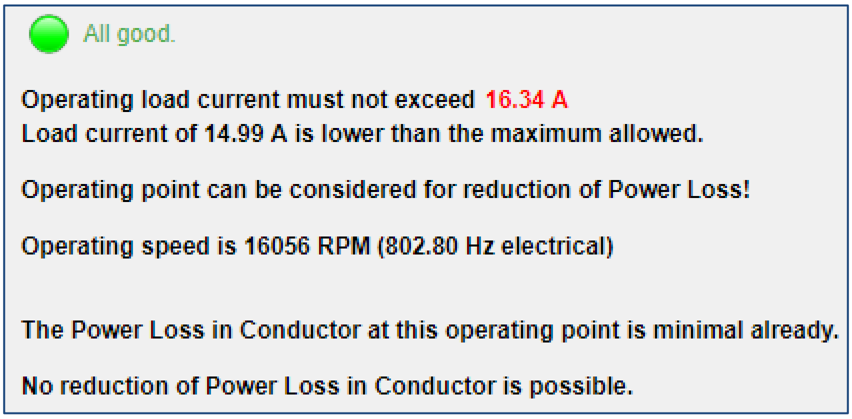

Fig. 7.67 – Power loss in conductor is already at minimum text message

In order to plot the main 2D graph of total power loss in conductor, the following equations were used: (7.24) for the surface itself and for the operating point, (7.42) for the maximum points, and (7.44) for the minimum points. The maximum torque producing current is calculated using equation (7.45). Equation (7.50) was used to construct both of the "Reduction of Power Loss in Conductor" 1D plots.

The "Reduction of Power Loss in Conductor" with respect to the motor's speed will remain its shape once the operating current will be set to a particular value. Changing the operating speed will result in the magenta operating point travelling along this one dimensional graph.

The "Reduction of Power Loss in Conductor" with respect to the motor's torque producing current will remain its shape once the operating speed will be set to a particular value. Changing the operating torque producing current i_q will result in the magenta operating point travelling along this 1D graph.

The "Current Best Operation Points" graph provides the user with the operating points of the motor with the current parameter configuration that result in a minimum total power loss in conductor for the currently chosen phase resistance.

The "Predicted Best Operation Points" graph provides the user with the operating points of the motor with the suggested phase resistance that result in a minimum total power loss in conductor. The suggested phase resistance is the estimated value that the program provides the user with in order to minimise the power loss at the required operating point.

Furthermore, the designed application has a robust error handling algorithm that improves the user's experience. The error messages of such algorithms are shown in Fig. 7.68 - Fig. 7.71. The presented error messages navigate the user providing with the hints on the origin of the particular error.

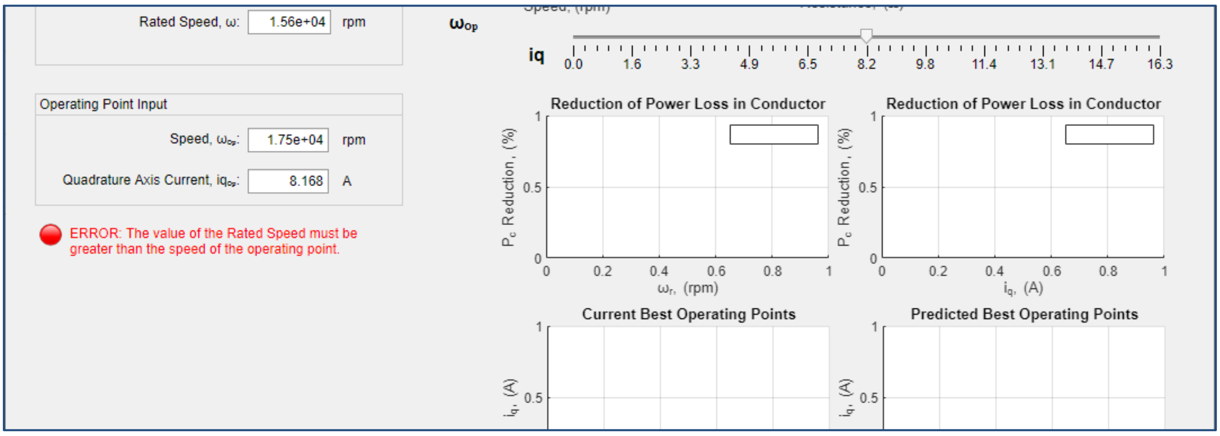

Fig. 7.68 – Error handling: operating speed exceeds rated speed

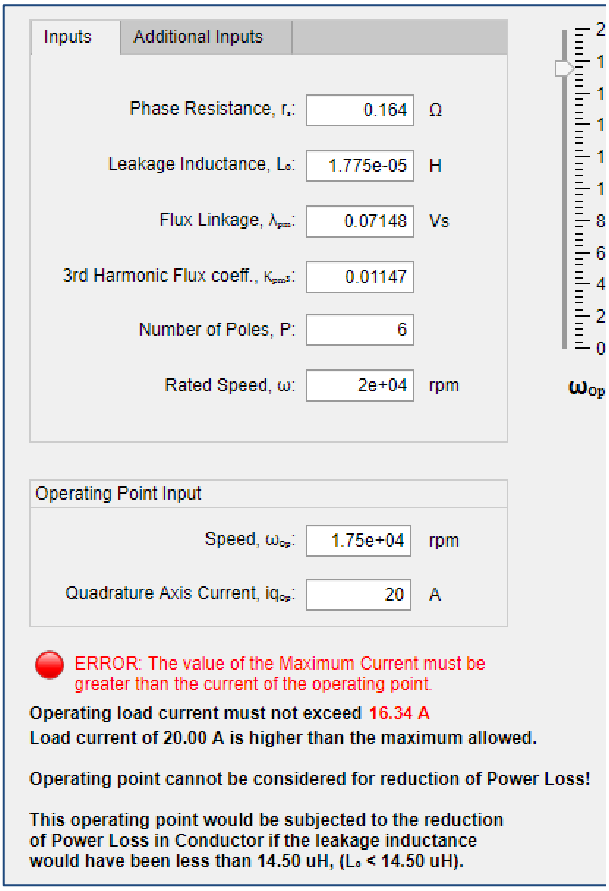

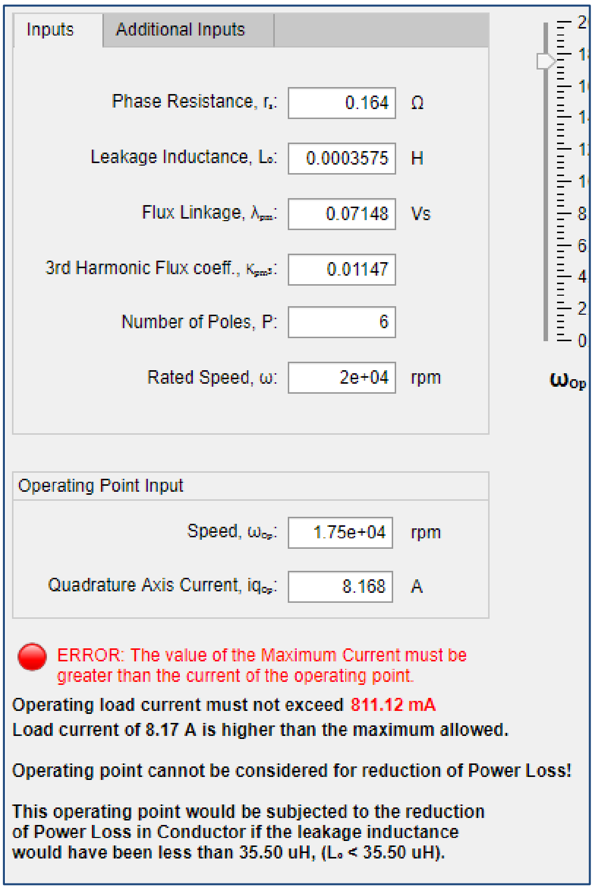

(a) (b)

Fig. 7.69 – Error handling: (a) – high operating point current, (b) - high leakage inductance

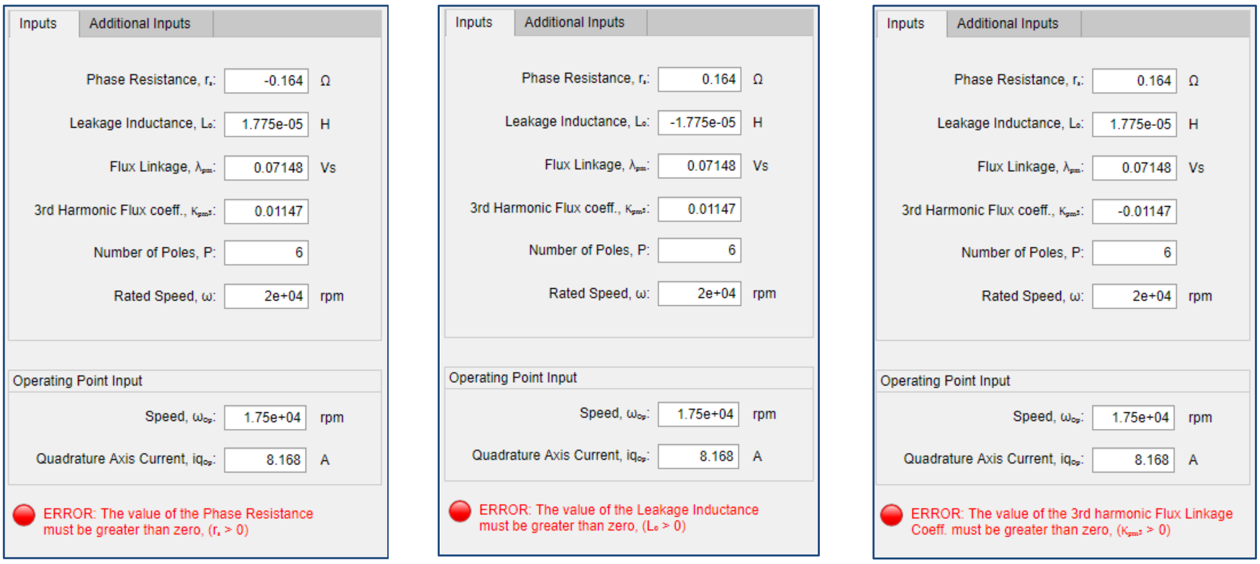

(a) (b) (c)

Fig. 7.70 – Error handling: (a) – phase resistance, (b) - leakage inductance, (c) – 3rd harmonic flux coefficient

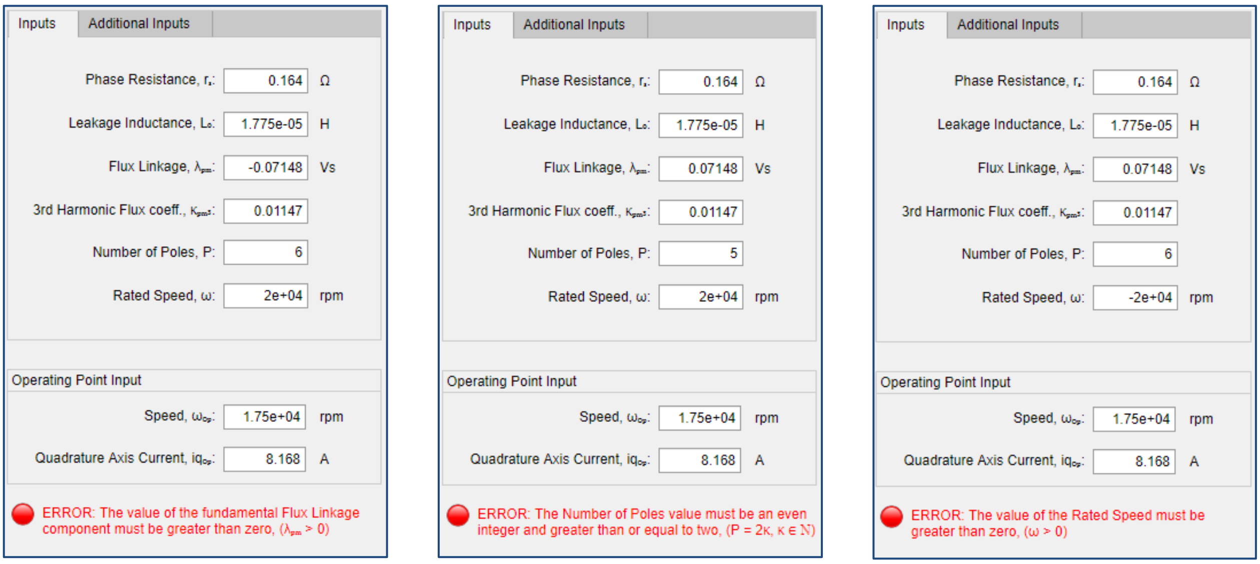

(a) (b) (c)

Fig. 7.71 – Error handling: (a) – flux linkage, (b) – pole number condition, (c) – rated speed value

7.3.2Discussion

The work produced and described in this chapter enabled the design and implementation of an algorithm and a specific software that is able to show how much power is lost due to the zero-sequence current choose the user an open-end winding configuration with common DC link for a particular permanent magnet synchronous motor.

The program identifies whether it is possible to reduce the power losses in conductor at a certain operating point. The parameters of the machine and the operating conditions the user specified along with the equations derived in 7.1 are used in the decision making process. In case it is possible to reduce the losses in conductor by the means of increasing the resistance, the program then determines how much power loss in conductor could be reduced. Subsequently, the program provides the user with an estimated value of the resistance increase. It is up to the user to decide how this change is going to be implemented.

Chapter 8

8 Conclusions, Contributions and Recommendations for Future Research

This chapter summaries the PhD research outcomes and draws the conclusions from the performed work, emphasising the contribution and proposing the further research work in the area.

8.1Conclusions and Contributions

There are two main sources of the zero-sequence current: the inverter side and the machine side. This research considers the machine side as the primary source of the zero-sequence current only.

This thesis introduced a concept of an uncontrolled zero-sequence current operation of an open-end winding permanent magnet motor drive with common DC link.

The novel technique for mitigating the influence of the zero-sequence current on the torque production was introduced in this thesis, validated in simulation and experimentally.

This thesis also introduced a helpful concept of a maximum zero-sequence current under an uncontrolled zero-sequence current operation. Not only did this concept become one of the key components in the proposed novel non-intrusive online stator temperature estimating method for an open-end winding permanent magnet synchronous motor with common DC link, but also the research showed that this concept appeared to be handy during the analysis of the power loss in conductor of the same types of motor configuration.

In this thesis an online identification of stator winding temperature for an open–end winding permanent magnet synchronous motor with common DC link is proposed. The method is based on the zero-sequence current flowing in the machine due to the third harmonic back EMF. Not only did the simulation validate the method, but also it showed that the temperature estimation is both accurate and resistant to the changes in the load torque and the speed of the machine. The independence of the rotor position grants the possibility for the exploitation of the proposed winding temperature estimation method in a variety of control techniques including the sensorless control to increase the robustness of the overall system.

An analytical approach was introduced for the estimation of power losses in conductor of an open-end winding permanent magnet motor drive with common DC link under an uncontrolled zero-sequence current operation. This analytical approach lead to a novel unintuitive method of reducing the machine's power losses in conductor. The method suggests that in some operational points of an OEW PMSM with common DC link operating under an uncontrolled zero-sequence current, it is possible to *reduce* the power losses in conductor by (ATTENTION!) increasing the phase resistance of the motor. The full mathematical derivation and simulation through Matlab validated the concept.

Chapter 7 described the results of the research performed regarding the power deprivation in the open-end winding permanent magnet synchronous motor with common DC bus configuration due to the zero-sequence current. The analysis of the power degradation due to the uncontrolled ZSC performed in this chapter revealed a potential for a novel idea that has been developed in order to mitigate the particular power loss in the conductor due to the zero-sequence current in some of the operational cases of OEW PMSM drives with common DC link.

A number of ideas to improve the performance of an open-end winding permanent magnet synchronous motor drive with common DC link control were introduced in chapter 7, the major one of which includes a proposed technique for the power loss in conductor reduction. This technique also includes the two new types of the current limiters for an OEW PMSM with common DC link.

Another contribution is the novel developed power loss in conductor reduction technique along with a software implemented in Matlab.

Not only is the developed software meant to aid engineers to understand the specifics of their system, but also it is meant to help them to reduce the motor's power losses in conductor.

In addition, the developed Matlab algorithm was used to understand some systems' behaviours and are aimed to aid the further research as it is widely known that visualization of the systems' processes could certainly help to identify a number of relationships and regularities. Moreover, not only could the developed "visualisation aid" provoke new ideas as to, for example, where the systems weak points might be, but also it could lead to the solutions to the existing problems as the human brain is known for an outstanding pattern recognition ability particularly in the presence of noise. [110] In addition, due to the interactive nature of the developed algorithms, they could be used for the educational purposes to aid the academics and the students to grasp some complex concepts easier and quicker.

Two new concepts of the current limiters for an open-end winding permanent magnet synchronous motor drives with common DC link are proposed. Both are verified analytically and in simulation.

It is show by the means of mathematical analysis that the proposed RMS current limiting technique appears to be the correct representation of the intended outcome, whereas the formula for the current limit presented in [71] and [109] is argued to be erroneous. The real representation of the RMS limit derived in 7.2.1 uses the amplitude of the zero-sequence current rather than the RMS value.

The novel developed peak current limiter for an OEW PMSM was tested and validated through the mathematical analysis and Matlab simulation.

Finally, the papers resulted from the research are attached to this thesis and can be found in Appendix F.

8.2Recommendation for Future Work

8.2.1Torque Quality Improvement Technique

Judging by the simulation results using the FEA and the estimated drive parameter it could be concluded that the proposed in this thesis torque quality improvement technique along with the online stator temperature estimation for the OEW PMSM with the common DC link is thought to have a better performance when an integrated motor drive is used. The reason for this is the compact design would mean the shorter lengths of the wires that in turn will result in both the lower internal resistance and the lower leakage inductance. This should make the zero-sequence current more prominent. Hence, it would be interesting from the research point of view to repeat the experiments using the integrated open-end winding high-speed drive with common DC link.

Further work could also include the comparison on the developed torque reduction technique and a model predictive control that uses a similar control principle as the one introduced in chapter 5.

8.2.2Non-Intrusive Online Stator Temperature Estimation Technique

A suitable experimental setup must be found for the proposed online non-intrusive estimation of the stator temperature to confirm the method experimentally. As it was already discussed, an integrated drive could be one of the options. Once the method will be confirmed, the future research could then be focused on the partially controlled zero-sequence current with the possibility to maintain the advantage of estimating the temperature of stator having the influence of the zero-sequence current reduced.

8.2.3Reduction of Power Loss in Conductor Technique

Regarding the proposed power loss in conductor reduction technique, the equations that are presented valid for the case of the constant torque operational region only, i.e. then the value of the direct axis current i_d is zero amperes.

The future work will involve the expansion of the proposed technique to the constant power region and the Maximum Torque per Ampere (MTPA) technique. This will involve incorporating the direct current axis variable into the existing method and rearranging all of the equations accordingly. As a consequence, the developed software will be more versatile, featuring new formulae.

The future work could also be focused on the identification of an optimal value for the phase resistance for more than one operational point. For example, when a motor is operating under a constant current control technique over a range of frequencies or when a motor is controlled using a speed control mode.

In addition, the experimental validation of the technique will need to be done using different permanent magnet synchronous motors in an open-end winding configuration with common DC link under uncontrolled current operation.

Furthermore, the developed in Matlab engineering aid can potentially be translated into a C/C++/Java/Python application with the further integration into a machine designing software. The research introduced in this thesis enables the potential for a collaboration with the industries producing machine design simulations.

Moreover, a whole new research can be done on an incorporation of the zero-sequence voltage due to the power converter into the developed method of reduction of the power loss in conductor. The introduction of the zero-sequence voltage from the inverter side of the drive would change the behaviour of the zero-sequence current and, therefore, the developed equations will have to be altered in a non-trivial way.

8.2.4Current Limiting Technique

It has been confirmed that the zero-sequence current affects the operation of an open-end winding permanent magnet synchronous motor with common DC Link. In particular, it affects the current limit that could be used. Further work could involve the research into the affection of identification of the base speed of an OEW PMSM with common DC link under the proper current limiting techniques introduced in this thesis, following by the investigation of the affection of the flux weakening control with the following experimental confirmation.

Also, the field of OEW PMSM with common DC link control lacks the research on a Maximum Torque per Ampere (MTPA) control technique for the Interior Permanent Magnet Synchronous Motors (IPMSM). This technique is likely to be affected due to the zero-sequence current that has to be incorporate in the current limiting algorithm.

8.2.5Other Further Work

The test rigs for testing of the high-speed high torque machines are expensive, the research could be stopped for a prolonged time. For example, the testing facility that was used for the experimental part of the research is unique. It was designed by Torquemeters specifically for the University of Nottingham. Hence, there is a long waiting time and a short time for the experiment testing to be conducted. In addition, it takes time to set up a rig and adapt the control. Furthermore, whilst the motor is running it is impossible to walk inside of the high-speed testing facilities to check the system, measure the outputs or ensure that the data acquisition tools are working correctly. Moreover, the inverter for the machine must remain in another room. This causes all sorts of unexpected inconveniences and disturbances which are sometimes hard to account for. The limited time of operation along with the health and safety precautions can hold the research back for many months, or even years.

All of the mentioned factors contribute to the success of the future PhD candidates and the success in the future research along with the possible collaboration with other research groups and industries. Hence, one of the directions of the future research could be based around the automation of the process of collection of the data from the high-speed facility in Nottingham. This automation could also include the algorithms that would gather all of the data necessary to make an accurate model of an open-end winding PMSM with common DC link, helping saving time and effort in predicting the behaviour of the drive itself. This process should include the possibility to predict the disturbances and collect the necessary data for its further analysis and use for the design of an accurate mathematical model of the drive. This accurate model could then be used to, for example, identify the frequency content of the zero-sequence current flowing in the system in order to realise the limitations of certain proposed concepts based on the assumption that the zero-sequence current has third harmonic only. This algorithm has to be universal, easily implemented on any types of control boards. Knowing the facility, it can be certain that there will be a need to implement some hardware as well in order to achieve the set goals.

Future work could also include the research on the improvement of the sensorless control that utilises the zero-sequence current reading in order to estimate the rotor’s position.

A high-speed operation could require faster switching, meaning that there is less time for the calculations determining the next control action, especially if one desires to implement, for example, a model predictive control with heavy calculations and an unacceptable number of states to go though. When there are too many states to find the minimum of, it is sometimes impossible to go through each of the states in a given period of sampling time. This is where genetic algorithm might be handy as it is known to work relatively well with a large number of possible solutions. A research into the incorporation of the model predictive control with the genetic algorithm for an open-end winding PMSM with the common DC link could be thought as one of the possible directions. The maximum time allowed for the calculations could be used as a stopping criterion for the algorithm.

Although the main focus of this thesis is to address the zero-sequence current related problems of the high-speed open-end winding permanent magnet synchronous machines with common DC link from the machine side only, there are other factors that could be taken into account, such as the effect of PWM on the machines with low inductance. However, analysing those is a complex matter on its own. The low inductance ensures the high current ripple if the inverter is not fast enough. For this reason, the current sensors must be carefully selected in order to not only withstand the current variations, but also measure the phase current accurately. The future work could include the combination of the results of the research discussed in this thesis with those problems as well.

Another interesting topic to research is the influence of the magnetic saturation on the zero-sequence current in high-speed low inductance machines. It is expected that the saturation would have an effect on the zero-sequence current. The future work could include the investigation of this behaviour.

References

[1] D. Gerada, A. Mebarki, N. L. Brown, C. Gerada, A. Cavagnino and A. Boglietti, "High-Speed Electrical Machines: Technologies, Trends, and Development," *IEEE TRANSACTIONS ON INDUSTRIAL ELECTRONICS,,* vol. 61, no. 6, p. 2946, 2014.

[2] H. L. Garbarino, A. K. Hawkes and J. A. Granath, "A weight analysis of modern aircraft electric systems," *Transactions of the American Institute of Electrical Engineers,* vol. 73, no. 6, pp. 463-469, 1955.

[3] Hui Zhang, L. M. Tolbert and B. Ozpineci, "Impact of SiC Devices on Hybrid Electric and Plug-In Hybrid Electric Vehicles," *IEEE TRANSACTIONS ON INDUSTRY APPLICATIONS,,* vol. 47, no. 2, pp. 912-921, 2011.

[4] G. Borgogna, T. Lamberti and A. F. Massardo, "Innovative power system for autonomous underwater vehicle," in *OCEANS 2015 - Genova*, Genoa, 2015.

[5] J. C. Rama and A. Giesecke, "High speed electric drive applications, experience, potential and pitfalls-a global overview," in *42nd Annual Petroleum and Chemical Industry Conference*, Denver, CO, 1995.

[6] Z. Lei, W. Xuhui, Z. Jian and W. Youlong, "Research of high power-density permanent magnet synchronous motor and driving system," in *2011 International Conference on Electric Information and Control Engineering*, Wuhan, 2011.

[7] P. Arumugam, Z. Xu, G. Vakil, T. Hamiti, S. Bozhko, C. Gerada and S. Pickering, "Solid rotor interior permanent magnet machines for high speed applications," in *41st Annual Conference of the IEEE Industrial Electronics Society*, Yokohama, 2015.

[8] A. Boglietti, C. Gerada and A. Cavagnino, "High-Speed Electrical Machines and Drives," *IEEE TRANSACTIONS ON INDUSTRIAL ELECTRONICS,* vol. 61, no. 6, pp. 2943-2945, 2014.

[9] L. Zheng, "Super High-speed Miniaturized Permanent Synchronous Motor," University of Central Florida, Electronic Theses and Dissertations, 2005.

[10] P. Thelin and H.-P. Nee, "Analytical calculation of the airgap flux density of PM synchronous motors with buried magnets including axial leakage, tooth and yoke saturations," in *2000 Eighth International Conference on Power Electronics and Variable Speed Drives (IEE Conf. Publ. No. 475)*, London, 2000.

[11] T. Z. Htet, "PM material analysis of permanent magnet synchronous generator in wind turbines," in *2017 2nd International Conference on System Reliability and Safety (ICSRS)*, Milan, 2017.

[12] B.-H. Bae, S.-K. Sul, J.-H. Kwon and J.-S. Byeon, "Implementation of sensorless vector control for super-high-speed PMSM of turbo-compressor," *IEEE Transactions on Industry Applications,* vol. 39, no. 3, pp. 811-818, 2003.

[13] S. Fang, H. Liu, H. Wang, H. Yang and H. Lin, "High Power Density PMSM With Lightweight Structure and High-Performance Soft Magnetic Alloy Core," *IEEE Transactions on Applied Superconductivity,* vol. 29, no. 2, 2019.

[14] D. Lusignani, D. Barater, G. Franceschini, G. Buticchi, M. Galea and C. Gerada, "A high-speed electric drive for the more electric engine," in *IEEE Energy Conversion Congress and Exposition (ECCE)* , Montreal, QC , 2015.

[15] L. Chu, Y.-f. Jia, D.-s. Chen, N. Xu and Y.-w. Wang, "Research on Control Strategies of an Open-End Winding Permanent Magnet Synchronous Driving Motor (OW-PMSM)-Equipped Dual Inverter with a Switchable Winding Mode for Electric Vehicles," *Energies,* vol. 10, no. 5, 2017.

[16] G. L. Calzo, P. Zanchetta, C. Gerada and F. Crescimbini, "Converter Topologies comparison for more electric aircrafts high speed Starter/Generator application," in *IEEE Energy Conversion Congress and Exposition (ECCE)*, Montreal, QC, 2015.

[17] B. C.Mecrow, A. G. Jack, J. A.Haylock and a. J. Coles, "Fault-tolerant permanent magent machine drives," *IEE Proc. Electric Power Appl,* vol. 143, no. 6, pp. 437-442, 1996.

[18] N. K. Nguyen, F. Meinguet, E. Semail and X. Kestelyn, "Fault-Tolerant Operation of an Open-End Winding Five-Phase PMSM Drive With Short-Circuit Inverter Fault," *IEEE TRANSACTIONS ON INDUSTRIAL ELECTRONICS,* vol. 63, no. 1, pp. 595-605, 2016.

[19] K. A. Corzine, S. D. Sudhoff and C. A. Whitcomb, "Performance characteristics of a cascaded two-level converter," *IEEE Transaction on Energy Conversion,* vol. 14, no. 3, pp. 433-439, 1999.

[20] Y. Lee and J.-I. Ha, “Hybrid Modulation of Dual Inverter for Open-End Permanent Magnet Synchronous Motor,” *IEEE Transactions on Power Electronics ,* vol. 30, no. 6, pp. 3286-3299, 2015.

[21] X. Lin, W. Huang and L. Wang, “SVPWM Strategy Based on the Hysteresis Controller of Zero-Sequence Current for Three-Phase Open-End Winding PMSM,” *IEEE Transactions on Power Electronics,* vol. 34, no. 4, pp. 3474 - 3486, 2019.

[22] Z. Shen, D. Jiang, L. Zhu, Y. Xu, T. Zou, Z. Liu and R. Qu, “A Novel Zero-Sequence Current Elimination PWM Scheme for an Open-Winding PMSM With Common DC Bus,” *IEEE Transactions on Power Electronics,* vol. 34, no. 12, pp. 12476 - 12490, 2019.

[23] H. Nian, Y. Zhou and H. Zeng, “Zero-Sequence Current Suppression Strategy for Open Winding PMSG Fed by Semicontrolled Converter,” *IEEE Transactions on Power Electronics,* vol. 31, no. 1, pp. 711 - 720, 2016.

[24] X. Zhang, W. Zhang, C. Xu, Y. Li, Y. Wang and D. Gao, “Three-Dimensional Vector Based Model Predictive Current Control for Open-End Winding PMSG System with Zero-Sequence Current Suppression,” *IEEE Journal of Emerging and Selected Topics in Power Electronics (Early Access),* 2019.

[25] L. Yao, S. Yang, Z. Xie and X. Zhang, “Eliminating scheme of zero-sequence currents in open-end winding induction motor drive with a single DC power supply,” in *2017 Chinese Automation Congress (CAC)*, Jinan, 2017.

[26] H. Nian, C. Ruan, W. Hu and D. Sun, “Improved modulation method with reduced switching frequency for OW-PMSM system with

common DC bus," *Electronics Letters ,* vol. 55, no. 18, pp. 1009 - 1012, 2019.

[27] Z. Song, X. Ma and Y. Yu, "Design of Zero-Sequence Current Controller for Open-End Winding PMSMs Considering Current Measurement Errors," *IEEE Transactions on Power Electronics,* vol. 35, no. 6, pp. 6127 - 6139, 2019.

[28] H. Zhan, Z. Q. Zhu, M. Odavic and Y. Li, "A Novel Zero-Sequence Model-Based Sensorless Method for Open-Winding PMSM With Common DC Bus," *IEEE Transactions on Industrial Electronics,* vol. 63, no. 11, pp. 6777 - 6789, 2016.

[29] X. Zhang and K. Wang, "Current Prediction Based Zero Sequence Current Suppression Strategy for the Semicontrolled Open-Winding PMSM Generation System With a Common DC Bus," *IEEE Transactions on Industrial Electronics,* vol. 65, no. 8, pp. 6066-6076, 2018.

[30] S. F. Zhao, X. Y. Huang, Y. T. Fang and J. Li, "A control scheme for a High Speed Railway traction system based on high power PMSM," in *2015 6th International Conference on Power Electronics Systems and Applications (PESA)*, Hong Kong, 2015.

[31] Q. An, G. Wang and L. Sun, "A fault-tolerant operation method of PMSM fed by cascaded two-level inverters," in *Proceedings of The 7th International Power Electronics and Motion Control Conference*, Harbin, 2012.

[32] J.-C. Hwang, "The Current Harmonics Elimination Control Strategy for Six-Leg Three-Phase Permanent Magnet Synchronous Motor Drives," *IEEE Transactions on Power Electronics,* vol. 29, no. 6, pp. 3032 - 3040, 2014.

[33] N. A. M. Said, J. E. Fletcher, R. Dutta and D. Xiao, “Analysis of common mode voltage using carrier-based method for dual-inverter open-end winding,” in *2014 Australasian Universities Power Engineering Conference (AUPEC)*, Perth, 2014.

[34] S. Foti, A. Testa, G. Scelba, S. D. Caro, M. Cacciato, G. Scarcella and T. Scimone, “An Open-End Winding Motor Approach to Mitigate the Phase Voltage Distortion on Multilevel Inverters,” *IEEE Transactions on Power Electronics,* vol. 33, no. 3, pp. 2404 - 2416, 2018.

[35] W. Zhou, D. Sun and B. Lin, “A modified flux weakening direct torque control for open winding PMSM system fed by hybrid inverter,” in *2014 17th International Conference on Electrical Machines and Systems (ICEMS)*, Hangzhou, 2015.

[36] P. Archana and K. Preetha, “EFFICIENCY IMPROVEMENT IN DUAL INVERTER FED OPEN-END PERMANENT MAGNET SYNCHRONOUS MOTOR,” *ARPN Journal of Engineering and Applied Sciences,* vol. 11, no. 3, pp. 2061-2070, 2016.

[37] W. Zhao, B. Wu, Q. Chen and J. Zhu, “Fault-Tolerant Direct Thrust Force Control for a Dual Inverter Fed Open-End Winding Linear Vernier Permanent-Magnet Motor Using Improved SVPWM,” *IEEE Transactions on Industrial Electronics,* vol. 65, no. 9, pp. 7458 - 7467, 2018.

[38] V. F. Pires and A. Cordeiro, “Dual Inverter with a Floating Bridge Controlled by a Vectorial Voltage Modulator,” in *2018 16th Biennial Baltic Electronics Conference (BEC)*, Tallinn, 2018.

[39] S. Chowdhury, P. W. Wheeler, C. Gerada and C. Patel, “Model Predictive Control for a Dual-Active Bridge Inverter With a Floating

Bridge," *IEEE Transactions on Industrial Electronics,* vol. 63, no. 9, pp. 5558 - 5568, 2016.

[40] S. Chowdhury, P. W. Wheeler, C. Patel and C. Gerada, "A Multilevel Converter With a Floating Bridge for Open-End Winding Motor Drive Applications," *IEEE Transactions on Industrial Electronics,* vol. 63, no. 9, pp. 5366 - 5375, 2016.

[41] R. U. Haque, M. S. Toulabi, A. M. Knight and J. Salmon, "Wide speed range operation of PMSM using an open winding and a dual inverter drive with a floating bridge," in *2013 IEEE Energy Conversion Congress and Exposition*, Denver, 2013.

[42] S. Chowdhury, P. Wheeler, Z. Huang, M. Rivera and C. Gerada, "Fixed switching frequency predictive control of an asymmetric source dual inverter system with a floating bridge for multilevel operation," *IET Power Electronics,* vol. 12, no. 3, pp. 450 - 457, 2019.

[43] Y. Zhou and H. Nian, "Zero-Sequence Current Suppression Strategy of Open-Winding PMSG System With Common DC Bus Based on Zero Vector Redistribution," *IEEE Transactions on Industrial Electronics,* vol. 62, no. 6, pp. 3399 - 3408, 015.

[44] W. Zhao, P. Zhao, D. Xu, Z. Chen and J. Zhu, "Hybrid Modulation Fault-Tolerant Control of Open-End Windings Linear Vernier Permanent-Magnet Motor With Floating Capacitor Inverter," *IEEE Transactions on Power Electronics,* vol. 34, no. 3, pp. 2563 - 2572, 2019.

[45] B. Lin and D. Sun, "Analysis on constant power range enhancement in hybrid-inverter open winding PMSM drive system," in *2014 17th*

International Conference on Electrical Machines and Systems (ICEMS), Hangzhou, 2014.

[46] X. Zhu, X. Bu, Y. Zuo, Y. Yuan and B. Shi, "Fault-Tolerant Control for Open Winding PMSM System with Common DC Bus Based on 120° Decoupled Modulation Strategy," in *2018 IEEE Energy Conversion Congress and Exposition (ECCE)*, Portland, 2018.

[47] C. Ruan, W. Hu, H. Nian and D. Sun, "Open-Phase Fault Control in Open-Winding PMSM System with Common DC Bus," in *2019 IEEE Applied Power Electronics Conference and Exposition (APEC)*, Anaheim, 2019.

[48] W. Hu, C. Ruan, H. Nian and D. Sun, "Simplified Modulation Scheme for Open-End Winding PMSM System With Common DC Bus Under Open-Phase Fault Based on Circulating Current Suppression," *IEEE Transactions on Power Electronics,* vol. 35, no. 1, pp. 10 - 14, 2020.

[49] G. C. Lim, H.-G. Choi and J.-I. Ha, "Single Phase Commutation Control of Open-End Winding PMSM Fed by Single DC-Link Dual Inverter," in *2019 10th International Conference on Power Electronics and ECCE Asia (ICPE 2019 - ECCE Asia)*, Busan, 2019.

[50] B. Zhu, C. Tan, M. Farshadnia and J. E. Fletcher, "Postfault Zero-Sequence Current Injection for Open-Circuit Diode/Switch Failure in Open-End Winding PMSM Machines," *IEEE Transactions on Industrial Electronics,* vol. 66, no. 7, pp. 5124 - 5132, 2019.

[51] M. Muenchhof, M. Beck and R. Isermann, "Fault Tolerant Actuators and Drives – Structures, Fault Detection Principles and Applications," *IFAC Proceedings Volumes,* vol. 42, no. 8, pp. 1294-1305, 2009.

[52] T. Komrska, T. Glasberger and Z. Peroutka, "PWM for Open-End Winding Drive in Fault Tolerant Mode with Minimum Infinity Norm

Calculation of Modulation Signals," in *IECON 2018 - 44th Annual Conference of the IEEE Industrial Electronics Society*, Washington, 2018.

[53] S. Khwan-on, L. d. Lillo, L. Empringham, P. Wheeler, C. Gerada, N. M. Othman, O. Jasim and J. Clare, "Fault tolerant power converter topologies for PMSM drives in aerospace applications," in *2009 13th European Conference on Power Electronics and Applications*, Barcelona, 2009.

[54] X. Yuan, C. Zhang and S. Zhang, "A Novel Deadbeat Predictive Current Control Scheme for OEW-PMSM Drives," *IEEE Transactions on Power Electronics,* vol. 34, no. 12, pp. 11990 - 12000, 2019.

[55] R. Baranwal, K. Basu and N. Mohan, "Carrier-Based Implementation of SVPWM for Dual Two-Level VSI and Dual Matrix Converter With Zero Common-Mode Voltage," *IEEE Transactions on Power Electronics,* vol. 30, no. 3, pp. 1471 - 1487, 2015.

[56] P. Zanchetta, C. Gerada, A. Lidozzi, M. Degano, F. Crescimbini and L. Solero, "Performance evaluation of converter topologies for high speed Starter/Generator in aircraft applications," in *40th Annual Conference of the IEEE Industrial Electronics Society*, Dallas, TX, 2014.

[57] L. Rovere, A. Formentini, G. L. Calzo, P. Zanchetta and T. Cox, "IGBT-SiC dual fed open end winding PMSM drive," in *Electric Machines and Drives Conference (IEMDC), 2017 IEEE International*, Miami, 2017.

[58] Q. An, J. Liu, Z. Peng, L. Sun and L. Sun, "Dual-Space Vector Control of Open-End Winding Permanent Magnet Synchronous Motor Drive

Fed by Dual Inverter," *IEEE Transactions on Power Electronics,* vol. 31, no. 12, pp. 8329-8342, 2016.

[59] N. Kalantari and L. A. C. Lopes, "Reduction of Dead-Time Effect on the Common Mode Voltage of an Open-End Winding Machine," in *2016 IEEE 25th International Symposium on Industrial Electronics (ISIE)*, Santa Clara, CA, USA, 2016.

[60] A. Somani, R. K. Gupta, K. K. Mohapatra and N. Mohan, "On the Causes of Circulating Currents in PWM Drives With Open-End Winding AC Machines," *IEEE Transactions on Industrial Electronics,* vol. 60, no. 9, pp. 3670-3678, 2013.

[61] H. Zhan, Z. Q. Zhu and M. Odavic, "Nonparametric Sensorless Drive Method for Open-Winding PMSM Based on Zero-Sequence Back EMF With Circulating Current Suppression," *IEEE Transactions on Power Electronics,* vol. 32, no. 5, pp. 3808 - 3817, 2017.

[62] J. Korhonen, J. Honkanen, T. J. Kärkkäinen, J. Nerg and P. Silventoinen, "Modulation and control methods to reduce zero sequence current in open-end winding motors," in *Electric Machines and Drives Conference (IEMDC), 2017 IEEE International*, Miami, FL, USA, 2017.

[63] N. M. Said, M. Priestley, R. Dutta and J. E. Fletcher, "Torque ripple minimization in dual inverter open-end winding PMSM drives with non-sinusoidal back-EMFs by harmonic current suppression," in *IECON 2016*, Florence, 2016.

[64] A. R. López-Núñez, J. D. Mina, J. Aguayo and G. Calderón, "Proportional Integral Resonant controller for current harmonics mitigation in a wind energy conversion system," in *Power Electronics*

(CIEP), 2016 13th International Conference on, Guanajuato, Mexico, 2016.

[65] X. Yuan, C. Zhang and S. Zhang, "Torque Ripple Suppression for Open-End Winding Permanent-Magnet Synchronous Machine Drives With Predictive Current Control," *IEEE Transactions on Industrial Electronics,* vol. 67, no. 3, pp. 1771 - 1781, 2020.

[66] L. Tarisciotti, G. L. Calzo, A. Gaeta, P. Zanchetta, F. Valencia and D. Saez, "A Distributed Model Predictive Control Strategy for Back-to-Back Converters," *IEEE Transactions on Industrial Electronics,* vol. PP, no. 99, pp. 1-11, 2016.

[67] J. Lara, J. Xu and A. Chandra, "Effects of Rotor Position Error in the Performance of Field-Oriented-Controlled PMSM Drives for Electric Vehicle Traction Applications," *IEEE Transactions on Industrial Electronics,* vol. 63, no. 8, pp. 4738 - 4751, 2016.

[68] S. Mohan, J. S. T.K, A. Gopinath, J. B and M. Namboothiripad, "Modeling and simulation of high power open end winding based electromechanical actuator for aerospace applications," in *International Conference on Power and Advanced Control Engineering (ICPACE), 2015*, Bangalore, India, 2015.

[69] B. Lin, D. Sun and Y. Chen, "Research on high-speed operation of hybrid-inverter fed open winding permanent magnet synchronous motor," in *International Conference on Electrical Machines and Systems (ICEMS), 2013*, Busan, South Korea, 2014.

[70] M. Neubert, S. Koschik and R. W. D. Doncker, "Performance comparison of inverter and drive configurations with open-end and star-connected windings," in *2014 International Power Electronics Conference (IPEC-Hiroshima 2014 - ECCE ASIA)*, Hiroshima, 2014.

[71] P. Sandulescu, F. Meinguet, X. Kestelyn, E. Semail and A. Bruyere, "Control Strategies for Open-End Winding Drives Operating in the Flux-Weakening Region," *IEEE Transactions on Power Electronics,* vol. 29, no. 9, pp. 4829 - 4842, 2014.

[72] P. Arumugam, Z. Xu, A. L. Rocca, G. Vakil, M. Dickinson, E. Amankwah, T. Hamiti, S. Bozhko, C. Gerada and S. J. Pickering, "High-Speed Solid Rotor Permanent Magnet Machines: Concept and Design," *IEEE Transactions on Transportation Electrification,* vol. 2, no. 3, pp. 391 - 400, 2016.

[73] G. Feng, C. Lai, K. L. V. Iyer and N. C. Kar, "Improved High-Frequency Voltage Injection Based Permanent Magnet Temperature Estimation for PMSM Condition Monitoring for EV Applications," *IEEE Transactions on Vehicular Technology,* vol. 67, no. 1, pp. 216-225, 2018.

[74] M. Pulvirenti, G. Scarcella, G. Scelba, A. Testa and M. M. Harbaugh, "On-Line Stator Resistance and Permanent Magnet Flux Linkage Identification on Open-End Winding PMSM Drives," *IEEE Transactions on Industry Applications,* vol. 55, no. 1, pp. 504-515, 2019.

[75] M. Dilshad, S. Ashok, V. Vijayan and P. Pathiyil, "An energy loss model based temperature estimation for Permanent Magnet Synchronous Motor (PMSM)," in *2016 2nd International Conference on Advances in Electrical, Electronics, Information, Communication and Bio-Informatics (AEEICB)*, Chennai, 2016.

[76] R. Mocanu and A. Onea, "Temperature estimation for condition monitoring of PMSM used in electric vehicles," in *2014 International Symposium on Fundamentals of Electrical Engineering (ISFEE)*, Bucharest, 2014.

[77] G. Kizir, Ş. Demirbaş and M. Şahin, "Real-time resistance estimation of permanent magnet synchronous motor," in *2018 IEEE 12th International Conference on Compatibility, Power Electronics and Power Engineering (CPE-POWERENG 2018)*, Doha, 2018.

[78] J. Yoshimoto, Y. Inoue, S. Morimoto and M. Sanada, "Ultra-high-speed PMSM sensorless drive using direct torque control," in *15th International Conference on Electrical Machines and Systems (ICEMS)*, Sapporo , 2012.

[79] B.-H. Bae, S.-K. Sul, J.-H. Kwon and J.-S. Byeon, "Implementation of sensorless vector control for super-high-speed PMSM of turbo-compressor," *IEEE Transactions on Industry Applications,* vol. 39, no. 3, pp. 811-818, 2003.

[80] S. Moon, J.-M. Choe, Y. Cho and J.-s. Lai, "Priority based current control design in high speed sensorless PMSM drives," in *9th International Conference on Power Electronics and ECCE Asia (ICPE-ECCE Asia)*, Seoul, 2015.

[81] C. Bian, S. Ren and L. Ma, "Sensorless DTC of Super High-speed PMSM," in *IEEE International Conference on Automation and Logistics* , Jinan , 2007.

[82] F. Genduso, R. Miceli, C. Rando and G. R. Galluzzo, "IEEE Transactions on Industrial Electronics," *IEEE Transactions on Industrial Electronics ,* vol. 57, no. 6, pp. 2092-2100, 2010.

[83] J.-W. Lee, "Adaptive sensorless control of high speed PMSM with back EMF constant variation," in *9th International Conference on Power Electronics and ECCE Asia (ICPE-ECCE Asia)* , Seoul, 2015.

[84] Y. LIANG and Y. LI, "Sensorless Control of PM Synchronous Motors Based on MRAS Method and Initial Position Estimation," in *Sixth*

International Conference on Electrical Machines and Systems, Beijing, China, 2003.

[85] G. Zhao, J. Liu and J. Feng, "The research of speed sensorless control of PMSM based on MRAS and high frequency signal injection method," in *International Conference on Computer, Mechatronics, Control and Electronic Engineering* , Changchun , 2010.

[86] L. Yongdong and Z. Hao, "Sensorless Control of Permanent Magnet Synchronous Motor – A Survey," in *2008 IEEE Vehicle Power and Propulsion Conference*, Harbin, 2008.

[87] W. Hu, H. Nian and T. Zheng, "Torque Ripple Suppression Method With Reduced Switching Frequency for Open-Winding PMSM Drives With Common DC Bus," *IEEE Transactions on Industrial Electronics,* vol. 66, no. 1, pp. 674 - 684, 2019.

[88] A. D. kiadehi, K. E. K. Drissi and C. Pasquier, "Angular Modulation of Dual-Inverter Fed Open-End Motor for Electrical Vehicle Applications," *IEEE Transactions on Power Electronics ,* vol. 31, no. 4, pp. 2980 - 2990, 2015.

[89] Y. Liu, B. Zhou, H. Wang and S. Fang, "A new sliding mode control for Permanent Magnet Synchronous Motor drive system based on reaching law control," in *2009 4th IEEE Conference on Industrial Electronics and Applications*, Xi'an, 2009.

[90] R. Abebe, G. Vakil, G. L. Calzo, T. Cox, C. Gerada and M. Johnson, "FEA Based Thermal Analysis of Various Topologies for Integrated Motor Drives (IMD)," in *IECON2015-Yokohama*, 2015.

[91] J. Wolmarans, M. Gerber, H. Polinder, S. D. Haan, J. Ferreira and D. Clarenbach, "A 50KW integrated fault tolerant permanent magnet

machine and motor drive," *IEEE Power Electronics Specialists Conference 2008,* pp. 345-451, 2008.

[92] J.-X. Xu, S. K. Panda, Y.-J. Pan, T. H. Lee and B. H. Lam, "A Modular Control Scheme for PMSM Speed Control With Pulsating Torque Minimization," *IEEE Transactions on Industrial Electronics,* vol. 51, no. 3, pp. 526-536, 2004.

[93] S. M. Lambert, B. C. Mecrow, R. Abebe, G. Vakil and C. M. Johnson, "Integrated Drives for Transport - A Review of the Enabling Thermal Management Technology," in *2015 IEEE Vehicle Power and Propulsion Conference (VPPC)*, Montreal, 2015.

[94] P. Xie, G. Vakil and C. Gerada, "Electric drive systems with long feeder cables," *IET Electric Power Applications,* vol. 14, no. 1, pp. 16 - 30, 2020.

[95] P. Krause, O. Wasynczuk, S. Sudhoff and S. Pekarek, Analysis of Electric Machinery and Drive Systems, Hoboken: John Wiley & Sons Inc, 2013.

[96] A. Navarrete, J. Rivera, J. J. Raygoza and S. Ortega, "Discrete-Time Modeling and Control of PMSM," in *IEEE Electronics, Robotics and Automotive Mechanics Conference (CERMA)*, Cuernavaca, Morelos, 2011.

[97] G. L. Calzo, "Power GEnerating Unit for the Future More Electric Aircraft: Power Electroc Converter Modelling and Design," *Thesis,* p. 51, 2014.

[98] L. Rovere, A. Formentini, G. L. Calzo, P. Zanchetta and T. Cox, "Zero-Sequence Voltage Elimination for Dual-Fed Common DC-Link Open-End Winding PMSM High-Speed Starter–Generator—Part I:

Modulation," *IEEE Transactions on Industry Applications,* vol. 55, no. 6, pp. 7804 - 7812, 2019.

[99] L. Rovere, A. Formentini, G. L. Calzo, P. Zanchetta and T. Cox, "Zero-Sequence Voltage Elimination for Dual-Fed Common DC-Link Open-End Winding PMSM High-Speed Starter-Generator—Part II: Deadtime Hysteresis Control of Zero-Sequence Current," *IEEE Transactions on Industry Applications,* vol. 55, no. 6, pp. 7813 - 7821, 2019.

[100] S. Konaka, Y. Inoue, S. Morimoto and M. Sanada, "Comparative study of control characteristics in ultra-high-speed PMSM drives," in *IEEE 5th International Symposium on Sensorless Control for Electrical Drives* , Hiroshima, 2014.

[101] A. Galassini, G. L. Calzo, A. Formentini, C. Gerada, P. Zanchetta and A. Costabeber, "uCube: Control platform for power electronics," in *2017 IEEE Workshop on Electrical Machines Design, Control and Diagnosis (WEMDCD)*, Nottingham, 2017.

[102] T. Limited, "4-Quadrant starter/generator test rig," Torquemeters Limited, 2020. [Online]. Available: https://torquemeters.com/case-studies/4-quadrant-starter-generator-test-rig/. [Accessed 10 02 2020].

[103] B. Jin, Y. Shen and D. Wu, "Permanent magnet synchronous motor parameter identification with multi-innovation least squares," in *2016 IEEE 11th Conference on Industrial Electronics and Applications (ICIEA)*, Hefei, China, 2016.

[104] A. Lidozzi, G. L. Calzo, L. Solero and F. Crescimbini, "Multiple resonant controller with load-adaptive phase compensation

capabilities," in *IECON 2013 - 39th Annual Conference of the IEEE Industrial Electronics Society*, Vienna, Austria, 2013.

[105] M. Ciobotaru, R. Teodorescu and F. Blaabjerg, "A new single-phase PLL structure based on second order generalized integrator," in *2006 37th IEEE Power Electronics Specialists Conference*, Jeju, 2006.

[106] A. Accetta, M. Pucci, A. Lidozzi, L. Solero and F. Crescimbini, "Compensation of static end effects in linear induction motor drives by frequency-adaptive synchronous controllers," in *2014 International Conference on Electrical Machines (ICEM)*, Berlin, 2014 .

[107] R. H. PAUL PETER URONE, College Physics, Houston,: OpenStax, 2017.

[108] F. A. Wolff and J. H. Dellinger, "The electrical conductivity of commercial copper," *Proceedings of the American Institute of Electrical Engineers,* vol. 29, no. 12, pp. 1981-2008, 1910.

[109] A. P. Sandulescu, F. Meinguet, X. Kestelyn, E. Semail and A. Bruyere, "Flux-weakening operation of open-end winding drive integrating a cost-effective high-power charger," *IET Electrical Systems in Transportation,* vol. 3, no. 1, pp. 10 - 21, 2013.

[110] J. Li, N. Barrett, Y.-Q. Zhang and D. A. Washburn, "Genetic granular cognitive fuzzy neural networks and human brains for pattern recognition," *2005 IEEE International Conference on Granular Computing ,* vol. 1, pp. 172-175, 2005.

[111] J. A. Güemes, A. M. Iraolagoitia, J. I. D. Hoyo and P. Fernández, "Torque Analysis in Permanent-Magnet Synchronous Motors: A

Comparative Study," *IEEE Transactions on Energy Conversion,* vol. 26, no. 1, pp. 55-63, 2011.

[112] C. Fraeger, "Influence of voltage harmonics and cogging torque on speed deviations of servo drives with permanent magnet synchronous motors," in *Proceedings of IKMT 2015, ETG/GMM-Symposium Innovative small Drives and Micro-Motor Systems*, Cologne, Germany, 2015.

Appendix A – Special FFT Algorithm

FFTsim.m – an algorithm to perform FFT of a vector variable from a Matlab/Simulink simulation in a more convenient way.

Special features:

- Automatic resampling of the signal in case a signal has a variable sampling time in order to perform a perfect FFT
- Ability to choose the signal range dynamically in order to perform an FFT of its particular part.
- Designed specifically for the variables that are taken from Simulink using "to Workspace" block, however, can be easily adapted to any signal in a vector form.
- Ability to limit the sampling time of the signal before FFT is performed
- Indication of the phase of the frequency components

The code itself:

```
function [freqArray, amplArray] = FFTsim(time, signal)
%
% ========== FFT for simulink "to Workspace" variables v1.5
========
% Developer: Nick Hunter,
% Date last modified:
% 14/03/2016 - v1.3 - Peforms FFT on the zoomed in signal
% 27/07/2018 - v1.4 - Perform FFT on the data between two
cursors selected
% by the user.
% Function has two arguments: Time and Amplitude
% Output is the Frequency array and Amplitude array
% Example: [frequency, amplitude] = FFTsim(Time, Current)
% ***** VERY IMPORTANT INFORMATION *****
% This function is for the Simulink output "to Workspace",
hence, the input
% arrays must be the column vectors!!!
% Pick TWO ponts of the graph using DATA CURSOR tool to
perform FFT on a
% part of the graph between those two cursors and click
"Perform FFT"
% button
% **************************************
```

```
% === changing Column to Row vectors ===
time = time';
signal = signal';
% ======================================

% === Declaration of the output ===
freqArray = [];     % to avoid complaints if the Original
Figure was closed
amplArray = [];     % before the output variables were
declared
% =================================

OrigFig = figure;
plot(time,signal);
set(OrigFig,'Position',[376 266 1172 567]);
title('Entire Signal in Time Domain');
ylabel('Amplitude');
xlabel('Time, s');
grid on;
OrigAx = gca;

FigPos = OrigFig.Position;  % in pixels
AxPos = OrigAx.Position;    % normalized

% === Create GUI in the figure ===
DisY = 1/FigPos(4);
btnSize = [90 30]./[FigPos(3) FigPos(4)];   % pxls to
normalised
btnPos = [(1+AxPos(1)+AxPos(3)-btnSize(1))/2, AxPos(2)];

editSize = [90 20]./[FigPos(3) FigPos(4)];   % pxls to
normalised
editPos = [(1+AxPos(1)+AxPos(3)-btnSize(1))/2,
AxPos(2)+btnSize(2)+DisY*100];

textSize = [90 15]./[FigPos(3) FigPos(4)];   % pxls to
normalised
text2Pos = [(1+AxPos(1)+AxPos(3)-btnSize(1))/2,
editPos(2)+editSize(2)+DisY];
text1Pos = [(1+AxPos(1)+AxPos(3)-btnSize(1))/2,
text2Pos(2)+textSize(2)-DisY];

btn  = uicontrol('Parent',
OrigFig,'Style','togglebutton','Units','normalized','String','
Perform FFT','Position', [btnPos btnSize]);
text = uicontrol('Parent', OrigFig, 'Style',
'text','Units','normalized','String',num2str(2^ceil(log2(lengt
h(time)))),'Position', [editPos editSize]);
uicontrol('Parent', OrigFig, 'Style',
'text','Units','normalized','String','of Points for
FFT:','Position', [text2Pos textSize]);
```

```
uicontrol('Parent', OrigFig, 'Style',
'text','Units','normalized','String','Maximum
Number','Position', [text1Pos textSize]);
% =================================
a = 0; % for Changing Phase Zoom with Freq-Amplitude zoom

fftFig = [];

    while ishandle(OrigFig)

        % === Obtaining the t1 and t2 from the current view
===
        while (ishandle(OrigFig) && (btn.Value==0)) % loops
until the button is pressed


            % kXLim = get(OrigAx,'XLim'); %


            pause(0.05);

            if a ~= 0
                % === Changing Phase Zoom with Freq-Amplitude
zoom ===
                if ishandle(sub2)
                    if a~=sub2.XLim
                        sub3.XLim = sub2.XLim;
                    end
                    a = sub2.XLim;
                end
                %
====================================================
            end

        % if isempty(gcf)     % if the graph is not closed
        % FFTgetFreqInfo(gcf);
        % end

        end


        if ~ishandle(OrigFig)    % if the Original Figure with
the graph is closed
            return
        else

            % === Calculataing limits from the two cursors X
axis data ===
            k = getCursorInfo(datacursormode(OrigFig)); %
cursor info

            if k(1).Position(1) > k(2).Position(1)
```

```
                kXLim(1) = k(2).Position(1); % Second cursor
as XLim min value
                kXLim(2) = k(1).Position(1); % First cursor
XLim max value
            elseif k(1).Position(1) < k(2).Position(1)
                kXLim(1) = k(1).Position(1); % First cursor
XLim min value
                kXLim(2) = k(2).Position(1); % Second cursor
XLim max value
            else
                warning('Select TWO data points...');
                btn.Value=1;
            end
            %
============================================================
        end


        btn.Value=0; % reset the buttons value
        %
=====================================================

        % === Set time limits for FFT according to the input
===
        t1 = kXLim(1); % seconds
        t2 = kXLim(2); % seconds

        StartIndex = find(time==t1);
        EndIndex = find(time==t2);
        Range = StartIndex:EndIndex;

        % === Changing the signal to a new range ===
        timeA =
linspace(time(StartIndex),time(EndIndex),2^ceil(log2(length(Ra
nge)))); % New Time array of size 2^n elements
        signalA =
interp1(time(Range),signal(Range),timeA,'spline'); % new
signal of size 2^ceil(log2(length(range)))
        % ==========================================


        Fs = length(timeA)/(timeA(end)-timeA(1));  % sampling
frequency (non-linearity of time is ignored)

        fftFig = figure;
        set(fftFig,'Position',[285 161 1220 757]);
        subplot(311);
        plot(timeA,signalA)
        axis tight
        title('Time Domain','FontSize',13)
        ylabel('Amplitude')
        xlabel('Time, s')
        grid on;
```

```
        n = 2^nextpow2(length(timeA));
        dim = 2;     % operate along row; 1 - along column
        Y = fft(signalA,n,dim);

        P2 = abs(Y/n);        % two-sided spectrum
        P1 = P2(1:n/2+1);    % single-sided spectrum
        P1(2:end-1) = 2*P1(2:end-1);     % to get the actual
amplitude

        freqArray = 0:(Fs/n):(Fs/2-Fs/n);
        amplArray = P1(1:n/2);

        sub2 = subplot(312);
        bar(freqArray,amplArray)
        title('Frequency Domain','FontSize',13)
        ylabel('Amplitude')
        xlabel('Frequency, Hz')
        grid on;
        pause(0.25)


        sub3 = subplot(313);

        p = unwrap(angle(Y))*180/pi;      % Phase
        % f2 = (0:n-1)*(Fs/n);              % Frequency vector
for two-sided spectrum
        f = 0:(Fs/n):(Fs/2-Fs/n);         % Frequency vector
for two-sided spectrum

        plot(f,p(1:n/2))
        title('Phase','FontSize',13)
        ylabel('Phase, degrees')
        xlabel('Frequency, Hz')
        grid on;


        % figure;
        % plot(ifft(Y))
        % size(Y)
        % title('Freq - to - Time','FontSize',13)
        % ylabel('Amplitude')
        % xlabel('Time, s')
        % grid on;

        if ishandle(sub2)     % if the graph is not closed
            a = sub2.XLim;
        end
    end
end
```

Appendix B – OEW PMSM Model for Simulink simulation

```
function [ia, ib, ic, Wr, Theta, Wc, WcP,Teabc,Teabc1,
TeWc,TeWcP, TeABC,TeDQ,TeDQ0, PcQD0,PcABC,PfQD0,PfABC,PemQD0,
PemABC,PmTot,PmABC,PmQD0, LqOut,LdOut, E0, Eabc, Vm, Ym] =
OpenEndPMSM(TL,Va,Vb,Vc,dt, Rs, Ld, Lq, Lls, Ypm, Kpm3, J, B,
C, P, LdNonLin, LqNonLin, IqOrId, Ilim)
%#codegen
% Va, Vb, Vc - phase voltages
% ia,ib,ic - phase currents
% we - electrical angular velocity in rad/s
% the - electrical position in rad
% Ypm - emf constant due to the permanent magnet
% Kfem - amount of 3rd harmonic w.r.t. fundamental.
% Lls - leakage inductance
% Ls - motor inductance neglecting mutual leakage terms

persistent iabc;          % ABC currents
persistent we;            % Electrical frequency
persistent the;           % Angle in rad
persistent the_old;       % for differentiation of Energy Wc to
obtain Torque
persistent Ls_old;        % Old Ls for differentiation
persistent LqINT;         % interpolated NON linear value of Lq
persistent LdINT;         % interpolated NON linear value of Ld
persistent LqINT_old;     % Old value of Lq
persistent LdINT_old;     % Old value of Ld
persistent Lls_old;       % Old Value of Lo
persistent Wc_old;        % Energy
persistent WcP_old;       % Old Value of Energy derived from
Power


% === Initial conditions ===
if isempty(LqINT)
    LqINT = Lq;
end

if isempty(WcP_old)
    WcP_old = 0;
end

if isempty(LdINT)
    LdINT = Ld;
end

if isempty(LqINT_old)
```

```
    LqINT_old = Lq;
end

if isempty(LdINT_old)
    LdINT_old = Ld;
end

if isempty(Lls_old)
    Lls_old = Lls;
end

if isempty(iabc)
    iabc = [0; 0; 0];
end

if isempty(we)
    we = 200*2*pi;
end

if isempty(the)
    the = 0;
end

if isempty(the_old)
    the_old = 0;
end

flag = 0; % Flag to get rid of the spike in the beginning of
simulation
if isempty(Ls_old)
    flag = 1; % Flag to get rid of the spike in the beginning
of simulation
    Ls_old =zeros(3,3);
end

if isempty(Wc_old)
    Wc_old = 0;
end
% ==========================

% === Vector of the phase voltages ===
Vabc = [Va;
        Vb;
        Vc];
% ====================================


% === THIRD HARMONIC!!! =====
% ===========================
% === Back EMF fundamental + 3rd harmonic ===
Ym = Ypm*[sin(the)         + Kpm3*sin(3*the);...
          sin(the-2/3*pi)  + Kpm3*sin(3*(the-2/3*pi));...
          sin(the+2/3*pi)  + Kpm3*sin(3*(the+2/3*pi))];
```

```
% =========================================

% === Derivative of Back EMF fundamental + 3rd harmonic ===
pYm = Ypm*we*[cos(the)        + 3*Kpm3*cos(3*the);...
              cos(the-2/3*pi) + 3*Kpm3*cos(3*(the-2/3*pi));...
              cos(the+2/3*pi) + 3*Kpm3*cos(3*(the+2/3*pi))];
% =========================================================

% === LA and LB from Lq & Ld and Lls ===
LA = (LqINT+LdINT-2*Lls)/3;
LB = (LqINT-LdINT)/3;
% ======================================

% === Inductance matrix ===
Ls = [Lls+LA+LB*cos(2*the),        -1/2*LA+LB*cos(2*(the-
pi/3)),    -1/2*LA+LB*cos(2*(the+pi/3));...
     -1/2*LA+LB*cos(2*(the-pi/3)),  Lls+LA+LB*cos(2*(the-
2/3*pi)), -1/2*LA+LB*cos(2*(the+pi));...
     -1/2*LA+LB*cos(2*(the+pi/3)), -1/2*LA+LB*cos(2*(the+pi)),
Lls+LA+LB*cos(2*(the+2/3*pi))];
% =========================

% === Derivative of inductance matrix Ls if Lls, LA & LB are
constant ===
if flag == 1            % if at the initialisation cycle
pLs = zeros(3,3);       % force pLs to be ZERO
else                    % if not at the initialisation cycle
pLs = (Ls-Ls_old)/dt;   % calculate derivative
end

Ls_old = Ls;            % save old as new
%
==============================================================
=========

% === Resistance Matrix ===
rs = diag([Rs Rs Rs]);
% =========================

piabc = Ls\(Vabc-(rs+pLs)*iabc-pYm); % Ls\(Vabc-(rs+pLs)*iabc-
pYm);  % calculating the change of current

iabc = iabc+piabc*dt;   % Euler Approximation

% === Phase currents to output ===
ia = iabc(1);
ib = iabc(2);
ic = iabc(3);
% ================================

% === Torque equation ===
```

```
% === Energy Original eqn (Wc ==
1/2*iabc'*Ls*iabc+iabc'*Ym+Wpm) ===
Wc = (1/2*Ls*iabc+Ym)'*iabc; % ignorring the change in cogging
energy '+ Wpm' term
%
================================================================
====

% === Electrical Torque from the Energy equation ===
if (the-the_old == 0) || (Wc-Wc_old == 0)
  TeWc = 0;
else
  TeWc = P/2*(Wc-Wc_old)/(the-the_old);
end
Wc_old = Wc;
% ====================================================

% === Electrical Torque from the Power equation ===
WcP = (Vabc-Rs*iabc)'*iabc*dt+WcP_old;    % Energy derived
from Power

if (the-the_old == 0) || (WcP-WcP_old==0)
    TeWcP = 0;
else
  TeWcP = P/2*(WcP-WcP_old)/(the-the_old);
end
WcP_old = WcP;
% ===================================================

Lmq = 1.5*(LA-LB);
Lmd = 1.5*(LA+LB);

TeABC = (P/2)*((Lmd-Lmq)/3*((ia^2-1/2*ib^2-1/2*ic^2-ia*ib-
ia*ic+2*ib*ic)*sin(2*the)+sqrt(3)/2*(ib^2-ic^2-
2*ia*ib+2*ia*ic)*cos(2*the))+Ypm*((ia-1/2*ib-
1/2*ic)*cos(the)+sqrt(3)/2*(ib-ic)*sin(the)));

K = 2/3*[cos(the) cos(the-2/3*pi) cos(the+2/3*pi); sin(the)
sin(the-2/3*pi) sin(the+2/3*pi); 0.5 0.5 0.5];
% Kinv = [cos(the) sin(the) 1; cos(the-2/3*pi) sin(the-2/3*pi)
1; cos(the+2/3*pi) sin(the+2/3*pi) 1];
Iqd0 = K*iabc; % iq = Iqd0(1), id = Iqd0(2), i0 = Iqd0(3)
Vqd0 = K*Vabc; % Vq = Vabc(1), Vd = Vabc(2), V0 = Vabc(3)

TeDQ = (3/2)*(P/2)*(Ypm*Iqd0(1)+(LdINT-
LqINT)*Iqd0(1)*Iqd0(2));  % in DQ0 without i0.
TeDQ0 = 3/2*P/2*(Ypm*Iqd0(1)+(LdINT-
LqINT)*Iqd0(1)*Iqd0(2)+6*Ypm*Kpm3*Iqd0(3)*cos(3*the));
Teabc = (P/2)*norm(cross(iabc,Ym+Ls*iabc));
Teabc1 = (P/2)*norm(cross(iabc,Ym));
% ====================================================

% === Power Loss in the conductor ===
```

```
PcQD0 = 3/2*Rs*(Iqd0(1)^2+Iqd0(2)^2+2*Iqd0(3)^2); % same as
(Rs*iabc)'*iabc
PcABC = Vabc'*iabc - (pLs*iabc)'*iabc - (Ls*piabc)'*iabc -
pYm'*iabc;


% === Power due to the rate of change of the magnetic Fields
===
pLq = (LqINT - LqINT_old)/dt;
pLd = (LdINT - LdINT_old)/dt;
pL0 = (Lls - Lls_old)/dt;

LqINT_old = LqINT;
LdINT_old = LdINT;
Lls_old = Lls;

PfQD0 = 3/2*(pLq*Iqd0(1)^2+pLd*Iqd0(2)^2+2*pL0*Iqd0(3)^2);
PfABC = (pLs*iabc)'*iabc - (Ls*piabc)'*iabc;


% === Electromechanital Power ===
PemQD0 = 3/2*we*(Ypm*Iqd0(1)+(LdINT-
LqINT)*Iqd0(1)*Iqd0(2)+6*Ypm*Kpm3*Iqd0(3)*cos(3*the));
PemABC = Vabc'*iabc - PcABC;


% === Total Power ===
PmTot = PcQD0+PfQD0+PemQD0;                          % Total
power
PmQD0 = 3/2*(Vqd0'*(diag([1 1 2])*Iqd0)); % Total power in QD0
PmABC = Vabc'*iabc;                       % Total power in ABC
% ===================================


% === Mechanical system ===
pwe  = P/2*(TeDQ0-TL)/J-B/J*we; % -2/P*C/J*we^2;
we = we + pwe*dt;           % current value of electrical
speed
% =========================

the_old = the;  % storing the old value of theta

% === Integration of speed to obtain the position ===
the = the + we*dt;  % the new theta calcualted here
% ====================================================

% === Inductance LUT ===

% Limiting Inductance
if Iqd0(1) >Ilim
    Iq = Ilim;
elseif Iqd0(1) < -Ilim
    Iq = -Ilim;
```

```
else
    Iq = Iqd0(1);
end

if Iqd0(2) >Ilim
    Id = Ilim;
elseif Iqd0(2) < -Ilim
    Id = -Ilim;
else
    Id = Iqd0(2);
end

% === Non-linearity of inductance according to current ===
LqINT = interp1(IqOrId,LqNonLin,abs(Iq),'pchip');
LdINT = interp1(IqOrId,LdNonLin,abs(Id),'pchip');
% ========================================================

Theta = 2/P*the;     % Mechanical Angle goes to the output
Wr = 2/P*30/pi*we;   % Mechanical Speed goes to the output
[rpm]

LqOut = LqINT*1e-6;
LdOut = LdINT*1e-6;

% ====================
% === NEW ADDITION ===
% ====================


% === 3rd Harmonic BACK EMF ===
E0 = Ypm*we*[3*Kpm3*cos(3*the);...
              3*Kpm3*cos(3*(the-2/3*pi));...
              3*Kpm3*cos(3*(the+2/3*pi))];
% =========================================================

% === Fundamental BACK EMF ===
Eabc = Ypm*we*[cos(the);...
              cos(the-2/3*pi);...
              cos(the+2/3*pi)]+E0;
% ============================

% === VOLTAGE lost on resistive part ===
Vm = Vabc - Eabc;
% ======================================



% ====================
% ====================
% ====================
```

Appendix C - Sample Calculations

Torque quality improvement sample calculation for the first row of TABLE IV in chapter 5 on page 108:

$$Torque\ Quality\ Improvment = \frac{x_{NC} - x_C}{x_{NC}} \cdot 100\% \tag{C.1}$$

where, x_{NC} is the peak-to-peak torque ripple without the proposed method and x_C is the peak-to-peak torque ripple when the proposed method is applied.

$$Torque\ Quality\ Improvment = \frac{3.29 - 1.66}{3.29} \cdot 100\% = 49.5\% \tag{C.2}$$

Torque quality improvement sample calculation of the first row of TABLE V in chapter 5 on page 109.

$$MSE = \frac{1}{N}\sum_{k=1}^{N}(x_k - \hat{x}_k)^2 \tag{C.3}$$

where N is the number of data points, x_k is the observed values, and $\hat{x}_k$ is the predicted values.

$$MSE\ Improvment = \frac{0.65 - 0.09}{0.65} \cdot 100\% = 86\% \tag{C.4}$$

Appendix D - Power Loss Reduction Algorithm

```
% === Power Loss Reduction Algorithm ===
clear;
clc;

disp('Power Loss in Conductor Reduction Calculator');

% === Inputs ===
% === Motor parameters ===
Rs = 164e-3;             % Phase Resistance
L0 = 17.75e-6;           % Leakage inductance (less than 5% of
Lq||Ld)
Ypm = 0.07147648494;     % Permanent magnet fundamental flux
linkage
Kpm3 = 0.0114748014533; % PM 3rd harmonic flux linkage
coefficient
P = 6;                   % Number of poles
RatedSpeedRPM = 20000;   % Rated speed in RPM
% ========================

% === User's Operating Point ===
OperatingSpeedRPM = 17500;  % Mechanical rotor speed in RPM
LoadCurrent = 8.168;        % Load current iq
% ==============================

% === Other inputs ===
N = 11;                     % Number of speed values
FontSize = 15;              % Font size for the axes
MinValPerc = 0;             % Minimum value percentage (0-
100)%
% ====================

% === Defining fuctions ===
% === Get Zero-Sequence Back EMF and Current ===
getE0  = @(we,Ypm,Kpm3) 3*we*Ypm*Kpm3;
getI0  = @(rs,we,I0max,L0)
I0max*we./sqrt((rs/(3*L0)).^2+we.^2);
% ==============================================

% === Get Gamma, Active, Reactive and Total Power of Zero-
Sequence ===
getGamma = @(we,L0,rs) atand(3*we.*L0./rs);     % Angle in
degrees
getPe0  = @(I0,E0,Gamma) 3/2*I0.*E0.*cosd(Gamma);% Active Power
(I0 and E0 are peak values)
```

```
getQe0 = @(I0,E0,Gamma)3/2*I0.*E0.*sind(Gamma); % Reactive
Power (I0 and E0 are peak values)
getSe0 = @(I0,E0) 3/2*I0.*E0;                     % Total Power
(I0 and E0 are peak values)
%
===============================================================
======

% === Get Power Loss in Conductor Components ===
getPc0fromWE = @(rs,we,I0max,L0)
3/2*rs.*(I0max.^2).*(we.^2)./((rs/(3*L0)).^2+we.^2);
getPc0fromI0 = @(rs,I0) 3/2*rs.*I0.^2;
getPcQ = @(rs,iq) 3/2*rs.*iq.^2;
% ==============================================

% === Get Total Power Loss in Conductor ===
getPcFromQ0 = @(PcQ,Pc0) PcQ+Pc0;
getPcFromWE = @(we,iq,rs,I0max,L0)
3/2*rs.*(iq.^2+I0max^2*(we.^2)./((rs/3/L0).^2+we.^2));
% =========================================

% === Get Rs when the Power Loss in Conductor is Max/Min ===
getRsMaxLoss = @(we,iq,I0max,L0)
3*sqrt(2)/2*we.*L0./iq.*sqrt(I0max^2-I0max*sqrt(I0max^2-
8*iq.^2)-2*iq.^2);
getRsMinLoss = @(we,iq,I0max,L0)
3*sqrt(2)/2*we.*L0./iq.*sqrt(I0max^2+I0max*sqrt(I0max^2-
8*iq.^2)-2*iq.^2);
% ==========================================================

% === Get Max/Min Power in Conductor Loss according to we and
iq ===
getPcMaxLoss = @(we,iq,I0max,L0)
9*sqrt(2)/4*L0*we.*iq.*(3*I0max-sqrt(I0max^2-
8*iq.^2)).*sqrt(I0max^2-I0max*sqrt(I0max^2-8*iq.^2)-
2*iq.^2)./(I0max-sqrt(I0max^2-8*iq.^2));
getPcMinLoss = @(we,iq,I0max,L0)
9*sqrt(2)/4*L0*we.*iq.*(3*I0max+sqrt(I0max^2-
8*iq.^2)).*sqrt(I0max^2+I0max*sqrt(I0max^2-8*iq.^2)-
2*iq.^2)./(I0max+sqrt(I0max^2-8*iq.^2));
%
===============================================================
====

% === Relative Error ===
getRelativeError = @(Old,New) (Old-New)./Old*100;
% ======================

% === One of the solutions for operating point ===
getWeOP = @(iq,rs,I0max,L0)
sqrt(2)/3/L0*rs.*iq./sqrt(I0max^2+I0max*sqrt(I0max^2-8*iq.^2)-
2*iq.^2);
```

```
getIqOP = @(we,rs,I0max,L0) (3*I0max*L0*we.*sqrt((rs -
3*L0*we).*(rs + 3*L0*we)))./(9*L0^2*we.^2 + rs.^2);
% ================================================

% === One of the solutions for operating point ===
getWeOPAll1 = @(iq,rs,I0max,L0)
sqrt(2)/3/L0*rs.*iq./sqrt(I0max^2+I0max*sqrt(I0max^2-8*iq.^2)-
2*iq.^2);
getWeOPAll2 = @(iq,rs,I0max,L0)  sqrt(2)/24*rs./iq/L0.*(I0max
+ sqrt(I0max^2 - 8*iq.^2)).*sqrt(I0max^2 + I0max*sqrt(I0max^2
- 8*iq.^2)+4*iq.^2)./sqrt(I0max^2 + iq.^2);

getIqOPAll1 = @(we,rs,I0max,L0) (3*I0max*L0*we.*sqrt((rs -
3*L0*we).*(rs + 3*L0*we)))./(9*L0^2*we.^2 + rs.^2);
getIqOPAll2 = @(we,rs,I0max,L0) -sqrt(6)/2*I0max./rs.*(3*L0*we
- sqrt(9*L0^2*we.^2 + rs.^2)).*sqrt(L0*we.*(3*L0*we +
sqrt(9*L0^2*we.^2 + rs.^2))./(9*L0^2*we.^2 + rs.^2));

getWeOPAll = @(iq,rs,I0max,L0) [getWeOPAll1(iq,rs,I0max,L0),
getWeOPAll2(iq,rs,I0max,L0)];
getIqOPAll = @(we,rs,I0max,L0)
getIqOPAll1(we,rs,I0max,L0).*(we<=rs/3/sqrt(3)/L0)+getIqOPAll2
(we,rs,I0max,L0).*(we>rs/sqrt(3)/3/L0);
% ================================================
% =========================

% === Define Maximum paramenters ===
I0max = Ypm*Kpm3/L0;    % Maximum value of the Zero-Sequence
Current
IqMax = sqrt(2)/4*I0max;% Maximum value of iq to be eligible
for
% ==================================

% === Units conversion ===
RatedSpeedHz = RatedSpeedRPM/60*P/2;    % Rated Electrical
speed in rad
RatedSpeedRad = RatedSpeedHz*2*pi;       % Rated Electrical
speed in Hz

SpeedHz = OperatingSpeedRPM/60*P/2; % Electrical speed of
operation in Hz
SpeedRad = SpeedHz*2*pi;            % Electrical speed of
operation in rad

Iq = LoadCurrent;                   % Single value of load
current iq
% ========================

fprintf(2,'Operating load current must not exceed %.2f
A\n',IqMax);

if Iq>IqMax
```

```
    fprintf('Load current of %.2f A is higher than the maximum
allowed.\n',Iq);
    fprintf('Operating point cannot be considered for
reduction of Power Loss in Conductor!\n');
    L0Min = sqrt(2)/4*Ypm*Kpm3/Iq;  % Minimum L0 for the
reduction to take place
    fprintf('If you would like to work at this load current,
then L0 must be lower than %.1fuH\n',L0Min*1e6);

else
    fprintf('Load current of %.2f A is lower than the maximum
allowed.\n',Iq);
    fprintf('Operating point can be considered for reduction
of Power Loss in Conductor!\n');

    fprintf('Operating speed is %.0f RPM (%.2f Hz
electrical)\n',OperatingSpeedRPM, SpeedHz);

    % === Define the variables' range ===
    fe = linspace(RatedSpeedHz*MinValPerc/100,RatedSpeedHz,N);
% Range of electrical speeds in Hz

    we = fe*2*pi;                          % Range of electrical
speeds in rad


    % === Resistance Ranges for the points of interest ===
    rsMaxRange = getRsMaxLoss(we,Iq,I0max,L0);  % For Maximum
Power Loss
    rsMinRange = getRsMinLoss(we,Iq,I0max,L0);  % For Minimum
Power Loss
    % ====================================================

    % === Vectors of Resistance and iq Current values ===
    if Rs > rsMinRange(end)
        rs = [rsMaxRange,(2*rsMaxRange(end)-rsMaxRange(end-
1)):(rsMaxRange(end)-rsMaxRange(end-1)):(Rs+(rsMaxRange(end)-
rsMaxRange(end-1)))];
    else
        rs = [rsMaxRange,(2*rsMaxRange(end)-rsMaxRange(end-
1)):(rsMaxRange(end)-rsMaxRange(end-
1)):(rsMinRange(end)+(rsMaxRange(end)-rsMaxRange(end-1)))];
    end
    iq = linspace(IqMax*MinValPerc/100,IqMax,length(rs));
    % ===================================================
    % ===================================

    % === Converting vectors to matrices ===
    [RS,WE] = meshgrid(rs,we);
    [IQ,~] = meshgrid(iq,we);
    % ======================================

    % === Power Loss in Conductor Components ===
```

```
    PC0 = getPc0fromWE(RS,WE,I0max,L0); % due to i0
    PCQ = getPcQ(RS,Iq);                % due to iq
    PC = getPcFromQ0(PCQ,PC0);          % Total
    % ==========================================

    % === Maximum/Minimum Power Loss for line graph ===
    PcMax = getPcMaxLoss(we,Iq,I0max,L0);
    PcMin = getPcMinLoss(we,Iq,I0max,L0);
    % =================================================

    % === Calculate User's Operating Point ===
    PcPoint = getPcFromWE(SpeedRad,Iq,Rs,I0max,L0); % Power
Loss in Conductor at user's operational point
    PcMinPoint = getPcMinLoss(SpeedRad,Iq,I0max,L0);% Minimum
Power Loss at Operational Point
    % ========================================

    % === Power Loss in Cinductor Reduction Analysis at user's
operating point ===
    if PcPoint>PcMinPoint
        PercReduction = getRelativeError(PcPoint,PcMinPoint);
% Relative Power in Conductor Reduction
        RsMinLoss = getRsMinLoss(SpeedRad,Iq,I0max,L0); %
Resistance for Minimum Loss at user's speed
        RsIncreas = RsMinLoss - Rs;                     %
Resistance to be added to the existing

        fprintf('\n%.2f%% Reduction of Power Loss in Conductor
is possible.\n',PercReduction);

        if Rs>RsMinLoss
            fprintf('\nThe resistance is too high.\n');
            Msg = 'Reduction in';
        else
            fprintf('\nThe resistance is too low.\n')
            Msg = 'Additional';
        end

        fprintf('The resistance must be %.3f
Ohm.\n',RsMinLoss);
        fprintf('Current resistance value: %.3f Ohm.\n',Rs);
        fprintf('%s resistance required: %.3f
Ohm.\n',Msg,abs(RsIncreas));
    else
        fprintf('\nThe Power Loss in Conductor at this
operating point is minimal already.\n');
        fprintf('\nNo reduction of Power Loss in Conductor is
possible.\n');
    end
    %
==============================================================
==============
```

```
    % === Power Loss in Conductor Graph ===
    figure(1); clf;
    surf(RS,WE/2/pi,PC,'FaceAlpha',1)
    hold on;

plot3(rsMaxRange,fe,PcMax,'ok','LineWidth',2,'MarkerSize',15,'
MarkerFaceColor','r');% Maximum values of the power loss in
conductor due to ZSC

plot3(rsMinRange,fe,PcMin,'ok','LineWidth',2,'MarkerSize',15,'
MarkerFaceColor','g');% Maximum values of the power loss in
conductor due to ZSC

plot3(Rs,SpeedHz,PcPoint,'ok','LineWidth',2,'MarkerSize',15,'M
arkerFaceColor','m'); % Maximum values of the power loss in
conductor due to ZSC
    set(gca,'FontSize',FontSize*1.3)
    title('Total Power Loss in Conductor');
    xlabel('Resistance, (\Omega)');
    ylabel('Electrical Angular Speed, (Hz)');
    zlabel('Total Power Loss in Conductor, (W)');
    legend('P_{c}','P_{c max}','P_{c min}','P_{c o/p}');
%     legend('P_{c}','P_{c max}','P_{c min}')

    % =====================================


    % === Maximum/Minimum Power Loss for surface graph ===
    PCMax = getPcMaxLoss(WE,IQ,I0max,L0);    % PCMax according
to WE and IQ
    PCMin = getPcMinLoss(WE,IQ,I0max,L0);    % PCMin according
to WE and IQ
    % ====================================================


    % === Relative Maximum Power Loss Reduction 1D ===
    figure(2); clf;

    % === Max Values Only ===
    PcMax1Dmax = getPcMaxLoss(we(end),iq,I0max,L0);
    PcMin1Dmax = getPcMinLoss(we(end),iq,I0max,L0);
    PLRmaxPerc = getRelativeError(PcMax1Dmax,PcMin1Dmax);
    % =======================

    plot(iq,PLRmaxPerc,'g-','LineWidth',3);
    hold on;

plot(iq,PLRmaxPerc,'o','LineWidth',1,'MarkerSize',6,'MarkerFac
eColor','g','MarkerEdgeColor','k')
    set(gca,'FontSize',FontSize*1.3)
    title('Relative Maximum Power Loss in Conductor
Reduction');
    xlabel('Torque Producing Current, (A)');
```

```
    ylabel('Maximum Power Loss in Conductor Reduction, (%)');
    grid on;
    % ================================================

    % === Relative Power Loss Reduction 1D at constant speed
===
    figure(3); clf;
    % === Operation Point ===
    PcMax1D = getPcFromWE(SpeedRad,iq,Rs,I0max,L0);
    PcMin1D = getPcMinLoss(SpeedRad,iq,I0max,L0);
    PLRperc1D = getRelativeError(PcMax1D,PcMin1D);
    % =======================

    % === Zero point ===
    ZeroIqNewPoint = getIqOPAll(SpeedRad,Rs,I0max,L0);
    % ==================

    % === Operation Point ===
    PcMaxPoint1D = getPcFromWE(SpeedRad,Iq,Rs,I0max,L0);
    PcMinPoint1D = getPcMinLoss(SpeedRad,Iq,I0max,L0);
    PLRpointPerc1D =
getRelativeError(PcMaxPoint1D,PcMinPoint1D);
    % =======================

    pLine = plot(iq,PLRperc1D,'g-','LineWidth',3);
    hold on;

plot(iq,PLRperc1D,'o','LineWidth',1,'MarkerSize',6,'MarkerFace
Color','g','MarkerEdgeColor','k');
    pPoint =
plot(Iq,PLRpointPerc1D,'o','LineWidth',1,'MarkerSize',10,'Mark
erFaceColor','m','MarkerEdgeColor','k');
    pZero =
plot(ZeroIqNewPoint,zeros(1,length(ZeroIqNewPoint)),'o','LineW
idth',1,'MarkerSize',10,'MarkerFaceColor','r','MarkerEdgeColor
','k');
    set(gca,'FontSize',FontSize*1.3);
    title(sprintf('Potential Reduction of Power Loss in
Conductor @ f_{e} = %.2f Hz',SpeedHz));
    xlabel('Torque Producing Current, (A)');
    ylabel('Power Loss in Conductor Reduction, (%)');
    grid on;
    legend([pLine,pPoint,pZero],{sprintf('@ f_{e o/p} = %.2f
Hz',SpeedHz),sprintf('i_{q o/p} = %.2f A',Iq),'Min Power
Loss'});
    %
==========================================================

    % === Relative Power Loss Reduction 1D with constant iq
===
    figure(4); clf;

    % === Line Construction Point ===
```

```
    if N<500
        % === New vector we with 200 points for better
resolution ===
        weNew =
linspace(RatedSpeedHz*MinValPerc/100,RatedSpeedHz,500)*2*pi;
        %
===========================================================
    else
        weNew = we;
    end
    PcMax1DweNew = getPcFromWE(weNew,Iq,Rs,I0max,L0);
    PcMin1DweNew = getPcMinLoss(weNew,Iq,I0max,L0);
    PLRperc1DweNew =
getRelativeError(PcMax1DweNew,PcMin1DweNew);
    % ===============================

    % === Minimum point of the graph ===
    ZeroWeNewPoint = getWeOPAll(Iq,Rs,I0max,L0);
    ZeroWeNewPoint =
ZeroWeNewPoint(ZeroWeNewPoint<=RatedSpeedRad);
    % ==================================

    % === Points Construction ===
    PcMax1Dwe = getPcFromWE(we,Iq,Rs,I0max,L0);
    PcMin1Dwe = getPcMinLoss(we,Iq,I0max,L0);
    PLRperc1Dwe = getRelativeError(PcMax1Dwe,PcMin1Dwe);
    % ===========================

    % === Operation Point ===
    PcMaxPoint1D = getPcFromWE(SpeedRad,Iq,Rs,I0max,L0);
    PcMinPoint1D = getPcMinLoss(SpeedRad,Iq,I0max,L0);
    PLRpointPerc1D =
getRelativeError(PcMaxPoint1D,PcMinPoint1D);
    % =======================

    pLine = plot(weNew/2/pi,PLRperc1DweNew,'g-
','LineWidth',3);
    hold on;

plot(we/2/pi,PLRperc1Dwe,'o','LineWidth',1,'MarkerSize',6,'Mar
kerFaceColor','g','MarkerEdgeColor','k');
    pZero =
plot(ZeroWeNewPoint/2/pi,zeros(1,length(ZeroWeNewPoint)),'o','
LineWidth',1,'MarkerSize',10,'MarkerFaceColor','r','MarkerEdge
Color','k');
    pPoint =
plot(SpeedHz,PLRpointPerc1D,'o','LineWidth',1,'MarkerSize',10,
'MarkerFaceColor','m','MarkerEdgeColor','k');
    set(gca,'FontSize',FontSize*1.3);
    title(sprintf('Potential Reduction of Power Loss in
Conductor @ i_{q} = %.2f A',Iq));
    xlabel('Electrical Angular Speed, (Hz)');
    ylabel('Power Loss in Conductor Reduction, (%)');
```

```
    grid on;
    legend([pLine,pPoint,pZero],{sprintf('@ i_{q o/p} = %.2f
A',Iq),sprintf('f_{e o/p} = %.2f Hz',SpeedHz),'Min Power
Loss'});
    %
=========================================================


    % === Relative Reduction of Power Loss in Conductor ===
    figure(5); clf;

    PercImprv =
getRelativeError(getPcFromWE(WE,Iq,RS,I0max,L0),getPcMinLoss(W
E,Iq,I0max,L0));
    PercImprvMax =
getRelativeError(getPcMaxLoss(we,Iq,I0max,L0),getPcMinLoss(we,
Iq,I0max,L0));
    PercImprvMin =
getRelativeError(getPcMinLoss(we,Iq,I0max,L0),getPcMinLoss(we,
Iq,I0max,L0));
    PercImprvPoint =
getRelativeError(getPcFromWE(SpeedRad,Iq,Rs,I0max,L0),getPcMin
Loss(SpeedRad,Iq,I0max,L0));

    surf(RS,WE/2/pi,PercImprv)
    hold on;
    set(gca,'FontSize',FontSize)
    title('Relative Potential Reduction of Power Loss in
Conductor');
    xlabel('Resistance, (\Omega)');
    ylabel('Electrical Angular Speed, (Hz)');
    zlabel('Power Loss in Conductor Reduction, (%)');

plot3(rsMaxRange,fe,PercImprvMax,'ok','LineWidth',2,'MarkerSiz
e',15,'MarkerFaceColor','r'); % Maximum values of the power
loss in conductor due to ZSC

plot3(rsMinRange,fe,PercImprvMin,'ok','LineWidth',2,'MarkerSiz
e',15,'MarkerFaceColor','g'); % Maximum values of the power
loss in conductor due to ZSC

plot3(Rs,SpeedHz,PercImprvPoint,'ok','LineWidth',2,'MarkerSize
',15,'MarkerFaceColor','m'); % Maximum values of the power
loss in conductor due to ZSC
    legend('P_{c reduction}','P_{c max reduction}','P_{c min
reduction}','P_{c o/p reduction}')
    % =====================================================


    % === Active, Reactive and Total Power Graph ===
    figure(6); clf;

    % ============================================
```

```
    % === Get Gamma, Active, Reactive and Total Power of Zero-
Sequence ===
    E0 = getE0(WE,Ypm,Kpm3);     % Amplitude of third harmonic
back EMF
    I0 = getI0(RS,WE,I0max,L0); % Amplitude of Zero-Sequence
Current
    Gamma = getGamma(WE,L0,RS); % Phase shit of i0
    PE0 = getPe0(I0,E0,Gamma);  % Active power of zero-
sequence component
    QE0 = getQe0(I0,E0,Gamma);  % Reactive power of zero-
sequence component
    SE0 = getSe0(I0,E0);        % Total power of zero-sequence
component

    % === Construct operating point ===
    E0op = getE0(SpeedRad,Ypm,Kpm3);    % Amplitude of third
harmonic back EMF
    I0op = getI0(Rs,SpeedRad,I0max,L0);% Amplitude of Zero-
Sequence Current
    Gammaop = getGamma(SpeedRad,L0,Rs);% Phase shit of i0
    PE0op = getPe0(I0op,E0op,Gammaop);  % Active power of
zero-sequence component
    QE0op = getQe0(I0op,E0op,Gammaop);  % Reactive power of
zero-sequence component
    SE0op = getSe0(I0op,E0op);        % Total power of zero-
sequence component
    % =================================


surf(RS,WE/2/pi,PE0,'EdgeColor','k','FaceColor','k','FaceAlpha
',0.1);
    hold on;

surf(RS,WE/2/pi,QE0,'EdgeColor','g','FaceColor','g','FaceAlpha
',0.1);

surf(RS,WE/2/pi,SE0,'EdgeColor','r','FaceColor','r','FaceAlpha
',0.1);

plot3(Rs,SpeedHz,PE0op,'ok','LineWidth',3,'MarkerFaceColor','m
','MarkerSize',20)

plot3(Rs,SpeedHz,QE0op,'og','LineWidth',3,'MarkerFaceColor','m
','MarkerSize',20)

plot3(Rs,SpeedHz,SE0op,'or','LineWidth',3,'MarkerFaceColor','m
','MarkerSize',20)
    set(gca,'FontSize',FontSize*1.3)
    title('Power Loss due to Zero-Sequence Component');
    xlabel('Resistance, (\Omega)');
    ylabel('Electrical Angular Speed, (Hz)');
    zlabel('Power Loss, (VA,VAr,W)');
```

```
    grid on;
    legend('P_{0} - active power','Q_{0} - reactive
power','S_{0} - total power','P_{0 o/p} - active power','Q_{0
o/p} - reactive power','S_{0 o/p} - total
power','Location','NorthWest');
    % ==============================================

    % === OPERATING POINT SOLUTIONS ===
    % === Potential reduction of power loss fe domain ===
    figure(7); clf;

    % === Line Construction Point ===
    if N<10000
        % === New vector we with 200 points for better
resolution ===
        weNew =
linspace(RatedSpeedHz*MinValPerc/100,RatedSpeedHz,10000)*2*pi;
        %
===========================================================
    else
        weNew = we;
    end
    % ===============================

    % === Drawing lines according to the current value ===
    Leg = {};    % Initiation for the legend strings

    IqNew = linspace(1,IqMax,16);
    WeOPminLM = getWeOPAll1(IqNew,Rs,I0max,L0);
    WeOPminZC = getWeOPAll2(IqNew,Rs,I0max,L0);
    WeOPminZC = WeOPminZC(WeOPminZC > Rs/3/sqrt(3)/L0 &
WeOPminZC <= RatedSpeedRad);     % Limit to the
    for c = 1:length(IqNew)

        % === Calculated the lines ===
        PcMax1DweNew =
getPcFromWE(weNew,IqNew(c),Rs,I0max,L0);
        PcMin1DweNew = getPcMinLoss(weNew,IqNew(c),I0max,L0);
        PLRperc1DweNew =
getRelativeError(PcMax1DweNew,PcMin1DweNew);
        % ==============================

        pLine(c) =
plot(weNew/2/pi,PLRperc1DweNew,'LineWidth',3);
        hold on;
        set(gca,'FontSize',FontSize*1.3);
        title(sprintf('Power Loss in Conductor Reduction
Potential @ i_{q} = %.2f A',IqNew(c)));
        xlabel('Electrical Angular Speed, (Hz)');
        ylabel('Power Loss in Conductor Reduction, (%)');
        grid on;
        Leg{end+1} = sprintf('i_{q} = %.2f A',IqNew(c));
```

```
    end
    pLM =
plot(WeOPminLM/2/pi,zeros(1,length(WeOPminLM)),'o','LineWidth'
,1,'MarkerSize',10,'MarkerFaceColor','r','MarkerEdgeColor','k'
);     % Local Minimum
    pZC =
plot(WeOPminZC/2/pi,zeros(1,length(WeOPminZC)),'o','LineWidth'
,1,'MarkerSize',10,'MarkerFaceColor','b','MarkerEdgeColor','k'
);     % Zero Crossing
    legend([pLine,pLM,pZC],[Leg,'Local minimum','Zero
crossing'],'NumColumns',2);
    % ====================================================


    % === All Operating Points for Minimum Power Loss in
Conductor at original Rs ===
    figure(8); clf;

    % === The line itself ===
    weOP = linspace(0,RatedSpeedRad,1000);   % New range for we
operating point
    iqOPAll = getIqOPAll(weOP,Rs,I0max,L0); % New range for iq
operating point
    % =======================

    % === Two in one piecewise funstions ===
    iqOPAll1 = getIqOPAll1(weOP,Rs,I0max,L0); % we(1)
    iqOPAll2 = getIqOPAll2(weOP,Rs,I0max,L0); % we(2)
    iqOPAll1 = iqOPAll1(weOP<=Rs/3/sqrt(3)/L0); % Clipping
    iqOPAll2 = iqOPAll2(weOP>Rs/3/sqrt(3)/L0); % Clipping
    weOP1 = weOP(weOP<=Rs/3/sqrt(3)/L0);
    weOP2 = weOP(weOP>Rs/3/sqrt(3)/L0);
    % ======================================

    % === Just points on the top ===
    weOPp = linspace(0,RatedSpeedRad,21);   % Range for we for
10 points only
    iqOPpAll = getIqOPAll(weOPp,Rs,I0max,L0);  % Range for iq
for 10 points only
    % ==============================

    pLine = plot(weOP/2/pi,iqOPAll,'g-','LineWidth',3);
    hold on;

plot(weOPp/2/pi,iqOPpAll,'o','LineWidth',1,'MarkerSize',6,'Mar
kerFaceColor','g','MarkerEdgeColor','k');
    pPoint =
plot(SpeedHz,Iq,'o','LineWidth',1,'MarkerSize',10,'MarkerFaceC
olor','m','MarkerEdgeColor','k');
    set(gca,'FontSize',FontSize*1.3);
    title(sprintf('All Operating Points for Minimum Power Loss
in Conductor @ r_{s} = %.3f \\Omega',Rs));
    xlabel('Electrical Angular Speed, (Hz)');
```

```
    ylabel('Torque Producing Current, (A)');
    grid on;
    legend([pLine,pPoint],'Min Power Loss O/Ps','Current
O/P','Location','southeast');
    %
===============================================================
=================

    % === All Operating Points for Minimum Power Loss in
Conductor at the suggested Rs ===
    figure(9); clf;

    % === The line itself ===
    weOP = linspace(0,RatedSpeedRad,1000);  % New range for we
operating point
    iqOPAll =
getIqOPAll(weOP,getRsMinLoss(SpeedRad,Iq,I0max,L0),I0max,L0);
% New range for iq operating point
    % ======================

    % === Just points on the top ===
    weOPp = linspace(0,RatedSpeedRad,11);   % Range for we for
10 points only
    iqOPpAll =
getIqOPAll(weOPp,getRsMinLoss(SpeedRad,Iq,I0max,L0),I0max,L0);
% Range for iq for 10 points only
    % ==============================

    pLine = plot(weOP/2/pi,iqOPAll,'g-','LineWidth',3);
    hold on;

plot(weOPp/2/pi,iqOPpAll,'o','LineWidth',1,'MarkerSize',6,'Mar
kerFaceColor','g','MarkerEdgeColor','k');
    pPoint =
plot(SpeedHz,Iq,'o','LineWidth',1,'MarkerSize',10,'MarkerFaceC
olor','m','MarkerEdgeColor','k');
    set(gca,'FontSize',FontSize*1.3);
    title(sprintf('All Operating Points for Minimum Power Loss
in Conductor @ r_{s} = %.3f
\\Omega',getRsMinLoss(SpeedRad,Iq,I0max,L0)));
    xlabel('Electrical Angular Speed, (Hz)');
    ylabel('Torque Producing Current, (A)');
    grid on;
    legend([pLine,pPoint],'Min Power Loss O/Ps','Current
O/P','Location','southeast');
    %
===============================================================
=================


end % end of the load current checking statement
```

Appendix E - Power Loss Reduction App

```
classdef PowerLossRedApp < matlab.apps.AppBase

    % Properties that correspond to app components
    properties (Access = public)
        UIFigure                     matlab.ui.Figure
        CurrentSlider                matlab.ui.control.Slider
        iqLabel                      matlab.ui.control.Label
        wOPLabel                     matlab.ui.control.Label
        SpeedSlider                  matlab.ui.control.Slider
        LampLabel                    matlab.ui.control.Label
        Lamp                         matlab.ui.control.Lamp
        TabGroup
matlab.ui.container.TabGroup
        InputsTab                    matlab.ui.container.Tab
        PhaseResistanceField
matlab.ui.control.NumericEditField
        LeakageInductanceEditField_2Label
matlab.ui.control.Label
        LeakageInductanceField
matlab.ui.control.NumericEditField
        FluxLinkageEditField_2Label  matlab.ui.control.Label
        FluxLinkageField
matlab.ui.control.NumericEditField
        rdHarmonicFluxcoeffEditField_2Label
matlab.ui.control.Label
        ZeroSequenceFluxCoeffField
matlab.ui.control.NumericEditField
        NumberofPolesPLabel          matlab.ui.control.Label
        NumberofPolesField
matlab.ui.control.NumericEditField
        RatedSpeedEditField_2Label   matlab.ui.control.Label
        RatedSpeedField
matlab.ui.control.NumericEditField
        PhaseResistanceUnit          matlab.ui.control.Label
        LeakageInductanceUnit        matlab.ui.control.Label
        FluxLinkageUnit              matlab.ui.control.Label
        RatedSpeedUnit               matlab.ui.control.Label
        PhaseResistanceEditField_2Label
matlab.ui.control.Label
        AdditionalInputsTab          matlab.ui.container.Tab
        OperatingPointInputPanel     matlab.ui.container.Panel
        SpeedOPField
matlab.ui.control.NumericEditField
        SpeedLabel                   matlab.ui.control.Label
        SpeedOPUnit                  matlab.ui.control.Label
        QuadratureCurrentOPField
matlab.ui.control.NumericEditField
```

```
        QuadratureAxisCurrentLabel   matlab.ui.control.Label
        QuadratureCurrentOPUnit      matlab.ui.control.Label
        PowerLossinConductorReductionCalculatorLabel
matlab.ui.control.Label
        OperatingloadcurrentmustnotexceedLabel
matlab.ui.control.Label
        LoadCurrentMaxValueLabel     matlab.ui.control.Label
        Output                       matlab.ui.control.Label
        TotalPowerLossAxes           matlab.ui.control.UIAxes
        CurrentVsReductionAxes       matlab.ui.control.UIAxes
        PredictedBestOPAxes          matlab.ui.control.UIAxes
        SpeedVsReductionAxes         matlab.ui.control.UIAxes
        CurrentBestOPAxes            matlab.ui.control.UIAxes
        ViewSwitchLabel              matlab.ui.control.Label
        ViewSwitch
matlab.ui.control.RockerSwitch
    end

    methods (Access = public)

        function DoCalculations(app)

            OutputText = {};    % Cell for the output string

            % === Motor parameters ===
            Rs = app.PhaseResistanceField.Value;         %
Phase Resistance
            L0 = app.LeakageInductanceField.Value;       %
Leakage inductance (less than 5% of Lq||Ld)
            Ypm = app.FluxLinkageField.Value;            %
Permanent magnet fundamental flux linkage
            Kpm3 = app.ZeroSequenceFluxCoeffField.Value; % PM
3rd harmonic flux linkage coefficient
            P = app.NumberofPolesField.Value;            %
Number of poles
            RatedSpeedRPM = app.RatedSpeedField.Value;   %
Rated speed in RPM
            % ========================

            % === Working out the units ===
            [RsLabel, RsUnit] = UnitChanger(app,Rs,
char(937));
            % =============================

            % === User's Operating Point ===
            OperatingSpeedRPM = app.SpeedOPField.Value;
% Mechanical rotor speed in RPM
            LoadCurrent = app.QuadratureCurrentOPField.Value;
% Load current iq
            N = 11;                          % Number of speed
values
            MinValPerc = 0;                  % Minimum value
percentage (0-100)%
```

```
            % ==============================


            % === Defining functions ===
            % === Get Zero-Sequence Back EMF and Current ===
            getE0 = @(we,Ypm,Kpm3) 3*we*Ypm*Kpm3;
            getI0 = @(rs,we,I0max,L0)
I0max*we./sqrt((rs/(3*L0)).^2+we.^2);
            % ==============================================

            % === Get Gamma, Active, Reactive and Total Power
of Zero-Sequence ===
            getGamma = @(we,L0,rs) atand(3*we.*L0./rs);     %
Angle in degrees
            getPe0 = @(I0,E0,Gamma) 3/2*I0.*E0.*cosd(Gamma);%
Active Power (I0 and E0 are peak values)
            getQe0 = @(I0,E0,Gamma)3/2*I0.*E0.*sind(Gamma); %
Reactive Power (I0 and E0 are peak values)
            getSe0 = @(I0,E0) 3/2*I0.*E0;                   %
Total Power (I0 and E0 are peak values)
            %
==============================================================
======

            % === Get Power Loss in Conductor Components ===
            getPc0fromWE = @(rs,we,I0max,L0)
3/2*rs.*(I0max.^2).*(we.^2)./((rs/(3*L0)).^2+we.^2);
            getPc0fromI0 = @(rs,I0) 3/2*rs.*I0.^2;
            getPcQ = @(rs,iq) 3/2*rs.*iq.^2;
            % ==============================================

            % === Get Total Power Loss in Conductor ===
            getPcFromQ0 = @(PcQ,Pc0) PcQ+Pc0;
            getPcFromWE = @(we,iq,rs,I0max,L0)
3/2*rs.*(iq.^2+I0max^2*(we.^2)./((rs/3/L0).^2+we.^2));
            % =========================================

            % === Get Rs when the Power Loss in Conductor is
Max/Min ===
            getRsMaxLoss = @(we,iq,I0max,L0)
3*sqrt(2)/2*we.*L0./iq.*sqrt(I0max^2-I0max*sqrt(I0max^2-
8*iq.^2)-2*iq.^2);
            getRsMinLoss = @(we,iq,I0max,L0)
3*sqrt(2)/2*we.*L0./iq.*sqrt(I0max^2+I0max*sqrt(I0max^2-
8*iq.^2)-2*iq.^2);
            %
==========================================================

            % === Get Max/Min Power in Conductor Loss
according to we and iq ===
            getPcMaxLoss = @(we,iq,I0max,L0)
9*sqrt(2)/4*L0*we.*iq.*(3*I0max-sqrt(I0max^2-
```

```
8*iq.^2)).*sqrt(I0max^2-I0max*sqrt(I0max^2-8*iq.^2)-
2*iq.^2)./(I0max-sqrt(I0max^2-8*iq.^2));
            getPcMinLoss = @(we,iq,I0max,L0)
9*sqrt(2)/4*L0*we.*iq.*(3*I0max+sqrt(I0max^2-
8*iq.^2)).*sqrt(I0max^2+I0max*sqrt(I0max^2-8*iq.^2)-
2*iq.^2)./(I0max+sqrt(I0max^2-8*iq.^2));
            %
==============================================================
====

            % === Relative Error ===
            getRelativeError = @(Old,New) (Old-New)./Old*100;
            % ======================

            % === One of the solutions for operating point ===
            getWeOP = @(iq,rs,I0max,L0)
2/3/sqrt(2)/L0*rs.*iq./sqrt(I0max^2+I0max*sqrt(I0max^2-
8*iq.^2)-2*iq.^2);
            getIqOP = @(we,rs,I0max,L0)
(3*I0max*L0*we.*sqrt((rs - 3*L0*we).*(rs +
3*L0*we)))./(9*L0^2*we.^2 + rs.^2);
            % ================================================

            % === Minimum power loss loss Operating points (we
domain) ===
            getIqOPAll1 = @(we,rs,I0max,L0)
(3*I0max*L0*we.*sqrt((rs - 3*L0*we).*(rs +
3*L0*we)))./(9*L0^2*we.^2 + rs.^2);
            getIqOPAll2 = @(we,rs,I0max,L0) -
sqrt(6)/2*I0max./rs.*(3*L0*we - sqrt(9*L0^2*we.^2 +
rs.^2)).*sqrt(L0*we.*(3*L0*we + sqrt(9*L0^2*we.^2 +
rs.^2))./(9*L0^2*we.^2 + rs.^2));

            getIqOPAll = @(we,rs,I0max,L0)
getIqOPAll1(we,rs,I0max,L0).*(we<=rs/3/sqrt(3)/L0)+getIqOPAll2
(we,rs,I0max,L0).*(we>rs/sqrt(3)/3/L0);
            %
============================================================

            % === Minimum power loss Operating points (iq
domain) ===
            getWeOPAll1 = @(iq,rs,I0max,L0)
sqrt(2)/3/L0*rs.*iq./sqrt(I0max^2+I0max*sqrt(I0max^2-8*iq.^2)-
2*iq.^2);
            getWeOPAll2 = @(iq,rs,I0max,L0)
sqrt(2)/24*rs./iq/L0.*(I0max + sqrt(I0max^2 -
8*iq.^2)).*sqrt(I0max^2 + I0max*sqrt(I0max^2 -
8*iq.^2)+4*iq.^2)./sqrt(I0max^2 + iq.^2);

            getWeOPAll = @(iq,rs,I0max,L0)
[getWeOPAll1(iq,rs,I0max,L0), getWeOPAll2(iq,rs,I0max,L0)];
            %
=======================================================
```

```
            % ========================


            % === Define Maximum paramenters ===
            I0max = Ypm*Kpm3/L0;    % Maximum value of the
Zero-Sequence Current
            IqMax = sqrt(2)/4*I0max;% Maximum value of iq to
be eligible for
            % ==================================


            % === Units conversion ===
            RatedSpeedHz = RatedSpeedRPM/60*P/2;   % Rated
Electrical speed in rad
            RatedSpeedRad = RatedSpeedHz*2*pi;      % Rated
Electrical speed in Hz

            SpeedHz = OperatingSpeedRPM/60*P/2; % Electrical
speed of operation in Hz
            SpeedRad = SpeedHz*2*pi;            % Electrical
speed of operation in rad

            Iq = LoadCurrent;                   % Single value
of load current iq
            % ========================


            % === Speed Slider Setup ===
            app.SpeedSlider.Limits = [0, RatedSpeedRPM];  %
Set the Limits to Rated Speed in Hz
            app.SpeedSlider.Value = OperatingSpeedRPM;    %
Set Speed Operating Point in Hz
            % ==========================

            % === Setting up Speed Slider's Ticks ===
            if app.SpeedSlider.MajorTicks(end)~=RatedSpeedRPM
% if the ticks are still old

                app.SpeedSlider.MajorTicks =
linspace(0,RatedSpeedRPM,11);  % Change the Major Ticks'
values
                app.SpeedSlider.MinorTicks =
linspace(0,RatedSpeedRPM,51);  % Change the Minor Ticks'
values

                for i =
1:length(app.SpeedSlider.MajorTickLabels)
                    [MajorTicksLabel, MajorTicksUnit] =
UnitChanger(app,app.SpeedSlider.MajorTicks(i), ''); % Change
units if necessary
                    app.SpeedSlider.MajorTickLabels{i} =
sprintf('%.1f%s',MajorTicksLabel, MajorTicksUnit);  % Create
new Major Tick Labels
```

```
                end

            end
            %
==================================================



            % === Maximum Iq string for the output ===
            app.OperatingloadcurrentmustnotexceedLabel.Visible
= 'on'; % Turn on the visibility
            app.LoadCurrentMaxValueLabel.Visible = 'on';
% Turn on the visibility

            [IqMaxLabel, IqMaxUnit] = UnitChanger(app,IqMax,
'A');        % Change units if needed
            app.LoadCurrentMaxValueLabel.Text = sprintf('%.2f
%s',IqMaxLabel,IqMaxUnit); % Output the value
            % ========================================

            % === Obtaining Units for the Operating Current
Value ===
            [IqLabel, IqUnit] = UnitChanger(app,Iq, 'A');
            %
========================================================


            if Iq>IqMax

             % === Clearing all of the axes ===
             cla(app.TotalPowerLossAxes);      % Clear axes
             cla(app.SpeedVsReductionAxes);    % Clear axes
             cla(app.CurrentVsReductionAxes);  % Clear axes
             cla(app.CurrentBestOPAxes);       % Clear axes
             cla(app.PredictedBestOPAxes);     % Clear axes
             % ================================


                % === Set the Lamp signal to red with the
correspondig error message ===
                app.LampLabel.FontColor = 'r';   % Text of a
red colour
                app.Lamp.Color = 'r';            % Turn lamp
red
                app.LampLabel.Text = {'ERROR: The value of the
Maximum Current must be';...
                                       'greater than the
current of the operating point.'};
                %
==============================================================
========
```

```
                OutputText{end+1} = sprintf('Load current of
%.2f %s is higher than the maximum
allowed.\n',IqLabel,IqUnit);
                OutputText{end+1} = sprintf('Operating point
cannot be considered for reduction of Power Loss!\n');
                L0Min = sqrt(2)/4*Ypm*Kpm3/Iq;   % Minimum L0
for the reduction to take place
                [L0MinLabel, L0MinUnit] =
UnitChanger(app,L0Min, 'H');
                OutputText{end+1} = sprintf('This operating
point would be subjected to the reduction\nof Power Loss in
Conductor if the leakage inductance\nwould have been less than
%.2f %s, (%s < %.2f
%s).',L0MinLabel,L0MinUnit,[char(76),char(8320)],L0MinLabel,L0
MinUnit);
            else
                % === Current Slider Setup ===
                app.CurrentSlider.Limits = [0, IqMax];   % Set
the Limits to Rated Speed in Hz
                app.CurrentSlider.Value = Iq;          % Set
Speed Operating Point in Hz
                % ============================

                % === Setting up Current Slider's Ticks ===
                if app.CurrentSlider.MajorTicks(end)~=IqMax %
if the ticks are still old

                    app.CurrentSlider.MajorTicks =
linspace(0,IqMax,11);  % Change the Major Ticks' values
                    app.CurrentSlider.MinorTicks =
linspace(0,IqMax,51);  % Change the Minor Ticks' values

                    for i =
1:length(app.CurrentSlider.MajorTickLabels)
                        [MajorTicksLabel, MajorTicksUnit] =
UnitChanger(app,app.CurrentSlider.MajorTicks(i), ''); % Change
units if necessary
                        app.CurrentSlider.MajorTickLabels{i} =
sprintf('%.1f%s',MajorTicksLabel, MajorTicksUnit);  % Create
new Major Tick Labels
                    end

                end
                %
=================================================

                OutputText{end+1} = sprintf('Load current of
%.2f %s is lower than the maximum allowed.\n',IqLabel,IqUnit);
                OutputText{end+1} = sprintf('Operating point
can be considered for reduction of Power Loss!\n');
```

```
                OutputText{end+1} = sprintf('Operating speed
is %.0f RPM (%.2f Hz electrical)\n',OperatingSpeedRPM,
SpeedHz);


                % === Calculate User's Operating Point ===
                PcPoint =
getPcFromWE(SpeedRad,Iq,Rs,I0max,L0); % Power Loss in
Conductor at user's operational point
                PcMinPoint =
getPcMinLoss(SpeedRad,Iq,I0max,L0);% Minimum Power Loss at
Operational Point
                % =======================================

                % === Power Loss in Cinductor Reduction
Analysis at user's operating point ===
                if PcPoint>PcMinPoint
                    PercReduction =
getRelativeError(PcPoint,PcMinPoint); % Relative Power in
Conductor Reduction
                    RsMinLoss =
getRsMinLoss(SpeedRad,Iq,I0max,L0); % Resistance for Minimum
Loss at user's speed
                    RsIncreas = RsMinLoss - Rs;
% Resistance to be added to the existing

                    OutputText{end+1} = sprintf('\n%.2f%%
reduction of Power Loss in Conductor is
possible.\n',PercReduction);

                    if Rs>RsMinLoss
                        OutputText{end+1} = sprintf('The
resistance is too high.\n');
                        Msg = 'Reduction in';
                    else
                        OutputText{end+1} = sprintf('The
resistance is too low.\n');
                        Msg = 'Additional';
                    end

                    % === Working out the units ===
                    [RsMinLossLabel, RsMinLossUnit] =
UnitChanger(app,RsMinLoss, char(937));
                    [absRsIncreasLabel, absRsIncreasUnit] =
UnitChanger(app,abs(RsIncreas), char(937));
                    % =============================

                    OutputText{end+1} = sprintf('The
resistance must be %.2f %s.',RsMinLossLabel, RsMinLossUnit);
                    OutputText{end+1} = sprintf('Current
resistance value: %.2f %s.',RsLabel, RsUnit);
                    OutputText{end+1} = sprintf('%s resistance
required: %.2f %s.',Msg,absRsIncreasLabel, absRsIncreasUnit);
```

```
                else
                    OutputText{end+1} = sprintf('\nThe Power
Loss in Conductor at this operating point is minimal
already.\n');
                    OutputText{end+1} = sprintf('No reduction
of Power Loss in Conductor is possible.');
                end
                %
==============================================================
==============


                % === Define the variables' range ===
                fe =
linspace(RatedSpeedHz*MinValPerc/100,RatedSpeedHz,N);    %
Range of electrical speeds in Hz

                we = fe*2*pi;                          % Range of
electrical speeds in rad


                % === Resistance Ranges for the points of
interest ===
                rsMaxRange = getRsMaxLoss(we,Iq,I0max,L0);  %
For Maximum Power Loss
                rsMinRange = getRsMinLoss(we,Iq,I0max,L0);  %
For Minimum Power Loss
                %
====================================================

                % === Vectors of Resistance and iq Current
values ===
                if Rs > rsMinRange(end)
                    rs = [rsMaxRange,(2*rsMaxRange(end)-
rsMaxRange(end-1)):(rsMinRange(end)-rsMinRange(end-
1)):(Rs+(rsMinRange(end)-rsMinRange(end-1)))];
                else
                    rs = [rsMaxRange,(2*rsMaxRange(end)-
rsMaxRange(end-1)):(rsMaxRange(end)-rsMaxRange(end-
1)):(rsMinRange(end)+(rsMaxRange(end)-rsMaxRange(end-1)))];
                end
                iq =
linspace(IqMax*MinValPerc/100,IqMax,length(rs));      % Vector
of iq of the lame length as Resistance
                %
===================================================
                % =====================================

                % === Converting vectors to matrices ===
                [RS,WE] = meshgrid(rs,we);
                [IQ,~] = meshgrid(iq,we);
                % ========================================
```

```
                % === Power Loss in Conductor Components ===
                PC0 = getPc0fromWE(RS,WE,I0max,L0); % due to
i0
                PCQ = getPcQ(RS,Iq);                % due to
iq
                PC = getPcFromQ0(PCQ,PC0);          % Total
                % =========================================

                % === Maximum/Minimum Power Loss for line
graph ===
                PcMax = getPcMaxLoss(we,Iq,I0max,L0);
                PcMin = getPcMinLoss(we,Iq,I0max,L0);
                %
=================================================

                % === Determine the state of the View Switch
===
                if strcmp(app.ViewSwitch.Value,'3D')
                    Mltplr = 1;
                else
                    Mltplr = 0;
                end
                %
==============================================

                % === Total Power Loss in Conductor Graph ===
                cla(app.TotalPowerLossAxes);          % Clear
axes before using
                surf(app.TotalPowerLossAxes,RS,WE/pi*60/P,PC);
% (RS and WErpm) vs PC
                hold(app.TotalPowerLossAxes,'on');

plot3(app.TotalPowerLossAxes,rsMaxRange,fe*120/P*Mltplr,PcMax,
'ok','LineWidth',2,'MarkerSize',15,'MarkerFaceColor','r'); %
Maximum values of the power loss in conductor due to ZSC

plot3(app.TotalPowerLossAxes,rsMinRange,fe*120/P*Mltplr,PcMin,
'ok','LineWidth',2,'MarkerSize',15,'MarkerFaceColor','g'); %
Maximum values of the power loss in conductor due to ZSC

plot3(app.TotalPowerLossAxes,Rs,OperatingSpeedRPM*Mltplr,PcPoi
nt,'ok','LineWidth',2,'MarkerSize',15,'MarkerFaceColor','m');
% Maximum values of the power loss in conductor due to ZSC
                legend(app.TotalPowerLossAxes,'P_{c}','P_{c
max}','P_{c min}','P_{c o/p}');
                grid(app.TotalPowerLossAxes,'on');
                % ============================================

                % === Setting 3D (1) or 2D (0) view ===
                if Mltplr
                    view(app.TotalPowerLossAxes,-26.3645,
20.7297); % Best chosen view
                else
```

```
                    view(app.TotalPowerLossAxes,0,0);
% Power vs Resistance
                end
                % =====================================


                % === Operation Point Percentage ===
                PLRpointPerc1D =
getRelativeError(PcPoint,PcMinPoint);
                % ==================================


                % === Relative Power Loss Reduction 1D with
constant iq ===

                % === Line Construction Point ===
                if N<500
                    % === New vector we with 200 points for
better resolution ===
                    weNew =
linspace(RatedSpeedRad*MinValPerc/100,RatedSpeedRad,500);
                    %
===========================================================
                else
                    weNew = we;
                end
                Pc1DweNew = getPcFromWE(weNew,Iq,Rs,I0max,L0);
                PcMin1DweNew =
getPcMinLoss(weNew,Iq,I0max,L0);
                PLRperc1DweNew =
getRelativeError(Pc1DweNew,PcMin1DweNew);
                % ===============================

                % === Zero point of the graph ===
                ZeroweNew =  getWeOPAll(Iq,Rs,I0max,L0);
                ZeroweNew =
ZeroweNew(ZeroweNew<=RatedSpeedRad);
                % ===============================

                % === Points Construction ===
                WeNew =
linspace(RatedSpeedRad*MinValPerc/100,RatedSpeedRad,10);
                Pc1Dwe = getPcFromWE(WeNew,Iq,Rs,I0max,L0);
                PcMin1Dwe = getPcMinLoss(WeNew,Iq,I0max,L0);
                PLRperc1Dwe =
getRelativeError(Pc1Dwe,PcMin1Dwe);
                % ===========================

                % === Change of Units ===
                [NewIqValue, NewIqUnit] = UnitChanger(app, Iq,
'A');
```

```
                [NewOperatingSpeedValue,
NewOperatingSpeedUnit] = UnitChanger(app, OperatingSpeedRPM, '
rpm');
                % =======================

                % === Plotting Reduction in Power Loss vs
Speed ===
                cla(app.SpeedVsReductionAxes);      % Clear
axes before using
                pLine =
plot(app.SpeedVsReductionAxes,weNew/pi*60/P,PLRperc1DweNew,'g-
','LineWidth',3); % The line itself
                hold(app.SpeedVsReductionAxes,'on');

plot(app.SpeedVsReductionAxes,WeNew/pi*60/P,PLRperc1Dwe,'o','L
ineWidth',1,'MarkerSize',4,'MarkerFaceColor','g','MarkerEdgeCo
lor','k'); % Plotting the point just for a better look

                pZero =
plot(app.SpeedVsReductionAxes,ZeroweNew/pi*60/P,zeros(1,length
(ZeroweNew)),'o','LineWidth',1,'MarkerSize',10,'MarkerFaceColo
r','r','MarkerEdgeColor','k');

                pPoint =
plot(app.SpeedVsReductionAxes,OperatingSpeedRPM,PLRpointPerc1D
,'o','LineWidth',1,'MarkerSize',10,'MarkerFaceColor','m','Mark
erEdgeColor','k');

                set(app.SpeedVsReductionAxes, 'XLimSpec',
'Tight');


legend(app.SpeedVsReductionAxes,[pLine,pPoint,pZero],{sprintf(
'@ iq_{op} = %.1f
%s',NewIqValue,NewIqUnit),sprintf('\\omega_{op} =
%.1f%s',NewOperatingSpeedValue,NewOperatingSpeedUnit),'Min
Power Loss'});
                %
=================================================



                % === Relative Power Loss Reduction 1D at
constant speed ===
                cla(app.CurrentVsReductionAxes);      % Clear
axes before using


                % === Operation Points Line Construction ===
                if N<100
                    % === New vector iq with 100 points for
better resolution ===
```

```
                    iqNew =
linspace(IqMax*MinValPerc/100,IqMax,100);     % Vector of iq
for
                    %
============================================================
                else
                    iqNew = iq;
                end
                Pc1Diq =
getPcFromWE(SpeedRad,iqNew,Rs,I0max,L0);
                PcMin1Diq =
getPcMinLoss(SpeedRad,iqNew,I0max,L0);
                PLRperc1D =
getRelativeError(Pc1Diq,PcMin1Diq);
                % ===========================================

                % === Points Construction ===
                IqNew =
linspace(IqMax*MinValPerc/100,IqMax,10); % just to make the
line look nice
                Pc1DiqP =
getPcFromWE(SpeedRad,IqNew,Rs,I0max,L0);
                PcMin1DiqP =
getPcMinLoss(SpeedRad,IqNew,I0max,L0);
                PLRperc1DiqP =
getRelativeError(Pc1DiqP,PcMin1DiqP);
                % ===========================

                % === Zero Point of of the graph ===
                ZeroIqNew = getIqOPAll(SpeedRad,Rs,I0max,L0);
                % ==================================



                pLine =
plot(app.CurrentVsReductionAxes,iqNew,PLRperc1D,'g-
','LineWidth',3);
                hold(app.CurrentVsReductionAxes,'on');

plot(app.CurrentVsReductionAxes,IqNew,PLRperc1DiqP,'o','LineWi
dth',1,'MarkerSize',4,'MarkerFaceColor','g','MarkerEdgeColor',
'k'); % For the line to look nice

                pZero =
plot(app.CurrentVsReductionAxes,ZeroIqNew,zeros(1,length(ZeroI
qNew)),'o','LineWidth',1,'MarkerSize',10,'MarkerFaceColor','r'
,'MarkerEdgeColor','k');
                pPoint =
plot(app.CurrentVsReductionAxes,Iq,PLRpointPerc1D,'o','LineWid
th',1,'MarkerSize',10,'MarkerFaceColor','m','MarkerEdgeColor',
'k');

                set(app.CurrentVsReductionAxes, 'XLimSpec',
'Tight');
```

```
legend(app.CurrentVsReductionAxes,[pLine,pPoint,pZero],{sprint
f('@ \\omega_{op} =
%.1f%s',NewOperatingSpeedValue,NewOperatingSpeedUnit),sprintf(
'iq_{op} = %.1f %s',NewIqValue,NewIqUnit),'Min Power Loss'});
                %
==========================================================


                % === Current Best Operating Points ===
                cla(app.CurrentBestOPAxes);     % Clear axes
before using


                % === Operation Points Line Construction ===
                iqOP = getIqOPAll(weNew,Rs,I0max,L0);
                % ==========================================

                % === Points Construction ===
                IqOP = getIqOPAll(WeNew,Rs,I0max,L0);
                % ===========================



                pLine =
plot(app.CurrentBestOPAxes,weNew/pi*60/P,iqOP,'g-
','LineWidth',3);
                hold(app.CurrentBestOPAxes,'on');

plot(app.CurrentBestOPAxes,WeNew/pi*60/P,IqOP,'o','LineWidth',
1,'MarkerSize',4,'MarkerFaceColor','g','MarkerEdgeColor','k');
% For the line to look nice

                pPoint =
plot(app.CurrentBestOPAxes,OperatingSpeedRPM,Iq,'o','LineWidth
',1,'MarkerSize',10,'MarkerFaceColor','m','MarkerEdgeColor','k
');

                set(app.CurrentBestOPAxes, 'XLimSpec',
'Tight');

legend(app.CurrentBestOPAxes,[pLine,pPoint],{sprintf('@ r_{s}
= %.2f %s',RsLabel,RsUnit),'Operating
Point'},'Location','southeast');
                % =====================================


                % === Predicted Best Operating Points ===
                cla(app.PredictedBestOPAxes);     % Clear axes
before using

                if PcPoint>PcMinPoint
                    % === Operation Points Line Construction
===
```

```
                    iqOPnew =
getIqOPAll(weNew,RsMinLoss,I0max,L0);
                    %
==========================================

                    % === Points Construction ===
                    IqOPnew =
getIqOPAll(WeNew,RsMinLoss,I0max,L0);
                    % ===========================


                    pLine =
plot(app.PredictedBestOPAxes,weNew/pi*60/P,iqOPnew,'g-
','LineWidth',3);
                    hold(app.PredictedBestOPAxes,'on');

plot(app.PredictedBestOPAxes,WeNew/pi*60/P,IqOPnew,'o','LineWi
dth',1,'MarkerSize',4,'MarkerFaceColor','g','MarkerEdgeColor',
'k'); % For the line to look nice

                    pPoint =
plot(app.PredictedBestOPAxes,OperatingSpeedRPM,Iq,'o','LineWid
th',1,'MarkerSize',10,'MarkerFaceColor','m','MarkerEdgeColor',
'k');

                    set(app.PredictedBestOPAxes, 'XLimSpec',
'Tight');

legend(app.PredictedBestOPAxes,[pLine,pPoint],{sprintf('@
r_{s} = %.2f %s',RsMinLossLabel,RsMinLossUnit),'Operating
Point'},'Location','southeast');
                end
                % =======================================

            end % end of the load current checking statement

            app.Output.Text = OutputText;

        end



        % === Function that checks for errors and calls
DoCalculations(app) if none detected ===
        function IfNoErrorsDoCalculations(app)

            app.Lamp.Enable = 'on';         % Enabling the
lamp
            app.Output.Text = '';           % Empty the Output
Label
            app.LampLabel.FontColor = 'r';  % Text of a red
colour
            app.Lamp.Color = 'r';           % Turn lamp red
```

```
            app.OperatingloadcurrentmustnotexceedLabel.Visible
= 'off';    % Turn off the visibility
            app.LoadCurrentMaxValueLabel.Visible = 'off';
% Turn off the visibility

            % === Clearing all of the axes ===
            cla(app.TotalPowerLossAxes);        % Clear axes
            cla(app.SpeedVsReductionAxes);      % Clear axes
            cla(app.CurrentVsReductionAxes);    % Clear axes
            cla(app.CurrentBestOPAxes);         % Clear axes
            cla(app.PredictedBestOPAxes);       % Clear axes
            % ================================

            % === Checking whether the Operating Point is
still within the Base Speed Range ===
            if app.PhaseResistanceField.Value <= 0
                app.LampLabel.Text = {'ERROR: The value of the
Phase Resistance';...
                                      sprintf('must be greater
than zero, (%s > 0)',[char(114),char(8347)])};
            elseif app.LeakageInductanceField.Value <= 0
                app.LampLabel.Text = {'ERROR: The value of the
Leakage Inductance';...
                                      sprintf('must be greater
than zero, (%s > 0)',[char(76),char(8320)])};
            elseif app.FluxLinkageField.Value <= 0
                app.LampLabel.Text = {'ERROR: The value of the
fundamental Flux Linkage';...
                                      sprintf('component must
be greater than zero, (%s >
0)',[char(955),char(8346),char(8344)])};
            elseif app.ZeroSequenceFluxCoeffField.Value <= 0
                app.LampLabel.Text = {'ERROR: The value of the
3rd harmonic Flux Linkage';...
                                      sprintf('Coeff. must be
greater than zero, (%s >
0)',[char(954),char(8346),char(8344),char(8323)])};
            elseif app.NumberofPolesField.Value < 2 ||
round(app.NumberofPolesField.Value) ~=
app.NumberofPolesField.Value ||
mod(app.NumberofPolesField.Value,2)
                app.LampLabel.Text = {'ERROR: The Number of
Poles value must be an even';...
                                      sprintf('integer and
greater than or equal to two, (P = 2%s, %s %s
%s)',char(954),char(954),char(8712),char(8469))};
            elseif app.RatedSpeedField.Value <= 0
                app.LampLabel.Text = {'ERROR: The value of the
Rated Speed must be';...
                                      sprintf('greater than
zero, (%s > 0)',char(969))};
            elseif app.RatedSpeedField.Value <
app.SpeedOPField.Value
```

```
                app.LampLabel.Text = {'ERROR: The value of the
Rated Speed must be';...
                                      'greater than the speed
of the operating point.'};
            elseif app.SpeedOPField.Value < 0
                app.LampLabel.Text = {'ERROR: The value of the
Speed of the Operating';...
                                      sprintf('Point must be
greater than or equal to zero, (%s >=
0)',[char(969),char(8338),char(8346)])};
            elseif app.QuadratureCurrentOPField.Value < 0
                app.LampLabel.Text = {'ERROR: The value of the
Current of the Operating';...
                                      sprintf('Point must be
greater than or equal to zero, (%s >=
0)',['iq',char(8338),char(8346)])};
            else
                app.LampLabel.Text = 'All good.';          %
Message to the user that there is no known errors
                app.Lamp.Color = 'g';                      %
Turn lamp green
                app.LampLabel.FontColor = [0.31 0.68 0.31];%
Text of a green colour
                DoCalculations(app);                       %
Recalculate the model
            end
            %
==============================================================
===================
        end
        %
==============================================================
========================


        % === Changes the Unit and the Value if necessary ===
        function [NewValue, NewUnit] = UnitChanger(app, Value,
Unit)

            % === Extracting the Sign ===
            if Value < 0
                Sign = -1;
            else
                Sign = 1;
            end
            % ===========================

            Value = abs(Value); % to work with the positive
values only

            % === Changes the Unit and the Value if necessary
===
            if Value > 1
```

```
                if Value >= 1e27
                    NewValue = Value; % Leaving the value as
it is
                    NewUnit = Unit;   % Leaving the unit as it
is
                elseif Value >= 1e24        % yotta (Y)
                    NewValue = Value*1e-24;
                    NewUnit = ['Y',Unit];
                elseif Value >= 1e21        % zetta (Z)
                    NewValue = Value*1e-21;
                    NewUnit = ['Z',Unit];
                elseif Value >= 1e18        % exa   (E)
                    NewValue = Value*1e-18;
                    NewUnit = ['E',Unit];
                elseif Value >= 1e15        % peta  (P)
                    NewValue = Value*1e-15;
                    NewUnit = ['P',Unit];
                elseif Value >= 1e12        % tera  (T)
                    NewValue = Value*1e-12;
                    NewUnit = ['T',Unit];
                elseif Value >= 1e9         % giga  (G)
                    NewValue = Value*1e-9;
                    NewUnit = ['G',Unit];
                elseif Value >= 1e6         % mega  (M)
                    NewValue = Value*1e-6;
                    NewUnit = ['M',Unit];
                elseif Value >= 1e3         % kilo  (k)
                    NewValue = Value*1e-3;
                    NewUnit = ['k',Unit];
                else                         % Range: (1,1000)
                    NewValue = Value; % Leaving the value as
it is
                    NewUnit = Unit;   % Leaving the unit as it
is
                end

            elseif Value < 1

                if Value <= 1e-24
                    NewValue = Value; % Leaving the value as
it is
                    NewUnit = Unit;   % Leaving the unit as it
is
                elseif Value < 1e-21      % yocto (y)
                    NewValue = Value*1e24;
                    NewUnit = ['y',Unit];
                elseif Value < 1e-18      % zepto (z)
                    NewValue = Value*1e21;
                    NewUnit = ['z',Unit];
                elseif Value < 1e-15      % atto  (a)
                    NewValue = Value*1e18;
                    NewUnit = ['a',Unit];
```

```
                elseif Value < 1e-12      % femto (f)
                    NewValue = Value*1e15;
                    NewUnit = ['f',Unit];
                elseif Value < 1e-9      % pico  (p)
                    NewValue = Value*1e12;
                    NewUnit = ['p',Unit];
                elseif Value < 1e-6       % nano  (n)
                    NewValue = Value*1e9;
                    NewUnit = ['n',Unit];
                elseif Value < 1e-3       % micro (u)
                    NewValue = Value*1e6;
                    NewUnit = ['u',Unit];
                else                       % milli (m)
                    NewValue = Value*1e3;
                    NewUnit = ['m',Unit];
                end

            else
                NewValue = Value; % Leaving the value as it is
                NewUnit = Unit;   % Leaving the unit as it is
            end

            % === Assign the Original Sign ===
            NewValue = NewValue * Sign;
            % ================================

        end
        % ===================================================

    end

    methods (Access = private)



    end


    % Callbacks that handle component events
    methods (Access = private)

        % Code that executes after component creation
        function startupFcn(app)

            % === Useful Special Caracters ===
            LambdaPM = [char(955),char(8346),char(8344)];
            OmegaE = [char(969),char(8337)];
            Omega = char(969);
            OmegaOP = [char(969),char(8338),char(8346)];
            ResS = [char(114),char(8347)];
            KappaPM3 =
[char(954),char(8346),char(8344),char(8323)];
            LZERO = [char(76),char(8320)];
```

```
            Ohms = char(937);
            Pi = char(960);
            Gamma = char(955);
            Sigma = char(963);
            PowOf3 = char(179);
            Infinity = char(8734);
            Micro = char(181);
            % ================================

            % === Initialise Axes ===
            view(app.TotalPowerLossAxes,3);          % 3D view
            title(app.TotalPowerLossAxes,'Total Power Loss in
Conductor');
            xlabel(app.TotalPowerLossAxes,'Resistance,
(\Omega)');
            ylabel(app.TotalPowerLossAxes,'Speed, (rpm)');
            zlabel(app.TotalPowerLossAxes,'Power Loss, (W)');
            plot3(app.TotalPowerLossAxes,0,0,0);     % Plot for
Legend
            legend(app.TotalPowerLossAxes,'');       % Set
Legend

            grid(app.TotalPowerLossAxes,'on');

            grid(app.CurrentVsReductionAxes,'on');
            grid(app.SpeedVsReductionAxes,'on');
            grid(app.CurrentBestOPAxes,'on');
            grid(app.PredictedBestOPAxes,'on');
            % =======================

            % === Renaming Input Labels ===
            app.PhaseResistanceEditField_2Label.Text = ['Phase
Resistance, ',ResS,':'];          % Rs
            app.LeakageInductanceEditField_2Label.Text =
['Leakage Inductance, ',LZERO,':'];    % L0
            app.FluxLinkageEditField_2Label.Text = ['Flux
Linkage, ',LambdaPM,':'];              % Ypm
            app.rdHarmonicFluxcoeffEditField_2Label.Text =
['3rd Harmonic Flux coeff., ',KappaPM3,':']; % Kpm3
            app.RatedSpeedEditField_2Label.Text = ['Rated
Speed, ',Omega,':'];                   % wrated
            % =============================

            % === Renaming Input Unint ===
            app.PhaseResistanceUnit.Text = Ohms;     % Unit for
Resistance
            % ============================

            % === Renaming Sliders Labels ===
            app.wOPLabel.Text = OmegaOP;
            % ================================

            % === Renaming Operating Point Labels ===
```

```
            app.SpeedLabel.Text = ['Speed, ',OmegaOP,':'];
% wrpm Operating Point
            app.QuadratureAxisCurrentLabel.Text = ['Quadrature
Axis Current, iq',[char(8338),char(8346)],':'];
            % =======================================

            % === Set the Lamp and its Label Off ===
            app.Lamp.Enable = 'off';     % Disabling the lamp
            app.LampLabel.Text = '';     % Getting rid of the
lamp's label for now
            % ======================================

            % === Hide the Maximum Current label ===
            app.OperatingloadcurrentmustnotexceedLabel.Visible
= 'off';     % Turn off the visibility
            % ======================================

        end

        % Value changed function: CurrentSlider
        function CurrentSliderValueChanged(app, event)
            IfNoErrorsDoCalculations(app);     % Recalculate
the model if there is no detected errors
        end

        % Value changing function: CurrentSlider
        function CurrentSliderValueChanging(app, event)
            app.CurrentSlider.Value = event.Value;
% Make the changing value current
            app.QuadratureCurrentOPField.Value = event.Value;
% Store rounded RPM values
            IfNoErrorsDoCalculations(app);     % Recalculate
the model if there is no detected errors
        end

        % Value changed function: FluxLinkageField
        function FluxLinkageFieldValueChanged(app, event)
            IfNoErrorsDoCalculations(app);     % Recalculate
the model if there is no detected errors
        end

        % Value changed function: LeakageInductanceField
        function LeakageInductanceFieldValueChanged(app,
event)
            IfNoErrorsDoCalculations(app);     % Recalculate
the model if there is no detected errors
        end

        % Value changed function: NumberofPolesField
        function NumberofPolesFieldValueChanged(app, event)
            IfNoErrorsDoCalculations(app);     % Recalculate
the model if there is no detected errors
        end
```

```
        % Value changed function: PhaseResistanceField
        function PhaseResistanceFieldValueChanged(app, event)
            IfNoErrorsDoCalculations(app);    % Recalculate
the model if there is no detected errors
        end

        % Value changed function: QuadratureCurrentOPField
        function QuadratureCurrentOPFieldValueChanged(app,
event)
            IfNoErrorsDoCalculations(app);    % Recalculate
the model if there is no detected errors
        end

        % Value changed function: RatedSpeedField
        function RatedSpeedFieldValueChanged(app, event)
            IfNoErrorsDoCalculations(app);    % Recalculate
the model if there is no detected errors
        end

        % Value changed function: SpeedOPField
        function SpeedOPFieldValueChanged(app, event)
            IfNoErrorsDoCalculations(app);    % Recalculate
the model if there is no detected errors
        end

        % Value changed function: SpeedSlider
        function SpeedSliderValueChanged(app, event)
            IfNoErrorsDoCalculations(app);    % Recalculate
the model if there is no detected errors
        end

        % Value changing function: SpeedSlider
        function SpeedSliderValueChanging(app, event)
            app.SpeedSlider.Value = event.Value;            %
Round the RPM value
            app.SpeedOPField.Value = ceil(event.Value);    %
Store rounded RPM value
            IfNoErrorsDoCalculations(app);    % Recalculate
the model if there is no detected errors
        end

        % Value changed function: ZeroSequenceFluxCoeffField
        function ZeroSequenceFluxCoeffFieldValueChanged(app,
event)
            IfNoErrorsDoCalculations(app);    % Recalculate
the model if there is no detected errors
        end

        % Value changed function: ViewSwitch
        function ViewSwitchValueChanged(app, event)
            IfNoErrorsDoCalculations(app);    % Recalculate
the model if there is no detected errors
```

```
        end
    end

    % Component initialization
    methods (Access = private)

        % Create UIFigure and components
        function createComponents(app)

            % Create UIFigure and hide until all components
are created
            app.UIFigure = uifigure('Visible', 'off');
            app.UIFigure.Position = [100 100 1073 750];
            app.UIFigure.Name = 'UI Figure';

            % Create CurrentSlider
            app.CurrentSlider = uislider(app.UIFigure);
            app.CurrentSlider.ValueChangedFcn =
createCallbackFcn(app, @CurrentSliderValueChanged, true);
            app.CurrentSlider.ValueChangingFcn =
createCallbackFcn(app, @CurrentSliderValueChanging, true);
            app.CurrentSlider.Position = [505 424 521 3];

            % Create iqLabel
            app.iqLabel = uilabel(app.UIFigure);
            app.iqLabel.HorizontalAlignment = 'center';
            app.iqLabel.FontSize = 16;
            app.iqLabel.FontWeight = 'bold';
            app.iqLabel.Position = [460 399 25 20];
            app.iqLabel.Text = 'iq';

            % Create wOPLabel
            app.wOPLabel = uilabel(app.UIFigure);
            app.wOPLabel.HorizontalAlignment = 'center';
            app.wOPLabel.FontSize = 16;
            app.wOPLabel.FontWeight = 'bold';
            app.wOPLabel.Position = [387 428 41 20];
            app.wOPLabel.Text = 'wOP';

            % Create SpeedSlider
            app.SpeedSlider = uislider(app.UIFigure);
            app.SpeedSlider.MajorTicks = [0 10 20 30 40 50 60
70 80 90 100];
            app.SpeedSlider.MajorTickLabels = {'0', '10',
'20', '30', '40', '50', '60', '70', '80', '90', '100'};
            app.SpeedSlider.Orientation = 'vertical';
            app.SpeedSlider.ValueChangedFcn =
createCallbackFcn(app, @SpeedSliderValueChanged, true);
            app.SpeedSlider.ValueChangingFcn =
createCallbackFcn(app, @SpeedSliderValueChanging, true);
            app.SpeedSlider.MinorTicks = [0 2.5 5 7.5 10 12.5
15 17.5 20 22.5 25 27.5 30 32.5 35 37.5 40 42.5 45 47.5 50
```

```
52.5 55 57.5 60 62.5 65 67.5 70 72.5 75 77.5 80 82.5 85 87.5
90 92.5 95 97.5 100];
            app.SpeedSlider.Position = [391 464 3 218];

            % Create LampLabel
            app.LampLabel = uilabel(app.UIFigure);
            app.LampLabel.VerticalAlignment = 'top';
            app.LampLabel.Position = [58 222 296 34];
            app.LampLabel.Text = 'Lamp';

            % Create Lamp
            app.Lamp = uilamp(app.UIFigure);
            app.Lamp.Position = [31 238 20 20];

            % Create TabGroup
            app.TabGroup = uitabgroup(app.UIFigure);
            app.TabGroup.Position = [27 400 327 289];

            % Create InputsTab
            app.InputsTab = uitab(app.TabGroup);
            app.InputsTab.Title = 'Inputs';

            % Create PhaseResistanceField
            app.PhaseResistanceField =
uieditfield(app.InputsTab, 'numeric');
            app.PhaseResistanceField.ValueChangedFcn =
createCallbackFcn(app, @PhaseResistanceFieldValueChanged,
true);
            app.PhaseResistanceField.Position = [189 216 74
22];
            app.PhaseResistanceField.Value = 0.164;

            % Create LeakageInductanceEditField_2Label
            app.LeakageInductanceEditField_2Label =
uilabel(app.InputsTab);

app.LeakageInductanceEditField_2Label.HorizontalAlignment =
'right';
            app.LeakageInductanceEditField_2Label.Position =
[9 182 173 15];
            app.LeakageInductanceEditField_2Label.Text =
'Leakage Inductance:';

            % Create LeakageInductanceField
            app.LeakageInductanceField =
uieditfield(app.InputsTab, 'numeric');
            app.LeakageInductanceField.ValueChangedFcn =
createCallbackFcn(app, @LeakageInductanceFieldValueChanged,
true);
            app.LeakageInductanceField.Position = [189 178 74
22];
            app.LeakageInductanceField.Value = 1.775e-05;
```

```
            % Create FluxLinkageEditField_2Label
            app.FluxLinkageEditField_2Label =
uilabel(app.InputsTab);

app.FluxLinkageEditField_2Label.HorizontalAlignment = 'right';
            app.FluxLinkageEditField_2Label.VerticalAlignment
= 'top';
            app.FluxLinkageEditField_2Label.Position = [9 144
173 15];
            app.FluxLinkageEditField_2Label.Text = 'Flux
Linkage:';

            % Create FluxLinkageField
            app.FluxLinkageField = uieditfield(app.InputsTab,
'numeric');
            app.FluxLinkageField.ValueChangedFcn =
createCallbackFcn(app, @FluxLinkageFieldValueChanged, true);
            app.FluxLinkageField.Position = [189 140 74 22];
            app.FluxLinkageField.Value = 0.07147648494;

            % Create rdHarmonicFluxcoeffEditField_2Label
            app.rdHarmonicFluxcoeffEditField_2Label =
uilabel(app.InputsTab);

app.rdHarmonicFluxcoeffEditField_2Label.HorizontalAlignment =
'right';
            app.rdHarmonicFluxcoeffEditField_2Label.Position =
[9 106 173 15];
            app.rdHarmonicFluxcoeffEditField_2Label.Text =
'3rd Harmonic Flux coeff.:';

            % Create ZeroSequenceFluxCoeffField
            app.ZeroSequenceFluxCoeffField =
uieditfield(app.InputsTab, 'numeric');
            app.ZeroSequenceFluxCoeffField.ValueChangedFcn =
createCallbackFcn(app,
@ZeroSequenceFluxCoeffFieldValueChanged, true);
            app.ZeroSequenceFluxCoeffField.Position = [189 102
74 22];
            app.ZeroSequenceFluxCoeffField.Value =
0.0114748014533;

            % Create NumberofPolesPLabel
            app.NumberofPolesPLabel = uilabel(app.InputsTab);
            app.NumberofPolesPLabel.HorizontalAlignment =
'right';
            app.NumberofPolesPLabel.Position = [9 70 173 15];
            app.NumberofPolesPLabel.Text = 'Number of Poles,
P:';

            % Create NumberofPolesField
            app.NumberofPolesField =
uieditfield(app.InputsTab, 'numeric');
```

```
            app.NumberofPolesField.ValueChangedFcn =
createCallbackFcn(app, @NumberofPolesFieldValueChanged, true);
            app.NumberofPolesField.Position = [189 66 74 22];
            app.NumberofPolesField.Value = 6;

            % Create RatedSpeedEditField_2Label
            app.RatedSpeedEditField_2Label =
uilabel(app.InputsTab);
            app.RatedSpeedEditField_2Label.HorizontalAlignment
= 'right';
            app.RatedSpeedEditField_2Label.Position = [17 32
165 15];
            app.RatedSpeedEditField_2Label.Text = 'Rated
Speed:';

            % Create RatedSpeedField
            app.RatedSpeedField = uieditfield(app.InputsTab,
'numeric');
            app.RatedSpeedField.ValueChangedFcn =
createCallbackFcn(app, @RatedSpeedFieldValueChanged, true);
            app.RatedSpeedField.Position = [189 28 74 22];

            % Create PhaseResistanceUnit
            app.PhaseResistanceUnit = uilabel(app.InputsTab);
            app.PhaseResistanceUnit.Position = [273 220 46
15];
            app.PhaseResistanceUnit.Text = 'Ohm';

            % Create LeakageInductanceUnit
            app.LeakageInductanceUnit =
uilabel(app.InputsTab);
            app.LeakageInductanceUnit.Position = [273 182 46
15];
            app.LeakageInductanceUnit.Text = 'H';

            % Create FluxLinkageUnit
            app.FluxLinkageUnit = uilabel(app.InputsTab);
            app.FluxLinkageUnit.Position = [273 144 46 15];
            app.FluxLinkageUnit.Text = 'Vs';

            % Create RatedSpeedUnit
            app.RatedSpeedUnit = uilabel(app.InputsTab);
            app.RatedSpeedUnit.Position = [273 32 46 15];
            app.RatedSpeedUnit.Text = 'rpm';

            % Create PhaseResistanceEditField_2Label
            app.PhaseResistanceEditField_2Label =
uilabel(app.InputsTab);

app.PhaseResistanceEditField_2Label.HorizontalAlignment =
'right';
            app.PhaseResistanceEditField_2Label.Position = [9
220 173 15];
```

```
            app.PhaseResistanceEditField_2Label.Text = 'Phase
Resistance:';

            % Create AdditionalInputsTab
            app.AdditionalInputsTab = uitab(app.TabGroup);
            app.AdditionalInputsTab.Title = 'Additional
Inputs';

            % Create OperatingPointInputPanel
            app.OperatingPointInputPanel =
uipanel(app.UIFigure);
            app.OperatingPointInputPanel.Title = 'Operating
Point Input';
            app.OperatingPointInputPanel.Position = [27 274
327 101];

            % Create SpeedOPField
            app.SpeedOPField =
uieditfield(app.OperatingPointInputPanel, 'numeric');
            app.SpeedOPField.ValueChangedFcn =
createCallbackFcn(app, @SpeedOPFieldValueChanged, true);
            app.SpeedOPField.Position = [189 48 72 22];
            app.SpeedOPField.Value = 17500;

            % Create SpeedLabel
            app.SpeedLabel =
uilabel(app.OperatingPointInputPanel);
            app.SpeedLabel.HorizontalAlignment = 'right';
            app.SpeedLabel.Position = [18 52 164 15];
            app.SpeedLabel.Text = 'Speed:';

            % Create SpeedOPUnit
            app.SpeedOPUnit =
uilabel(app.OperatingPointInputPanel);
            app.SpeedOPUnit.Position = [273 52 26 15];
            app.SpeedOPUnit.Text = 'rpm';

            % Create QuadratureCurrentOPField
            app.QuadratureCurrentOPField =
uieditfield(app.OperatingPointInputPanel, 'numeric');
            app.QuadratureCurrentOPField.ValueChangedFcn =
createCallbackFcn(app, @QuadratureCurrentOPFieldValueChanged,
true);
            app.QuadratureCurrentOPField.Position = [189 11 72
22];
            app.QuadratureCurrentOPField.Value = 8.1684;

            % Create QuadratureAxisCurrentLabel
            app.QuadratureAxisCurrentLabel =
uilabel(app.OperatingPointInputPanel);
            app.QuadratureAxisCurrentLabel.HorizontalAlignment
= 'right';
```

```
            app.QuadratureAxisCurrentLabel.Position = [9 15
173 15];
            app.QuadratureAxisCurrentLabel.Text = 'Quadrature
Axis Current:';

            % Create QuadratureCurrentOPUnit
            app.QuadratureCurrentOPUnit =
uilabel(app.OperatingPointInputPanel);
            app.QuadratureCurrentOPUnit.Position = [273 15 25
15];
            app.QuadratureCurrentOPUnit.Text = 'A';

            % Create
PowerLossinConductorReductionCalculatorLabel
            app.PowerLossinConductorReductionCalculatorLabel =
uilabel(app.UIFigure);

app.PowerLossinConductorReductionCalculatorLabel.HorizontalAli
gnment = 'center';

app.PowerLossinConductorReductionCalculatorLabel.FontSize =
20;

app.PowerLossinConductorReductionCalculatorLabel.FontWeight =
'bold';

app.PowerLossinConductorReductionCalculatorLabel.Position = [1
715 944 26];

app.PowerLossinConductorReductionCalculatorLabel.Text = 'Power
Loss in Conductor Reduction Calculator';

            % Create OperatingloadcurrentmustnotexceedLabel
            app.OperatingloadcurrentmustnotexceedLabel =
uilabel(app.UIFigure);

app.OperatingloadcurrentmustnotexceedLabel.FontWeight =
'bold';

app.OperatingloadcurrentmustnotexceedLabel.Position = [27 208
233 15];
            app.OperatingloadcurrentmustnotexceedLabel.Text =
'Operating load current must not exceed';

            % Create LoadCurrentMaxValueLabel
            app.LoadCurrentMaxValueLabel =
uilabel(app.UIFigure);
            app.LoadCurrentMaxValueLabel.FontWeight = 'bold';
            app.LoadCurrentMaxValueLabel.FontColor = [1 0 0];
            app.LoadCurrentMaxValueLabel.Position = [259 208
95 15];
            app.LoadCurrentMaxValueLabel.Text = '';
```

```
            % Create Output
            app.Output = uilabel(app.UIFigure);
            app.Output.VerticalAlignment = 'top';
            app.Output.FontWeight = 'bold';
            app.Output.Position = [27 6 434 199];
            app.Output.Text = '';

            % Create TotalPowerLossAxes
            app.TotalPowerLossAxes = uiaxes(app.UIFigure);
            title(app.TotalPowerLossAxes, 'Power Loss in
Conductor')
            xlabel(app.TotalPowerLossAxes, 'Resistance,
(\Omega)')
            ylabel(app.TotalPowerLossAxes, 'Speed, (rpm)')
            app.TotalPowerLossAxes.PlotBoxAspectRatio =
[2.60591133004926 1 1];
            app.TotalPowerLossAxes.Position = [460 446 577
259];

            % Create CurrentVsReductionAxes
            app.CurrentVsReductionAxes = uiaxes(app.UIFigure);
            title(app.CurrentVsReductionAxes, 'Reduction of
Power Loss in Conductor')
            xlabel(app.CurrentVsReductionAxes, 'i_{q}, (A)')
            ylabel(app.CurrentVsReductionAxes, 'P_{c}
Reduction, (%)')
            app.CurrentVsReductionAxes.Position = [738 190 300
185];

            % Create PredictedBestOPAxes
            app.PredictedBestOPAxes = uiaxes(app.UIFigure);
            title(app.PredictedBestOPAxes, 'Predicted Best
Operating Points')
            xlabel(app.PredictedBestOPAxes, '\omega_{r},
(rpm)')

            ylabel(app.PredictedBestOPAxes, 'i_{q}, (A)')
            app.PredictedBestOPAxes.Position = [739 1 300
185];

            % Create SpeedVsReductionAxes
            app.SpeedVsReductionAxes = uiaxes(app.UIFigure);
            title(app.SpeedVsReductionAxes, 'Reduction of
Power Loss in Conductor')
            xlabel(app.SpeedVsReductionAxes, '\omega_{r},
(rpm)')
            ylabel(app.SpeedVsReductionAxes, 'P_{c} Reduction,
(%)')
            app.SpeedVsReductionAxes.Position = [440 190 300
185];

            % Create CurrentBestOPAxes
            app.CurrentBestOPAxes = uiaxes(app.UIFigure);
```

```
            title(app.CurrentBestOPAxes, 'Current Best
Operating Points')
            xlabel(app.CurrentBestOPAxes, '\omega_{r}, (rpm)')
            ylabel(app.CurrentBestOPAxes, 'i_{q}, (A)')
            app.CurrentBestOPAxes.Position = [441 1 300 185];

            % Create ViewSwitchLabel
            app.ViewSwitchLabel = uilabel(app.UIFigure);
            app.ViewSwitchLabel.HorizontalAlignment =
'center';
            app.ViewSwitchLabel.FontWeight = 'bold';
            app.ViewSwitchLabel.Position = [965 458 33 22];
            app.ViewSwitchLabel.Text = 'View';

            % Create ViewSwitch
            app.ViewSwitch = uiswitch(app.UIFigure, 'rocker');
            app.ViewSwitch.Items = {'2D', '3D'};
            app.ViewSwitch.ValueChangedFcn =
createCallbackFcn(app, @ViewSwitchValueChanged, true);
            app.ViewSwitch.FontWeight = 'bold';
            app.ViewSwitch.Position = [971 510 20 45];
            app.ViewSwitch.Value = '3D';

            % Show the figure after all components are created
            app.UIFigure.Visible = 'on';
        end
    end

    % App creation and deletion
    methods (Access = public)

        % Construct app
        function app = PowerLossRedApp

            % Create UIFigure and components
            createComponents(app)

            % Register the app with App Designer
            registerApp(app, app.UIFigure)

            % Execute the startup function
            runStartupFcn(app, @startupFcn)

            if nargout == 0
                clear app
            end
        end

        % Code that executes before app deletion
        function delete(app)

            % Delete UIFigure when app is deleted
            delete(app.UIFigure)
```

```
        end
    end
end
```

Appendix F - Published Papers

The research resulted in two published conference papers:

- N. Hunter, T. Cox, P. Zanchetta, S. Odhano and L. Rovere, “Torque Quality Improvement of an Open-End Winding PMSM” *2018 IEEE Energy Conversion Congress and Exposition (ECCE)*, Portland, 2018.

- N. Hunter, T. Cox, P. Zanchetta, S. Odhano and L. Rovere, “Non-Intrusive Online Stator Temperature Estimation for Open-End Winding PMSM” *2018 IEEE Energy Conversion Congress and Exposition (ECCE)*, Portland, 2018.